Reactive Transport Modelling of In-situ Diffusion Experiments for the Mont Terri Project

MIN3P-THCm Code Enhancements and Numerical Simulations

NWMO-TR-2014-25 **December 2014**

Mingliang Xie[1], Pejman Rasouli[1], K. Ulrich Mayer[1] and Kerry T. B. MacQuarrie[2]

[1]Department of Earth, Ocean and Atmospheric Sciences, University of British Columbia
[2]Department of Civil Engineering, University of New Brunswick

nwmo
NUCLEAR WASTE MANAGEMENT ORGANIZATION
SOCIÉTÉ DE GESTION DES DÉCHETS NUCLÉAIRES

Nuclear Waste Management Organization
22 St. Clair Avenue East, 6th Floor
Toronto, Ontario
M4T 2S3
Canada

Tel: 416-934-9814
Web: www.nwmo.ca

Reactive Transport Modelling of In-situ Diffusion Experiments for the Mont Terri Project

MIN3P-THCm Code Enhancements and Numerical Simulations

NWMO-TR-2014-25

December 2014

Mingliang Xie[1], Pejman Rasouli[1], K. Ulrich Mayer[1] and Kerry T. B. MacQuarrie[2]
[1]Department of Earth, Ocean and Atmospheric Sciences, University of British Columbia
[2]Department of Civil Engineering, University of New Brunswick

Document History

Title:	Reactive Transport Modelling of In-situ Diffusion Experiments for the Mont Terri Project MIN3P-THCm Code Enhancements and Numerical Simulations		
Report Number:	NWMO-TR-2014-25		
Revision:	R000	Date:	December 2014
[1]Department of Earth, Ocean and Atmospheric Sciences, University of British Columbia [2]Department of Civil Engineering, University of New Brunswick			
Authored by:	Mingliang Xie[1], Pejman Rasouli[1]		
Verified by:	Kerry T. B. MacQuarrie[2]		
Approved by:	K. Ulrich Mayer[1]		
Nuclear Waste Management Organization			
Reviewed by:	Tammy Yang, Monique Hobbs, Laura Kennell		
Accepted by:	Mark Jensen		

ABSTRACT

Title: **Reactive Transport Modelling of In-situ Diffusion Experiments for the Mont Terri Project**
MIN3P-THCm Code Enhancements and Numerical Simulations
Report No.: **NWMO-TR-2014-25**
Author(s): Mingliang Xie[1], Pejman Rasouli[1], K. Ulrich Mayer[1] and Kerry T. B. MacQuarrie[2]
Company: [1]Department of Earth, Ocean and Atmospheric Sciences, University of British Columbia
[2]Department of Civil Engineering, University of New Brunswick
Date: December 2014

Abstract
The DR-A in-situ borehole diffusion experiment conducted at the Mont Terri Underground Research Laboratory and a series of associated benchmarking tasks were simulated using the reactive transport code MIN3P-THCm. The simulations of the DR-A diffusion experiment included both Phase I (diffusion of mixed tracers including HTO, I^-, Br^-, $^{85}Sr^{2+}$, Cs^+, $^{60}Co^{2+}$ and Eu^{3+}) and Phase II (replacement of the initial synthetic porewater in the borehole with a more saline solution). To facilitate these simulations several code enhancements were undertaken, including the implementation of a multisite ion exchange (MIE) model, a multicomponent diffusion (MCD) model, and a hybrid multicomponent diffusion (HMD) model that, in an empirical manner, accounts for anion exclusion and enhanced cation diffusion.

For the benchmarking tasks, excellent agreement was achieved with other modelling groups (PSI and University of Bern, Switzerland (using the reactive ransport code FLOTRAN); IDAEA-CSIC, Spain and LBNL, USA (using the reactive transport code CrunchFlow)). The application of the HMD model to the DR-A in-situ diffusion experiment illustrates that this approach provides a simple, but effective method for simulations involving several tracers. The HMD model allows the inclusion of multiple tracers in a single simulation by using factors that modify effective porosity and/or tortuosity for individual species, accounting for processes such as anion exclusion and interlayer/surface diffusion in clayey materials.

A comparison of simulated results and observational data from the DR-A diffusion experiment shows good agreement for HTO and anions, but a less favorable agreement for reactive cations – especially for strongly sorbing cations such as Cs^+, Eu^{3+}, $^{60}Co^{2+}$ and $^{85}Sr^{2+}$. Therefore, a sensitivity analysis and alternative scenarios were investigated for simulating cation migration. The simulation results suggest that the presence of colloidal clay particles in the gap and/or the filter may contribute to the observed rapid decline of tracer concentrations in the borehole at early time. For Eu^{3+}, additional adsorption on equipment, such as the Teflon filter, may explain the experimental data.

The simulation results for Phase II of the DR-A experiment suggest that the diffusion parameters of the Opalinus Clay change in response to the replacement of the circulation solution (i.e. the synthetic OPA porewater) with a more saline solution. Consequently, diffusion parameters obtained via calibration for Phase I had to be recalibrated for Phase II. Such modifications are consistent with the hypothesis that the diffuse double layer (DDL) thickness, which is not directly simulated, is reduced in response to the replacement of the Phase I borehole solution with a solution of higher ionic strength. By using a modified parameter set for the simulation of Phase II, good agreement with the experimental observed data was obtained for the test tracers.

TABLE OF CONTENTS

LIST OF TABLES

Page

LIST OF FIGURES

Page

1. INTRODUCTION

Clay formations are being considered internationally as potential host rocks for radioactive waste disposal owing to their special properties (i.e., low permeability, diffusion dominated solute transport and favorable retention capability). A series of in-situ diffusion experiments (DI, DI-A, DI-B, DR) were previously performed in the Opalinus Clay (OPA) at the Mont Terri Underground Rock Laboratory (Switzerland) to investigate the transport and retardation behaviour of different tracers (HTO, cations and anions; conservative and sorbing) using synthetic OPA porewater (Palut et al. 2003; Yllera et al. 2003; van Loon et al. 2003; Wersin et al. 2008). The most recent diffusion, retention and perturbation (DR-A) experiment was initiated in 2011 to investigate the response of tracers in a solution out of equilibrium with the host rock, which in the test interval was shaley facies OPA (Wersin et al. 2008; Gimmi et al. 2013). The experiment involved a variety of tracers including HTO, anions (Br^-, I^-), and cations ($^{85}Sr^{2+}$, Cs^+, $^{60}Co^{2+}$, and Eu^{3+}) and produced data sets that allow the quantitative characterization of solute migration by reactive transport modelling. The DR-A experiment was performed in two phases: Phase I – diffusion of tracers in synthetic OPA porewater for 189 days; Phase II – diffusion of the tracers after changing to a borehole solution with much higher salinity.

Due to the low permeability of the OPA formation at the Mont Terri Underground Research Laboratory, solute transport is diffusion controlled. Previous reactive transport modelling (Appelo and Wersin 2007; Appelo et al. 2010) has revealed that anion migration is inhibited by anion exclusion, while cation transport (i.e. $^{22}Na^+$, $^{85}Sr^{2+}$, and Cs^+) is enhanced by preferential migration through the diffusive double layer (DDL). Conceptual simulations by Soler (2010) have provided insight into the geochemical evolution of the OPA when exposed to strongly oxidizing or high pH fluids.

A model intercomparison was initiated to interpret experimental data from the DR-A experiment. The participated teams are: IDAEA-CSIC (Spain); PSI, University of Bern (Uni. Bern, Switzerland); University of British Columbia (Canada); and the Lawrence Berkeley National Laboratory (LBNL, USA) (Soler et al. 2014). The codes used for the simulations were: CrunchFlow (by LBNL and IDAEA-CSIC), Flotran (PSI and Uni. Bern), COMSOL (PSI) and MIN3P-THCm (UBC). For the first task, the participating groups simulated a series of simplified benchmark scenarios, as defined by the Mont Terri steering committee (Leupin 2012). The purpose of this exercise was to evaluate the modelling capabilities of different reactive transport codes to simulate simplified diffusion scenarios and to demonstrate that equivalent results can be obtained with different codes. Task 1 included four sub-tasks:

- Task 1.1: Simulation of diffusion of a non-sorbing solute from a vertical borehole into the Opalinus Clay (OPA) host rock;
- Task 1.2a: Simulation of diffusion of a weakly sorbing solute (with a sorption coefficient K_d=0.2 L kg^{-1}) from a vertical borehole into the OPA host rock;
- Task 1.2b: Simulation of diffusion of a strongly sorbing solute (with a sorption coefficient K_d=500 L kg^{-1}) from a vertical borehole into the OPA host rock;
- Task 1.3: Simulation of reactive Cs diffusion (subject to multisite ion exchange on illite).

The actual design of the DR-A experiment is characterized by more complex conditions than captured in the above description of Task 1 (Fierz and Rösli 2012). For example, the borehole was equipped with a 4 mm thick Teflon filter to separate the circulation chamber from the borehole wall. Between the filter and the borehole wall, there was a small water-filled gap with an average thickness of 3 mm, which further complicated the modelling. The presence of the filter and gap had to be taken into consideration for the accurate simulation of the in-situ experiment. As a result, Task 2.1 (see below) included a set of simulations analogous to Task 1, but including the filter and gap between the circulation chamber and the host rock. These simulations were defined by the following four sub-tasks:

- Task 2.1a: Simulation of diffusion of a non-sorbing solute from a vertical borehole through a filter and water-filled gap into the OPA host rock;

- Task 2.1bw: Simulation of diffusion of a weakly sorbing solute (K_d=0.2 L kg^{-1}) from a vertical borehole through a filter and water-filled gap into the host rock;

- Task 2.1bs: Simulation of diffusion of a strongly sorbing solute (K_d=500 L kg^{-1}) from a vertical borehole through a filter and water-filled gap into the host rock;

- Task 2.1c: Simulation of reactive Cs diffusion through a filter and water-filled gap into the OPA (subject to multisite ion exchange on illite).

Simulation of the in-situ borehole diffusion experiment after initial tracer injection (HTO, I^-, Br^-, $^{85}Sr^{2+}$, Cs^+, $^{60}Co^{2+}$ and Eu^{3+}, up to 189 days), i.e. Phase I of the DR-A diffusion experiment, was defined as Task 2.2. The chemical compositions of the porewater and sorption properties were based on experimental data published by van Loon et al. (2009) as suggested by the Mont Terri Consortium. In addition, several sensitivity analyses for $^{85}Sr^{2+}$ and $^{60}Co^{2+}$ were included to explore potential causes for discrepancies between simulated and observed results for both species.

Task 3.1 simulations were designed to reproduce Phase II of the DR-A experiment. This phase was initiated by increasing the ionic strength of the borehole solution at day 189 of the experiment. For this task, measured concentrations of the tracers and the major ions were provided up to 413 days. Sensitivity analyses were performed to further investigate ion migration behaviour (Table 1).

The circulation of the borehole solution and data collection continued beyond 413 days until initiation of overcoring (starting at 728 days for one week). During the overcoring, some water was detected above the packer, which unfortunately could not be removed before retrieving the packer and equipment. Consequently, the water gathered at the bottom of the borehole and contacted the clay at the borehole wall for the remainder of the week. These events were taken into consideration when simulating Task 3.2 (Table 1). Two steps were undertaken within this task: the first step (Task 3.2a) used the calibrated parameters from Task 3.1b and extended the prediction to 728 days. The second step (Task 3.2b) considered the contact with the formation water that occurred during the overcoring (from 728 to 735 days). Finally, the simulated and measured concentration profiles of aqueous species in porewater, as well as, adsorbed species in the overcored samples were compared.

An overview of the tasks is presented in Table 1.

Table 1: Overview of the Simulation Tasks

Task	Subtask	Description	Remark
Task 1	Diffusion of tracer from borehole without filter and gap		
	Task 1.1	Diffusion of a non-sorbing tracer	Benchmark case
	Task 1.2a	Diffusion of a weakly sorbing tracer (K_d=0.2 L kg^{-1})	Benchmark case
	Task 1.2b	Diffusion of a strongly sorbing tracer (K_d=500.0 L kg^{-1})	Benchmark case
	Task 1.3	Diffusion of Cs^+ with cation exchange	Benchmark case
Task 2.1	Diffusion of tracer from borehole with filter and gap		
	Task 2.1a	Diffusion of a non- sorbing tracer (based on task 1.1)	Benchmark case
	Task 2.1bw	Diffusion of a weakly sorbing tracer, K_d=0.2 L kg^{-1} (based on task 1.2a)	Benchmark case
	Task 2.1bs	Diffusion of a strongly sorbing tracer, K_d=500 L kg^{-1} (based on task 1.2b)	Benchmark case
	Task 2.1c	Diffusion of Cs^+ with cation exchange	Benchmark case
Task 2.2	Simulations of DR-A experiment (Phase I) after initial tracer injection (HTO, I^-, Br^-, $^{85}Sr^{2+}$, Cs^+, $^{60}Co^{2+}$, and Eu^{3+}) up to day 189		
	Task 2.2a	Open gap scenario (without Cs and Eu)	Reference case
	Task 2.2b	Filled gap scenario (without Cs and Eu)	Sensitivity case
	Task 2.2c	Open gap and surface diffusion in filter	Sensitivity case
	Task 2.2d	Simulations of Cs^+ diffusion and retardation	Sensitivity case
	Task 2.2e	Simulations of Eu^{3+}diffusion and retardation	Sensitivity case
	Task 2.2f	Simulation of Cs^+ diffusion and retardation, with parameter optimization using PEST	Sensitivity case
Task 3.1	Simulations of DR-A experiment (Phase II) after increasing the ionic strength of the borehole solution at day 189 of the experiment		
	Task 3.1a	Simulation by direct extension of Task 2.2	Reference case
	Task 3.1b	Sensitivity analysis, modified transport parameters for Phase II	Sensitivity case
Task 3.2	Simulations of DR-A experiment (Phase II) up to day 735 of the experiment and consideration of overcoring data		
	Task 3.2a	Simulation by direct extension of Task 3.1b	Reference case
	Task 3.2b	Simulation of overcoring	Reference case

2. REACTIVE TRANSPORT PROCESSES IN CLAYEY MATERIALS

Clayey materials typically have high total porosity; however, not all of the pore space is available for mass transport processes (Diamond 1970; Bourke et al. 1993; Pearson 1999; García-Gutiérrez et al. 2004; Appelo et al. 2010; Shackelford and Moore 2013). Owing to the extremely small particle size of clay minerals – such as montmorillonite – clayey materials have a large specific surface area, high cation exchange capacity (CEC), and a large fraction of

micropores. When solutes migrate through such materials, processes such as anion exclusion, multicomponent diffusion, and interlayer diffusion may be important. This leads to the species-dependent effective porosity concept, as shown in Figure 1 (Shackelford and Moore 2013).

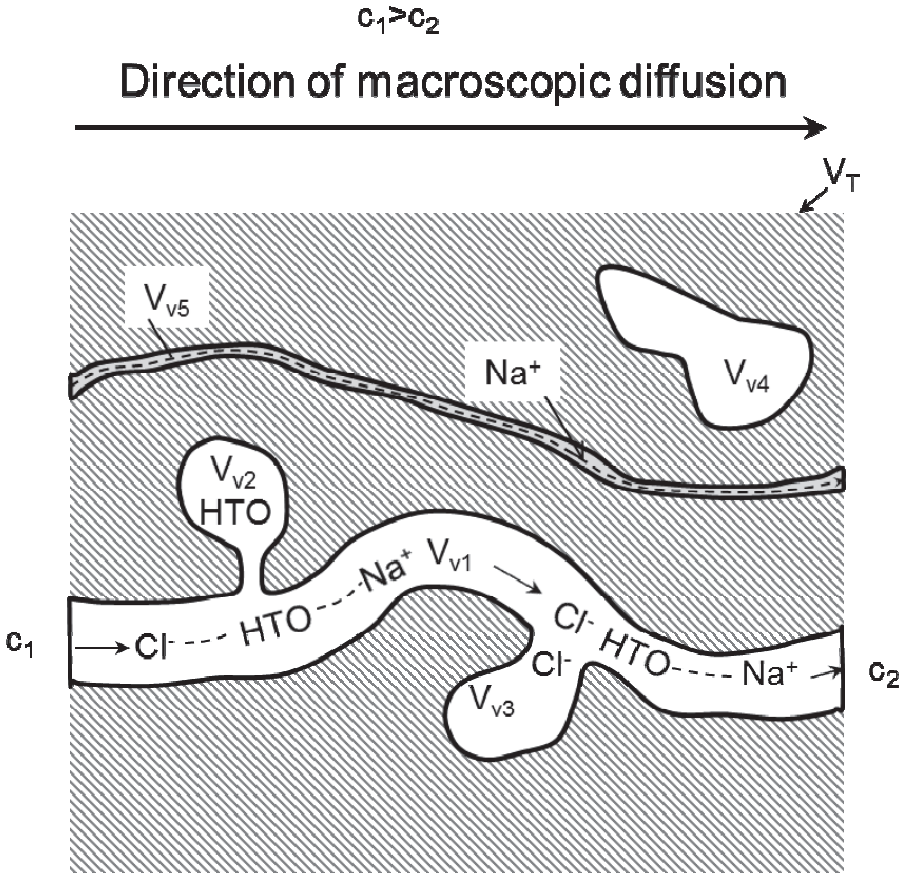

Figure 1: Concept of Species-dependent Porosity in Clayey Material (Modified from Shackelford and Moore 2013)

Based on this concept, the total porosity, ϕ, can be expressed as a function of the different types of pore space:

$$\phi = \frac{V_{v1} + V_{v2} + V_{v3} + V_{v4} + V_{v5}}{V_T} \qquad \text{Equation 2-1}$$

in which, V_T is the total volume, and V_{v1} to V_{v5} are the volumes of different pore types shown in Figure 1. V_{v1} represents the interconnected pore volume, which is available for all species, while V_{v2} and V_{v3} refer to accessible, but non-interconnected (dead end) pores. V_{v2} is available for uncharged species and cations, but not for anions, owing to the anion exclusion effect, while V_{v3} is the dead end pore volume accessible to all species. V_{v4} represents inaccessible or occluded voids, which are unavailable for flow and mass transport. V_{v5} is the volume that is only available to cations, such as the volume associated with the DDL or interlayers.

The effective porosity for uncharged HTO ($\phi_{e,HTO}$) can be expressed as:

$$\phi_{e,HTO} = \frac{V_{v1} + V_{v2} + V_{v3}}{V_T} \qquad \text{Equation 2-2}$$

The effective porosity for a cation such as Na^+ ($\phi_{e,Na}$) can be expressed as:

$$\phi_{e,Na^+} = \frac{V_{v1} + V_{v2} + V_{v3} + V_{v5}}{V_T} \qquad \text{Equation 2-3}$$

The effective porosity for an anion such as Cl^- ($\phi_{e,Cl}$) will be lower because of the well-known anion exclusion effect (Molera et al. 2003; van Loon et al. 2007; Tournassat and Appelo 2011):

$$\phi_{e,Cl^-} = \frac{V_{v1} + V_{v3}}{V_T} \qquad \text{Equation 2-4}$$

Because the charge and radius of individual species are different, the effective porosity for each species in the clayey material may be different. In other words, the effective porosity can be conceptualized as being species-dependent. In a similar manner, the effective tortuosity (τ_e), a measure of the mass transport path, also can be different or species-dependent (Figure 2).

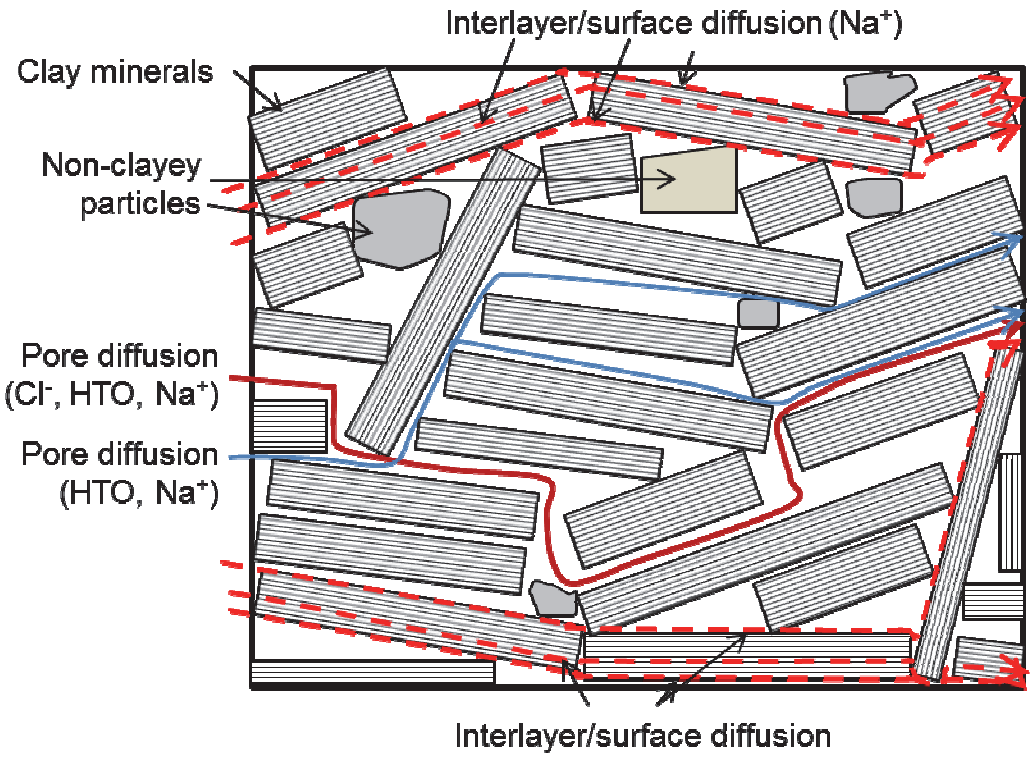

Figure 2: Concept of Species-dependent Tortuosity in Clayey Material

The effective diffusion coefficient D_e can be defined as:

$$D_e = \phi_e \tau_e D_0 = \phi_e D_p \qquad \text{Equation 2-5}$$

in which, D_p is the pore diffusion coefficient, D_0 is the diffusion coefficient of species in free water, and τ_e is the effective tortuosity.

In addition, for cations interlayer/surface diffusion may be important in densely compacted bentonite (Melkior et al. 2009; Glaus et al. 2007; Muurinen et al. 1990). A summary of some experimental results, illustrating the importance of interlayer/surface diffusion, is provided in Table 2. According to Lide (1994), the free phase diffusion coefficient (D_0) of HTO is 2.23×10^{-9} m^2 s^{-1}, which is higher (almost double) than that of Na^+ in free aqueous solution under standard conditions (1.33×10^{-9} m^2 s^{-1}). Melkior et al. (2009) investigated the D_e of Na^+ and HTO in three types of bentonite at a bulk dry density of 1.60 Mg m^{-3}. The measured D_e values of Na^+ in Na-bentonite and Ca-bentonite were higher than those of HTO. With a decrease of the ionic strength of the background solution, the D_e of Na^+ increased, while the D_e of HTO remained relatively unchanged. Other investigators (e.g., Glaus et al. 2007; Muurinen et al. 1990) reported even higher D_e values for Na^+ in densely compacted bentonite with a bulk dry density of 1.80 - 1.90 Mg m^{-3}. In some conditions, experimentally determined effective diffusion coefficients exceed free phase diffusion coefficients for Na^+ (Table 2). This behaviour can only be explained by interlayer/surface diffusion, which is positively correlated with the thickness of the DDL that increases with decreasing ionic strength of the solution (Melkior et al. 2009).

Table 2: Summary of Experimental Effective Diffusion Coefficient (D_e) for Na^+ and HTO in Densely Compacted Bentonite

	Density [Mg m^{-3}]	D_e [x 10^{-11} m^2 s^{-1}]				
		Na^+			HTO	
Ionic strength [M]		**0.1**	**0.01**	**0.001**	**0.1**	**0.01**
Na-bentonite[a]	1.6	7.5	23.0		5.3	5.0
Ca-bentonite[a]	1.6	9.9	12.0		5.1	5.1
Cs-bentonite[a]	1.6	4.8	7.2		9.1	10.8
Na-Montmorillonite[b]	1.9	37.0	140.0			
Na-bentonite[c]	1.8			160.0		
D_0 in infinite dilute aqueous solution[d]			133.4			223.0

[a]Melkior et al. (2009); [b]Glaus et al. (2007); [c]Muurinen et al.(1990); [d]Lide (1994)

3. MODEL FORMULATION AND DEVELOPMENT

MIN3P-THCm (v1.0.129.0) was utilized in this project. This code was developed on the basis of the original MIN3P code (Mayer 1999; Mayer et al. 2002) and further developments included in MIN3P-D (Henderson et al. 2009) and MIN3P-NWMO (Bea et al. 2011). MIN3P-THCm is a general purpose multicomponent reactive transport code for variably saturated porous media. It is characterized by a high degree of flexibility and is applicable to a wide range of

hydrogeological and geochemical problems. Chemical processes included are homogeneous reactions in the aqueous phase, as well as a variety of heterogeneous reactions. The code can simulate groundwater flow, advective-diffusive solute transport, and geochemical reactions under variable density, non-isothermal, and highly saline conditions (Bea et al. 2011; 2012). For the work presented here, the code has been enhanced to include multicomponent diffusion (MCD) and electrochemical migration following the approach of Giambalvo et al. (2002). The MCD module has been further developed into a hybrid multicomponent diffusion (HMD) model that empirically accounts for anion exclusion and cation interlayer/surface diffusion. In addition, multisite ion exchange was implemented to facilitate simulation of ion exchange processes that are believed to occur in the Opalinus Clay formations. The governing equations, with a focus on the new code developments, are detailed below. For additional details on the general code capabilities, the reader is referred to Mayer et al. (2002), Henderson et al. (2009), and Bea et al. (2011).

3.1 GOVERNING EQUATIONS FOR REACTIVE TRANSPORT

Diffusion is commonly simulated as part of the hydrodynamic dispersion term (Bear 1972; Mayer et al. 2002), with the diffusion coefficient and tortuosity of all species assumed equal. However, for clay-rich materials (e.g., compacted bentonite) mass transport may be dominated by more complex phenomena, such as anion exclusion, species-dependent diffusion, and interlayer/surface diffusion. To account for these processes, alternative and enhanced model formulations are required (Shackelford and Moore 2013). Different approaches have been reported in the literature to address the complex phenomena for diffusion in dense clayey materials. These include modified diffusion/adsorption models that account for the volume of the adsorbed phase (Bourg et al. 2003), and diffuse double layer (DDL) models based on the Donnan equilibrium assumption (Wersin et al. 2004; Appelo et al. 2008; Galindez et al. 2011). All formulations include more detailed descriptions of surface reactivity and/or of the mobility of interlayer species.

3.1.1 Hybrid Multicomponent Diffusion

Working toward the goal of simulating complex ion migration phenomena in low permeability rock formations, a multicomponent diffusion (MCD) module was recently implemented in MIN3P-THCm (Rasouli 2015). The revised code enables the simulation of species-dependent diffusion and related electro-chemical migration processes (Rasouli 2015). Further development of a hybrid multicomponent diffusion (HMD) approach combines the multicomponent diffusion module with modified equations for the effective porosity and tortuosity. In essence, correction factors are introduced for the effective porosity and tortuosity for each individual species to capture the net effect of processes such as anion exclusion and interlayer/surface diffusion. While this is an empirical approach that requires calibration of the individual correction factors to experimental results, it does allow for the efficient simulation of several processes that may influence solute migration in low permeability, clay-rich media.

The general equation for diffusion-dominated reactive solute transport in fully saturated porous media can be derived as:

$$\frac{\partial(\phi_e T_j^a)}{\partial t} + \frac{\partial T_j^s}{\partial t} + \nabla \cdot J_j^a = Q_j^{a,a} + Q_j^{a,m} + Q_j^{a,ext} \qquad j = 1, N_c \qquad \text{Equation 3-1}$$

subject to the following definitions:

T_j^a total aqueous component concentration of the j^{th} component in [mol L^{-3} H_2O], defined as:

$$T_j^a = C_j^c + \sum_{i=1}^{N_x} \nu_{ij}^x C_i^x$$

T_j^s total concentration [mol L^{-3} porous medium] of the j^{th} aqueous component on the exchanger;
$Q_j^{a,a}$ internal source and sink terms from intra-aqueous kinetic reactions [mol L^{-3} porous medium T^{-1}];
$Q_j^{a,m}$ source-sink term due to mineral dissolution/precipitation reactions [mol L^{-3} porous medium T^{-1}];
$Q_j^{a,ext}$ external source and sink term [mol L^{-3} porous medium T^{-1}];
C_j^c concentrations of the components as species in solution [mol L^{-3} H_2O];
C_i^x concentrations of complexed species in solution [mol L^{-3} H_2O];
ν_{ij}^x stoichiometric coefficients of the j^{th} component in the i^{th} complexed species;
ϕ_e effective porosity [-];
N_x number of aqueous complexes;
N_c number of aqueous components;
J_j^a total diffusive flux of the j^{th} component [M L^{-3} T^{-1}], described by the extended Nernst-Planck equation (Giambalvo et al. 2002):

$$J_j^a = -\left[\tau_e \phi_e \left(D_{0,j}^c \nabla C_j^c + \sum_i^{N_x} D_{0,i}^x \nu_{ij}^x \nabla C_i^x \right) - T_j^\varepsilon \frac{\sum_l^{N_c} z_l \left(\tau_e \phi_e D_{0,k}^c \nabla C_l^c + \sum_i^{N_x} \nu_{li}^x \tau_e \phi_e D_{0,i}^x \nabla C_i^x \right)}{\sum_k^{N_c} z_k T_k^\varepsilon} \right] \quad \text{Equation 3-2}$$

where:

$D_{0,j}^c$ free diffusion coefficient of the j^{th} component as species in solution [L^2 T^{-1}];
$D_{0,i}^x$ free diffusion coefficient of the i^{th} complexed species in solution [L^2 T^{-1}];
ϕ_e the effective porosity [-];
τ_e effective tortuosity [-];
z_j the charge number [-].

The variables T_j^ε (also applicable for T_k^ε) in Equation 3-2 are defined as (Giambalvo et al. 2002):

$$T_j^{\varepsilon} = \tau_e \phi_e D_{0,j}^c z_j C_j^c + \sum_{i=1}^{N_x} \tau_e \phi_e D_{0,i}^x \nu_{ij}^x C_i^x \qquad \text{Equation 3-3}$$

The formulation outlined in Equation 3-1 through Equation 3-3 assumes that the effective porosity and the effective tortuosity are identical for all species. This formulation can be further extended by defining species-dependent values for these parameters. The revised approach is termed the hybrid multicomponent diffusion (HMD) approach. As discussed above, this approach incorporates the effects of anion exclusion (i.e., leading to a reduction of effective tortuosity and porosity for anionic species) and enhanced cation diffusion through surface and interlayer diffusion (i.e., leading to an increase of effective tortuosity and porosity for cationic species). Applying this approach consistently to Equation 3-1 through Equation 3-3 leads to:

$$\frac{\partial T_j^{\varepsilon,s}}{\partial t} + \frac{\partial T_j^{s}}{\partial t} + \nabla \cdot J_j^a = Q_j^{a,a} + Q_j^{a,m} + Q_j^{a,ext} \qquad j = 1, N_c \qquad \text{Equation 3-4}$$

with

$$T_j^{\varepsilon,s} = f_{\phi,j}^c \phi_e C_j^c + \sum_{i=1}^{N_x} f_{\phi,i}^x \phi_e \nu_{ij}^x C_i^x \qquad \text{Equation 3-5}$$

$$J_j^a = -\left[\begin{array}{l} (f_{\phi,j}^c \phi_e f_{\tau,j}^c \tau_e D_{0.j}^c \nabla C_j^c + \sum_{i=1}^{N_x} f_{\phi,i}^x \phi_e f_{\tau,i}^x \tau_e D_{0,i}^x \nu_{ij}^x \nabla C_i^x) - \\ \qquad T_j^{\varepsilon,d} \dfrac{\sum_{l=1}^{N_c} z_l (f_{\phi,l}^c \phi_e f_{\tau,l}^c \tau_e D_{0,l}^c \nabla C_l^c + \sum_{i=1}^{N_x} f_{\phi,i}^x \phi_e f_{\tau,i}^x \tau_e D_{0,i}^x \nu_{li}^x \nabla C_i^x)}{\sum_{k=1}^{N_c} z_k T_k^{\varepsilon,d}} \end{array} \right] \qquad \text{Equation 3-6}$$

and

$$T_j^{\varepsilon,d} = f_{\tau,j}^c \tau_e f_{\phi,j}^c \phi_e D_{0.j}^c z_j C_j^c + \sum_{i=1}^{N_x} f_{\tau,i}^x \tau_e f_{\phi,i}^x \phi_e D_{0,i}^x \nu_{ij}^x C_i^x \qquad \text{Equation 3-7}$$

Equation 3-5 and Equation 3-7 are species-normalized total concentration terms for the mass storage term and diffusive transport terms, respectively, accounting for species-dependent effective porosities, effective tortuosities and free phase diffusion coefficients. Species-dependent effective tortuosities and porosities are expressed relative to a reference value using the correction factors $f_{\tau,j}^c$, $f_{\phi,j}^c$, $f_{\tau,i}^x$ and $f_{\phi,i}^x$, which are defined as:

$f_{\tau,j}^c$ effective tortuosity correction factor for the j^{th} component as species in solution [-];
$f_{\phi,j}^c$ effective porosity correction factor for the j^{th} component as species in solution [-];
$f_{\tau,i}^x$ effective tortuosity correction factor for the i^{th} complexed species in solution [-];
$f_{\phi,i}^x$ effective porosity correction factor for the i^{th} complexed species in solution [-];

The above equations are expressed in general terms, and apply to a Cartesian coordinate system. For a one-dimensional radial coordinate system, the gradient terms in Equation 3-2 and Equation 3-6 can be replaced with the following term:

$$\nabla^2 C_i^{c,x} = \frac{\partial^2 C_i^{c,x}}{\partial r^2} + \frac{1}{r}\frac{\partial C_i^{c,x}}{\partial r} \qquad \text{Equation 3-8}$$

in which *r* denotes the radial axis.

For simplicity, effective porosity and tortuosity correction factors are only applied to the primary species (i.e., species as components in solution). This approach is justified considering that the primary species of the tracers are dominant (> 90% of the total concentrations in all cases) for the conditions simulated.

3.1.2 Multisite Ion Exchange

Multicomponent cation exchange can be formulated using the Gaines-Thomas activity convention (Appelo and Postma 2003). Written in general form, cation exchange between the cations A_k^d and A_j^d can be expressed as:

$$\frac{A_k^d}{Z_k^d} + \frac{A_{ij}^d \sim (X_i)_{Z_j^d}}{Z_j^d} \leftrightarrow \frac{A_{ik}^d \sim (X_i)_{Z_k^d}}{Z_k^d} + \frac{A_j^d}{Z_j^d}, \qquad i = 1, N_{ex} \qquad \text{Equation 3-9}$$

where Z_k^d and Z_j^d define the charge of the cations A_k^d and A_j^d in [meq mmol^{-1}], while $(Z_k^d)^{-1}$ and $(Z_j^d)^{-1}$ can be interpreted as the stoichiometric coefficients of the reaction equation. X_i is the i^{th} exchange site and N_{ex} is the number of exchange sites. To simplify the description, it is convenient to redefine the ion-exchange species as:

$$A_{ij}^s = A_{ij}^d \sim (X_i)_{Z_j^d} \qquad \text{Equation 3-10}$$

$$\mathrm{A_{ik}^s = A_{ik}^d \sim (X_i)_{Z_k^d}} \qquad \text{Equation 3-11}$$

Substituting Equation 3-10 and Equation 3-11 into Equation 3-9 leads to:

$$\frac{A_k^d}{Z_k^d} + \frac{A_{ij}^s}{Z_j^d} \leftrightarrow \frac{A_{ik}^s}{Z_k^d} + \frac{A_j^d}{Z_j^d}, \qquad i = 1, N_{ex} \qquad \text{Equation 3-12}$$

Equation 3-12 can be rearranged to obtain a stoichiometric relationship with a unit stoichiometric coefficient for the cation exchange species A_{ij}^s:

$$A_{ij}^s \leftrightarrow \frac{Z_j^d}{Z_k^d} A_{ik}^s + A_j^d - \frac{Z_j^d}{Z_k^d} A_k^d, \qquad i = 1, N_{ex} \qquad \text{Equation 3-13}$$

The stoichiometric relationship in Equation 3-13 expresses cation exchange reactions in a general way involving any pair of dissolved cations on the exchange site X_i. This formulation has to be adjusted to facilitate its incorporation into the existing model equations. In this context, ion-exchange reactions will be limited to exchange reactions involving cations, which are defined in the geochemical system as components. Equation 3-13 can be further generalized for any pair of ion-exchange reactions as:

$$A_{ij}^s \leftrightarrow v_{ij}^s A_{ik}^s + \sum_{l=1}^{N_c} v_{ijl}^s A_l^d, \qquad i = 1, N_{ex};\ j = 1, N_i^s \qquad \text{Equation 3-14}$$

where v_{ij}^s is the stoichiometric coefficient of the ion-exchanged species A_{ik}^s in the j^{th} ion exchange reaction on the i^{th}exchange site, which is defined by the ratio of the charge of the two competing cations. The parameters v_{ijl}^s are the stoichiometric coefficients of the components in the j^{th} ion exchange reaction on the i^{th}exchange site. N_i^s is the number of the ion-exchanged species on the i^{th} exchange site. The cations in dissolved form A_l^d can be expressed by the corresponding component concentration. However, because A_{ij}^s cannot be expressed exclusively in terms of aqueous components, but is dependent on the ion-exchanged species, A_{ik}^s , on each cation exchange site, one of the ion-exchanged species has to be chosen to represent A_{ik}^s. Based on the stoichiometry defined in reaction Equation 3-14, the law of mass action can be applied to obtain a relationship that defines the activities of the ion-exchanged species A_{ij}^s in terms of equivalent fractions:

$$\beta_{ij}^s = \left[K_{ij}^s\right]^{-1} [\beta_{ik}^s]^{v_{ij}^s} \prod_{l=1}^{N_c} (\gamma_l^c C_l^c)^{v_{ijl}^s}, \qquad i = 1, N_{ex};\ j = 1, N_i^s \qquad \text{Equation 3-15}$$

where β_{ij}^s and β_{ik}^s are the activities of the ion-exchanged species A_{ij}^s and A_k^s on the i^{th} exchange site in [meq meq^{-1}], and K_{ij}^s refers to the selectivity coefficient for the j^{th} ion-exchange reaction on the i^{th} ion-exchange site. Equation 3-15 only provides an explicit relationship for the calculation of β_{ij}^s if the activity β_{ik}^s of the ion-exchanged species A_{ik}^s is known. Because it is not possible to determine β_{ik}^s using Equation 3-15, an additional relationship is needed. This relationship can be defined as the sum of the activities of all ion-exchanged species on the exchange site X_i, which equals 1 for each type of ion exchange site (Appelo and Postma 2003):

$$1 = \sum_{j=1}^{N_s} \beta_{ij}^s, \qquad i = 1, N_{ex} \qquad \text{Equation 3-16}$$

Equation 3-15 and Equation 3-16 constitute the set of equations defining the ion-exchange sub-problem for the multisite cation exchange model.

3.2 NUMERICAL IMPLEMENTATION AND SOLUTION STRATEGY

The governing equations are implemented using a finite volume technique for spatial discretization and implicit time weighting for the temporal discretization. The reactive transport

equations are solved using the global implicit approach, employing Newton's method for linearization (Mayer et al. 2002; Mayer and MacQuarrie 2010).

3.3 MODEL VERIFICATION

3.3.1 Multicomponent Diffusion

The multicomponent diffusion formulation implemented in MIN3P-THCm (version 1.0.129.0) was verified for several benchmarks (Rasouli 2015) by making comparisons to results obtained using CrunchFlow (Steefel 2008) and PHREEQC (Appelo and Wersin 2007; Appelo et al. 2010).

One of the problems, involving the diffusion of nitric acid into a NaCl solution, is presented here to demonstrate the effect of electromigration and to serve as a verification example. In this example, the electrostatic forces between species in solution result in the electromigration of species present in the background solution (NaCl) in the absence of a concentration gradient. The electrochemical interactions act to slow down the diffusion of the species with higher D_0 values (H^+ and Cl^-) and speed up the diffusion of species with lower D_0 values (NO_3^- and Na^+).

The electromigration problem was simulated in a 1 m long, one-dimensional, horizontal domain, with a dilute NaCl background solution with pH = 6 (Figure 3). Nitric acid was allowed to diffuse into the domain from the left hand side boundary. The model was discretized into 100 cells with $\Delta x = 0.01$ m and the simulations were executed for a period of 100 days. The key model parameters are summarized in Table 3.

Table 3: Selected Model Parameters Used for the Simulation of Nitric Acid Diffusion in Saltwater

Transport Parameters	Symbol	Value	Units
Porosity	ϕ	0.25	-
Molecular diffusion coefficients (D_0)	$D_0(H^+)$	9.311×10^{-9}	$m^2\,s^{-1}$
	$D_0(Na^+)$	1.334×10^{-9}	
	$D_0(Cl^-)$	2.032×10^{-9}	
	$D_0(NO_3^-)$	1.902×10^{-9}	

Figure 3 compares the species concentration profiles at 100 days. The concentration profiles of Na^+ and Cl^- within the domain show differing concentration gradients, although both species were initially present at the same concentration throughout the column (Figure 3). This behavior is caused by the multicomponent diffusion effect. Because H^+ diffuses faster than the anion NO_3^- (e.g., Table 3), a charge imbalance is generated within the domain that, in turn, provides the driving force for the diffusion of Na^+ and Cl^- to maintain charge balance in the solution. Na^+ is displaced from the domain, while Cl^- is drawn into the domain to maintain charge balance. Consequently, the concentration of Cl^- is higher than Na^+. The concentration difference of H^+ and NO_3^- reaches a maximum at a position of x=0.3 m after 100 days, coinciding with the location where the concentrations of Na^+ and Cl^- differ the most (Figure 3). Excellent agreement is obtained between MIN3P-THCm, CrunchFlow and PHREEQC.

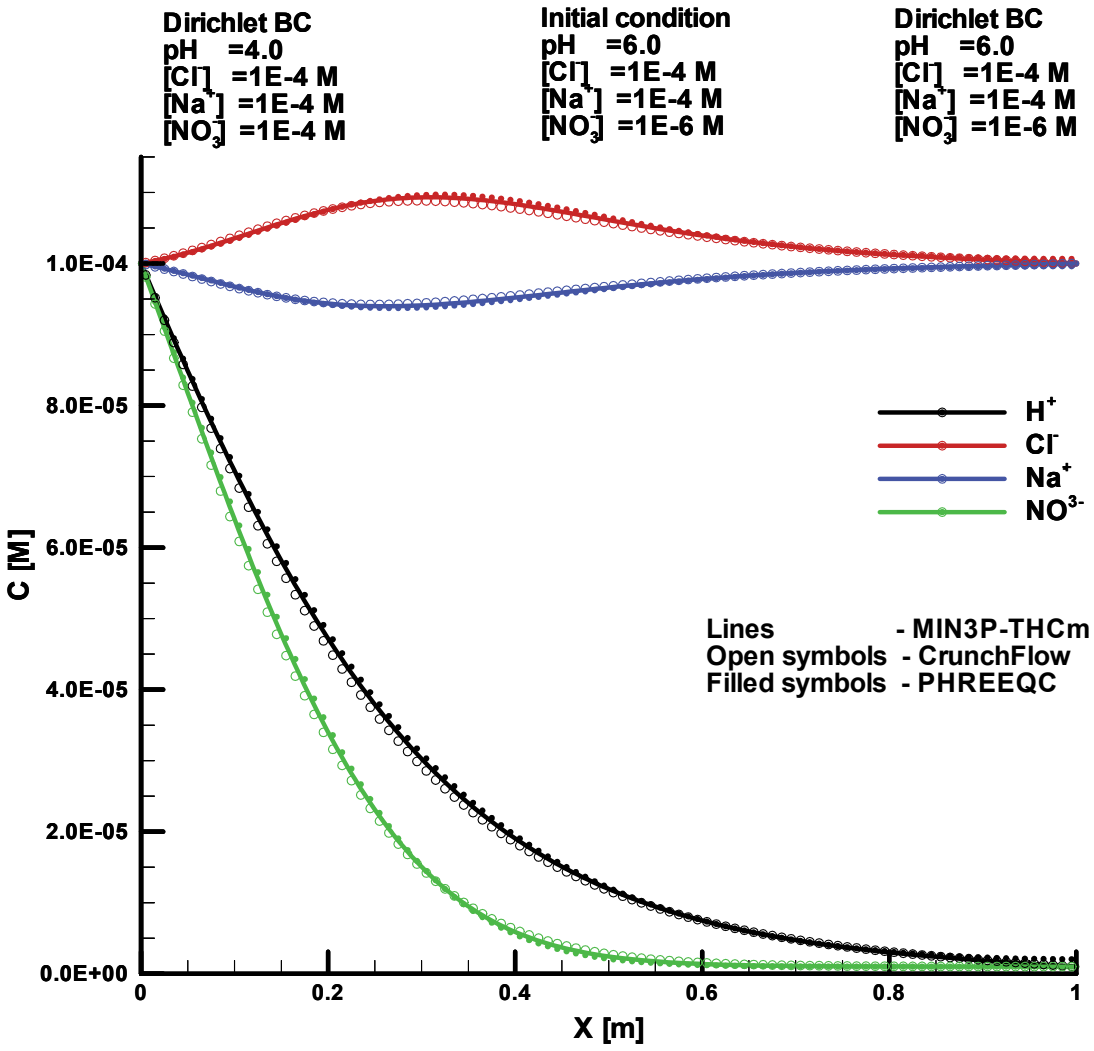

Figure 3: Comparison of Simulated Concentration Profiles and Charge Balance Error (CBE) Obtained from MIN3P–THCm (Lines), CrunchFlow (Open Symbols) and PHREEQC (Filled Symbols) at 100 Days.

3.3.2 Multisite Ion Exchange

3.3.2.1 Definition

This hypothetical benchmark is a multisite ion exchange problem with two material zones subject to steady state flow conditions. The MIN3P-THCm implementation was verified via code inter-comparison with CrunchFlow. CrunchFlow was previously applied for the simulation of Cs^+ migration and retardation in the DI-A2 in-situ diffusion experiment in OPA at the Mont Terri Underground Rock Laboratory (Wersin et al. 2008) and to investigate Cs^+ release mechanisms at the Hanford site (Washington) (Zachara et al. 2002; Steefel et al. 2003; Chang et al. 2011). The simulations described in Task 1.3 and Task 2.1c in Section 5 serve as two additional

verification examples. For all the simulations using MIN3P-THCm and CrunchFlow, the Gaines-Thomas activity convention was applied.

3.3.2.2 Model Set Up

A 1D domain, 16.0 m in length, was discretized into 101 control volumes, yielding a discretization interval of 0.16 m for the interior control volumes and 0.08 m for the control volumes on the boundary. The domain contains two materials: Material I is present from 0-8.0 m, while the remainder of the domain is composed of Material II. For simplicity, both materials have the same hydraulic and transport parameters; porewater with the same initial chemical composition is present throughout the domain. The only difference lies in the fractions of the two ion exchange sites in the materials (see Table 5 below). Boundary conditions for the flow problem consist of a specified hydraulic head of 1.4 m on the left boundary and 0.0 m on the right boundary. A plume with higher concentrations of Zn^{2+}, Pb^{2+} and Ca^{2+} enters the domain from the left boundary and then undergoes multisite ion exchange reactions in response to advective and diffusive transport. The initial condition of the pore water is obtained by determining the exchanger composition on the two exchange sites in equilibrium with the porewater. Consequently, the dominant sorbed species within Material I are Mg-X_2 and Na-X, and Mg-Y_2 and Na-Y within Material II (Figure 4). The chemical compositions of the initial and boundary waters are listed in Table 4.

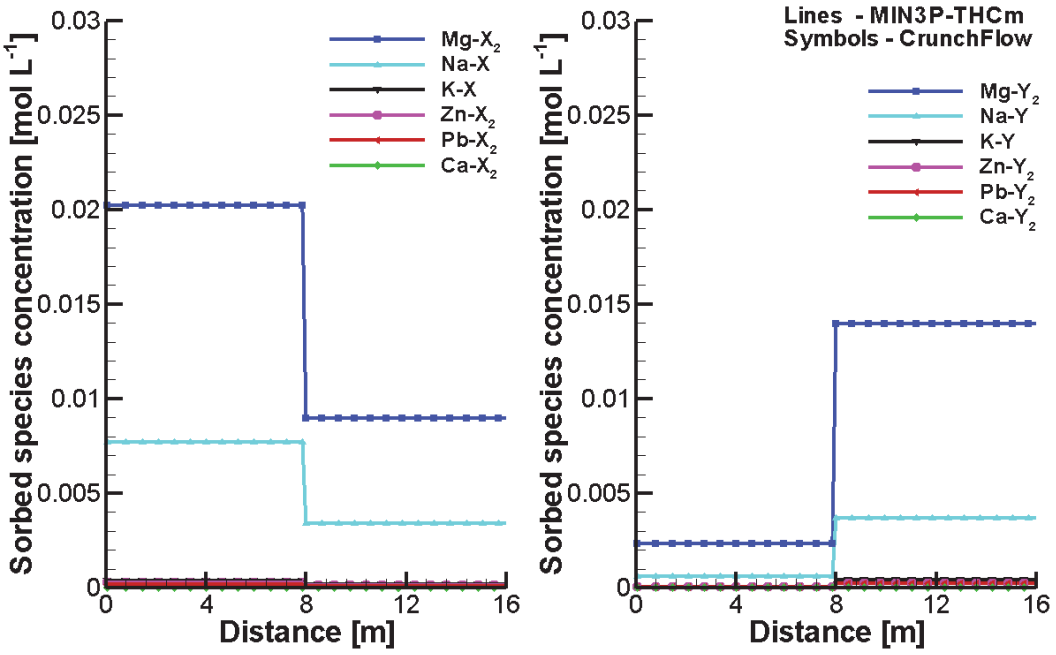

Figure 4: Initial Sorbed Species Concentration Profiles Simulated by MIN3P-THCm (Lines) and CrunchFlow (Symbols); Left Panel – Sorbed Species on Site –X, Right Panel- Sorbed Species on Site –Y

Table 4: Compositions of Initial and Boundary Porewaters

Component	Boundary water	Initial Water	Unit
H^+	3.0	8.0	pH
SO_4^{2-}	3.645×10^{-3}	5.147×10^{-4}	[mol L^{-1}] charge
Zn^{2+}	10^{-3}	10^{-7}	[mol L^{-1}]
Pb^{2+}	10^{-3}	10^{-7}	[mol L^{-1}]
Ca^{2+}	10^{-3}	10^{-10}	[mol L^{-1}]
Mg^{2+}	10^{-10}	10^{-5}	[mol L^{-1}]
K^+	10^{-10}	10^{-5}	[mol L^{-1}]
Na^+	10^{-10}	10^{-3}	[mol L^{-1}]

3.3.2.3 Parameters

The physical parameters (material properties), and the parameters for the multisite ion exchange reactions are summarized in Table 5.

Table 5: Physical and Chemical Parameters for Benchmark

Parameter	Symbol	Value	Unit
Length of domain	L	16.0	[m]
Porosity	ϕ	0.25	[-]
Hydraulic conductivity	K_{zz}	$1.0\text{x}10^{-3}$	[m s^{-1}]
Free phase diffusion coefficient	D_0	$1.0\text{x}10^{-9}$	[m^2 s^{-1}]
Longitudinal dispersivity	α_l	0.01	[m]
Soil bulk density	ρ_d	1.875	[g cm^{-3}]
Cation Exchange Capacity (CEC)	CEC	0.733	[meq $(100g)^{-1}$ solid]
CEC fraction of site –X in material I	$F\text{-}X_1$	90%	[-]
CEC fraction of site –Y in material I	$F\text{-}Y_1$	10%	[-]
CEC fraction of site –X in material II	$F\text{-}X_2$	40%	[-]
CEC fraction of site –Y in material II	$F\text{-}Y_2$	60%	[-]

The ion exchange reactions for both sites ‘-X’ and ‘-Y’ are listed in Table 6. Exchange coefficients for the ‘–Y’ sites were assumed to be 50% larger than for the ‘–X’ sites, to provide a testing platform for the multisite ion exchange model.

Table 6: Ion Exchange Reactions Used in the Verification Example

	Cation exchange reactions	Selectivity coefficients (log K_c)
1	$2Na\text{-}X + Mg^{2+} \rightleftharpoons Mg\text{-}X_2 + 2Na^+$	0.6
2	$Na\text{-}X + K^+ \rightleftharpoons K\text{-}X + Na^+$	0.7
3	$2Na\text{-}X + Zn^{2+} \rightleftharpoons Zn\text{-}X_2 + 2Na^+$	0.8
4	$2Na\text{-}X + Pb^{2+} \rightleftharpoons Pb\text{-}X_2 + 2Na^+$	1.0458
5	$2Na\text{-}X + Ca^{2+} \rightleftharpoons Ca\text{-}X_2 + 2Na^+$	0.8
6	$Na\text{-}X + Na^+ \rightleftharpoons Na\text{-}X + Na^+$	0.0
7	$2Na\text{-}Y + Mg^{2+} \rightleftharpoons Mg\text{-}Y_2 + 2Na^+$	0.9
8	$Na\text{-}Y + K^+ \rightleftharpoons K\text{-}Y + Na^+$	1.05
9	$2Na\text{-}Y + Zn^{2+} \rightleftharpoons Zn\text{-}Y_2 + 2Na^+$	1.2
10	$2Na\text{-}Y + Pb^{2+} \rightleftharpoons Pb\text{-}Y_2 + 2Na^+$	1.5687
11	$2Na\text{-}Y + Ca^{2+} \rightleftharpoons Ca\text{-}Y_2 + 2Na^+$	1.2
12	$Na\text{-}Y + Na^+ \rightleftharpoons Na\text{-}Y + Na^+$	0.0

3.3.2.4 Results

Due to the ingress of water with higher concentrations of Zn^{2+}, Pb^{2+} and Ca^{2+}, the Mg^{2+} and Na^+ ions become displaced from the exchange sites, resulting in a decrease of the exchanged species concentrations $Mg\text{-}X_2$, $Mg\text{-}Y_2$, Na-X and Na-Y, and an increase of $Zn\text{-}X_2$, $Zn\text{-}Y_2$, $Pb\text{-}X_2$, $Pb\text{-}Y_2$, $Ca\text{-}X_2$ and $Ca\text{-}Y_2$ (Figure 5, Figure 6). Displaced Mg^{2+} and Na^+ are thus transported downgradient. Owing to the stronger selectivity of both ion exchange sites for Mg when compared to Na, Mg is displacing Na from both '–X' and '–Y' sites. Breakthrough curves of total aqueous component concentrations, pH, and concentrations of the sorbed species at the outflow are depicted in Figure **7**. The simulated results obtained by MIN3P-THCm are in excellent agreement with the results simulated by CrunchFlow. It demonstrates that the multisite ion exchange model was implemented successfully into MIN3P-THCm.

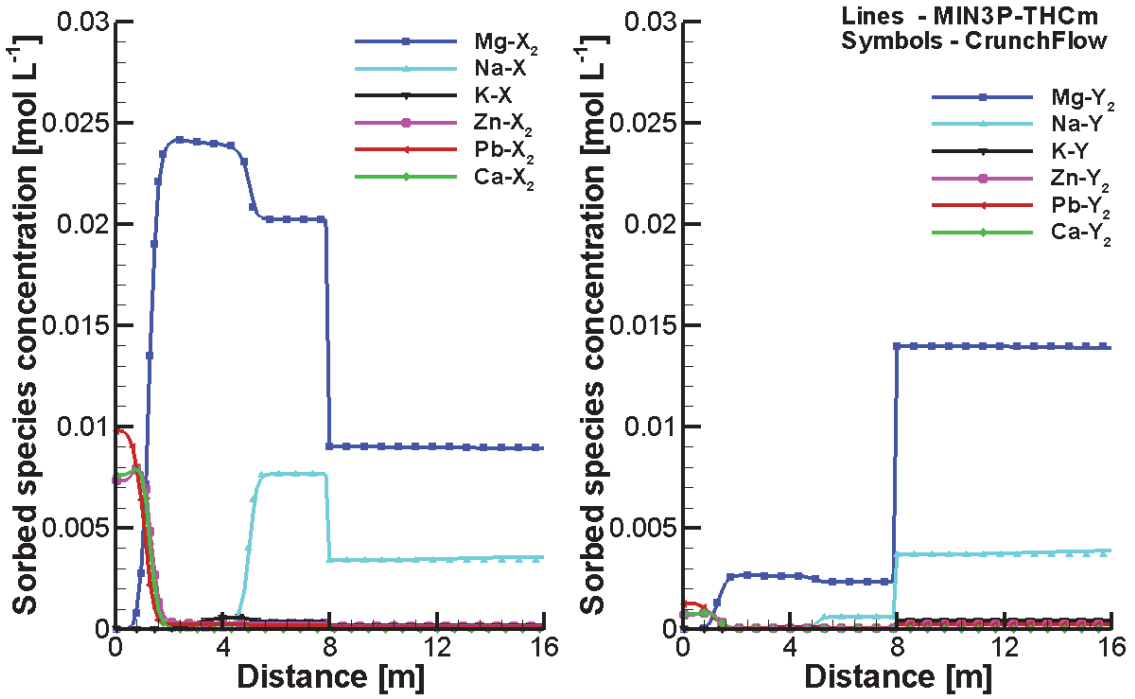

Figure 5: Comparison of Sorbed Species Concentration Profiles at 10 Hours Simulated by MIN3P-THCm (Lines) and CrunchFlow (Symbols); Left – Sorbed Species on Site –X, Right - Sorbed Species on Site –Y

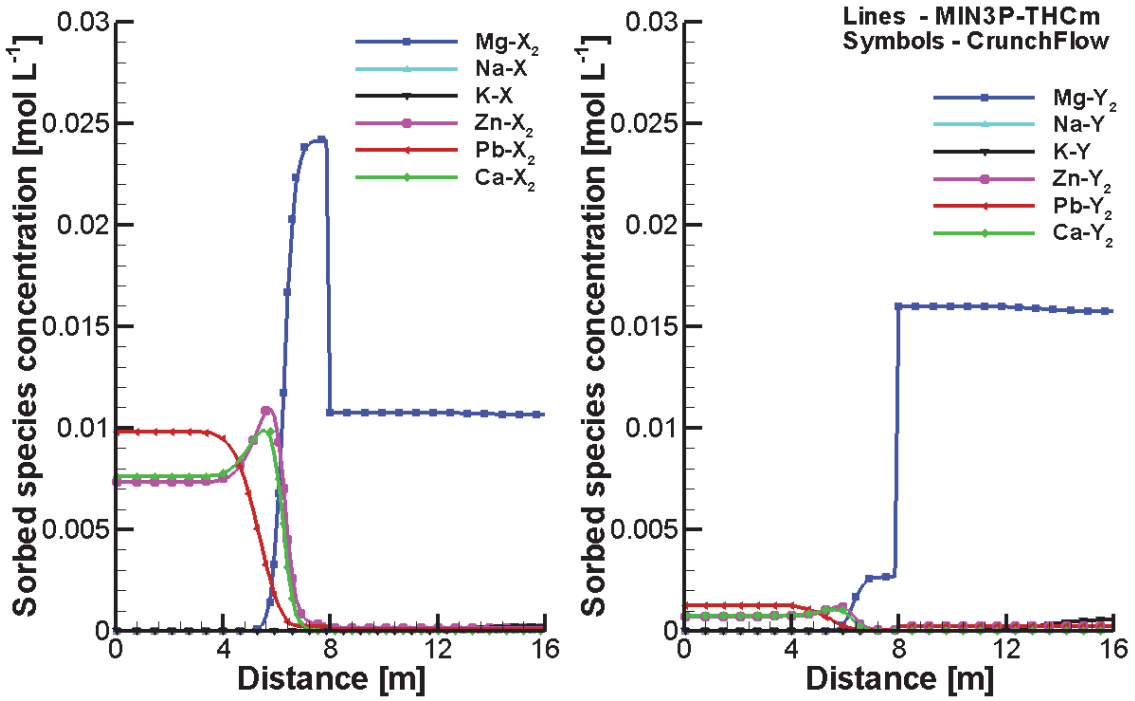

Figure 6: Comparison of Sorbed Species Concentration Profiles at 50 Hours Simulated by MIN3P-THCm (Lines) and CrunchFlow (Symbols); Left – Sorbed Species on Site –X, Right - Sorbed Species on Site –Y

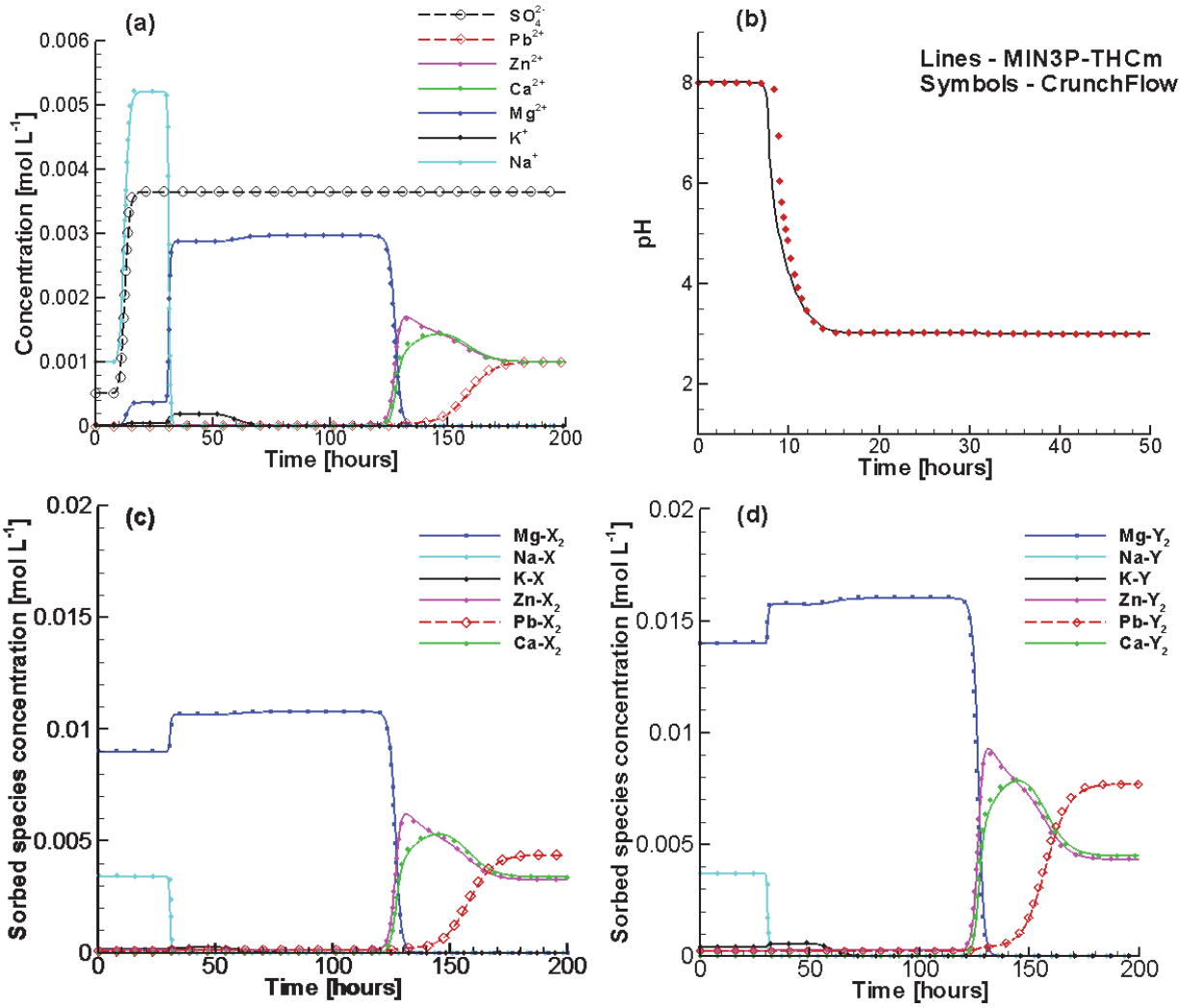

Figure 7: Comparison of Breakthrough Curves at the Outflow Boundary Calculated by MIN3P-THCm (Lines) and CrunchFlow (Symbols): (a) Total Concentrations of Components in the Aqueous Phase, (b) pH, (c) Sorbed Concentrations on Site –X, (d) Sorbed Concentrations on Site –Y

4. CONCEPTUAL MODEL AND KEY PARAMETERS FOR SIMULATIONS OF THE DR-A EXPERIMENT

4.1 MODEL SETUP

The simulations for the DR-A tasks were based on the in-situ diffusion experiment described in Soler (2010) and Fierz and Rösli (2012) (Figure 8). The experiment was undertaken by injecting tracers into the borehole, followed by measurement of the tracer concentration time curve in the solution circulating through the borehole circulation chamber (Fierz and Rösli 2012).

To ensure measurement of pure diffusion conditions, the porewater pressure was automatically adjusted, and the flow rate was monitored until no net flux was observed, before the tracer diffusion experiment began (Fierz and Rösli 2012). The diffusion of the tracers from the injection solution into the surrounding media can be represented by a 1D axial symmetric model, as shown in Figure 9.

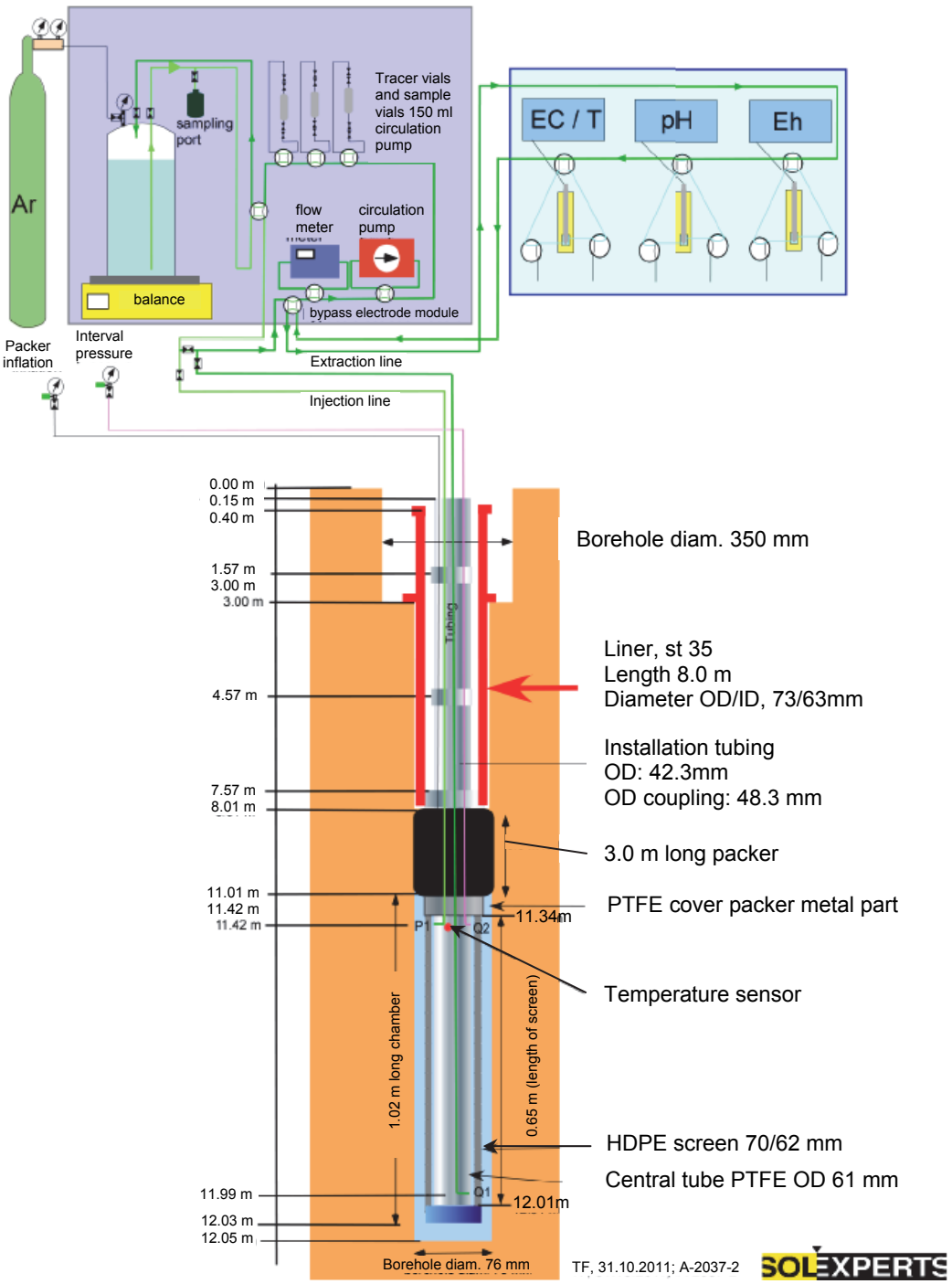

Figure 8: Schematic Depiction of the Mont Terri DR-A in Situ Diffusion and Retention Experiment (Fierz and Rösli 2012)

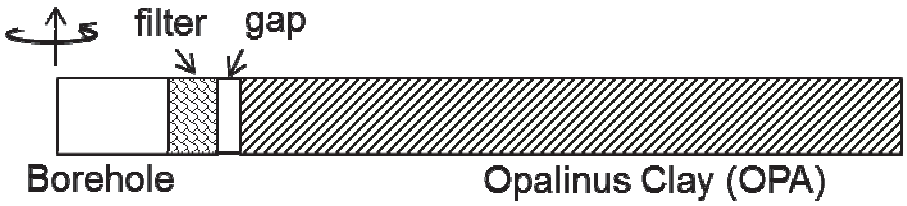

Figure 9: Schematic Diagram of the Simulation Domain Representing the Experimental Set-up Including the Inner Borehole (Radius= 3.1 cm) that Contains the Tracers in Solution, Filter (4 mm in Thickness), Gap (3 mm in Thickness), and OPA up to a Radius of 61.5 cm. The Thickness is h = 1.04 m. A Radial Coordinate System was Used for the Simulations

It is important to note that the OPA at Mont Terri has a dip angle of 30 – 35˚ (averaging 32.5˚) (NAGRA 2012). Due to the anisotropic diffusion properties of the layered clay material, the measured diffusion coefficient parallel to the bedding is higher than that perpendicular to the bedding (Samper et al. 2006). As the borehole for the DR-A experiment is oriented vertically (Fierz and Rösli 2012), the heterogeneous diffusion effect can be considered for the simplified 1D model by modifying the geometry to account for the equivalent solute volume, as depicted in Figure 10 and Table 7. r'_{iBH} is the equivalent radius of a circle with the same circumference as an oval with a = 4.56 cm and b= 3.8 cm, representative of the dip angle. This approach was used by all participating modelling groups.

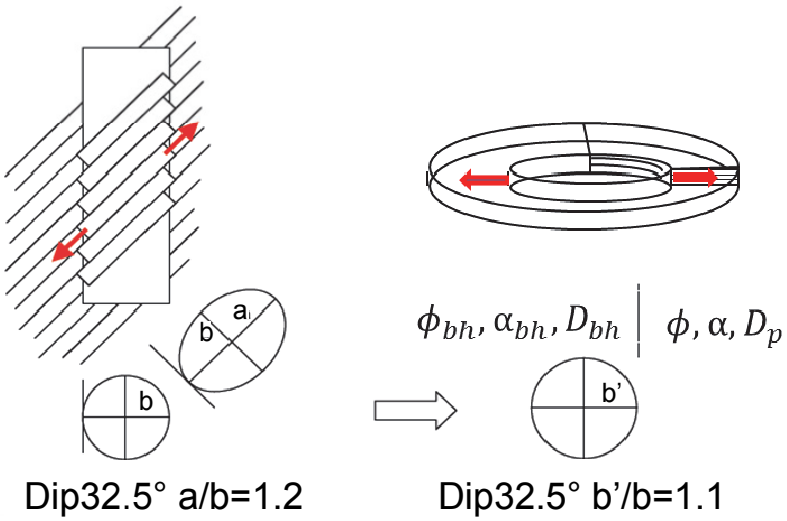

Figure 10: Conceptual Model of Coordinate Transformation (Gimmi et al. 2012)

Based on this transformation, the equivalent outer radius of each segment in the borehole (i.e., r'_{iBH} for circulation chamber, r'_F for filter, and r'_{Gap} for gap) as well as the equivalent borehole capacity (α') can be calculated for the cases including a filter and gap (Table 7). In MIN3P-THCm, the borehole capacity is described by an effective porosity that represents the total

tracer mass in the circulation chamber and tracer circulation system. Physically, α' is equivalent to the ratio between the total circulation solution volume and the volume of the circulation chamber.

Table 7: Calculated Equivalent Outer Radius of Circulation Chamber (r'_{iBH}), Filter (r'_F), and Gap (r'_{Gap}) and Borehole Capacity of the Circulation Chamber (α')

Option	r_{iBH} [m]	r'_{iBH} [m]	r'_F [m]	r'_{Gap} [m]	α' [-]
Task 1- no filter, no gap	0.038	0.0416	-	-	2.374
Task 2 & 3 – with filter and gap	0.031	0.0339	0.0383	0.0416	3.567

r_{iBH} – actual radius of the circulation chamber

4.2 IN-SITU DIFFUSION EXPERIMENT

The in-situ diffusion experiment was performed in two phases. For Phase I, seven tracers (HTO, Cs^+, Eu^{3+}, $^{85}Sr^{2+}$, $^{60}Co^{2+}$, I^- and Br^-) were added to a tank with synthetic Opalinus porewater (Table 8) and injected into the test interval through the circulation system. The concentrations of all tracers were measured at designated times. The measured results, after making any necessary corrections for decay, are listed in Table 9. The concentrations of major ions were measured at the beginning of the experiment and at 168.8 days only, because they were in equilibrium with the OPA and thus expected to be unchanged. These concentrations are presented in Table 11.

Table 8: Composition of the Synthetic OPA Porewater Used in the DR-A Diffusion and Sorption Experiment - Phase I (van Loon et al. 2003)

Element	Total concentration [mol L^{-1}]
Na^+	2.40×10^{-01}
K^+	1.60×10^{-03}
Mg^{2+}	1.70×10^{-02}
Ca^{2+}	2.60×10^{-02}
Sr^{2+}	5.10×10^{-04}
Cl^-	3.00×10^{-01}
SO_4^{2-}	1.40×10^{-02}
CO_3^{2-}/HCO_3^-	4.76×10^{-04}
pH	7.6
Sum of cations	0.328 eq L^{-1}
Sum of anions	0.328 eq L^{-1}
Ionic strength	0.39 mol L^{-1}

Table 9: Measured Tracer Concentrations [mol L^{-1}] during the DR-A In-situ Diffusion Experiment - Phase I (Calculated Based on NAGRA 2012 and Gimmi 2013)

Time	Cs^+	Eu^{3+}	HTO	$^{85}Sr^{2+}$	$^{60}Co^{2+}$	I^-	Br^-
0.0	2.09×10^{-04}	2.11×10^{-07}	1.20×10^{-10}	5.88×10^{-14}	2.18×10^{-13}	1.11×10^{-02}	1.11×10^{-02}
0.1	1.81×10^{-04}	2.11×10^{-07}	1.11×10^{-10}	5.81×10^{-14}	1.92×10^{-13}	1.04×10^{-02}	1.05×10^{-02}
0.3	1.45×10^{-04}	1.38×10^{-07}	1.08×10^{-10}	5.27×10^{-14}	1.55×10^{-13}	1.00×10^{-02}	1.01×10^{-02}
0.9	1.15×10^{-04}	9.21×10^{-08}	1.05×10^{-10}	5.19×10^{-14}	1.23×10^{-13}	1.00×10^{-02}	1.02×10^{-02}
1.2	1.02×10^{-04}	7.24×10^{-08}	1.05×10^{-10}	5.00×10^{-14}	1.10×10^{-13}	9.95×10^{-03}	1.00×10^{-02}
2.0	8.73×10^{-05}	5.26×10^{-08}	1.06×10^{-10}	4.95×10^{-14}	9.04×10^{-14}	9.94×10^{-03}	1.00×10^{-02}
3.0	7.67×10^{-05}	3.95×10^{-08}	1.04×10^{-10}	4.92×10^{-14}	7.92×10^{-14}	9.81×10^{-03}	9.98×10^{-03}
4.0	6.74×10^{-05}	3.29×10^{-08}	1.04×10^{-10}	4.81×10^{-14}	7.04×10^{-14}	9.88×10^{-03}	9.95×10^{-03}
5.0	6.11×10^{-05}	3.29×10^{-08}	1.03×10^{-10}	4.68×10^{-14}	6.23×10^{-14}	9.79×10^{-03}	9.90×10^{-03}
7.0	5.08×10^{-05}	2.63×10^{-08}	1.01×10^{-10}	4.70×10^{-14}	5.39×10^{-14}	9.77×10^{-03}	9.87×10^{-03}
10.0	4.27×10^{-05}	1.97×10^{-08}	9.92×10^{-11}	4.40×10^{-14}	4.71×10^{-14}	9.63×10^{-03}	9.71×10^{-03}
14.0	3.52×10^{-05}	1.32×10^{-08}	9.77×10^{-11}	4.25×10^{-14}	3.87×10^{-14}	9.58×10^{-03}	9.66×10^{-03}
21.0	2.84×10^{-05}	u.d.	9.61×10^{-11}	4.01×10^{-14}	2.87×10^{-14}	9.56×10^{-03}	9.65×10^{-03}
29.0	2.20×10^{-05}	u.d.	9.49×10^{-11}	3.76×10^{-14}	2.11×10^{-14}	9.46×10^{-03}	9.55×10^{-03}
43.0	1.74×10^{-05}	u.d.	9.28×10^{-11}	3.49×10^{-14}	1.02×10^{-14}	9.43×10^{-03}	9.50×10^{-03}
63.0	1.28×10^{-05}	u.d.	8.92×10^{-11}	3.14×10^{-14}	7.96×10^{-15}	9.19×10^{-03}	9.24×10^{-03}
85.4	-	u.d.	-	2.93×10^{-14}	u.d.	9.07×10^{-03}	9.05×10^{-03}
113.0	-	u.d.	8.67×10^{-11}	2.77×10^{-14}	-	8.87×10^{-03}	8.94×10^{-03}
168.8	6.66×10^{-06}	u.d.	8.17×10^{-11}	2.37×10^{-14}	-	8.46×10^{-03}	8.69×10^{-03}

- Not measured, u.d. – under detection limit

Table 10: Composition of the Synthetic OPA Porewater Used in the DR-A Diffusion and Sorption Experiment - Phase II

Element	Total concentration [mol L^{-1}]
Na^+	5.00×10^{-01}
K^+	5.60×10^{-01}
Mg^{2+}	1.47×10^{-02}
Ca^{2+}	2.30×10^{-02}
Sr^{2+}	4.49×10^{-04}
Cl^-	1.15
SO_4^{2-}	2.37×10^{-04}
CO_3^{2-}/HCO_3^-	4.76×10^{-04}
pH	7.6
Sum cations	1.14 eq L^{-1}
Sum anions	1.15 eq L^{-1}
Ionic strength	1.18 mol L^{-1}

Phase II of the DR-A in-situ diffusion test was conducted immediately after the first phase, beginning at 189 days, by changing the circulation solution to a solution with much higher concentrations of Cl^-, Na^+ and K^+, and a much lower concentration of SO_4^{2-} (to create a higher ionic strength solution perturbation). A summary of the major ion concentrations, based on the

measured data, is listed in Table 11. A spike of 3.64 Bq/g was also added for $^{85}Sr^{2+}$. All other tracers remained at the same concentrations as measured just before the exchange of the solution. During Phase II, the concentration of the major ions and tracers in the circulation solution were analyzed and these are listed in Table 11 and Table 12, respectively. It should be noted that the initial model calibration was based on data up to 413 days. By November 2014, additional concentration data became available for tracers and major ions covering the time period from 535 days until the overcoring started at 728 days (Table 11 and Table 12).

Table 11: Measured Major Ion Concentrations [mol L^{-1}] in the Circulation Solution during the DR-A In-situ Diffusion Experiment Phase I and II until Overcoring (Calculated Based on NAGRA (2012, 2014) and Gimmi 2013)

Time [days]	Ca^{2+}	Mg^{2+}	Na^{+}	K^{+}	Cl^{-}	SO_4^{2-}	Sr^{2+}
0	2.12×10^{-02}	1.85×10^{-02}	2.56×10^{-01}	1.80×10^{-03}	3.13×10^{-01}	1.45×10^{-02}	5.85×10^{-04}
168.8	1.88×10^{-02}	1.80×10^{-02}	2.59×10^{-01}	1.64×10^{-03}	2.98×10^{-01}	1.37×10^{-02}	5.54×10^{-04}
189.2	2.30×10^{-02}	1.47×10^{-02}	5.05×10^{-01}	5.60×10^{-01}	1.16	2.37×10^{-04}	4.50×10^{-04}
189.3	-	-	5.00×10^{-01}	5.60×10^{-01}	1.15	2.37×10^{-04}	4.50×10^{-04}
189.9	-	-	-	-	-	1.00×10^{-03}	-
190.1	-	-	-	-	-	1.09×10^{-03}	-
190.2	-	-	-	-	-	1.41×10^{-03}	-
190.9	-	-	4.78×10^{-01}	4.83×10^{-01}	1.05	1.49×10^{-03}	5.19×10^{-04}
191.2	2.99×10^{-02}	2.07×10^{-02}	-	-	-	1.58×10^{-03}	-
192.9	2.55×10^{-02}	1.72×10^{-02}	4.92×10^{-01}	4.65×10^{-01}	1.05	1.72×10^{-03}	6.55×10^{-04}
195.9	3.19×10^{-02}	2.14×10^{-02}	-	-	-	1.90×10^{-03}	-
200.0	2.77×10^{-02}	1.88×10^{-02}	4.78×10^{-01}	4.09×10^{-01}	1.02	2.03×10^{-03}	6.54×10^{-04}
204.2	2.84×10^{-02}	1.95×10^{-02}	4.78×10^{-01}	3.96×10^{-01}	1.01	2.20×10^{-03}	6.84×10^{-04}
206.9	-	-	-	-	-	2.35×10^{-03}	-
213.9	2.94×10^{-02}	2.00×10^{-02}	4.78×10^{-01}	3.81×10^{-01}	1.02	2.56×10^{-03}	7.02×10^{-04}
220.8	-	-	-	-	-	2.68×10^{-03}	-
234.8	3.37×10^{-02}	2.51×10^{-02}	5.00×10^{-01}	3.53×10^{-01}	1.01	3.29×10^{-03}	8.16×10^{-04}
291.1	3.94×10^{-02}	2.99×10^{-02}	5.09×10^{-01}	2.92×10^{-01}	9.79×10^{-01}	3.82×10^{-03}	1.15×10^{-03}
322.9	3.54×10^{-02}	2.26×10^{-02}	3.85×10^{-01}	2.74×10^{-01}	1.06	4.82×10^{-03}	9.64×10^{-04}
353.2	3.94×10^{-02}	3.18×10^{-02}	5.13×10^{-01}	2.49×10^{-01}	8.63×10^{-01}	4.02×10^{-03}	1.09×10^{-03}
385.8	3.92×10^{-02}	3.45×10^{-02}	5.31×10^{-01}	2.33×10^{-01}	8.52×10^{-01}	3.95×10^{-03}	1.14×10^{-03}
412.9	4.17×10^{-02}	3.43×10^{-02}	5.05×10^{-01}	2.06×10^{-01}	8.57×10^{-01}	4.65×10^{-03}	1.15×10^{-03}
535.1	4.54×10^{-02}	3.45×10^{-02}	4.52×10^{-01}	1.44×10^{-01}	7.93×10^{-01}	4.89×10^{-03}	1.24×10^{-03}
563.9	4.49×10^{-02}	3.71×10^{-02}	5.26×10^{-01}	1.54×10^{-01}	7.62×10^{-01}	5.02×10^{-03}	1.42×10^{-03}
597.1	4.44×10^{-02}	3.83×10^{-02}	5.00×10^{-01}	1.37×10^{-01}	8.26×10^{-01}	5.29×10^{-03}	1.48×10^{-03}
662.1	4.54×10^{-02}	3.95×10^{-02}	5.22×10^{-01}	1.29×10^{-01}	7.31×10^{-01}	4.98×10^{-03}	1.52×10^{-03}
692.1	4.32×10^{-02}	4.01×10^{-02}	5.31×10^{-01}	1.24×10^{-01}	7.50×10^{-01}	5.26×10^{-03}	1.54×10^{-03}
717.9	4.77×10^{-02}	4.03×10^{-02}	5.18×10^{-01}	1.17×10^{-01}	7.19×10^{-01}	5.12×10^{-03}	1.54×10^{-03}
728.9	4.28×10^{-02}	3.92×10^{-02}	4.87×10^{-01}	1.09×10^{-01}	7.71×10^{-01}	5.01×10^{-03}	1.49×10^{-03}

- Not measured. Note: The major ions were analyzed by Bachema AG (Fierz and Rosli 2012).

Table 12: Measured Tracer Concentrations [mol L^{-1}] in the Circulation Solution during the DR-A In-situ Diffusion Experiment - Phase II until Overcoring (Calculated Based on NAGRA 2012)

Time [days]	Cs^{+}	Eu^{3+}	HTO	$^{85}Sr^{2+}$	$^{60}Co^{2+}$	I^{-}	Br^{-}
189.2	6.37×10^{-06}	n.d	-	-	-	-	-
189.3	6.23×10^{-06}	n.d	-	-	-	-	-
189.3	-	-	7.80×10^{-11}	5.42×10^{-14}	n.d	8.60×10^{-03}	8.86×10^{-03}
189.9	7.75×10^{-06}	n.d	-	-	-	-	-
189.8	-	-	7.93×10^{-11}	5.08×10^{-14}	n.d	8.63×10^{-03}	8.91×10^{-03}
190.1	1.05×10^{-05}	n.d	7.72×10^{-11}	4.99×10^{-14}	n.d	8.50×10^{-03}	8.87×10^{-03}
190.2	1.48×10^{-05}	n.d	-	-	-	-	-
190.3	-	-	7.80×10^{-11}	4.89×10^{-14}	n.d	8.48×10^{-03}	8.80×10^{-03}
190.9	1.78×10^{-05}	n.d	-	-	-	-	-
190.8	-	-	8.04×10^{-11}	4.82×10^{-14}	n.d	8.65×10^{-03}	8.87×10^{-03}
191.2	1.86×10^{-05}	n.d	-	-	-	-	-
191.3	-	-	7.82×10^{-11}	4.81×10^{-14}	n.d	8.68×10^{-03}	8.88×10^{-03}
192.9	2.42×10^{-05}	n.d	-	-	-	-	-
192.9	-	-	7.73×10^{-11}	4.78×10^{-14}	n.d	8.68×10^{-03}	8.86×10^{-03}
195.9	2.81×10^{-05}	9.13×10^{-08}	7.64×10^{-11}	4.64×10^{-14}	n.d	8.50×10^{-03}	8.90×10^{-03}
199.9	-	-	7.54×10^{-11}	4.69×10^{-14}	n.d	8.60×10^{-03}	8.63×10^{-03}
200.0	3.18×10^{-05}	n.d	-	-	-	-	-
204.2	3.44×10^{-05}	n.d	7.67×10^{-11}	4.62×10^{-14}	n.d	-	-
206.9	3.53×10^{-05}	n.d	-	-	-	-	-
206.9	-	-	7.57×10^{-11}	4.71×10^{-14}	n.d	8.71×10^{-03}	8.72×10^{-03}
213.9	3.37×10^{-05}	n.d	-	-	-	-	-
214.0	-	-	7.43×10^{-11}	4.70×10^{-14}	n.d	7.89×10^{-03}	8.61×10^{-03}
220.8	3.35×10^{-05}	n.d	-	-	-	-	-
221.2	-	-	7.29×10^{-11}	4.66×10^{-14}	n.d	8.08×10^{-03}	8.74×10^{-03}
234.8	3.03×10^{-05}	n.d	-	-	-	-	-
234.9	-	-	7.05×10^{-11}	4.43×10^{-14}	n.d	7.87×10^{-03}	8.31×10^{-03}
291.1	2.70×10^{-05}	n.d	6.73×10^{-11}	4.12×10^{-14}	n.d	8.02×10^{-03}	8.16×10^{-03}
322.9	2.30×10^{-05}	n.d	6.13×10^{-11}	4.12×10^{-14}	n.d	7.72×10^{-03}	7.84×10^{-03}
353.1	-	-	6.00×10^{-11}	3.96×10^{-14}	n.d	7.27×10^{-03}	7.63×10^{-03}
353.2	2.06×10^{-05}	n.d	-	-	-	-	-
385.8	1.85×10^{-05}	n.d	5.81×10^{-11}	3.53×10^{-14}	n.d	7.00×10^{-03}	7.27×10^{-03}
412.9	1.57×10^{-05}	n.d	5.67×10^{-11}	3.70×10^{-14}	n.d	6.79×10^{-03}	7.39×10^{-03}
535.1	1.10×10^{-05}	n.d	5.03×10^{-11}	3.75×10^{-14}	n.d	6.27×10^{-03}	7.56×10^{-03}
563.9	1.05×10^{-05}	n.d	4.82×10^{-11}	3.18×10^{-14}	n.d	6.05×10^{-03}	7.51×10^{-03}
597.1	1.06×10^{-05}	n.d	4.75×10^{-11}	2.99×10^{-14}	n.d	6.72×10^{-03}	6.80×10^{-03}
662.1	-	n.d	4.48×10^{-11}	3.83×10^{-14}	n.d	5.96×10^{-03}	6.34×10^{-03}
692.1	7.60×10^{-06}	n.d	4.32×10^{-11}	2.87×10^{-14}	n.d	5.85×10^{-03}	6.00×10^{-03}
717.9	7.15×10^{-06}	n.d	4.20×10^{-11}	2.82×10^{-14}	n.d	6.15×10^{-03}	6.41×10^{-03}
728.9	7.28×10^{-06}	-	-	-	-	6.39×10^{-03}	6.26×10^{-03}

- Not measured, n.d. - not detected. Note: The tracers Cs^{+} and Eu^{3+} were analyzed by Bachema AG. Other elements were analyzed by PSI (Fierz and Rosli 2012).

Overcoring was used to obtain OPA samples for chemical analysis. Samples were extracted at depths ranging from 11.55 m to 11.85 m, corresponding to the depth interval where the filter was located. The samples were labeled based on depth with additional identifiers A, B and D. The overcored samples were analyzed by PSI (samples labeled "A" and "D") and University of Bern (Switzerland) (samples labeled "B"). Chemical analyses of rock samples provided concentration profiles of dissolved tracers and ions in the Opalinus Clay (Figure 11 - Figure 13), as well as concentrations of the sorbed species (Figure 14 and Figure 15), perpendicular to the borehole. Major ions and the tracers $^{60}Co^{2+}$and HTO in porewater were analyzed through aqueous extraction. The sorbed species were analyzed using extractions in nickel-ethylenediamine (Ni-en) solutions prepared on site (NAGRA 2014). Ni-en is a powerful, highly selective complex that displaces all exchangeable cations from the clay minerals into solution (Maes and Cremers 1986; Baeyens and Bradbury 1994). The concentrations of sorbed species were calculated based on the concentrations obtained by Ni-en extracts by subtracting the porewater concentrations. Using this method, the concentrations of tracers and major ions sorbed onto the overcored samples (Co-X_2, Sr-X_2, Na-X, Ca-X_2, K-X, Mg-X_2) were quantified. In addition, the method also allowed for the quantification of adsorbed concentrations of other elements (e.g. Cu, Mn, Cr, Mo, and Zn) down to concentrations of 0.002 meq $(100g)^{-1}$. For elements not included in the simulations, the measured data are not included in this report, but can be found in NAGRA (2014). Unfortunately, analysis of the overcored samples did not produce data for the tracers Cs^{+} and Sr^{2+} in the porewater, or adsorbed Cs.

The concentration profiles of all aqueous species consistently showed a signal of back diffusion from the OPA towards the borehole (Figure 11 - Figure 13). Back diffusion was caused by the presence of porewater in the space above the packer, which could not be removed before the overcoring. Consequently, this water gathered at the bottom of the borehole after retrieving the equipment. Most probably, this water was original formation water as listed in Table 8 (NAGRA 2014). Water of this composition was used to simulate the impact of the overcoring process on the concentration distributions.

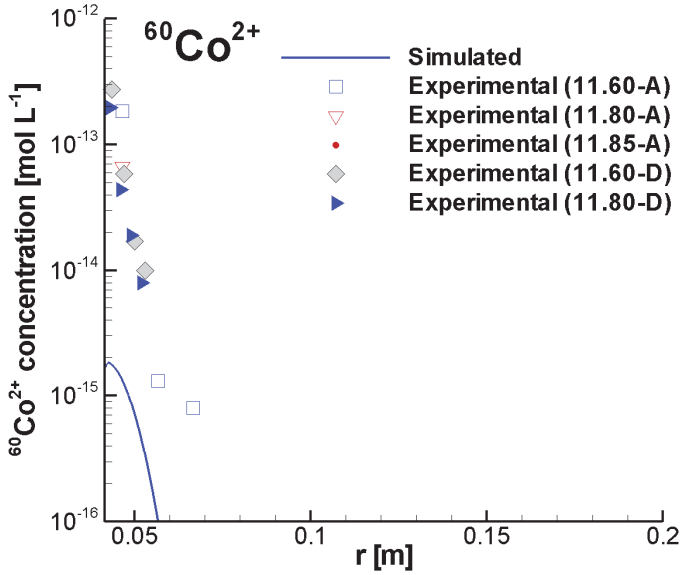

Figure 11: Profiles of $^{60}Co^{2+}$ Concentration Measured in the Porewater of the Overcored Opalinus Clay Samples (NAGRA 2014). The Labels in the Legend (e.g. 11.60-A) Represent the Sample Number

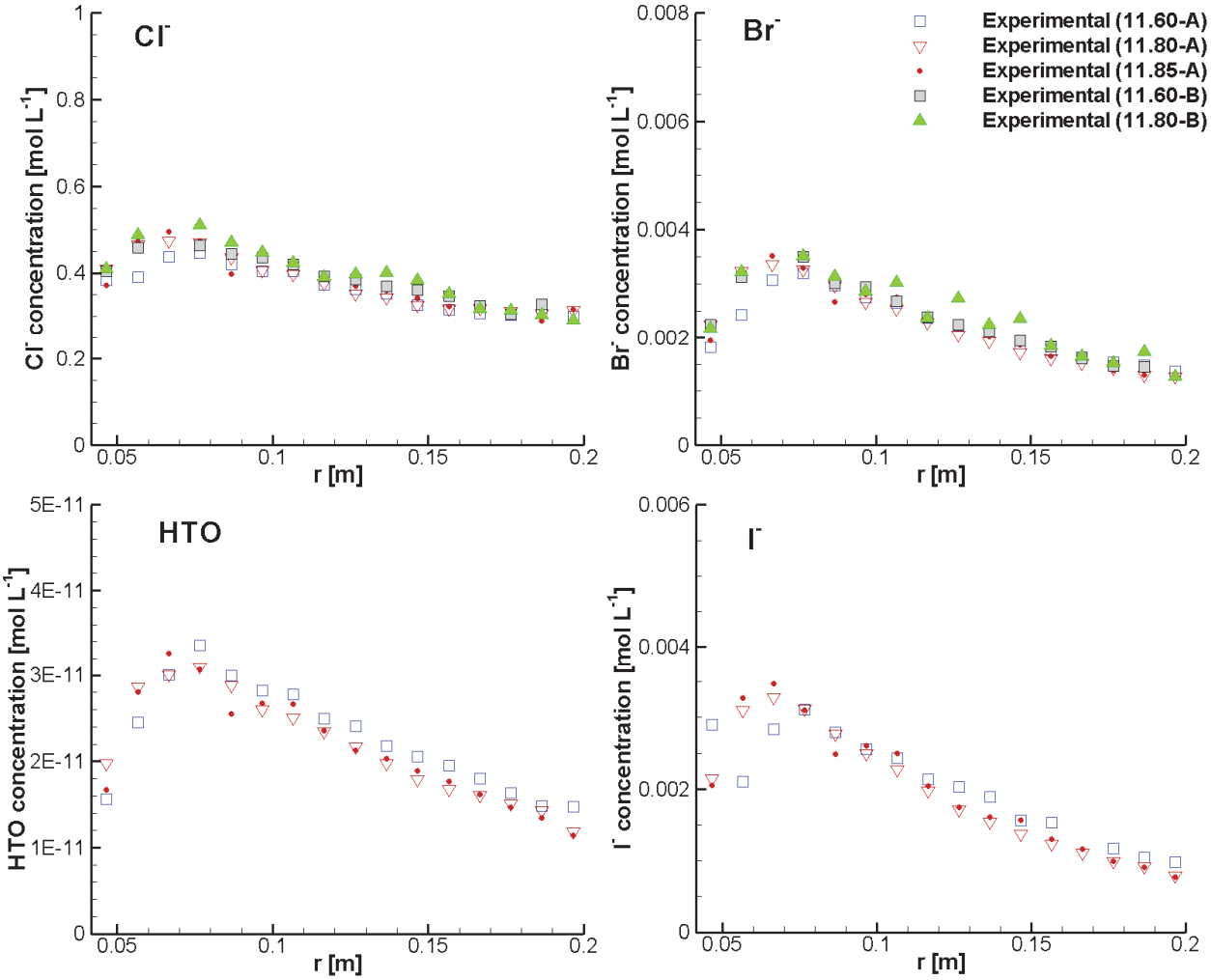

Figure 12: Profiles of Total Concentrations of Cl^-, Br^-, HTO and I^- Measured in the Porewater of the Overcored Opalinus Clay Samples (NAGRA 2014). The Labels in the Legend (e.g. 11.60-A) Represent the Sample Number

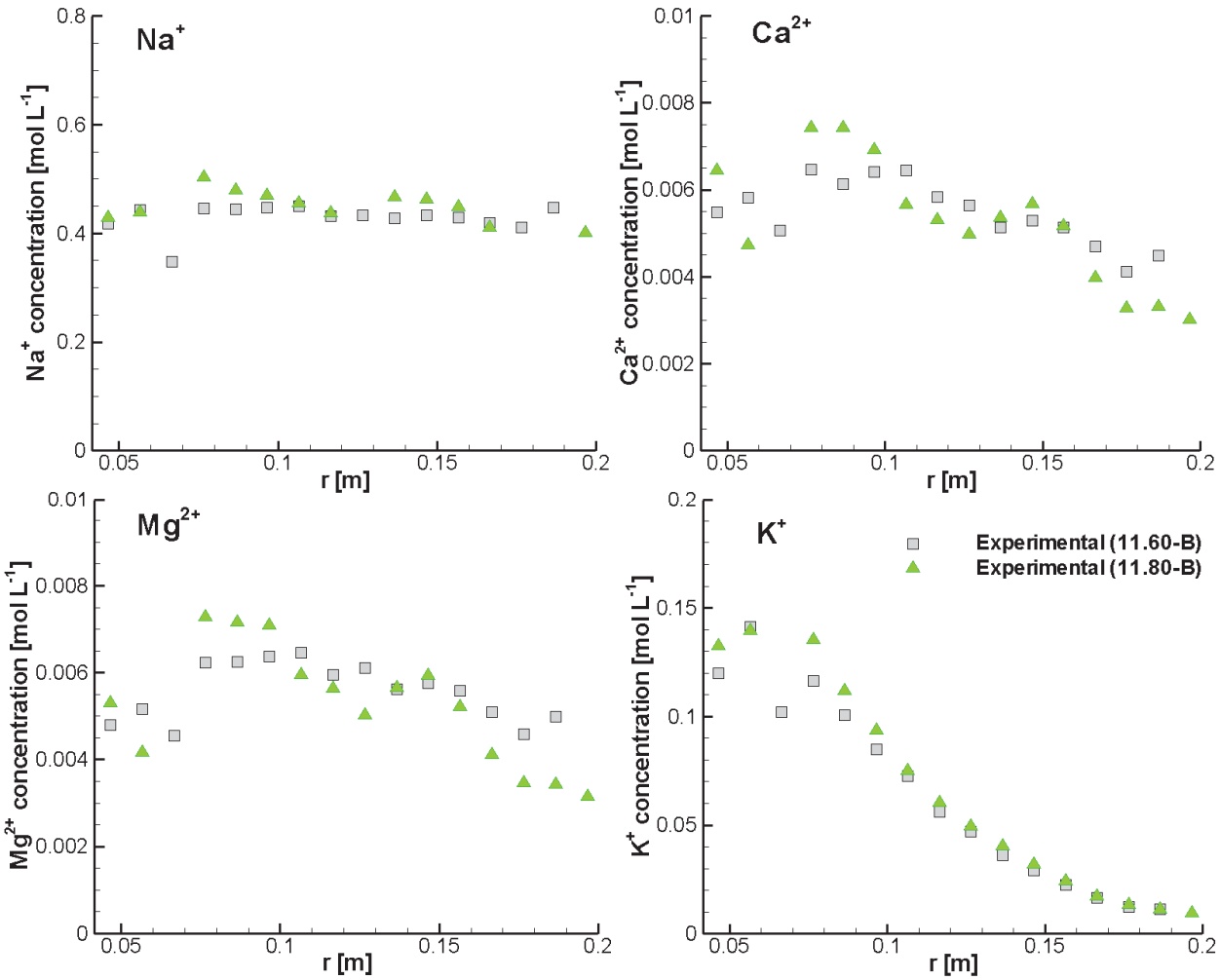

Figure 13: Profiles of Total Concentrations of Na^+, Ca^{2+}, Mg^{2+} and K^+ Measured in the Overcored Opalinus Clay Porewater (NAGRA 2014). The Labels in the Legend (e.g. 11.60-B) Represent the Sample Number

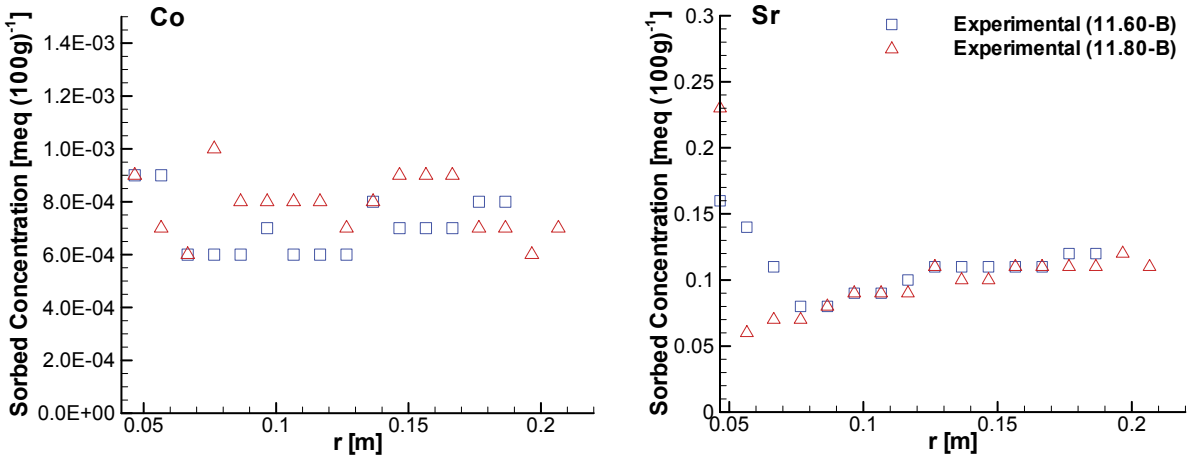

Figure 14: Profiles of Total Concentrations of Adsorbed Species Co (left) and Sr (right) Determined in the Overcored Opalinus Clay Samples (NAGRA 2014). The Labels in the Legend (e.g. 11.60-B) Represent the Sample Number.

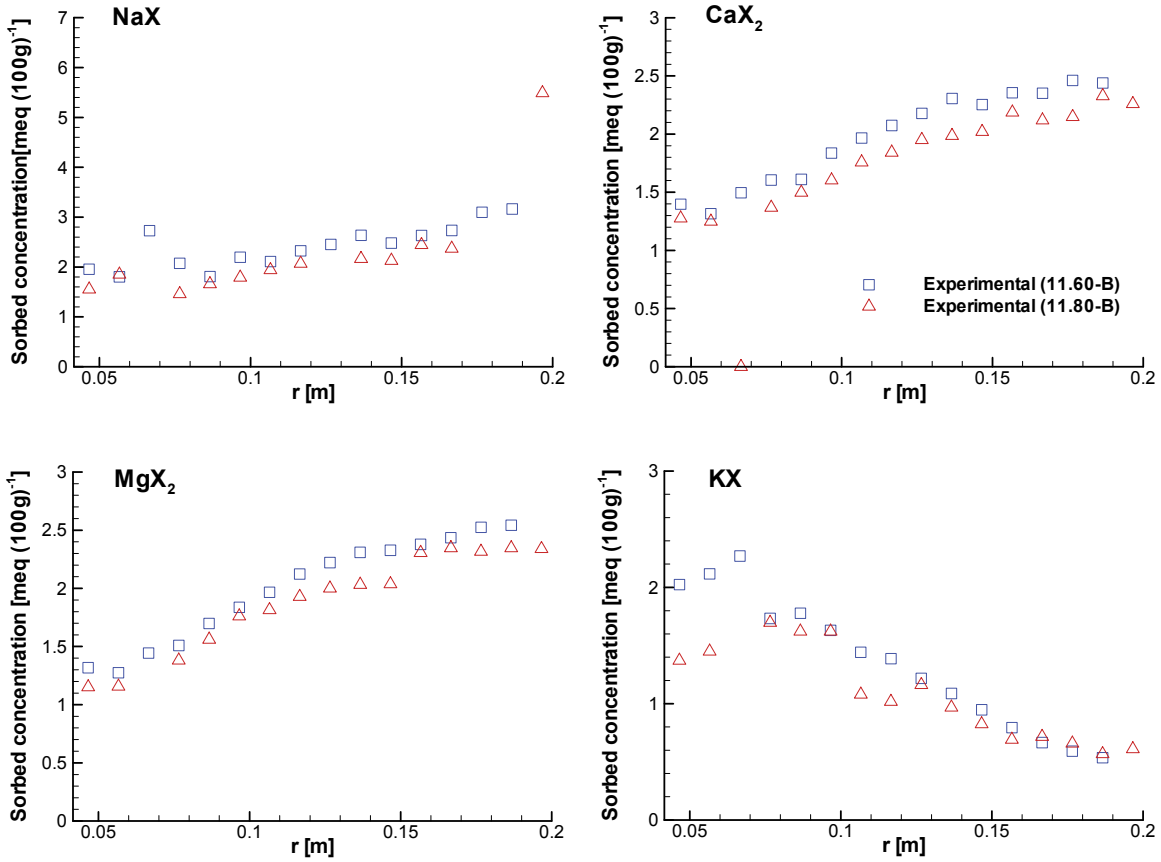

Figure 15: Profiles of Total Sorbed Concentrations of Major Ions Determined in the Overcored Opalinus Clay Samples (NAGRA 2014). The Labels in the Legend (e.g. 11.60-B) Represent the Sample Number

4.3 MATERIAL PROPERTIES AND MODEL PARAMETERS

Key modelling parameters used in the simulations are listed in Table 13. The simulation time was 365 days for the benchmark cases of Task 1 and Task 2.1, 189 days for Task 2.2 (simulations of the DR-A experiment - Phase I) and 450 days for Task 3 (simulations of the DR-A experiment - Phase II). Simulations including the overcoring data extended to 735 days (also Task 3).

Diffusion coefficients for all species are based on the definition of the effective diffusion coefficient D_e (Equation 2-5). For Task 1 and Task 2.1, the pore diffusion coefficient D_p (Equation 2-5) of the tracer was 2.7×10^{-10} m^2 s^{-1}, with an effective porosity of 0.15 for the Opalinus Clay according to the task definition (Leupin 2012). For other simulations (e.g., Task 2.2, the in-situ diffusion experiment) including tracers and all chemical components in the background solution, the free aqueous diffusion coefficients D_0 listed in Table 14 were used; these parameters were obtained from the CRC Handbook of Chemistry and Physics (Lide 1994), unless otherwise noted. The base (or reference) effective porosity was 0.15 and base (or reference) tortuosity was 0.12, which was derived from the numerical simulation of the DR-A in-situ experimental data for HTO (refer to Table 9).

Table 13: Parameters for the Circulation Chamber, Filter, Gap and OPA

Parameter		Borehole	Filter	Gap	OPA
Porosity [-]		2.37[a]	0.45	1.0	0.15
Solid dry bulk density [kg m^{-3}]		-	-	-	2310.0[b]
K_d [L kg^{-1}]	Task 1.1 and Task 2.1a	0.0	0.0	0.0	0.0
	Task 1.2a and Task 2.1b	0.0	0.0	0.0	0.2
	Task 1.2b and Task 2.1c	0.0	0.0	0.0	500

[a] borehole capacity; [b] Bossart (2013)

Table 14: Free Aqueous Phase Diffusion Coefficients (D_0) (Lide 1994)

Species	D_0 [$x10^{-9}$ m^2 s^{-1}]	Species	D_0 [$x10^{-9}$ m^2 s^{-1}]
Cs^+	2.056	SO_4^{2-}	1.065
Na^+	1.334	CO_3^{2-}	0.923
K^+	1.957	I^-	2.045
Mg^{2+}	0.706	Br^-	2.08
Ca^{2+}	0.792	Eu^{3+}	0.602
Sr^{2+}	0.791	Co^{2+}	0.732
Cl^-	2.032	HTO	2.23[#]
H^+	9.311		

[#] from O'Reilly and Peterson (1971)

The Opalinus Clay (OPA) is composed of up to 60 wt.% clay minerals (van Loon et al. 2009). The clay minerals, especially illite and illite/smectite mixed layers (with an average fraction of 40 wt.%), are the primary sites for the sorption of cations (Lauber et al. 2000; Wersin et al. 2008;

Bradbury and Baeyens 2011). Through extensive batch experiments, the sorption properties of Cs^+ have been well described by a three-site ion exchange model and the main parameters for the model are summerized in Table 15 (based on van Loon et al. (2009), with modified selectivity coefficients for Cs^+ for Type II and planar sites (PS) according to information provided by Gimmi et al. 2012). This multisite ion exchange model is especially important for the simulation of the tracer Cs^+ because the sorption of Cs^+ and K^+ on illite (the main clay mineral in OPA) occurs via an ion exchange mechanism involving three different exchange sites. The affinity of Cs^+ for all three sites is different. The frayed edge sites (FES), which are located at the edge of the clay, have the highest selectivity but lowest fraction (0.101%). The planar sites have the lowest affinity for Cs^+ but the highest fraction (about 92 % of the total sites). The type II sites, which are also located at the edges of the clay, are characterized by a moderate affinity for Cs^+ and are present at an intermediate fraction (van Loon et al. 2009). For other cationic reactive tracers, namely $^{85}Sr^{2+}$ and $^{60}Co^{2+}$, such information was not availbale and a linear sorption model was used for the simulations. The distribution coefficients (K_d) for $^{85}Sr^{2+}$ and $^{60}Co^{2+}$ were 1.0 L kg^{-1} and 90.0 L kg^{-1}, respectively (Wersin et al. 2008).

Table 15: Parameters for the Generalized Cs^+ Cation Exchange Model for Illite (van Loon et al. 2009; as Modified by Gimmi 2012)

Site types	**Site capacity**
Frayed edge sites (**FES**)	0.101% of the CEC
Type II sites (**II**)	8.12% of the CEC
Planar sites (**PS**)	91.779% of the CEC
CEC of illite	*0.1035 eq kg^{-1} (=10.35 meq $(100g)^{-1}$)*
Cation exchange reactions	**Selectivity coefficients (log K_s)**
$Na\text{-}FES + Cs^+ \leftrightharpoons Cs\text{-}FES + Na^+$	7.0
$Na\text{-}FES + K^+ \leftrightharpoons K\text{-}FES + Na^+$	2.4
$K\text{-}FES + Cs^+ \leftrightharpoons Cs\text{-}FES + K^+$	4.6
$Na\text{-}II + Cs^+ \leftrightharpoons Cs\text{-}II + Na^+$	3.2
$Na\text{-}II + K^+ \leftrightharpoons K\text{-}II + Na^+$	2.1
$K\text{-}II + Cs^+ \leftrightharpoons Cs\text{-}II + K^+$	1.1
$Na\text{-}PS + Cs^+ \leftrightharpoons Cs\text{-}PS + Na^+$	1.6
$Na\text{-}PS + K^+ \leftrightharpoons K\text{-}PS + Na^+$	1.1
$K\text{-}PS + Cs^+ \leftrightharpoons Cs\text{-}PS + K^+$	0.5
$2Na\text{-}PS + Ca^{2+} \leftrightharpoons Ca\text{-}PS_2 + 2Na^+$	0.67
$2Na\text{-}PS + Mg^{2+} \leftrightharpoons Mg\text{-}PS_2 + 2Na^+$	0.59
$2Na\text{-}PS + Sr^{2+} \leftrightharpoons Sr\text{-}PS_2 + 2Na^+$	0.59

Surface complexation was identified as an alternative to the K_d sorption model for $^{60}Co^{2+}$ and Eu^{3+}, and their surface complexation constants were determined (Bradbury and Baeyens 2011). The surface complexation reactions are associated with the surface hydroxyl groups (=SOH) situated along the edges of the clay platelets, which can protonate and deprotonate as a function of pH and form surface complexes with aqueous metal species. Bradbury and Baeyens (2011) proposed a two-site protolysis non-electrostatic surface complexation and cation exchange model to describe the $^{60}Co^{2+}$ and Eu^{3+} complex retardation effect on Opalinus Clay. The two sites can be distinguished as strong (=SOH(s)) and weak (=SOH(w)) types. The

capacity of the =SOH(s) site is 2.0×10^{-3} moL kg^{-1}, much smaller than that of the =SOH(w) site of 4.0×10^{-2} moL kg^{-1}. However, the surface complexes formed on the =SOH(s) site are considerably stronger and dominate the sorption of the tracer concentrations used in this experiment. The main surface complexation reactions and equilibrium constants were derived from Bradbury and Baeyens (2011) (Table 16). In the current simulation, only illite and illite/smectite mixed layers at 40 wt.% were considered for the surface complexation reactions. Other parameters for the OPA were: an average BET surface area of 31.0 $m^2\ g^{-1}$, and a dry bulk density of 2.31 Mg m^{-3}, according to Bossart (2013). The derived properties for the strong and weak sites for the simulations are listed in Table 17.

Table 16: Surface Complexation Constants ($\log K_s$) on Strong Sites (=SOH(s)) and Weak Sites (=SOH(w)) for the Sorption of Co^{2+} and Eu^{3+} (Bradbury and Baeyens 2011)

Surface complexation reactions	Surface complexation constants ($\log K_s$)
$=SOH(s) + H^+ \leftrightharpoons =SOH_2^+(s)$	4.0
$=SOH(s) \leftrightharpoons =SO^-(s) + H^+$	-6.2
$=SOH(w) + H^+ \leftrightharpoons =SOH_2^+(w)$	8.5
$=SOH(w) \leftrightharpoons =SO^-(w) + H^+$	-10.5
$=SOH(s) + Co^{2+} \leftrightharpoons =SOCo^+(s) + H^+$	0.0
$=SOH(s) + Co^{2+} + H_2O \leftrightharpoons =SOCoOH(s) + 2H^+$	-7.0
$=SOH(s) + Co^{2+} + 2H_2O \leftrightharpoons =SOCo(OH)_2(s) + 3H^+$	-16.5
$=SOH(w) + Co^{2+} \leftrightharpoons =SOCo^+(w) + H^+$	-1.8
$=SOH(s) + Eu^{3+} \leftrightharpoons =SOEu^{2+}(s) + H^+$	1.9
$=SOH(s) + Eu^{3+} + H_2O \leftrightharpoons =SOEuOH^+(s) + 2H^+$	-4.6
$=SOH(s) + Eu^{3+} + 2H_2O \leftrightharpoons =SOEu(OH)_2(s) + 3H^+$	-12.8
$=SOH(s) + Eu^{3+} + 3H_2O \leftrightharpoons =SOEu(OH)_3^+(s) + 4H^+$	-24.0
$=SOH(w) + Eu^{3+} \leftrightharpoons =SOEu^{2+}(w) + H^+$	0.3
$=SOH(w) + Eu^{3+} + H_2O \leftrightharpoons =SOEuOH^+(w) + 2H^+$	-6.2

Table 17: Parameters of the Strong Sites (=SOH(s)) and Weak Sites (=SOH(w)) for the Sorption of Co^{2+} and Eu^{3+} (Bradbury and Baeyens 2011)

Surface sites	Mass [g solid/L H_2O]	Surface Area [m^2/g solid]	Site density [sites/nm^2]
=SOH(s)	5049	31	7.11×10^{-3}
=SOH(w)	5049	31	1.42×10^{-1}

It is well known that some tracers, especially Eu^{3+}, can be strongly sorbed on equipment/ materials. Previous investigations after the field diffusion test, DI-A2, at the Mont Terri test site revealed that some tracers, especially $^{60}Co^{2+}$ and Eu^{3+}, were adsorbed by various equipment components, including the pump, PEEK lines, the tracer reservoir and the filter screen (porous Teflon®) (Wersin et al. 2008). Over 68 wt.% of the total injected Eu^{3+} was found to be absorbed on porous Teflon. This is due to the negative charge on the surface of Teflon while in contact with an aqueous electrolyte solution (Preocanin et al. 2012). Figure 16 depicts the surface

charge density on Teflon as a function of pH of the surrounding aqueous electrolyte solution. For pH > 3.0, a negative surface charge develops at the 0-plane (i.e., on the inert surface of Teflon). The surface charge density value increases rapidly when pH increases to 4.5, and more slowly when pH increases from 4.5 up to 5.5. The concentration of the solution slightly influences the surface charge density as well. Consequently, adsorption of dissolved ions occurs on the surface of Teflon, which creates an interfacial charge and an associated electrical double layer. In the absence of data for this process, and to facilitate illustrative simulations of Eu-sorption onto equipment, the reactions were assumed to be analogous to Eu^{3+} surface complexation on OPA, as shown in Table 18. For illustrative purposes in these code inter-comparisons, the Eu-sorption was simulated using the parameters for surface complexation on the strong sites of OPA as reported by Bradbury and Baeyens (2011). The surface charge density was assumed to be 0.04 C m^{-2} = 0.25 sites nm^{-2} (based on Preočanin et al. 2012, Figure 16). A summary of the relevant parameters is provided in Table 18 and Table 19.

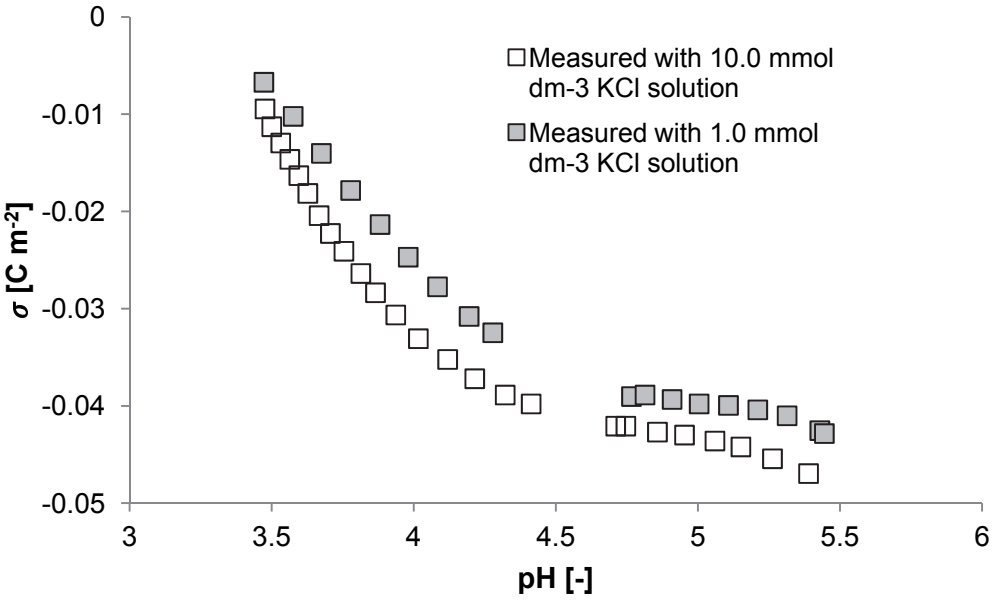

Figure 16: Surface Charge Density σ at the 0-plane of Teflon Evaluated from Potentiometric Mass Titration Data of Teflon Particles as a Function of the pH of the Contacting KCl Solution. Filled Symbols: Measured with 1.0 mmol dm^{-3} KCl Solution; open symbols: Measured with 10.0 mmol dm^{-3} KCl Solution (Based on Preočanin et al. 2012, Fig. 8)

Table 18: Assumed Surface Complexation Reactions and Constants (logK_s) on Teflon Sites (=TOH) for the Sorption of Eu^{3+}

Surface complexation reactions	Surface complexation constants (log K_s)
$=TOH + H^+ \leftrightharpoons =TOH_2^+$	4.0
$=TOH \leftrightharpoons =TO^- + H^+$	-6.2
$=TOH + Eu^{3+} \leftrightharpoons =TOEu^{2+} + H^+$	1.9
$=TOH + Eu^{3+} + H_2O \leftrightharpoons =TOEuOH^+ + 2H^+$	-4.6
$=TOH + Eu^{3+} + 2H_2O \leftrightharpoons =TOEu(OH)_2 + 3H^+$	-12.8
$=TOH + Eu^{3+} + 3H_2O \leftrightharpoons =TOEu(OH)_3^+ + 4H^+$	-24.0

Table 19: Assumed Parameters of the Sites (=TOH) for the Sorption of Eu^{3+}

Surface sites	Mass [g solid/L H_2O]	Surface area [m^2/g solid]	Site density [sites/nm^2]
=TOH	350.0	0.15	2.50×10^{-1}

All simulations were undertaken using the transformed geometry derived from the actual geometry of the DR-A in-situ experiment (Figure 8, Figure 9 and Table 7). The same approach was adopted by the other modelling teams. The radius of each component (i.e., circulation chamber, filter, gap) was transformed to account for the dip angle of the Opalinus Clay (Figure 10), as presented in Table 7. The total mass of tracers was calculated from the initial concentration in the borehole solution multiplied by the total solution volume, including the tank and circulation tubes. This is expressed in the one-dimensional model by a borehole capacity (represented by porosity in the model) of the circulation chamber, as listed in Table 7. As OPA has an extremely low hydraulic conductivity (2.0×10^{-14} to 1.0×10^{-12} m s^{-1}, Bossart (2013)), the mass transport was simulated as purely diffusive.

For the simulation of the in-situ experiment, all tracers were added to the solution in the circulation chamber at their reported initial concentrations. To ensure initial charge balance of the solution, the initial Cl^- concentration was allowed to vary. As for the reactive transport boundary conditions, no-flux boundaries were set at both ends of the solution domain. The diffusion parameters were: free aqueous diffusion coefficients (D_0) according to the CRC handbook (Lide 1994), the base (reference) tortuosity (τ_e) and base (reference) porosity (ϕ_e) for the OPA derived by fitting the experimental diffusion data for uncharged HTO (Table 20).

Effective porosity correction factors (f_ϕ) and effective tortuosity correction factors (f_τ) for the tracers and other dissolved species were set to 1.0 for the simulations with constant effective porosity and tortuosity.

Table 20: Diffusion Coefficients for HTO and Base Tortuosity (τ_e) and Base Porosity (ϕ_e)

	D_0[#] [m^2/s]	D_p [m^2/s]	D_e [m^2/s]	τ_e [-]	ϕ_e [-]
Filter	2.23×10^{-9}	2.23×10^{-9}	1.00×10^{-9}	1.0	0.45
Open gap	2.23×10^{-9}	2.23×10^{-9}	2.23×10^{-9}	1.0	1.0
Opalinus Clay	2.23×10^{-9}	3.35×10^{-10}	4.01×10^{-11}	0.12	0.15 **(HTO)**

[#] - Lide (1994)

An overview of the various simulation tasks is provided in Table 1. In the following section, the results are described for each of the tasks.

5. SIMULATION RESULTS

5.1 TASK 1: DIFFUSION OF A TRACER FROM BOREHOLE WITHOUT FILTER AND GAP

This task simulates the diffusion of conservative and reactive tracers from the borehole (with an equivalent circulation chamber radius of 4.16 cm and a borehole capacity of 2.374, Table 7) into OPA without considering the presence of the filter and gap. The task includes four sub-tasks.

5.1.1 Task 1.1: Diffusion of a Non-sorbing Tracer

In this sub-task, only one non-sorbing tracer was simulated. The pore diffusion coefficient, D_p, of the tracer was 2.7×10^{-10} m^2 s^{-1}, and the effective porosity was 0.15. The effective diffusion coefficient of the tracer was assumed to be 100 times higher in the circulation chamber to mimic complete mixing. Simulation results indicate that the relative tracer concentration in the circulation chamber decreases from 1.0 (initial) to 0.72 after 180 days, with a further decrease to 0.60 after 365 days (Figure 17).

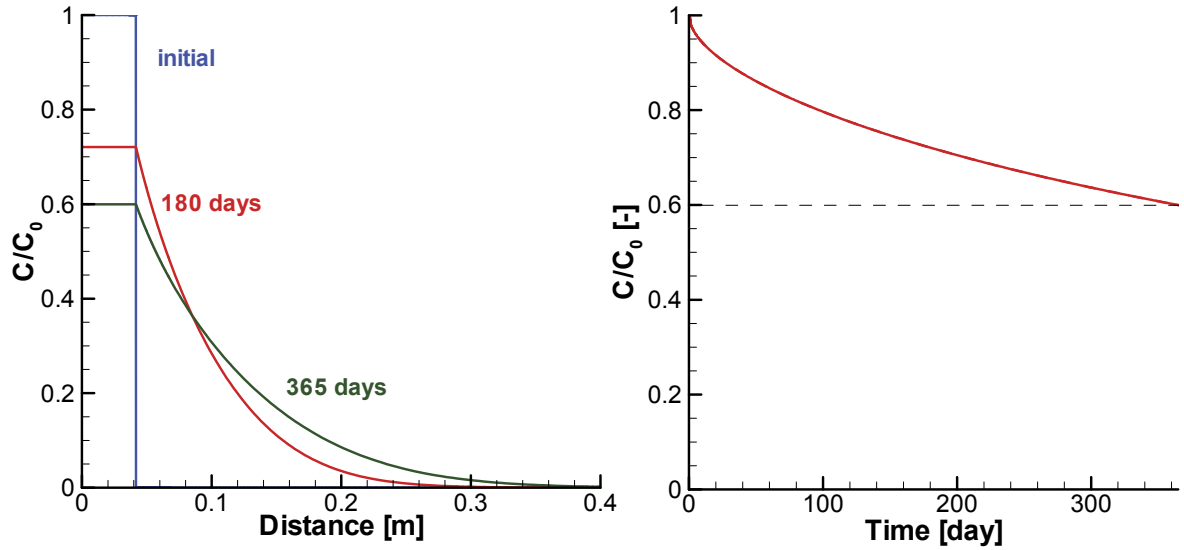

Figure 17: Simulated Tracer Concentration Profiles at 180 Days and 365 Days (Left) and Circulation Chamber Concentration versus Time (Right) for Task 1.1

The results for Task 1.1 obtained with MIN3P-THCm agree with the results presented by Gimmi (2012) (Figure 18) and Soler (2012) (Figure 19). As digital data were not available, the comparisons provided here are based on overlaying the MIN3P-THCm results on diagrams presented by Gimmi (2012) and Soler (2012).

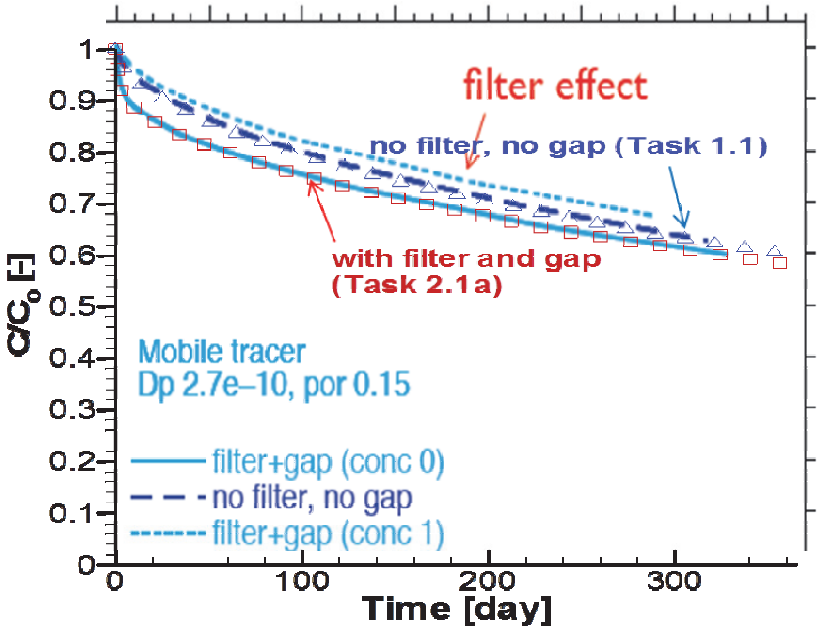

Figure 18: Comparison of the Results Obtained with MIN3P-THCm (Symbols) and Those Presented by Gimmi (2012) (Lines) for Task 1.1 (No Filter) and Task 2.1a (with Filter and Gap)

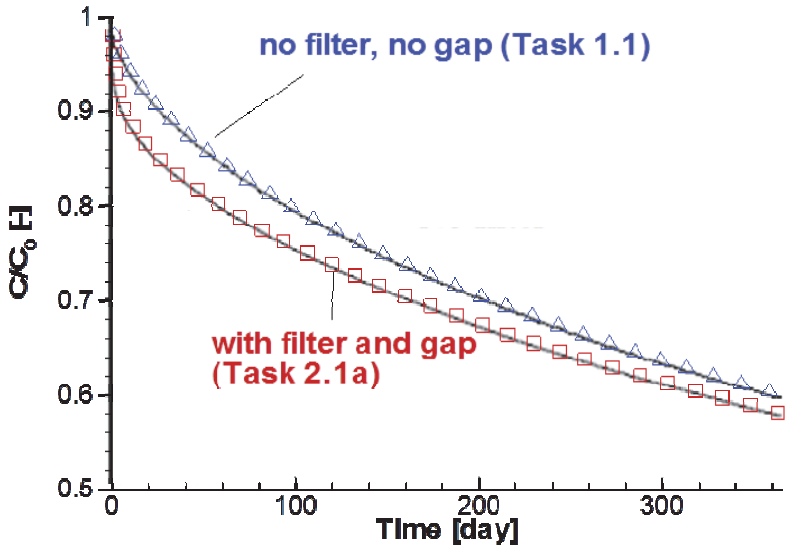

Figure 19: Comparison of the Results Obtained with MIN3P-THCm (Symbols) and Those Presented by Soler (2012) (Lines) for Task 1.1 (no Filter) and Task 2.1a (with Filter and Gap)

5.1.2 Task 1.2a: Diffusion of a Weakly Sorbing Tracer

The simulation for Task 1.2a is identical to Task 1.1, with the exception that the tracer is a weakly sorbing solute with $K_d = 0.2$ L kg^{-1}.

The relative tracer concentration in the circulation chamber decreases from 1.0 (initial) to 0.60 after 180 days, and further to 0.47 after 365 days of simulation time (Figure 20). In comparison to Task 1.1, the tracer concentration in the circulation chamber decreases faster, owing to sorption in the adjacent clay. The migration of the tracer in the clay is also retarded relative to the results obtained in Task 1.1; consequently, the tracer migration front after 365 days (Figure 20, left) has not penetrated as deeply into the clay as for the non-sorbing tracer (Figure 17, left).

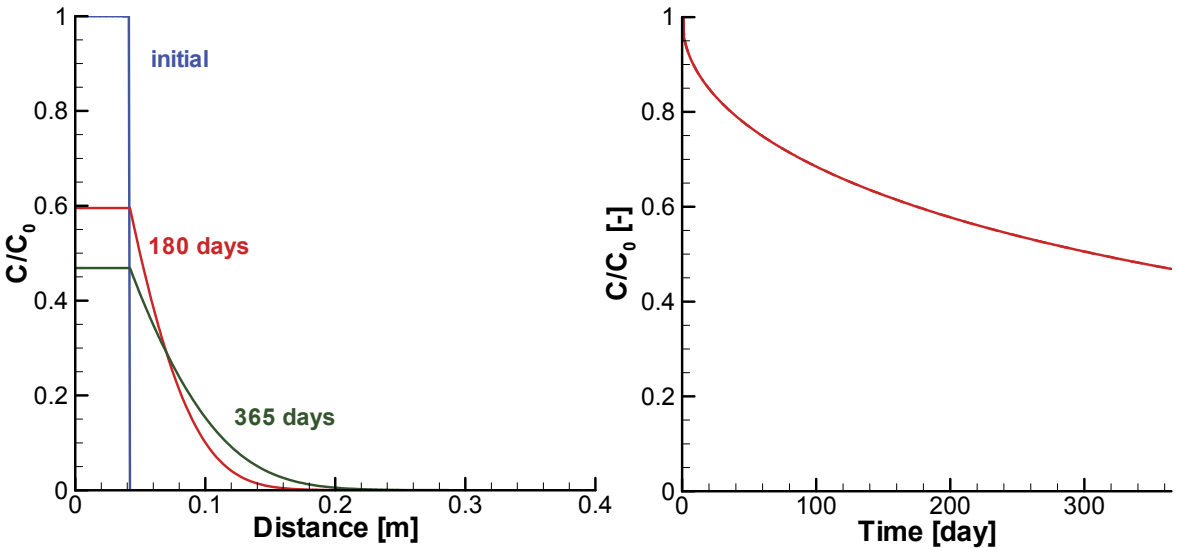

Figure 20: Simulated Tracer Concentration Profiles at 180 Days and 365 Days (Left) and Circulation Chamber Concentration versus Time (Right) for Task 1.2a

The results obtained with MIN3P-THCm agree well with those calculated with Flotran, as presented by Gimmi (2012) (Figure 21), and those simulated with CrunchFlow, as presented by Soler (2012) (Figure 22).

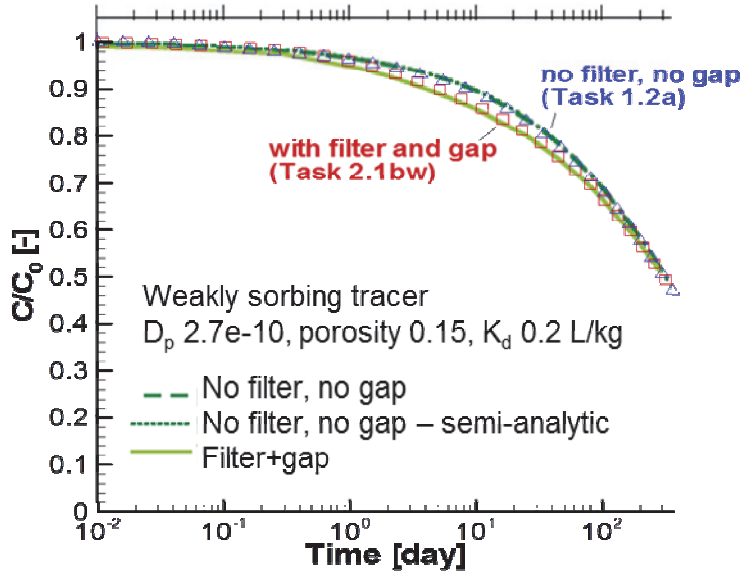

Figure 21: Comparison of Results Obtained with MIN3P-THCm (Symbols) and Those Presented by Gimmi (2012) (Lines) for a Weakly Sorbing Tracer: Task 1.2a (No Filter) and Task 2.1bw (with Filter and Gap)

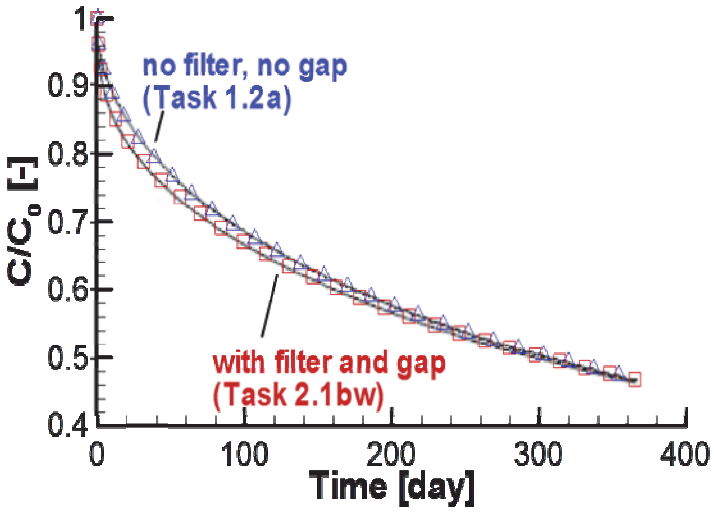

Figure 22: Comparison of Results Obtained with MIN3P-THCm (Symbols) and Those Presented by Soler (2012) (Lines) for a Weakly Sorbing Tracer: Task 1.2a (No Filter) and Task 2.1bw (with Filter and Gap)

5.1.3 Task 1.2b: Diffusion of a Strongly Sorbing Tracer

As noted in Table 1, the Task 1.2b simulation considered a more strongly sorbing tracer with a K_d = 500.0 L kg^{-1}. In this case, the relative tracer concentration in the circulation chamber decreases from 1.0 (initial) to 0.032 after 180 days, with a further decrease to 0.023 after 365 days (Figure 23). The tracer concentration decreases dramatically at early time; for

example, after only one day the relative tracer concentration in the circulation chamber drops over 60% from 1.0 to 0.38 (Figure 23, right). The tracer migrates less than 0.05 m into the clay after 365 days (Figure 23, left), which is much less than the tracer migration distance simulated in Task 1.2a (Figure 20, left).

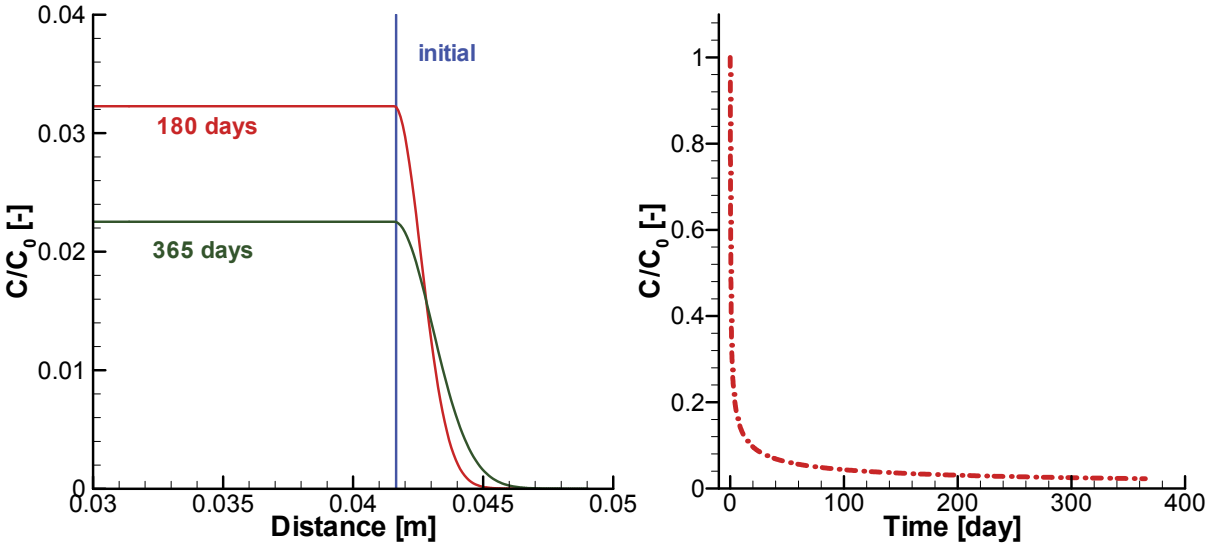

Figure 23: Simulated Tracer Concentration Profiles at 180 Days and 365 Days (Left) and Circulation Chamber Concentration versus Time (Right) for Task 1.2b

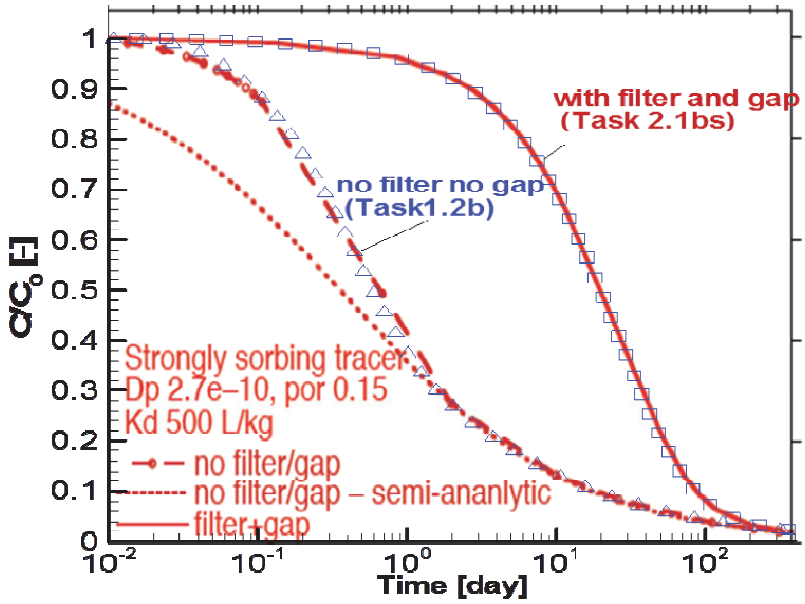

Figure 24: Comparison of Results Obtained with MIN3P-THCm (Symbols) and Those Presented by Gimmi (2012) (Lines) for a Strongly Sorbing Tracer: Task 1.2b (No Filter) and Task 2.1bs (with Filter and Gap)

The simulation results obtained with MIN3P-THCm again agree well with those calculated with Flotran, as presented by Gimmi (2012) (Figure 24), and those obtained with CrunchFlow, as shown by Soler (2012) (Figure 25).

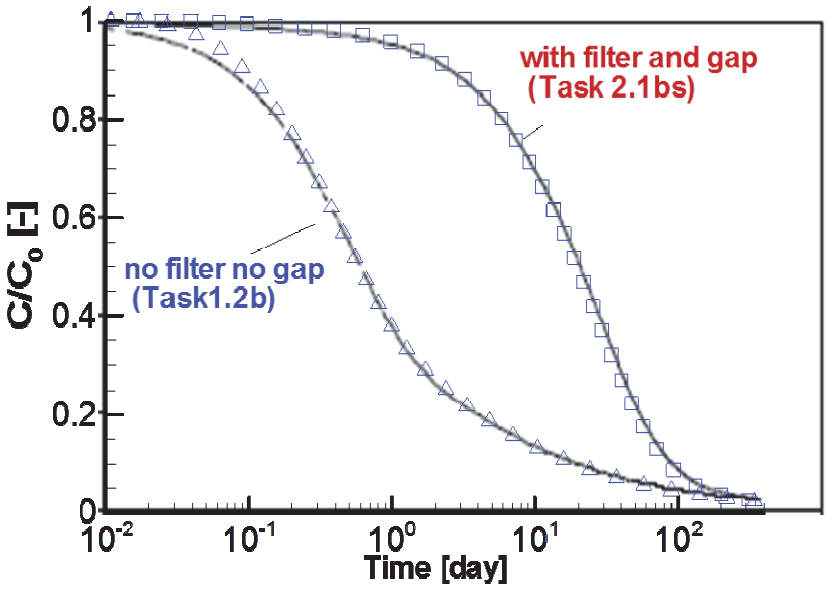

Figure 25: Comparison of Results Obtained with MIN3P-THCm (Symbols) and Those Presented by Soler (2012) (Lines) for a Strongly Sorbing Tracer: Task 1.2b (No Filter) and Task 2.1bs (with Filter and Gap)

5.1.4 Task 1.3: Diffusion of Cs^+ with Cation Exchange

Task 1.3 was designed to simulate the retardation of Cs^+ by OPA using a multisite ion exchange model (van Loon et al. 2009). In the simulation, Cs^+ was assumed to exchange with sorbed Na^+, K^+, Ca^{2+}, Mg^{2+}, and Sr^{2+} on the three ion exchange sites (PS, Type-II and FES as described in Section 4.3). The corresponding selectivity coefficients are listed in Table 15 in Section 4.3. Initially, Cs^+ was present only in the circulation chamber at a concentration of 2.02×10^{-4} mol L^{-1}. Aqueous Na^+ concentrations in the circulation chamber were set to 0.24 mol L^{-1} and were assumed to be the same as in the porewater of the OPA. The same assumption was also applied for the concentration of K^+, which was set at 1.6×10^{-3} mol L^{-1}.

The simulated results are shown in Figure 26 to Figure 28. The results show that the concentration of Cs^+ in the circulation chamber decreases with time (Figure 27), owing to the diffusive migration into the clay rock and ion exchange with the clay minerals present in the rock (Figure 26). The decrease in the concentration of Cs^+ is most apparent within the first 10 days (Figure 27). Due to ion exchange, Na^+ and K^+ diffuse back into the circulation chamber and the concentrations of these ions increase slightly in the circulation chamber. The K^+ concentration reaches a peak value of 1.62×10^{-3} mol L^{-1} at about 29 days, while Na^+ concentrations increase only marginally from 0.24000 mol L^{-1} to 0.24008 mol L^{-1} at about 85 days. Decreasing concentrations of Na^+ after 85 days and K^+ after 29 days in the circulation chamber indicate that

the ion exchange processes triggered by the injection of Cs^+ into the circulation chamber and migration into the OPA are slowing down (Figure 27).

The migration of Cs^+ into the clay rock is very limited (Figure 28). The maximum sorbed Cs on Type-II sites occurs close the borehole surface with the highest concentration of 0.42 meq $(100\ g)^{-1}$ (Figure 26). Sorbed concentrations decrease rapidly with distance from the borehole surface. Similar concentration distribution trends characterize sorbed Cs on the PS sites with a maximum concentration of 0.11 meq $(100\ g)^{-1}$ near the borehole surface. The concentration of Cs on the FES sites shows an almost even distribution between the borehole surface and 0.054 m. This occurs because the selectivity coefficient for Cs on FES sites is the highest among the three ion exchange sites. The FES sites are first occupied as long as Cs^+ is available. Only when these sites are almost fully occupied do the Type II and PS sites become populated with Cs^+. However, the CEC fraction of the FES sites is only 0.1%, implying that the maximum amount of Cs sorbed onto the FES sites remains lower than the sorbed Cs concentrations on Type II and PS sites (Figure 26). The results obtained using MIN3P-THCm agree well with those calculated with Flotran, as presented by Gimmi (2012) (Figure 29), and those simulated with CrunchFlow, as presented by Soler (2012) (Figure 30). The small difference between the MIN3P-THCm and Flotran results at the early time can be attributed to differences in time discretization and time step size (Figure 29).

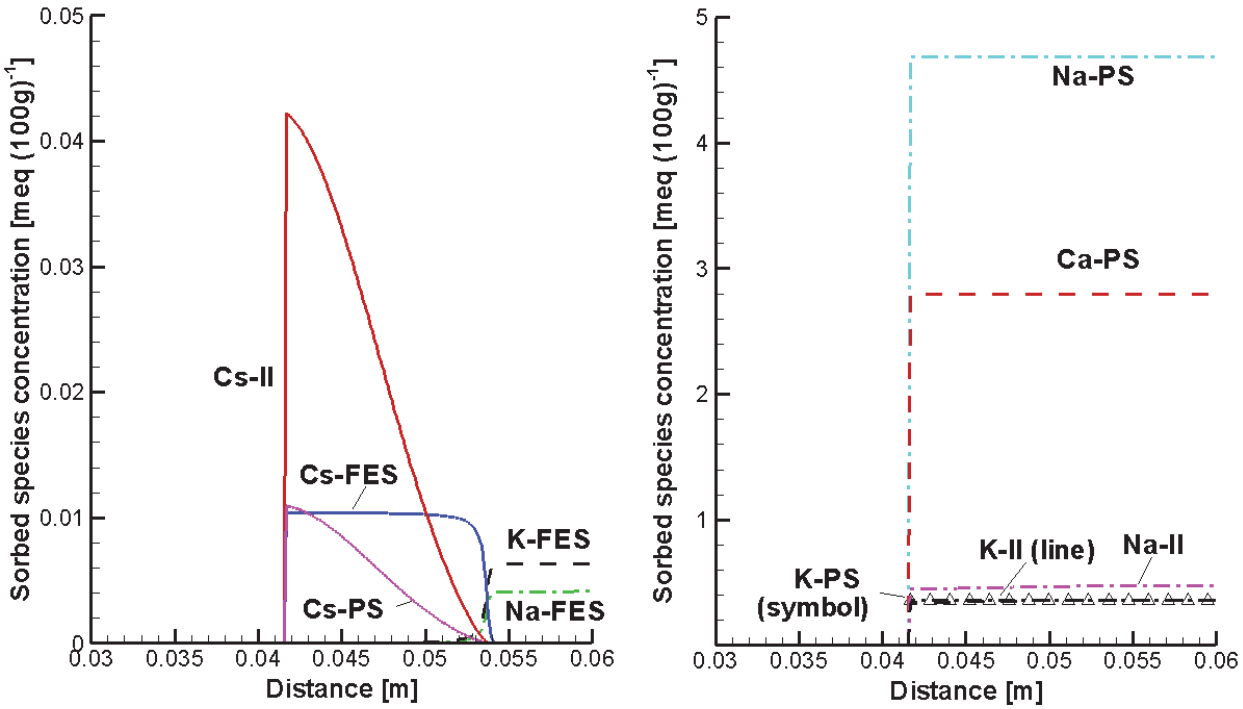

Figure 26: Simulated Sorbed Concentration Profiles for Ion Exchanged Species after 365 Days for Task 1.3 (Left: Sorbed Cs Species and K-FES, Na-FES; Right: Other Sorbed Cations)

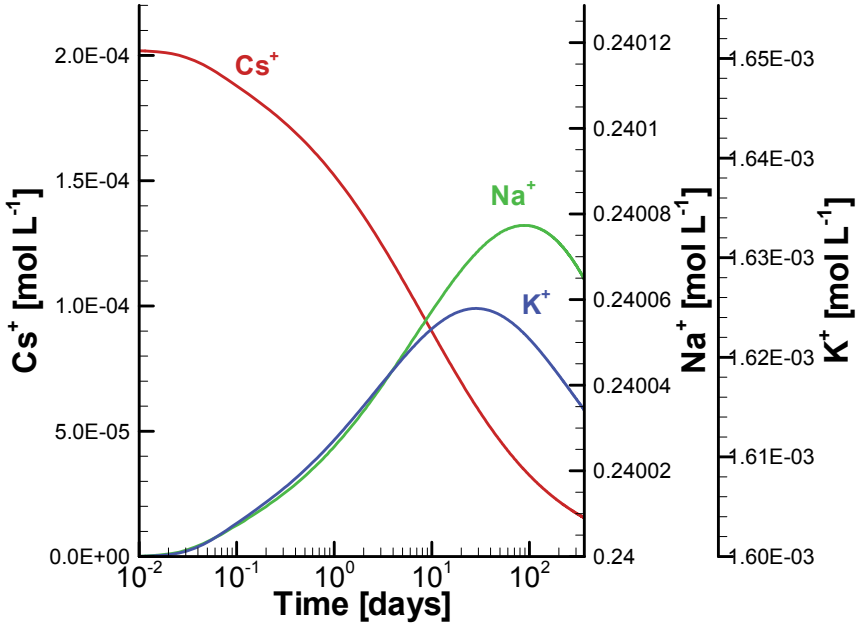

Figure 27: Simulated Circulation Chamber Aqueous Concentrations versus Time for Task 1.3

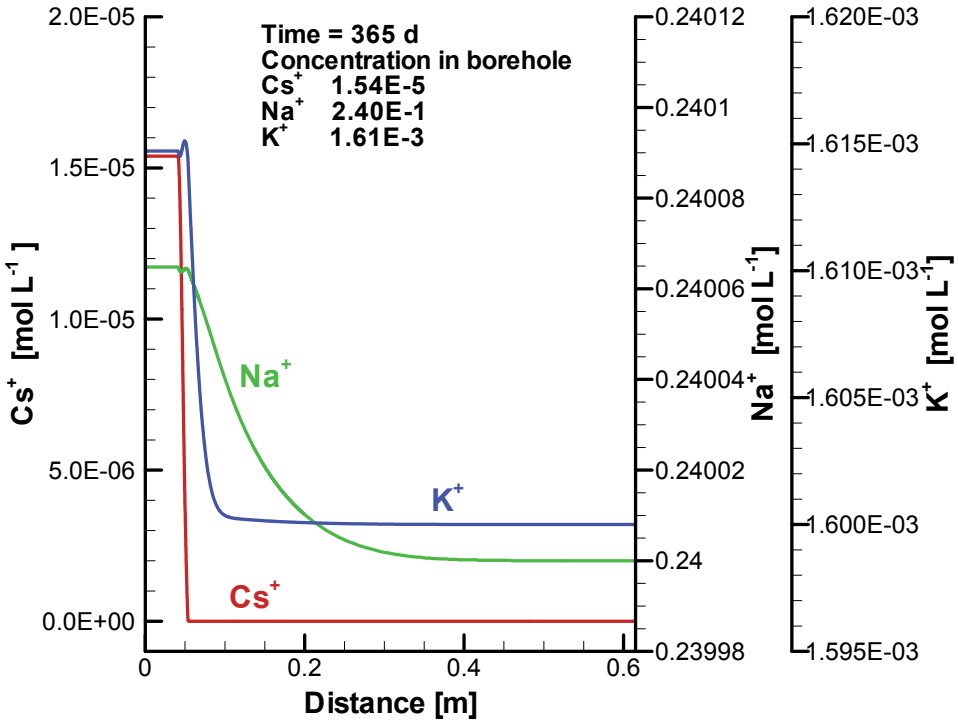

Figure 28: Simulated Cs^+, Na^+ and K^+ Concentration Profiles at 365 Days for Task 1.3

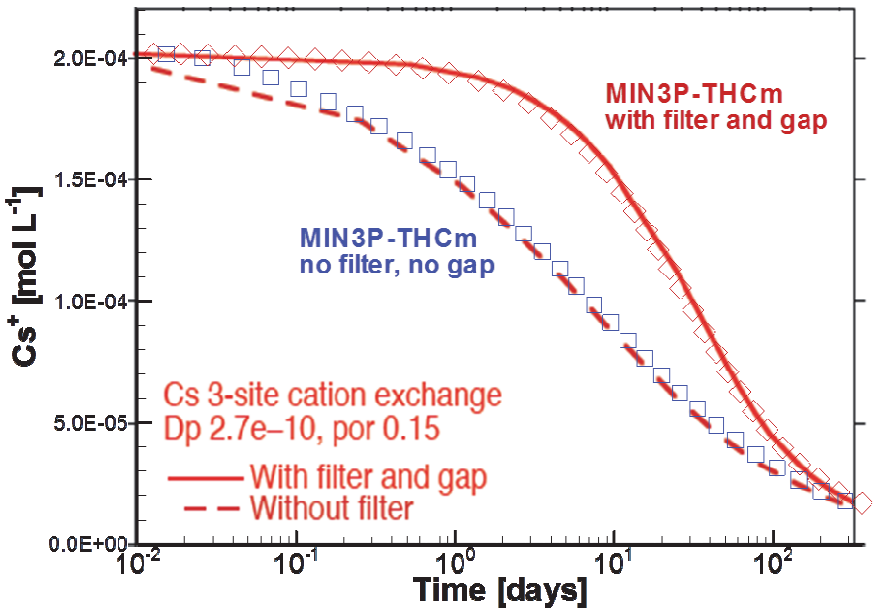

Figure 29: Comparison of Cs^+ Concentrations in the Borehole Circulation Chamber Obtained Using MIN3P-THCm (Symbols) and Those Presented by Gimmi (2012) (Lines) for Task 1.3 (No Filter, No Gap) and Task 2.1c (with Filter and Gap)

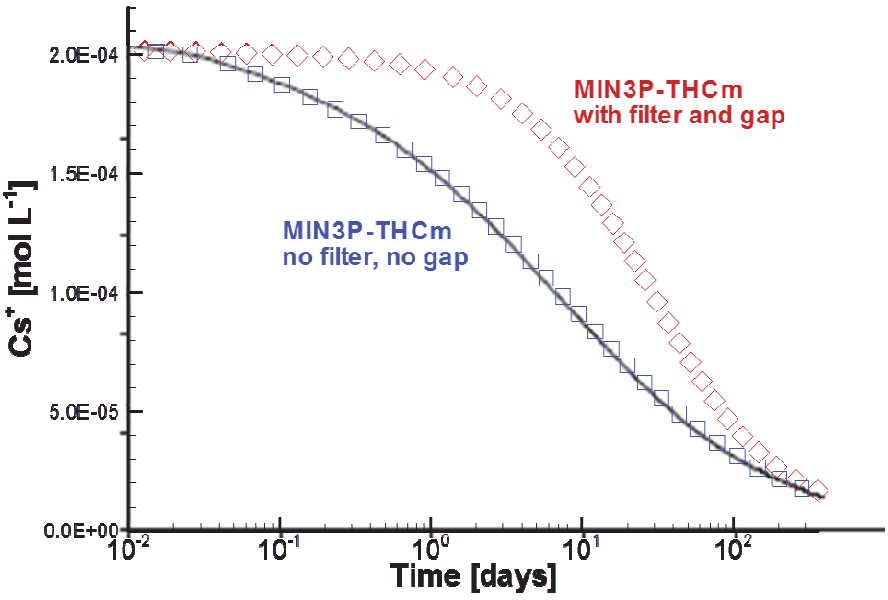

Figure 30: Comparison of Cs^+ Concentrations in the Borehole Circulation Chamber Obtained Using MIN3P-THCm (Symbols) and Those Presented by Soler (2012) (Line) for Task 1.3 (No Filter, No Gap) and Task 2.1c (with Filter and Gap)

5.1.5 Summary

Task 1 defined four benchmarks with increasing geochemical complexity and well-defined model and problem parameters. Through code inter-comparison with other reactive transport codes Flotran and CrunchFlow, the individual functions of MIN3P-THCm related to ion diffusion and retardation were verified for a borehole setting.

5.2 TASK 2: DIFFUSION OF A TRACER FROM BOREHOLE WITH FILTER AND GAP

This task includes two sub-tasks: Task 2.1 involves a comparative simulation of all cases defined in Task 1, but modified to include the effect of a filter and gap on the tracer migration; Task 2.2 is the numerical simulation and comparison to observed data (Table 9) from Phase I of the DR-A experiment.

5.2.1 Task 2.1: Diffusion of Sorbing and Non-sorbing Tracer

5.2.1.1 Task 2.1a: Diffusion of a Non-sorbing Tracer

Task 2.1a was based on Task 1.1, but modified by including a filter and gap. The equivalent circulation chamber radius is 3.39 cm, the equivalent outer radius of the filter is 3.83 cm, and the equivalent outer radius of the gap or borehole is 4.16 cm (Table 7). The borehole capacity (represented by porosity) of the circulation chamber is 3.567, which is larger than that in Task 1 because the circulation chamber is now smaller. The porosity of the Teflon filter is 0.45 and its tortuosity is assumed to be 1.0. The tracer migrates from the circulation chamber through the filter and gap into the OPA. The effective diffusion coefficient of the tracer is assumed to be 100 times higher in the circulation chamber to ensure complete mixing of the tracer within the chamber. The tracer is assumed to exist initially only in the circulation solution, and no tracer is initially present in the filter and gap.

The simulated tracer profiles exhibit a slight decrease of the tracer concentration through the filter at 180 and 365 days (Figure 31 left), which occurs because of the diffusive resistance of the filter. The relative tracer concentration in the circulation chamber decreases from 1.0 (initial) to 0.69 after 180 days, and further to 0.58 after 365 days (Figure 31). When compared to the case that does not consider the filter and gap, the tracer concentration in the circulation chamber is generally lower for the case that includes the filter (Figure 12 left). This is because of a rapid concentration decrease at early time, owing to the dilution of the tracer by the porewater that is present in the filter and the gap. The differences observed between the borehole tracer concentration in the cases of ‘with’ and ‘without’ a filter decrease with time, which indicates that the dilution effect is only important at early time. In the long term, tracer migration is mainly controlled by uptake into the OPA.

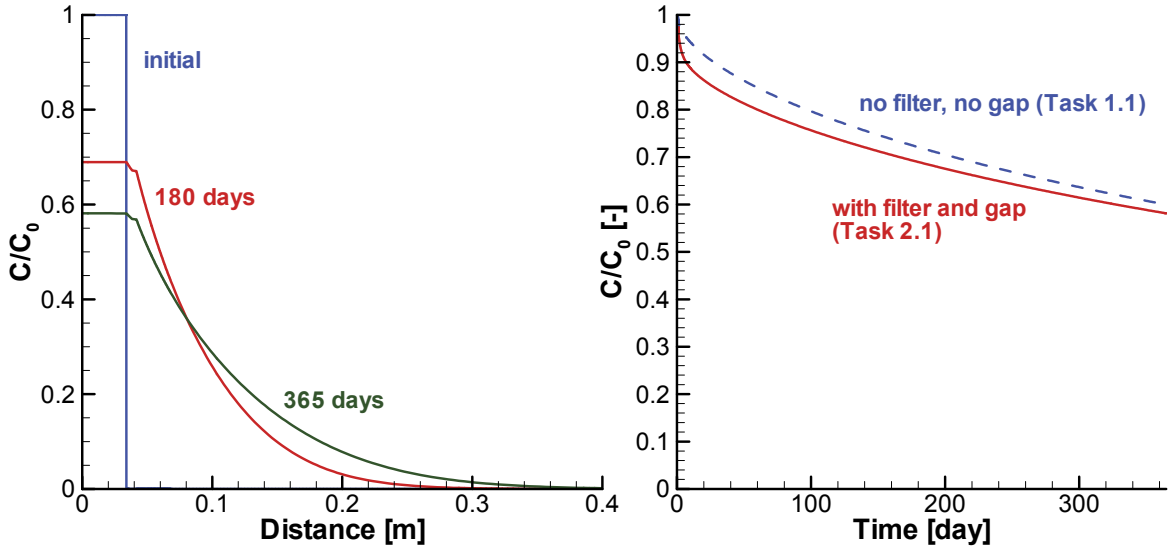

Figure 31: Simulated Tracer Concentration Profiles for Task 2.1a (Left) and Comparison of the Tracer Concentration Time Curves in the Circulation Chamber for Task 2.1a and Task 1.1 (Right)

The MIN3P-THCm results compare well with those calculated with Flotran, presented by Gimmi (2012) (Figure 18), and those obtained by Soler (2013) (Figure 19) using the same conceptual approach.

5.2.1.2 Task 2.1bw: Diffusion of a Weakly Sorbing Tracer

Task 2.1bw is based on Task 1.2a, but it is modified by adding the filter and gap. The additional model parameters are the same as described in Task 2.1a. Similar to the results for Task 2.1a, simulated tracer profiles show a slight decrease in the tracer concentration through the filter at 180 and 365 days (Figure 32 left). The relative tracer concentration in the circulation chamber decreases from 1.0 (initial) to 0.59 after 180 days, and further to 0.47 after 365 days (Figure 32). When compared to the results of Task 2.1a, the concentrations are lower at each point in time. The tracer penetration is also less pronounced, which reveals the effect of sorption on the tracer concentrations. By comparing the tracer concentration time curves to Task 1.2a (no filter no gap), the dilution effect, due to the presence of the filter and gap, can be easily identified (Figure 32 right). Nevertheless, the dilution effect plays a role only during early time and disappears after about 300 days. Afterward, tracer migration is mainly controlled by tracer diffusion and retardation in the OPA.

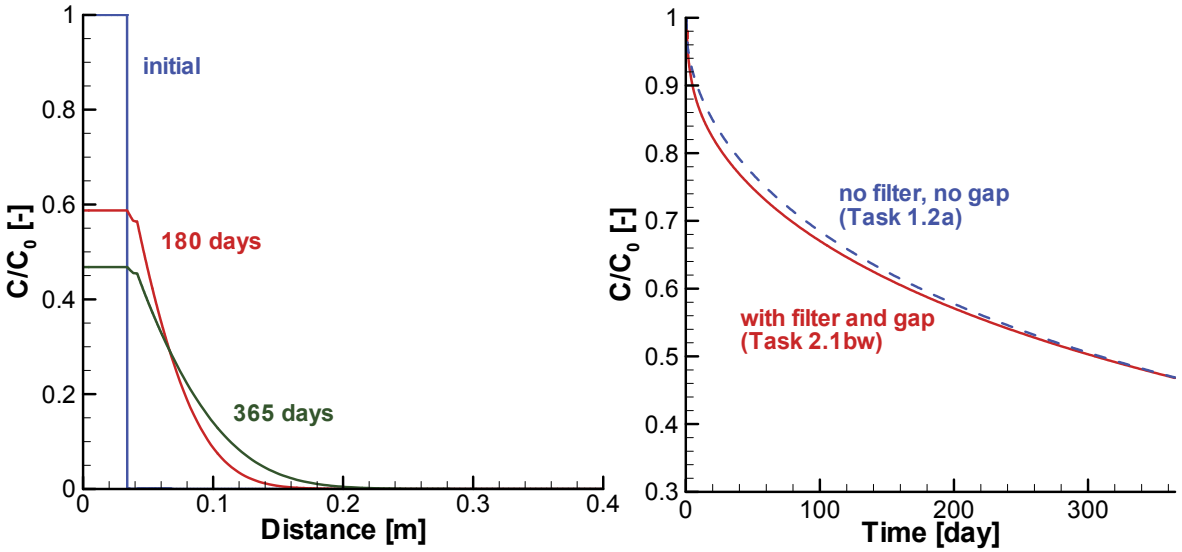

Figure 32: Simulated Tracer Concentration Profiles for Task 2.1bw (Left) and Comparison of the Tracer Concentration Time Curves in the Circulation Chamber for Task 2.1bw and Task 1.2a (Right)

The results obtained with MIN3P-THCm agree well with the results obtained with Flotran by Gimmi (2012) (Figure 21), and those calculated with CrunchFlow by Soler (2012, 2013) (Figure 22), verifying the codes with one another for the case of diffusion with weak sorption.

5.2.1.3 Task 2.1bs: Diffusion of a Strongly Sorbing Tracer

The simulation of Task 2.1bs is based on Task 1.2b, but modified by adding the filter and gap into the model. Additional model setup parameters are the same as described in Task 2.1a. Simulated tracer profiles show a slight decrease in the tracer concentration through the filter at 180 and 365 days (Figure 33 left). The relative tracer concentration in the circulation chamber decreases from 1.0 (initial) to 0.040 after 180 days, and further to 0.024 after 365 days (Figure 33 right). The rapid decrease of the tracer concentration in the circulation chamber is due to the strong sorption of the tracer onto the OPA. In comparison to the results of Task 1.2b, however, the concentrations are higher at each point in time. This indicates that the resistance of the filter substantially slows tracer migration into the clay. This phenomenon is clearly visualized by comparing the tracer concentration time curve to that obtained in Task 1.2b (no filter no gap) (Figure 33 right). The dilution effect, due to the presence of the filter and gap, as observed at early time, is overwhelmed by the strong sorption. The resistance effect of the filter only plays a temporary role and dissipates after about 200 days. Tracer migration is controlled primarily by the strong sorption characteristics.

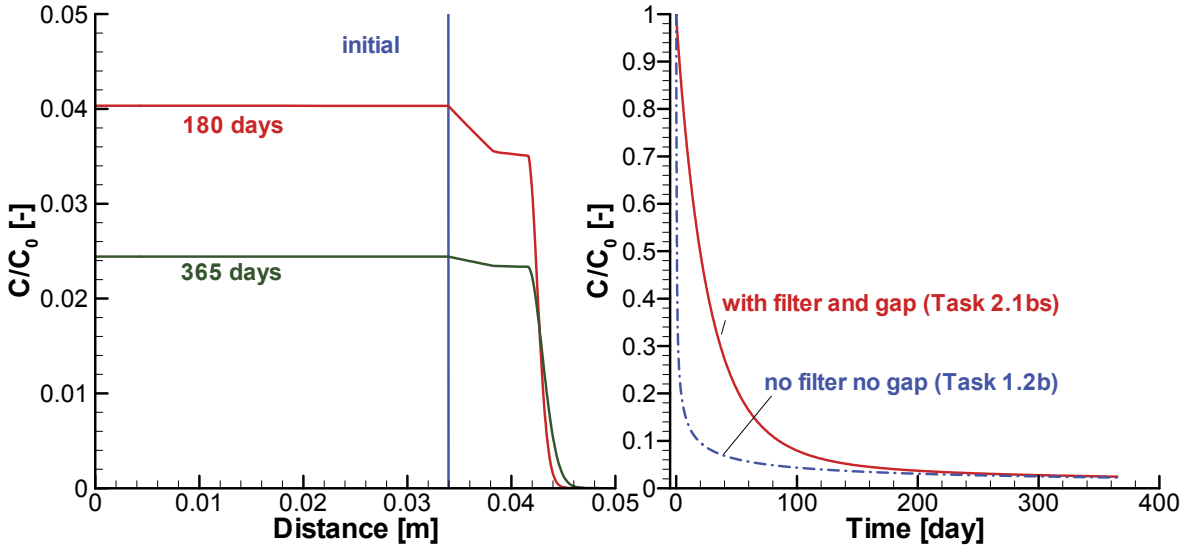

Figure 33: Simulated Tracer Concentration Profiles for Task 2.1bs (Left) and Comparison of the Tracer Concentration Time Curves in the Circulation Chamber for Task 2.1bs and Task 1.2b (Right)

The results predicted using MIN3P-THCm closely match the results calculated with Flotran by Gimmi (2012) (Figure 24) and simulated with CrunchFlow by Soler (2013) (Figure 25).

5.2.1.4 Task 2.1c: Diffusion of Cs^+ with Cation Exchange

The simulation of Task 2.1c is based on Task 1.3, but modified by adding the filter and gap. Model parameters specific to the filter and gap are the same as described in Task 2.1a. Simulated results are depicted in Figure 34 to Figure 36. Similar to Task 1.3 (Figure 26), the majority of sorbed Cs is present on Type-II sites near the borehole surface, but with a slightly higher concentration of 0.44 meq $(100\ g)^{-1}$ solid (Figure 34) in comparison to Task 1.3 (Figure 34). The migration front of Cs sorbed on FES sites is slightly less than 0.54 m, which is due to the retardation effect of the filter on Cs^+ migration (compare Figure 34 and Figure 26). Consequently, the Cs^+ concentration in the borehole decreases more slowly in comparison to Task 1.3 without filter (compare Figure 35 and Figure 27). The concentration peaks of K^+ (with 1.62×10^{-3} mol L^{-1}) and Na^+ (with 0.24 mol L^{-1}) appear at 103 days and 162 days, substantially later than for Task 1.3 at 29 days for K^+ and 85 days for Na^+, respectively (compare Figure 35 and Figure 27). Figure 36 depicts the concentration profiles of Cs^+, Na^+ and K^+ at 365 days. Similar to Task 1.3, there is a rapid concentration decrease for all three species in the clay near the borehole surface. An additional decrease in Cs^+ concentration in the filter becomes evident as well, owing to the retardation effect of the filter (compare Figure 36 and Figure 27).

The temporal changes in the Cs^+ concentration in the borehole obtained using MIN3P-THCm agree well with the results of Flotran presented by Gimmi (2012) (Figure 29).

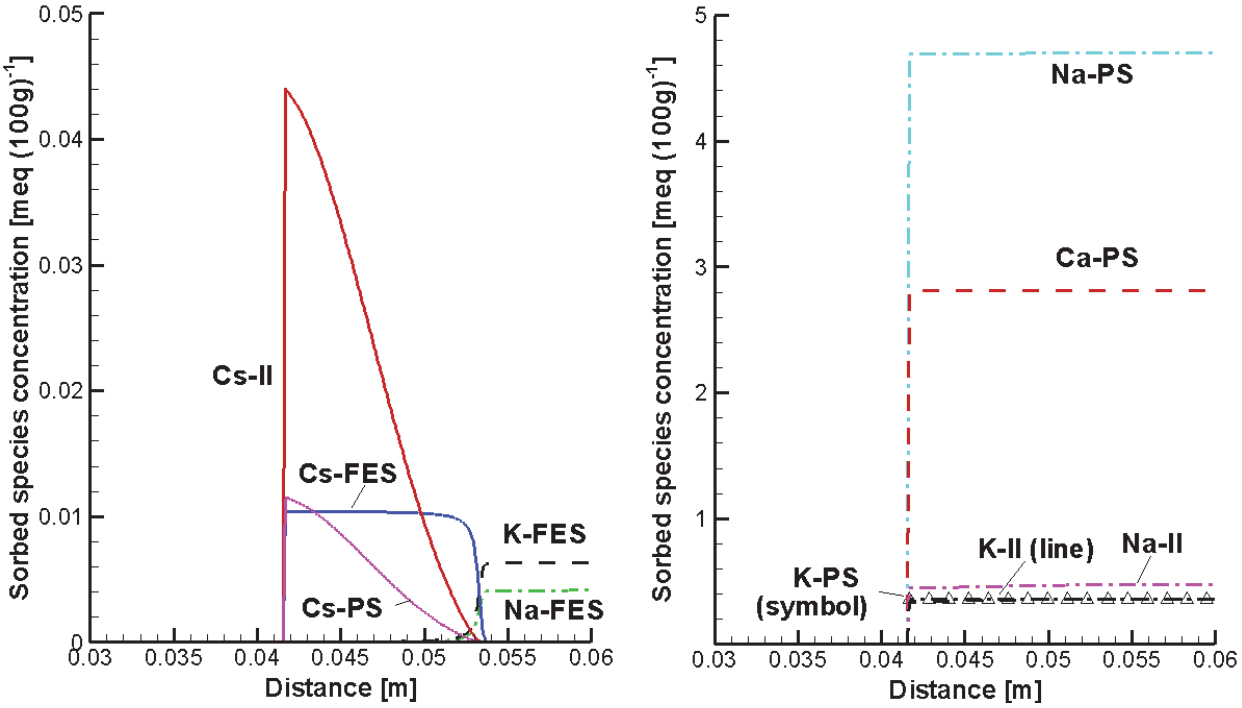

Figure 34: Simulated Concentration Profiles of Sorbed Species After 365 Days for Task 2.1c (Left: Sorbed Cs Species and K-FES, Na-FES; Right: Other Sorbed Species)

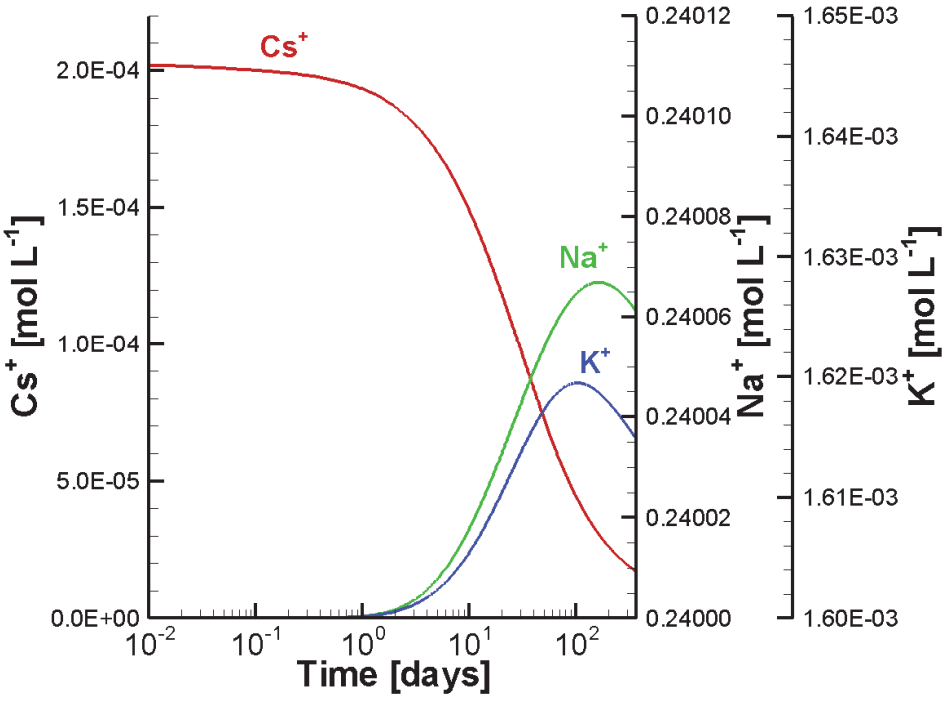

Figure 35: Simulated Aqueous Concentration Time Curves in the Circulation Chamber for Task 2.1c

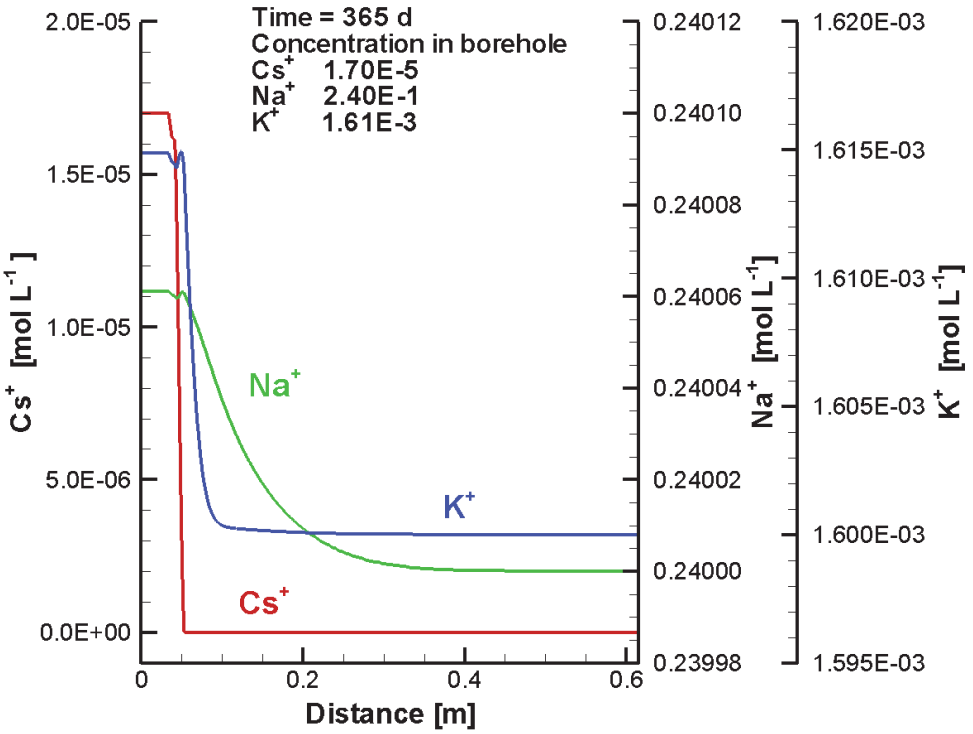

Figure 36: Simulated Cs^+, Na^+ and K^+ Concentration Profiles at 365 Days for Task 2.1c

5.2.1.5 Summary

Task 2.1 extended the four benchmarks defined in Task 1 by including the filter and gap to investigate their influence on the ion migration processes. In the benchmarks with non-sorbing and weakly sorbing tracers, the ion concentrations in the circulation chamber decrease slower in comparison to the corresponding benchmarks without a filter. In the benchmarks with a strongly sorbing tracer including Cs^+ , which is subject to ion exchange reactions, the opposite effect was observed. The inclusion of a filter inhibits the tracer in the circulation chamber from reaching the Opalinus Clay for all cases. For strongly sorbing tracers, the process most strongly affecting the concentration decrease in the borehole is sorption, which steepens the gradient and enhances diffusive transport. Because the strongly sorbing tracers can more easily reach the Opalinus Clay for the case without a filter, the concentration drops faster in comparison to the case with a filter. Such retardation effects are most significant at early time. At late time, the ion migration is mainly controlled by the clay rather than by the filter. All simulation results obtained with MIN3P-THCm agree well with those from Flotran, as presented by Gimmi (2012), and CrunchFlow, as reported by Soler (2012). This code inter-comparison thus provides a greater degree of confidence that these codes are capable of simulating the diffusion of both conservative and reactive tracers from the borehole including the effects of the filter and gap.

5.2.2 Task 2.2: Simulation of DR-A Experiment − Phase I

The objective of this task was to simulate Phase I of the in-situ diffusion experiment (DR-A) at the Mont Terri Underground Rock Laboratory (Switzerland). The experimental design was based on the previous DI-A1 and DI-A2 tests with an artificial porewater that matches the local geochemical conditions, but includes a mixture of tracers (HTO, I^-, Br^-, Cs^+, $^{85}Sr^{2+}$, $^{60}Co^{2+}$ and Eu^{3+}) (Gimmi et al. 2013). The observed tracer concentration data from the first phase are presented in Table 9 (see Section 4.2).

Numerical simulations were undertaken for the experiment using the HMD module, as described in Section 3.1 for two scenarios – open and filled gap scenarios. The filled gap scenario assumes that groundwater in the gap contains dispersed clay particles, providing additional sorption capacity, as discussed in Section 5.2.2.2. Anion exclusion was accounted for by reducing the effective porosity and effective tortuosity for anions by applying porosity and tortuosity correction factors (f_ϕ and f_τ, respectively). A linear sorption model was used for the simulation of $^{85}Sr^{2+}$ and $^{60}Co^{2+}$. For the simulation of Cs^+, a multisite ion exchange model was adopted in separate calculations. Several sensitivity analyses were performed in order to evaluate other simulation approaches (applied by different teams) for $^{85}Sr^{2+}$, $^{60}Co^{2+}$ and Cs^+. An additional simulation for Eu^{3+} was undertaken using Eu-teflon surface complexation reactions as introduced in Section 4.3. In all cases, the 1-D conceptual model including filter and gap was applied using a radial coordinate system. The chemical composition of the artificial porewater (Table 10) was applied as the initial condition in all simulations described in this subsection.

5.2.2.1 Task 2.2a: Open Gap Scenario

The first simulation for the diffusion experiment considered the anion exclusion effect by setting the effective porosity correction factor (f_ϕ) and the effective tortuosity correction factor (f_τ) for anions to values less than 1.0, as listed in Table 21. For the anions I^- and Br^-, the f_ϕ factors were calculated based on the measured accessible porosity of 0.08 and 0.10 (Wersin et al. 2008) divided by the base (reference) effective porosity of 0.15 (Table 21). The effective tortuosity factors were fitted parameters. In this simulation, both f_ϕ and f_τ were assumed to be 1.0 for all cations and uncharged species, which means there were no modifications of the effective porosity and tortuosity for any of the cations in relation to HTO.

Table 21: Effective Porosity Correction Factors (f_ϕ) and Effective Tortuosity Correction Factors (f_τ) for the Simulations of Diffusion in OPA

Species	f_ϕ [-]	f_τ [-]	Species	f_ϕ [-]	f_τ [-]
Co^{2+}	1.0	1.0	**Eu^{3+}**	1.0	1.0
Sr^{2+}	1.0	1.0	**I^-**	0.53	0.55
HTO	1.0	1.0	**Br^-**	0.67	0.38
Cs^+	1.0	1.0			

The best-fit parameters for HTO, as listed in Table 20, are identical to those presented by Gimmi (2012). One of the key parameter changes for the simulation was an increase of the

tortuosity of the filter from 0.4, which was provided in the initial task definition, to 1.0. This change reflects the fact that the barrier effect of the filter is actually only due to its porosity, but not its tortuosity. In other words, the pores in the filter are assumed to be well connected, such that elongated diffusion paths do not exist. By employing this parameter modification, the observed HTO concentration time curve was well simulated, especially during the early time period (Figure 37 left). Using this approach, good fits could also be obtained for Br^- and I^- (Figure 37 right). Based on these observations, the tortuosity of the filter was set to 1.0 for the remaining simulations.

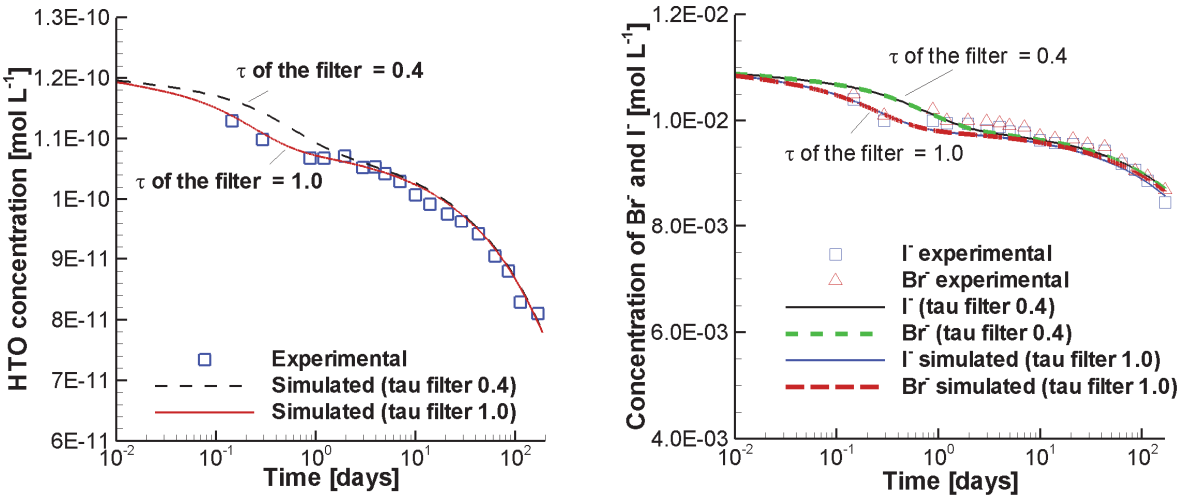

Figure 37: Influence of the Filter Tortuosity on the Simulated HTO (Left), Br^- and I^- (Right) Concentration Time Curves (Lines – Simulated Results; Symbols – Experimental Data)

The simulated results for all species are shown in Figure 38. The simulated concentrations of HTO show very good agreement with the experimental data. The calculated results for Br^- and I^- also show good agreement to observational data if the anion exclusion effect is taken into account using both f_ϕ and f_τ, as listed in Table 21 (Figure 38). For the tracers $^{60}Co^{2+}$ and $^{85}Sr^{2+}$, however, the simulated results do not agree well with the experimental data (Figure 38). This indicates that there must be additional processes that lead to the more rapid decrease in the observed tracer concentrations. One of the most likely possibilities is a higher degree of accessible pore space for cations, and faster diffusion due to surface and/or interlayer diffusion. These phenomena can be captured by increasing the porosity and tortuosity factors to values greater than 1.0. Sensitivity analysis on the influence of effective tortuosity factors f_τ on $^{85}Sr^{2+}$ diffusion show good agreement between the simulated and observed results if f_τ is equal to 3.5 (Figure 39 left). Using the same approach for $^{60}Co^{2+}$; however, did not produce an adequate match to the experimental results, even with an unrealistically high value of f_τ = 300.0 (Figure 39 right). The simulated $^{60}Co^{2+}$ concentrations at early time remain at significantly higher levels than observed. This result suggests that the rapid decrease in $^{60}Co^{2+}$ concentration at early time is not controlled by diffusion into the OPA and subsequent adsorption. The discrepancy indicates that an additional retardation effect, before $^{60}Co^{2+}$ reaches the clay, may exist. This hypothesis will be discussed in the next two sections. The effective porosity may also be

species-dependent for cations; however, this parameter was not varied in the current simulations, but was taken into consideration in the simulations discussed in section 5.2.2.6.

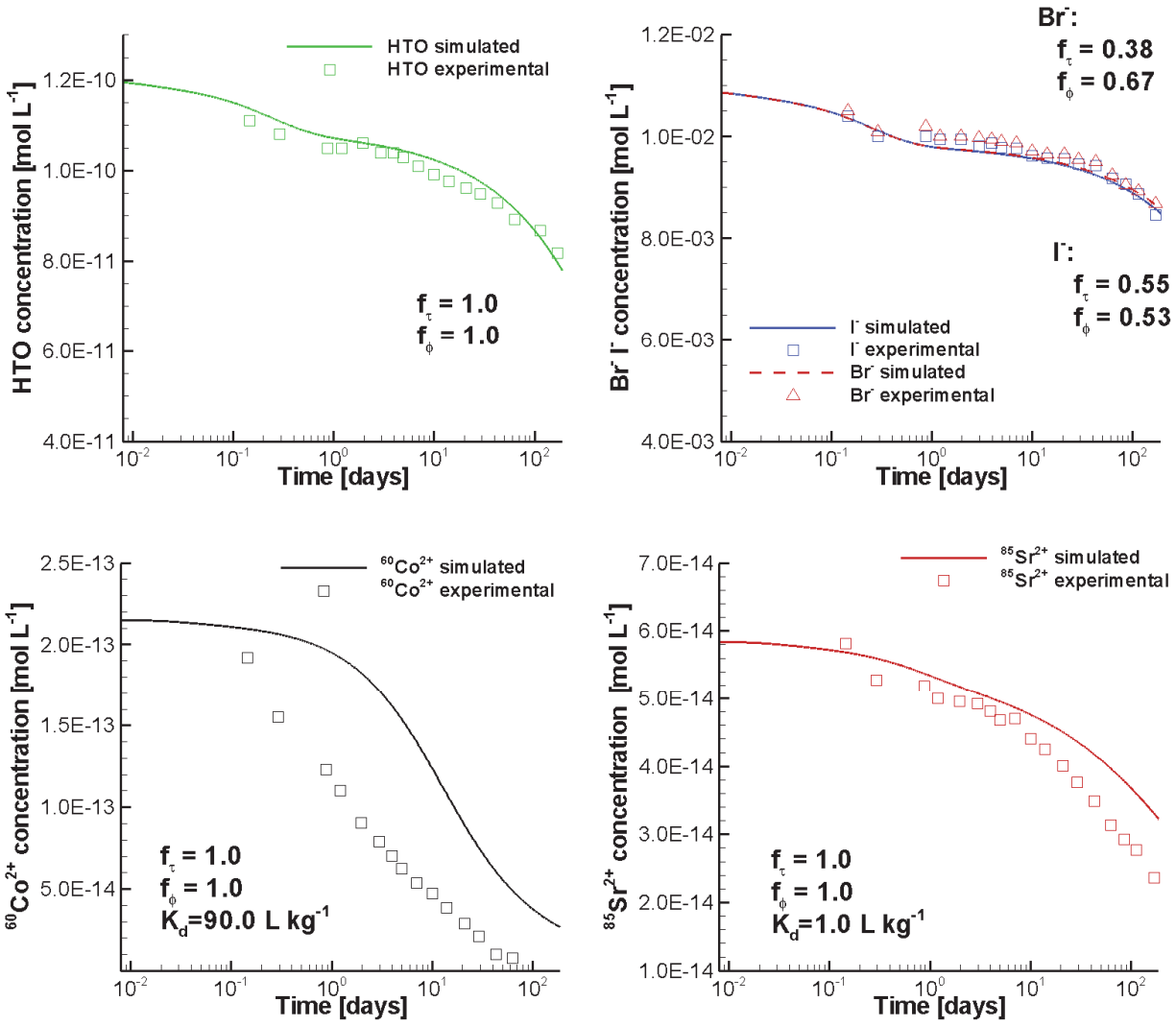

Figure 38: Comparison of Simulated (Lines) and Experimental (Symbols) Results for HTO, Br^-, I^-, $^{60}Co^{2+}$ and $^{85}Sr^{2+}$ Concentrations for the DR-A In-situ Diffusion Experiment Phase I (Task 2.2a)

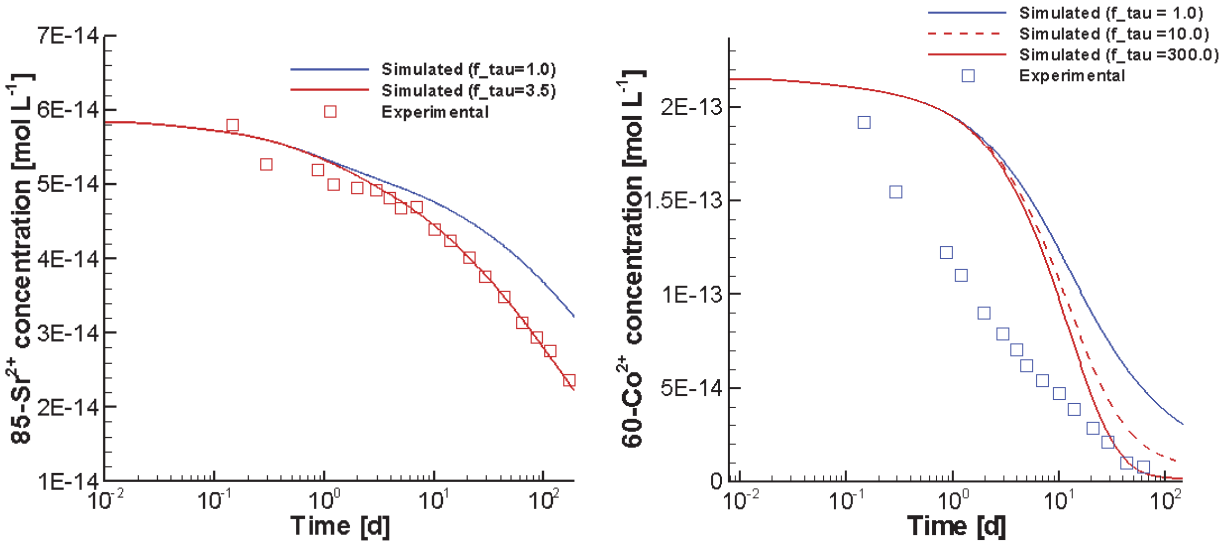

Figure 39: Sensitivity Analysis of the Effective Tortuosity Correction Factors (f_τ) in Opalinus Clay on the Diffusion of Tracers $^{85}Sr^{2+}$ (Left) and $^{60}Co^{2+}$ (Right)

5.2.2.2 Task 2.2b: Filled Gap Scenario

The results presented above in section 5.2.2.1 indicate that additional retardation for $^{60}Co^{2+}$, before it contacts the Opalinus Clay, may have been occurring. In order to explore this hypothesis, a test simulation was performed assuming that colloidal clay particles were dispersed in the solution within the gap and filter. Clay minerals tend to swell when in contact with artificial porewater during the initial stabilization phase of the experiment, which can eventually result in the dislocation and dispersion of clay minerals into the gap and, possibly, the filter, providing additional sorption capacity outside of the clay. A test simulation with the following assumptions was undertaken using MIN3P-THCm:

- Colloidal clay particles were uniformly dispersed in the solution within the gap and filter.
- In the gap and filter, colloidal clay particles exist as a solid phase. The volume fraction of colloidal clay particles (illite/smectite) in the gap was assumed to be 15%, while that in the filter is 5%. These values were chosen for illustrative purposes, i.e., to evaluate the potential effect of the presence of colloids.
- The sorption properties of the filled gap are the same as Opalinus Clay for all tracers.
- Porosity in the gap was reduced from 1.0 to 0.85, and for the filter from 0.45 to 0.40.

Simulation results for this scenario are shown in Figure 40. The simulated concentrations for the tracers HTO, Br^-, and I^- slightly change in comparison to the case of a completely open gap, owing to the effect of porosity reduction in the filter and gap. These tracers are not sorbed onto the colloidal clay particles and the presence of the collids therefore has only a minor effect on HTO and anionic tracer migration. Simulated results for the weakly sorbing tracer $^{85}Sr^{2+}$ show good agreement with the observed data, similar to the results depicted in Figure 39. For the strongly sorbing tracer $^{60}Co^{2+}$, simulated results show substantially improved agreement to the experimental data in comparison to the simulations introduced above (Figure 39), indicating that

the presence of colloids in the filter and gap provides a plausible explanation for the observed discrepancies between the data and the model.

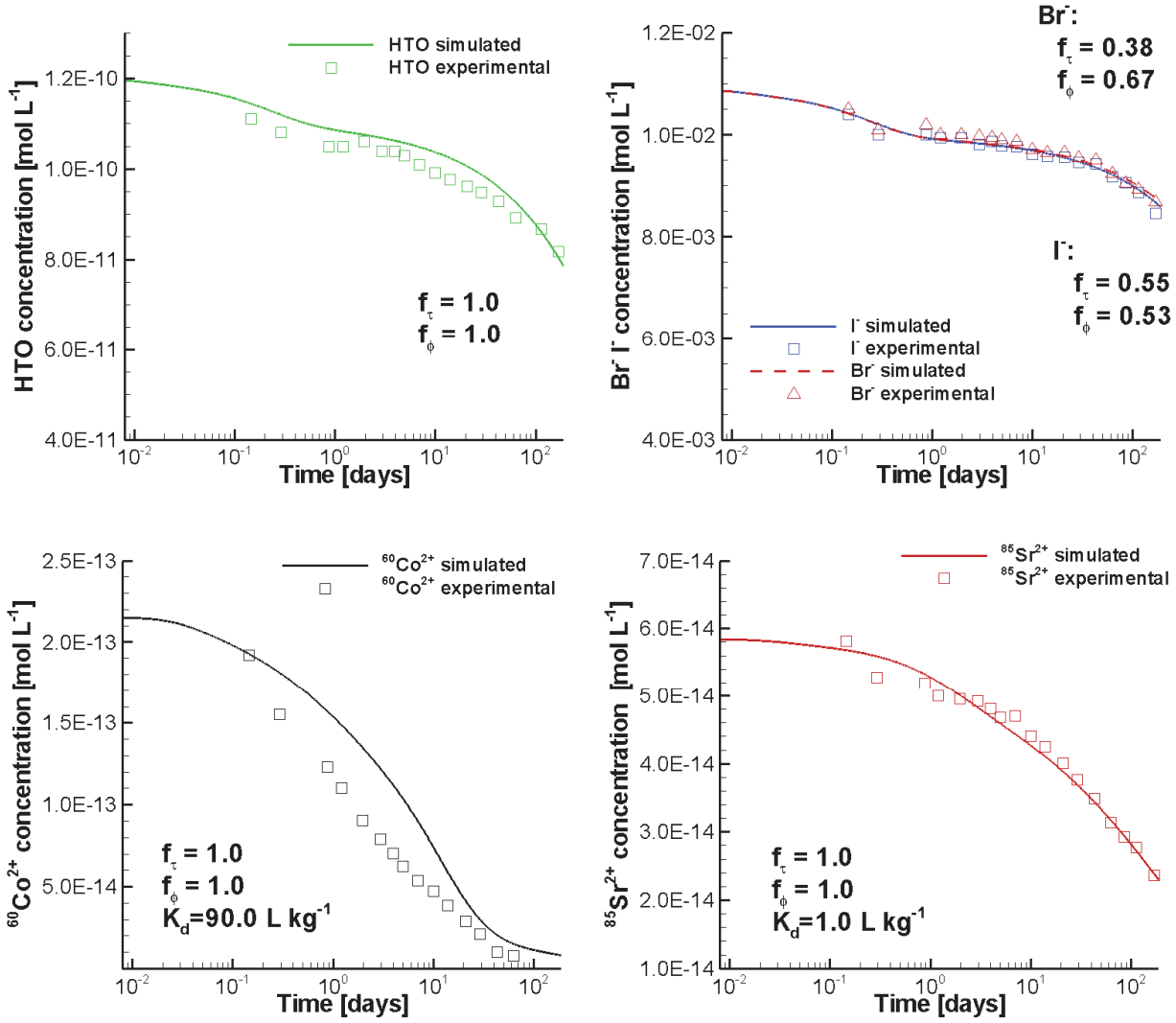

Figure 40: Comparison of Simulated and Experimental Results for HTO, Br^-, I^-, $^{60}Co^{2+}$ and $^{85}Sr^{2+}$ Concentrations for the DR-A In-situ Diffusion Experiment (Task 2.2b)

5.2.2.3 Task 2.2c: Open Gap and Surface Diffusion in Filter Scenario

Another possible mechanism for the rapid decrease in the concentrations of strongly sorbing cations at early time may be surface diffusion on the negatively charged Teflon filter, similar to surface diffusion on clay minerals. To evaluate whether this process can provide an explanation for the observed behavior, an additional simulation with the filter tortuosity increased by a factor of 15.0 was performed, while the effective porosity of the filter remained at 0.45. This implies that the effective diffusion coefficients for $^{85}Sr^{2+}$ and $^{60}Co^{2+}$ are 5.34×10^{-9} m^2 s^{-1} and 4.94×10^{-9} m^2 s^{-1}, respectively. The simulated results for $^{60}Co^{2+}$ and $^{85}Sr^{2+}$ show overall good agreement with the experimental results (Figure 41), suggesting that this process may also contribute to the observed behavior.

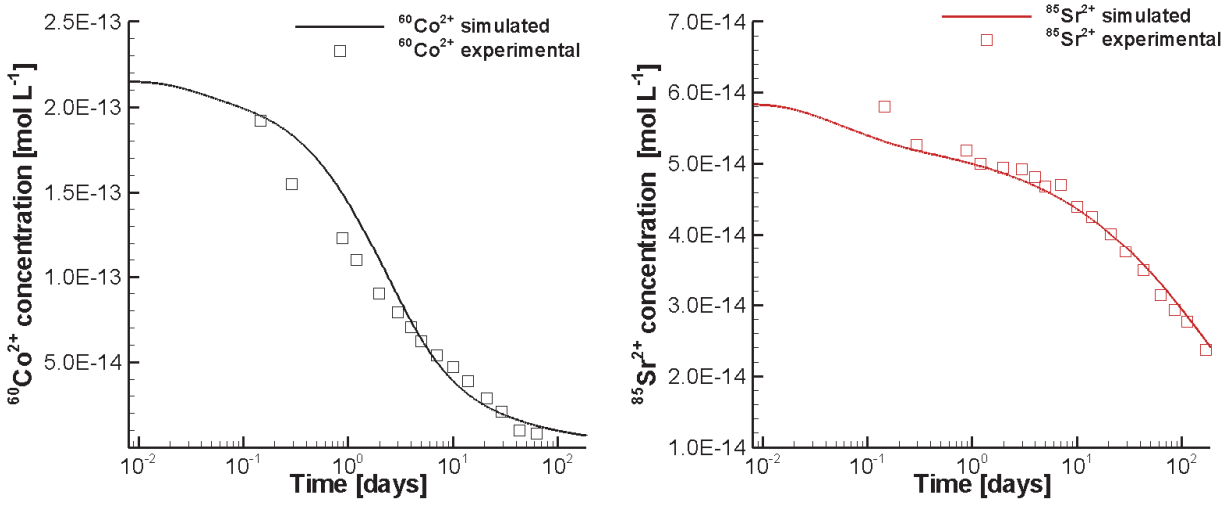

Figure 41: Comparison of Simulated and Experimental Results for $^{60}Co^{2+}$ and $^{85}Sr^{2+}$ Concentrations for the DR-A In-situ Diffusion Experiment (Case Task 2.2c) Using a Linear Sorption Approach and Surface Diffusion Through the Filter

5.2.2.4 Task 2.2d: Simulations of Cs Migration and Retardation

During the Mont Terri workshop in 2012, Gimmi (2012) and Soler (2012) reported simulation results of Cs^+ concentration evolution in the injection chamber that were significantly different than the experimental data. These simulation results had been obtained using the diffusion parameters published by van Loon et al. (2009). Therefore, to further explore the impact of these diffusion parameters, sensitivity analyses and alternative models were investigated. The following simulations report on results obtained using Case 1 as the reference case and sensitivity analyses in line with the approaches used by Gimmi (2012) (Case 2) and by Soler (2012) (Case 3). None of these three cases consider the electromigration effect. Therefore, an additional simulation was added using the hybrid multicomponent diffusion (HMD) model (Case 4).

The four cases were:

1) Case 1: Reference case, multisite ion exchange (MIE) model with parameters defined in the task description (Table 15). The free phase diffusion coefficient for Cs^+, D_0=1.0x10^{-9} m^2 s^{-1}; for clay, τ_e=0.27 and ϕ_e=0.15; for the filter, τ_e=1.0 and ϕ_e=0.45.
2) Case 2: MIE with parameters defined in the task description (Table 15), but with a literature value for the free phase diffusion coefficient for Cs^+ (D_0 = 2.06×10^{-9} m^2 s^{-1}, Lide (1994)); for clay, τ_e =0.63 and ϕ_e=0.15; for the filter, τ_e=1.0 and ϕ_e=0.45. All other parameters are as specified in the reference case. This approach results in an increased pore diffusion coefficient in Opalinus Clay (D_p =1.3×10^{-9} m^2 s^{-1}), as suggested by Gimmi (2012).
3) Case 3: MIE with parameters defined in the task description (Table 15), but with modified log K for Cs^+ on the Type II sites to the original value of -3.6 (Bradbury and

Baeyens 2000); for clay, τ_e =0.39 and ϕ_e=0.15; for the filter, τ_e=32400 and ϕ_e=0.45. All other parameters are as specified in the reference case. This simulation follows the approach by Soler (2012) and results in increased pore diffusion coefficients in the clay and filter (clay: D_p = 8.0×10^{-10} m^2 s^{-1}, filter: D_e = 3.0×10^{-5} m^2 s^{-1}). The very high pore diffusion coefficient in the filter mimics advective mixing through the filter.

4) Case 4: HMD and MIE model. When using the HMD approach, the molecular diffusion coefficients D_0 for each individual species, as listed in Table 14, are applied. The effective porosity (i.e. 0.15) and tortuosity (i.e. 0.12) of HTO from Table 20 were applied. At the same time, the effective diffusion coefficient for Cs^+ was kept the same as in Case 2 at 1.95x10^{-10} m^2 s^{-1} (Table 22) by assigning the tortuosity correction factor f_τ = 5.4, and a porosity correction factor f_ϕ = 1.0. The parameters of f_τ and f_ϕ for anions and other cations are the same as in Task2.2a.

A summary of the diffusion parameters used for the four simulation cases is provided in Table 22. Simulated time curves for Cs^+ concentrations in the borehole for the four cases are depicted in Figure 42. The simulated results of Case 2 agree better with the experimental data than those of Case 1, and show good agreement after 30 days. The D_e of Cs^+ for Case 2 is 1.95×10^{-10} m^2 s^{-1}, which is in good agreement with the reported value (approx. 10^{-10} m^2 s^{-1}) found in the previous in-situ diffusion experiment DI-A2 (Wersin et al. 2004). However, the substantial differences between simulated and measured concentrations up to about 30 days require further explanation.

Table 22: Diffusion Parameters for Cs^+ Used for the Sensitivity Cases

Case	Material	D_0 [m^2 s^{-1}]	τ_e	ϕ_e	D_p [m^2 s^{-1}]	D_e [m^2 s^{-1}]
1	Borehole	1.00×10^{-09}	100.0	3.262	1.00×10^{-07}	3.26×10^{-07}
	Filter	1.00×10^{-09}	1.0 [b]	0.45 [a]	1.00×10^{-09}	4.50×10^{-10}
	Gap	1.00×10^{-09}	1.0	1.00	1.00×10^{-09}	1.00×10^{-09}
	Clay	1.00×10^{-09}	0.27	0.15[a]	2.70×10^{-10}[a]	4.05×10^{-11}[a]
2	Borehole	2.06×10^{-09}	100	3.262	2.06×10^{-07}	6.71×10^{-07}
	Filter	2.06×10^{-09}	1.0	0.45	2.06×10^{-09}	9.25×10^{-10}
	Gap	2.06×10^{-09}	1.0	1.0	2.06×10^{-09}	2.06×10^{-09}
	Clay	2.06×10^{-09}	0.63	0.15	1.30×10^{-09}[b]	1.95×10^{-10}
3	Borehole	2.06×10^{-09}	100	3.262	2.06×10^{-07}	6.71×10^{-07}
	Filter	2.06×10^{-09}	32400	0.45	6.66×10^{-05}	3.00×10^{-05}[c]
	Gap	2.06×10^{-09}	1.0	1.0	2.06×10^{-09}	2.06×10^{-09}[c]
	Clay	2.06×10^{-09}	0.39	0.15	8.00×10^{-10}	1.20×10^{-10}[c]
4	Borehole	2.06×10^{-09}	100	3.262	2.06×10^{-07}	6.71×10^{-07}
	Filter	2.06×10^{-09}	1.0	0.45	2.06×10^{-09}	9.25×10^{-10}
	Gap	2.06×10^{-09}	1.0	1.0	2.06×10^{-09}	2.06×10^{-09}
	Clay	2.06×10^{-09}	0.12	0.15	2.47×10^{-10}	1.95×10^{-10}[d]

[a]Task definition; [b]Gimmi (2012); [c]Soler (2013); [d] D_e=f_τ $\tau_e f_\phi$ $\phi_e D_0$

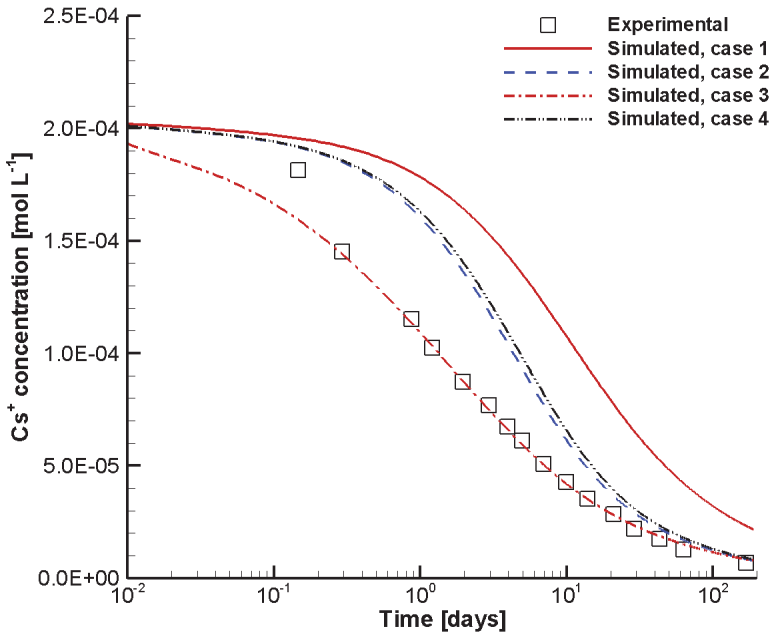

Figure 42: Comparison of Experimental and Simulation Results for Cs^+ Concentrations - DR-A In-situ Diffusion Experiment (Task 2.2d)

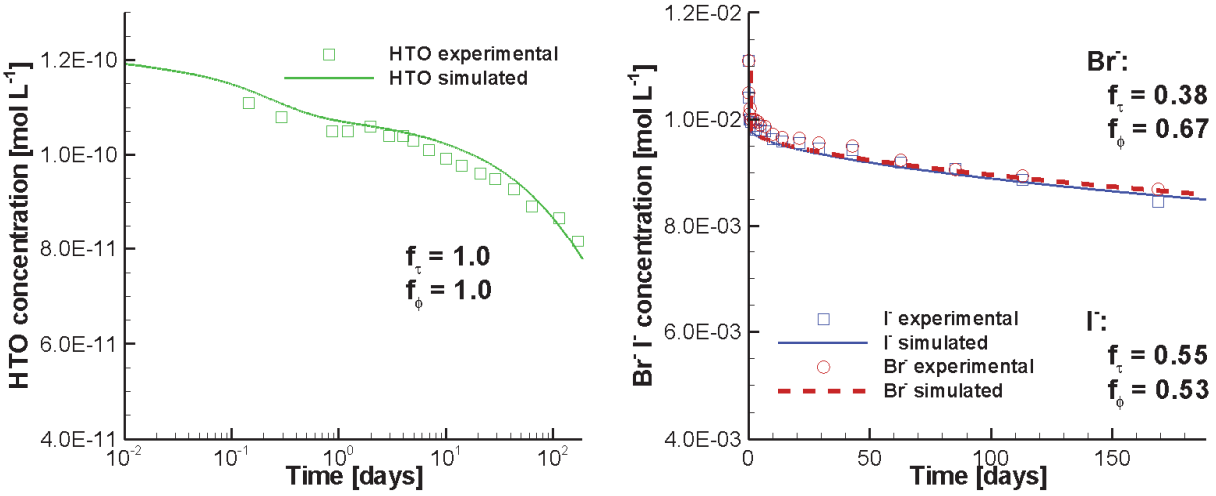

Figure 43: Comparison of Experimental and Simulated Concentration Time Curves for HTO (left), Br^- and I^- (right) - DR-A Field Diffusion Experiment Phase I (Task 2.2d Case 4)

The approach used for Case 3 shows much better agreement between observed and simulated data. The good agreement was obtained due to the extremely high value of D_e (3×10^{-5} m^2 s^{-1}) for the filter, mimicking advective mixing. This approach mimics rapid migration of Cs^+ through the filter induced by fluid migration in the circulation chamber, which leads to a rapid decrease of Cs^+ concentration in the borehole. The simulated Cs^+ concentration time curve in the borehole for Case 4 is very close to that for Case 2 (Figure 42). The calculated time curves for HTO, Br^- and I^- all show good agreement to the experimental data (Figure 43), very similar to

the results obtained in Task2.2a. For HTO, this is expected, because HTO is uncharged and non-sorbing, and thus the migration is solely controlled by Fickian diffusion. The good agreement of simulation results for the anions between Task 2.2a and Task 2.2d (Case 4), suggests that electrochemical effects are of limited relevance for anion migration.

5.2.2.5 Task 2.2e: Simulations of Eu Migration and Retardation

The simulation invoking the Eu-Teflon surface complexation model (SCM), as introduced in section 4.3, was conducted to explore the potential of this retardation mechanism to reproduce the observed behavior of Eu^{3+}. The main model parameters are listed in Table 17 to Table 19. For comparison, a similar simulation without Eu-Teflon surface complexation was conducted. The simulations demonstrate that sorption of Eu onto Teflon can reproduce the rapid decrease in Eu^{3+} concentration in the borehole and, overall, good agreement is achieved with the experimental data (Figure 44). The disagreement between observed and simulated data at very early time may be due to kinetic limitations and/or incomplete mixing within the circulation chamber and sampling apparatus during sample collection. On the other hand, assuming conservative transport through the filter does not reproduce the observed behavior (Figure 44). These results suggest that Eu sorption directly onto the filter, or onto clay particles trapped in the filter, may provide an explanation for the observed behavior.

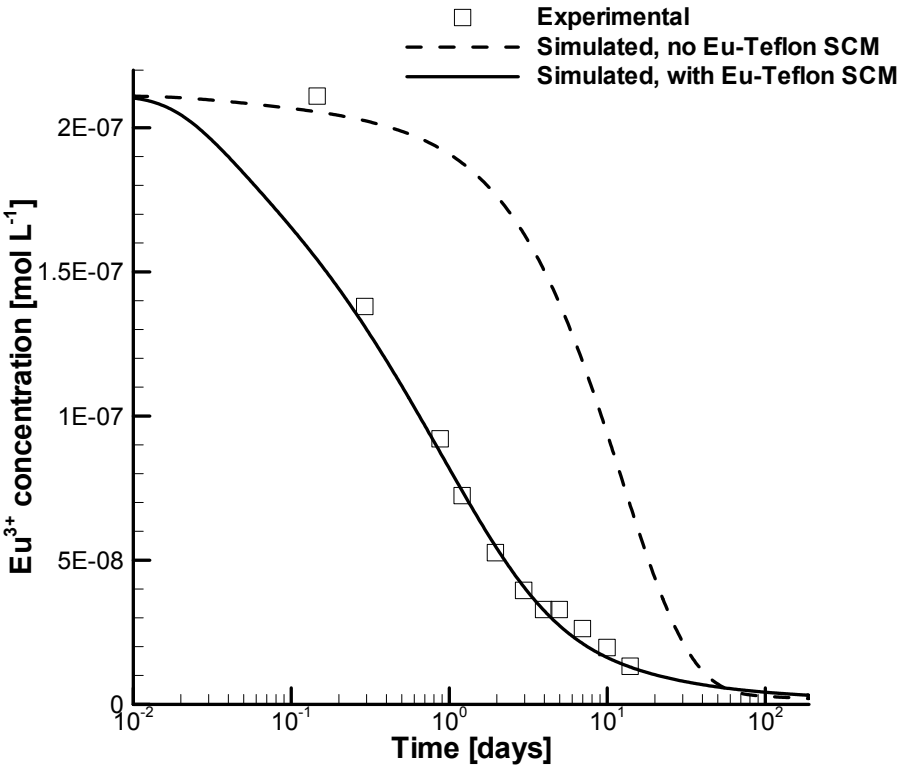

Figure 44: Comparison of Measured and Simulated Eu^{3+} Concentrations in the Borehole for Models with and without Eu Sorption onto the Teflon Filter (Task 2.2e)

5.2.2.6 Task 2.2f: Parameter optimization using PEST for the simulation of Cs

The software PEST (Doherty 2010) was used in combination with MIN3P-THCm for the simulation of Cs^+ to further optimize model fits and model parameters. Three scenarios were considered: (1) Open gap scenario; (2) Filled gap scenario; and (3) Filled gap and filter scenario.

Based on Task 2.2d, the open gap scenario was optimized for two parameters – the effective porosity correction factor (f_ϕ) and the effective tortuosity correction factor (f_τ). The simulated Cs^+ concentration evolution in the borehole is depicted in Figure 45. The optimized parameters are f_ϕ=1.0, which corresponds to the lower limit of the optimization range, and f_τ=20.0, which corresponds to the upper limit of the optimization range. However, using this approach, good agreement with the experimental data could not be obtained.

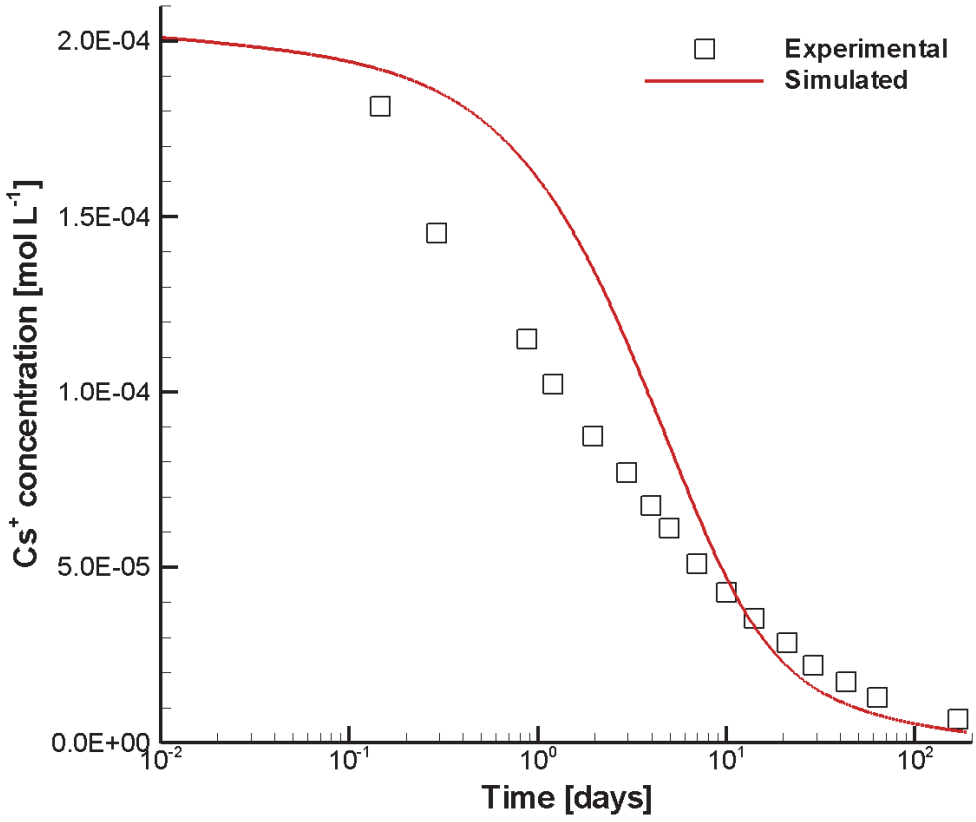

Figure 45: Comparison of Experimental and Simulated Cs^+ Concentration Time Curves Using MIN3P-THCm and PEST for the Open Gap Scenario (Task 2.2f)

The filled gap scenario involved optimization of f_ϕ, f_τ, and the volume fraction of colloidal clay in the gap. The optimized parameters are: f_ϕ=2.0, f_τ=4.77, and a clay volume fraction in the gap of 19.4%. The simulated results with the optimized parameters are compared to the experimental data in Figure 47, which shows good agreement after 5 days. However, the rapid decrease in Cs^+ concentrations at early times could not be reproduced using this approach.

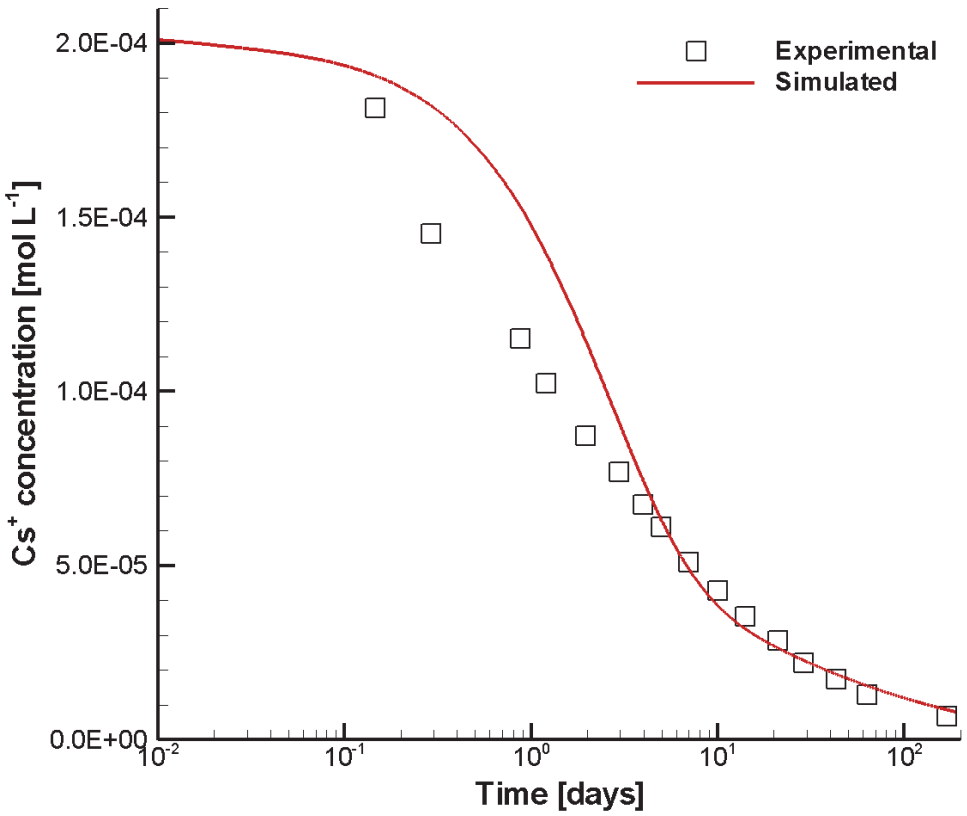

Figure 46: Comparison of Experimental and Simulated Cs^+ Concentration Time Curves Using MIN3P-THCm and PEST for the Filled Gap Scenario (Task 2.2f)

The filled gap and filter scenario assumed that the filter is partially filled with colloidal clay, similar to the scenario for $^{60}Co^{2+}$. For this simulation, an additional parameter was included in the parameter optimization, i.e., the clay volume fraction in the filter. The optimized parameters are: f_ϕ=1.54, f_τ=7.6, and clay volume fractions in filter and gap are 6.2% and 7.0%, respectively. The simulated results with the optimized parameters are compared to the experimental data in Figure 47, which shows very good agreement after 0.29 days. The mismatch at early time may be due to kinetic limitations of sorption reactions. These results suggest that the presence of colloidal clay particles in the gap and filter may provide a plausible explanation for the observed behavior. It is important to point out that colloidal particles were neither visually observed nor measured during the experiment, and that this scenario remains a hypothesis. Considering the substantial fraction of clay minerals and swelling properties of the Opalinus Clay, and the relatively low salinity of the Opalinus Clay porewater (ionic strength = 0.35 mol L^{-1} according to Bossart (2013)), there is a possibility that clay particles could be dispersed through the swelling process from the unsupported drill hole wall during the test preparation and operation period. It is also noteworthy that a filter was also used to prevent clogging of the circulation pump in the in-situ DI diffusion experiment (Palut et al. 2002). Clogging of the filter was believed to be one of the reasons for the dispersion of measured tracer concentrations in the DI-B in-situ experiment (Yi et al. 2012).

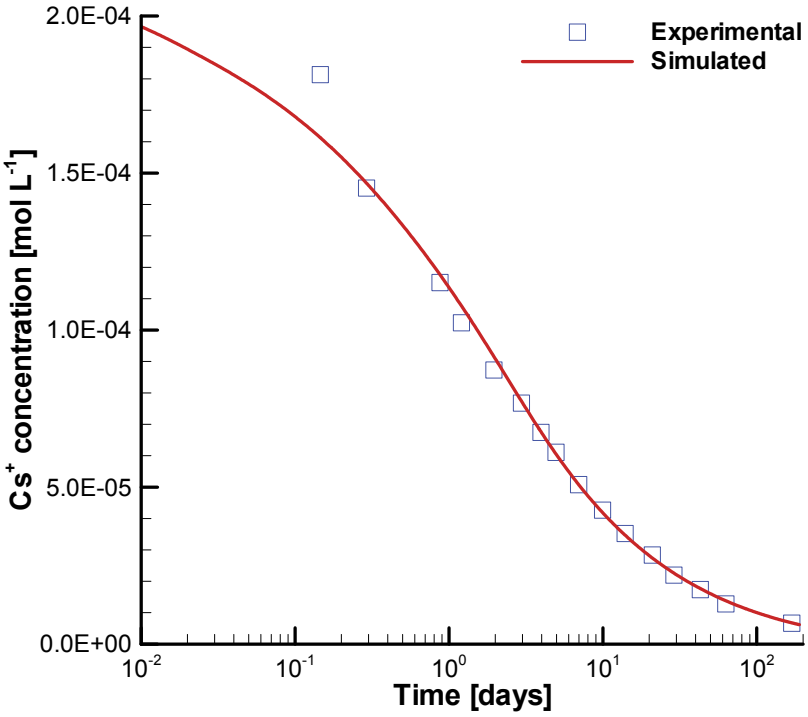

Figure 47: Comparison of Experimental and Simulated Cs^+ Concentration Time Curves Using MIN3P-THCm and PEST for the Filled Gap and Filter Scenario (Task 2.2f)

The parameter optimization simulations illustrate that the scenarios with dispersed colloidal clay particles in the filter and gap are able to reproduce the rapid concentration decrease of Cs^+ at early time. These simulations emphasize the importance of the filter properties on the early time behavior of sorbing cations in the experiment. However, the long-term influence of the filter appears limited, which agrees with the findings of other modelling teams (Gimmi 2012; Soler 2013).

5.3 TASK 3.1: SIMULATION OF DR-A EXPERIMENT − PHASE II

The simulations for Phase II of the DR-A in-situ diffusion experiment included three parts:

1) Direct extension of the simulations from Phase I using the estimated parameters from Task 2.2, and replacing the circulation solution in the borehole with the higher ionic strength solution shown in Table 10.

2) Recalibration of the effective porosity and tortuosity of the OPA for Phase II of the in-situ diffusion experiment. Using different transport parameters during Phase I and Phase II is justified because the replacement of the dilute borehole solution with a highly saline solution (compare Table 8 to Table 10) will tend to decrease the thickness of the diffuse double layer on the clay surface (Xie et al. 2004; Wersin et al. 2004). As a result, it is expected that the effective porosity and tortuosity of the Opalinus Clay for HTO and anions will increase during

Phase II. For cations, however, surface diffusion through the DDL will become inhibited. These processes are dynamic and closely related to the diffusion processes of the major ions in clay and can only be accurately accounted for by using the diffuse double layer model (Appelo and Wersin 2007). Such a model is currently not available in MIN3P-THCm, but may be implemented in the future. At the current stage, constant effective porosities and tortuosities were assigned at the time of the solution replacement.

3) In the simulations of Task 2.2, the tracers $^{60}Co^{2+}$ and $^{85}Sr^{2+}$ were simulated using a simple linear sorption model, while Cs^{+} was simulated using a multisite ion exchange model. Therefore, two separate simulations were undertaken to account for the different retardation models for Task 3.1: i) $^{60}Co^{2+}$, $^{85}Sr^{2+}$, HTO, Br^{-} and I^{-} using a simple linear sorption model; and ii) Cs^{+} using a multisite ion exchange model.

5.3.1 Task 3.1a Direct EXTENSION of PHASE I Simulations

5.3.1.1 Simulations for $^{60}Co^{2+}$, $^{85}Sr^{2+}$, HTO, Br^{-}, and I^{-}

Simulations for $^{60}Co^{2+}$ and $^{85}Sr^{2+}$were based on the open gap scenario described in Section 5.2.2.1 and Figure 39. A linear sorption model with the same parameters as those used for the simulations for Phase I of the diffusion experiment were adopted. This case used an effective tortuosity correction factor (f_τ) of 3.5 for $^{85}Sr^{2+}$ and f_τ of 10 for $^{60}Co^{2+}$. This case is selected as a foundation for the present simulation because it was used as the reference case for Phase I. Figure 48 shows that simulated concentrations of HTO, Br^{-} and I^{-} during the Phase II (after 189 days) remain higher than the observed data, while concentrations of $^{85}Sr^{2+}$ show very good agreement immediately after replacement of the borehole solution, but tend to trend lower beyond 10 days of the Phase II diffusion experiment. Simulated results for $^{60}Co^{2+}$ were relatively consistent with observed results (Figure 48).The concentration of the strongly sorbing $^{60}Co^{2+}$ in the borehole was very low and fell below the detection limit after about 70 days (Table 9). For the Phase II experiment, $^{60}Co^{2+}$ was not added to the borehole circulation solution. However, simulated results show the reappearance of low concentrations of $^{60}Co^{2+}$ in the borehole during this phase. This behavior can be explained by the presence of sorbed $^{60}Co^{2+}$ on the OPA Clay as a result of the Phase I experiment, which desorbs and diffuses back into the borehole during Phase II.

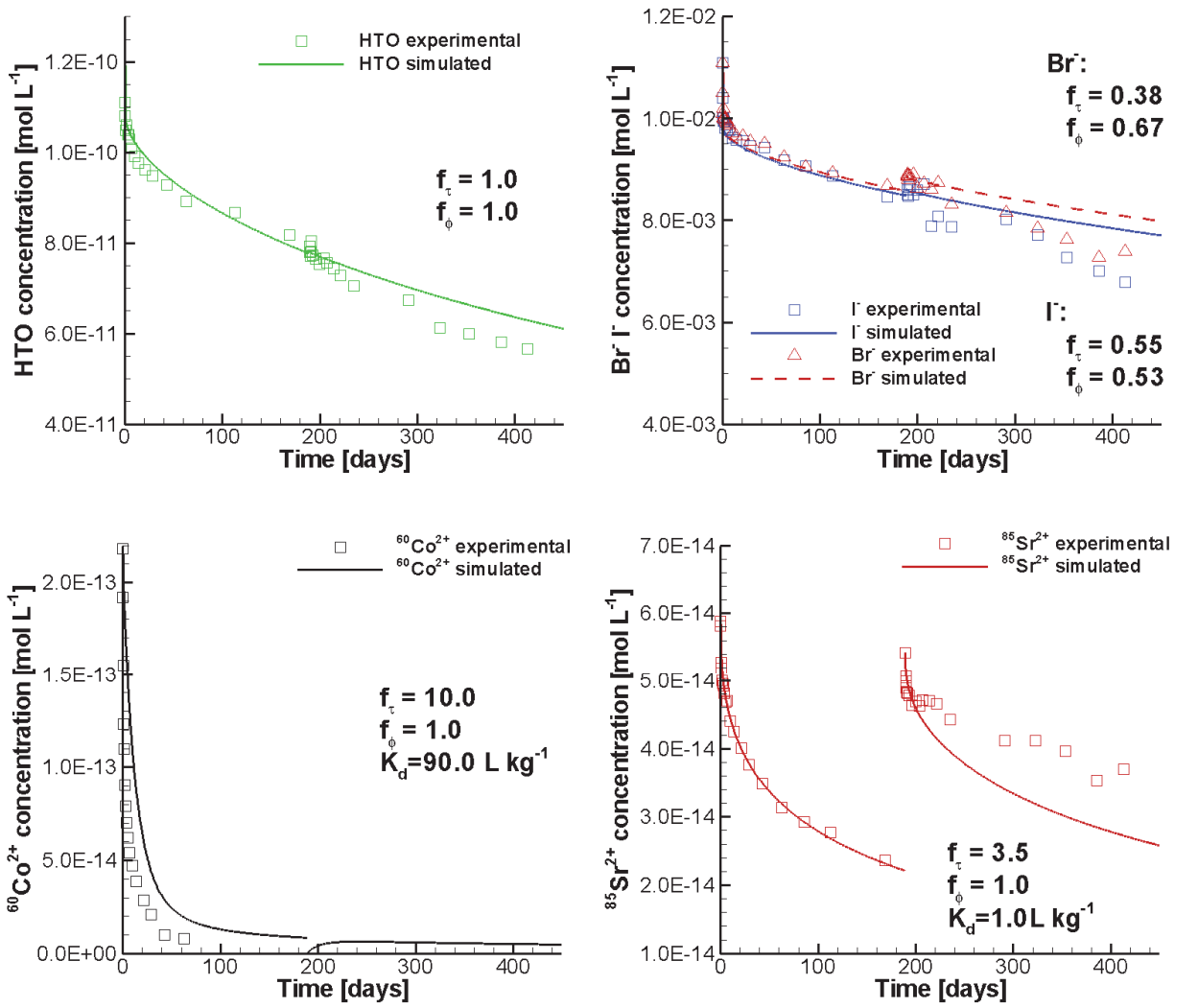

Figure 48: Comparison of Simulated and Experimental Results for HTO, Br^-, I^-, $^{60}Co^{2+}$ and $^{85}Sr^{2+}$ Concentrations for the DR-A In-situ Diffusion Experiment - Phase I and II (Task 3.1a)

5.3.1.2 Simulation for Cs^+

An extension of the simulation for Cs^+ was undertaken on the basis of Task 2.2d, Case 4, as described in Section 5.2.2.4 through the replacement of the chemical composition of the borehole solution, while retaining all parameters from Task 2.2d. For the simulation, the hybrid multicomponent diffusion model and the three-site ion exchange model for Cs were used.

The parameters f_τ and f_Φ were set to 5.4 and 1.0. Simulated results are depicted in Figure 49 and show an overall good agreement with the observational data during the second phase of the diffusion experiment. The simulated results indicate that a fraction of Cs^+ adsorbed onto the clay surface became displaced and diffused back into the borehole owing to the elevated concentrations of K^+, Na^+ and Ca^{2+} in the saline borehole solution (Figure 50). The concentration of Cs sorbed on the most abundant Type-II sites by the end of Phase I (Figure 50

left) decreases substantially after only one day of the Phase II diffusion experiment (Figure 50 right). The concentrations of Cs sorbed on the other two sites, Cs-FES and Cs-PS, also decrease near the borehole interface.

Reusing the same parameters as calibrated for Phase I qualitatively produces the trends observed in the experiment; however, it appears that systematic deviations exist. These results suggest that the transport parameters (i.e., effective porosity and effective tortuosity) of the OPA are modified, as expected, due to contact with the saline borehole solution with high ionic strength.

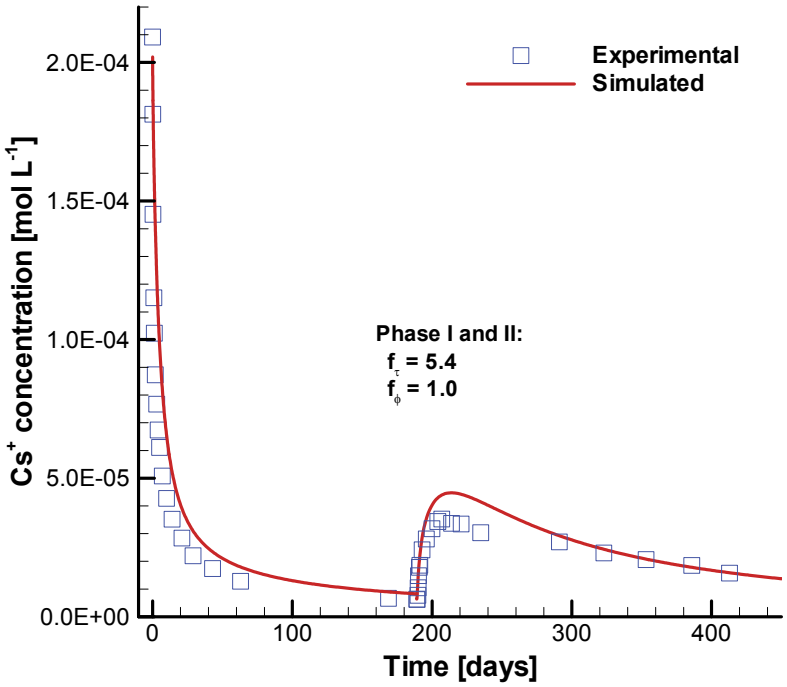

Figure 49: Comparison of Simulated and Experimental Results for Cs^+ Concentrations for the DR-A In-situ Diffusion Experiment - Phase I (Case 4 of Task 2.2d) and Phase II (Task 3.1a)

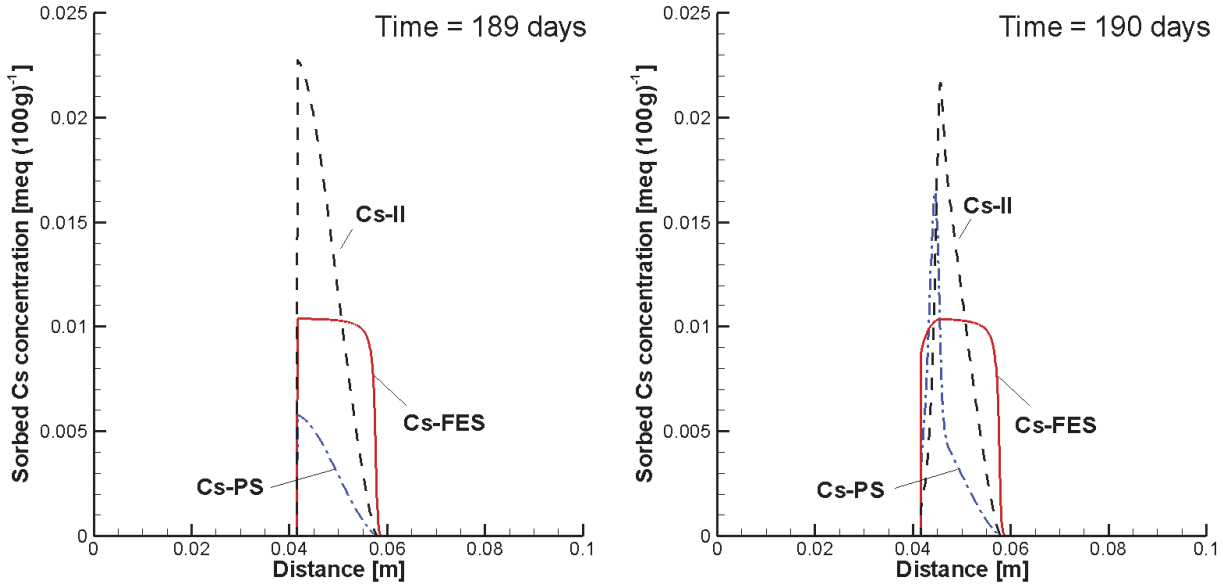

Figure 50: Simulated Sorbed Cs^+ Concentration Profiles at the End of Phase I (189 days Left) and One Day after the Initiation of Phase II (190 days, Right)

5.3.2 Task 3.1b: Sensitivity Analysis

Building on the extended simulations, the effective porosity and tortuosity of the OPA were recalibrated using the measured HTO concentration time curve during the second phase of the diffusion experiment. The best fit values for the effective porosity and effective tortuosity were 0.19 and 0.15, respectively. Both values are greater than those calibrated for the Phase I simulations, consistent with the hypothesis that a reduction of the DDL thickness enhances transport properties for HTO and the anions Br^- and I^-.

5.3.2.1 Simulations for $^{60}Co^{2+}$, $^{85}Sr^{2+}$, HTO, Br^-, and I^-

The simulated concentration profiles for $^{60}Co^{2+}$, $^{85}Sr^{2+}$, HTO, Br^-, and I^- are depicted in Figure 51. To obtain a better fit, the effective tortuosity factors (f_τ) for cations had to be decreased from 10.0 to 3.0 for $^{60}Co^{2+}$, and from 3.5 to 0.5 for $^{85}Sr^{2+}$, which can be explained by increased porosities and tortuosities and an associated decrease of surface diffusion.

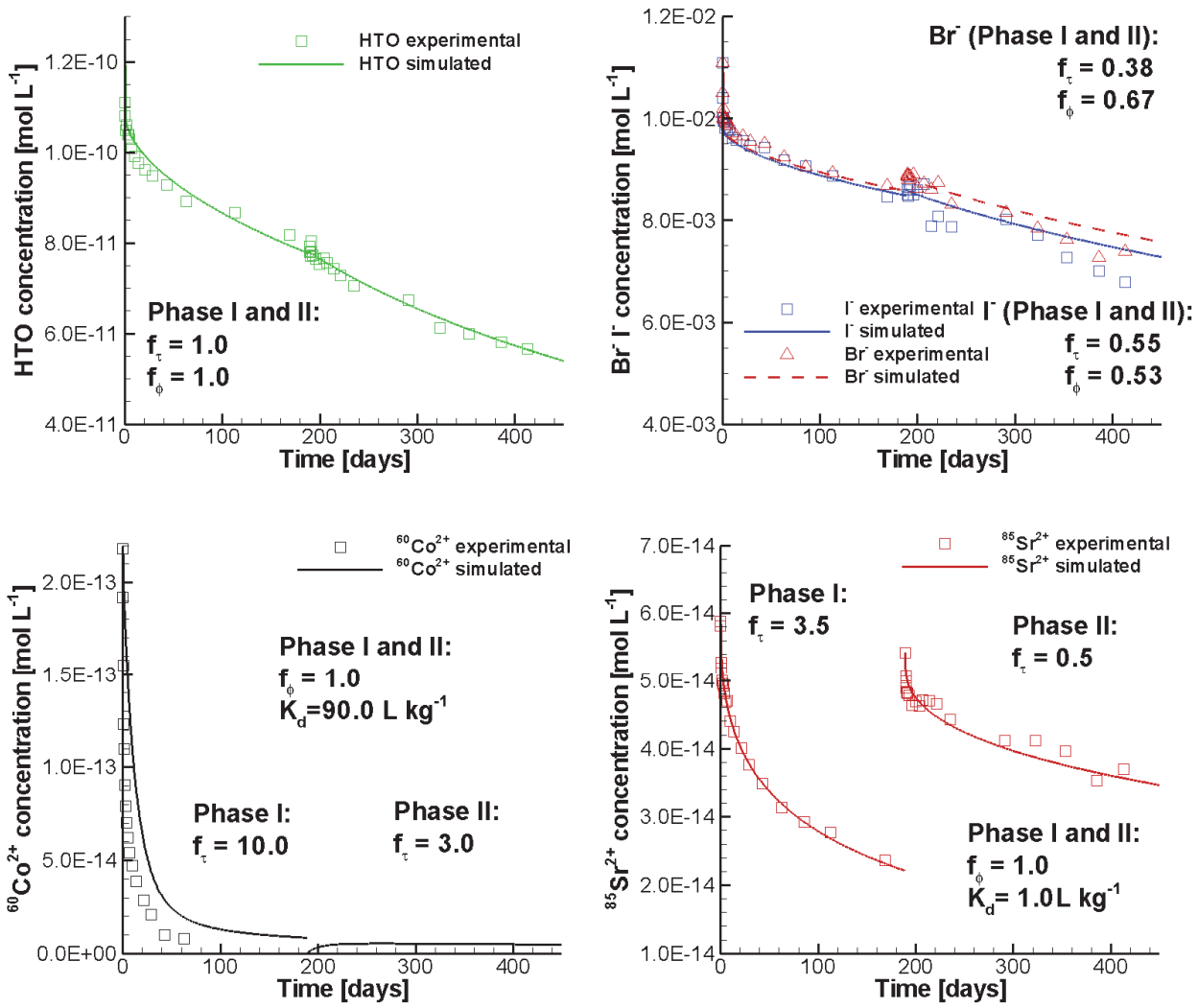

Figure 51: Comparison of Simulated and Experimental Results for HTO, Br^-, I^-, $^{60}Co^{2+}$ and $^{85}Sr^{2+}$ Concentrations for the DR-A In-situ Diffusion Experiment - Phase I and Phase II (Case Task 3.1b) after Increasing the Effective Porosity of the Opalinus Clay to 0.19 and the Effective Tortuosity to 0.15, and Modifications of f_τ for $^{60}Co^{2+}$ and $^{85}Sr^{2+}$

5.3.2.2 Simulations for Cs^+

The simulated Cs^+ concentration evolution is depicted in Figure 52. The simulation results for the concentration profiles of tracers and major ions in the porewater, as well as adsorbed species for the Phase I experiment in Task 2.2d Case 4, were used as the initial conditions. For the simulation of Phase II, the diffusion parameters (i.e. the effective diffusion coefficient and tortuosity of Opalinus Clay) were adjusted in the same way as for the previous simulations (i.e. ϕ_e is increased from 0.15 to 0.19, τ_e is increased from 0.12 to 0.15). If f_τ remains at 5.4 as it was for Phase I, the simulated results are closer to the experimental data during early time of Phase II, but start to deviate after about 280 days in comparison to the direct simulation as described

in Section 5.3.1.2. By decreasing f_τ from 5.4 to 2.0 for Cs^+, simulated results agree very well with the experimental data (Figure 52). For the major cations Na^+, K^+, Ca^{2+}, and Mg^{2+}, an slight increase of f_ϕ from 1.0 to 1.28 was required to improve the model fit. Using this approach, simulated concentration time curves for most major ions show good agreement with the observed data (Figure 53). This can be explained by a variation of diffusion parameters in the OPA caused by an ionic strength increase that is restricted to the region near the borehole interface, which is not considered in the current simulations.

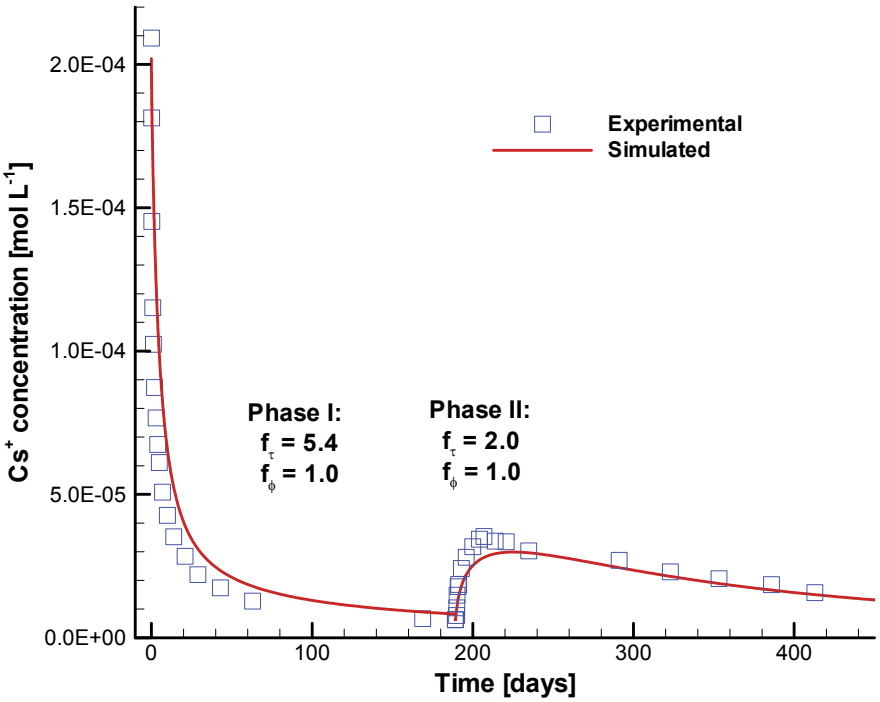

Figure 52: Comparison of Simulated and Experimental Results for Cs^+ Concentrations for the DR-A Field Diffusion Experiment - Phase I and Phase II (Case Task 3.1b) after Increasing the Effective Porosity of the Opalinus Clay to 0.19 and the Effective Tortuosity to 0.15

In the simulation, the multisite ion exchange model was applied together with the hybrid multicomponent diffusion model. This approach captures the interactions of tracer elements as well as major ions through ion exchange, different diffusion rates for the various species owing to individual D_0, and the local charge balance in the whole system. Therefore, the simulated concentration time curves for major ions showed good agreement to the experimental data, with the exception of Mg^{2+}, reflecting the perturbation by changing the circulation solution to a solution with much higher concentrations of Cl^-, Na^+ and K^+ and a much lower concentration of SO_4^{2-} (Figure 53).

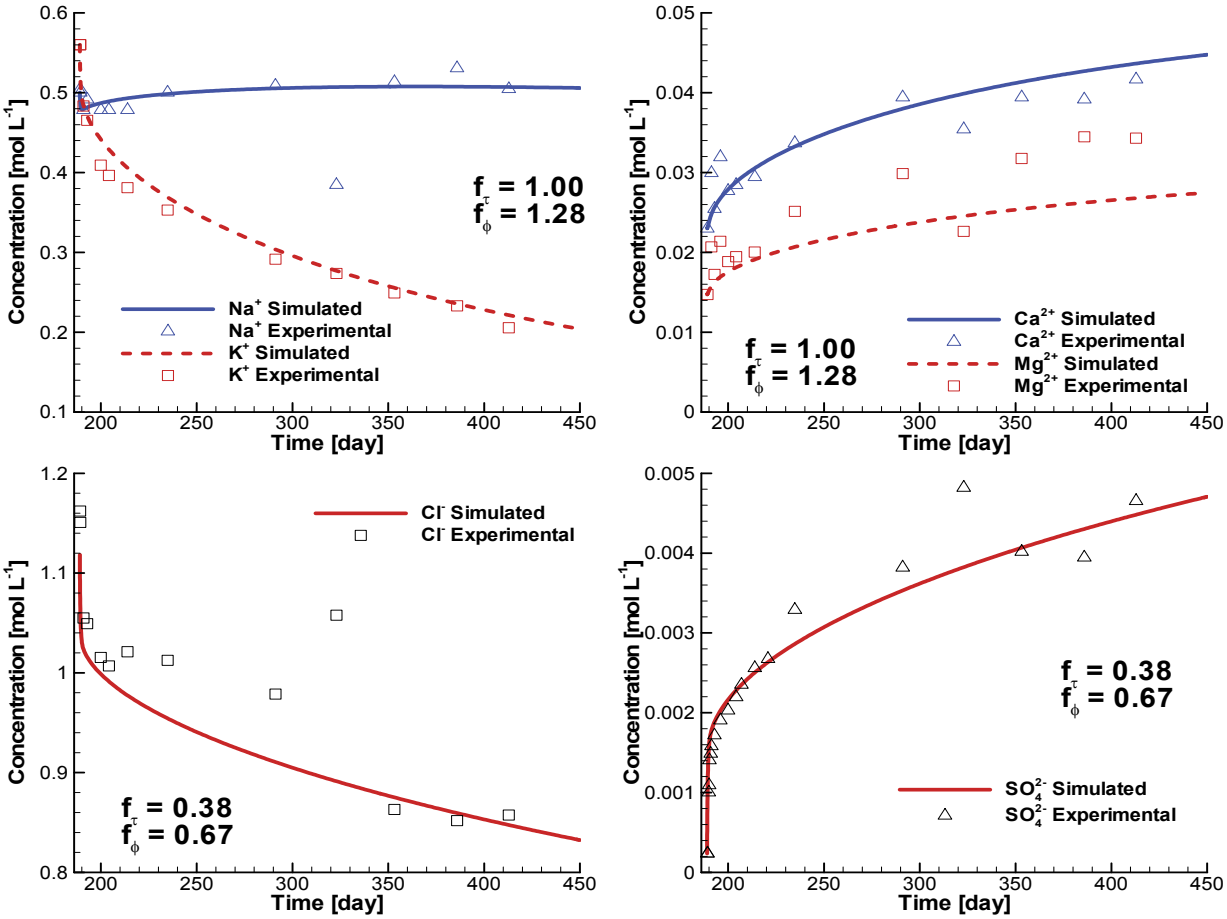

Figure 53: Comparison of Simulated and Experimental Results for Major Ion Concentrations for the DR-A In-situ Diffusion Experiment - Phase I and Phase II (Case Task 3.1b) after Increasing the Effective Porosity of the Opalinus Clay to 0.19 and the Effective Tortuosity to 0.15

5.4 TASK 3.2: SIMULATION OF DR-A EXPERIMENT − OVERCORING

The simulations taking into consideration the experimental results from the overcored Opalinus Clay samples were undertaken in two steps. In the first step (Task 3.2a), the simulations for the DR-A experiment Phase II were extended (from Task 3.1a) until the overcoring event (728 days). In the second step (Task3.2b), back diffusion from the OPA formation into the borehole due to the presence of Opalinus Clay formation water (Table 8) was included from 728 to 735 days. The simulations for both steps included two calculations using different retardation models: i) a linear adsorption model with constant K_d for $^{60}Co^{2+}$, and $^{85}Sr^{2+}$; and ii) the multisite ion exchange model for Cs^+. All simulations used the calibrated diffusion parameters as provided in Task 3.1b.

5.4.1 Task 3.2a: Extended Simulations Using the Optimized Parameters from Phase II

5.4.1.1 Simulations for $^{60}Co^{2+}$, $^{85}Sr^{2+}$, HTO, Br^-, and I^-

Simulated concentration time curves for HTO, Br^-, I^-, $^{60}Co^{2+}$ and $^{85}Sr^{2+}$ in the borehole circulation solution are depicted in Figure 54. These results show very good agreement to the

experimental data up to 728 days, even though the calibration of material and diffusion parameters was performed based on a more limited set of the experimental data (only until 413 days). This result provides confidence in the predictive capabilities of the simulation approach.

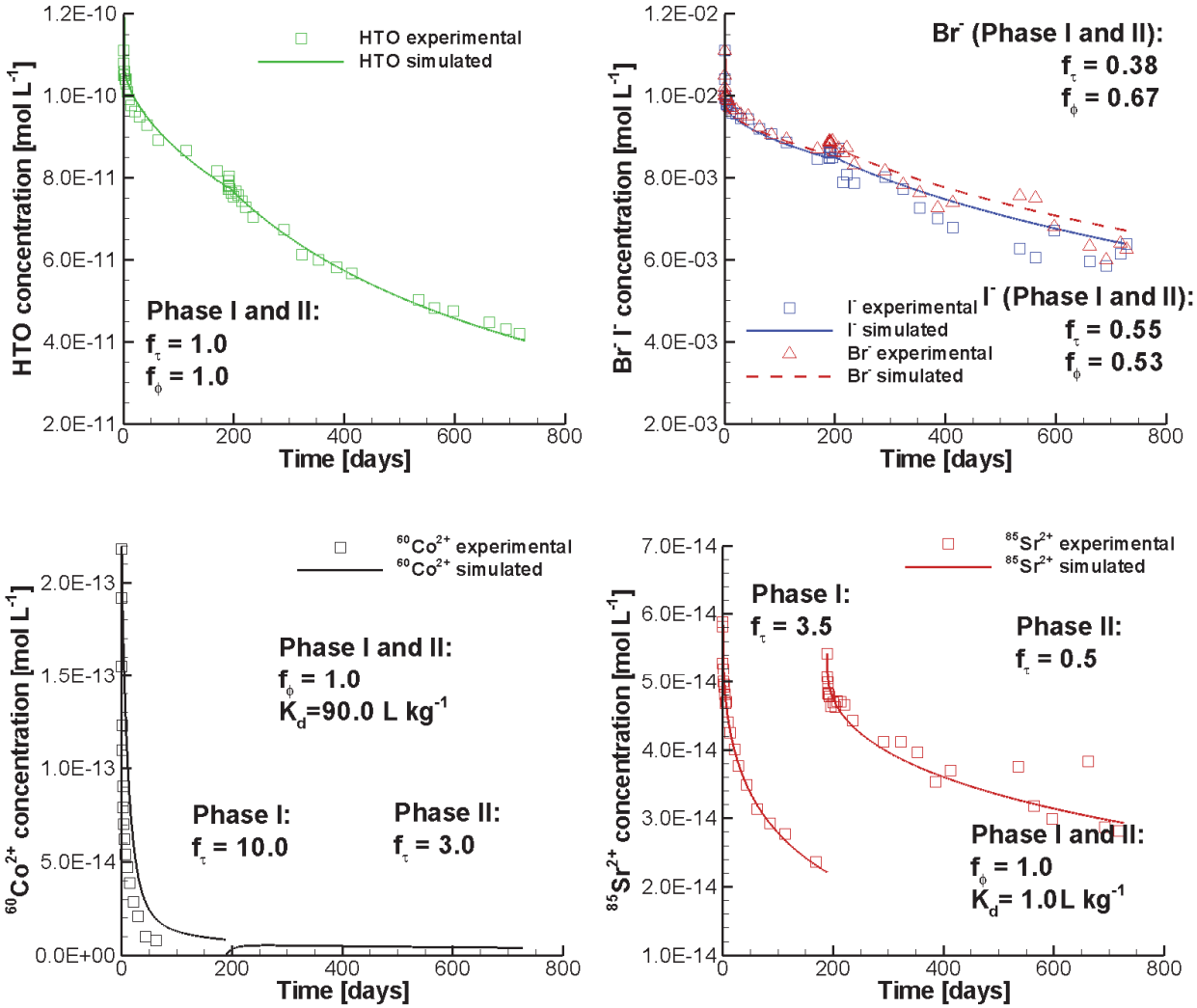

Figure 54: Comparison of Simulated and Experimental Results for HTO, Br^-, I^-, $^{60}Co^{2+}$ and $^{85}Sr^{2+}$ Concentrations for the DR-A In-situ Diffusion Experiment - from the Start until Overcoring (728 days) (Case Task 3.2a) based on Task 3.1b

The simulated total concentration (including both aqueous and sorbed species) profiles of HTO, $^{60}Co^{2+}$, Br^-, Sr^{2+}, I^-, and Cl^- in the Opalinus Clay at 728 days are depicted in Figure 55. Experimental data was not available for aqueous Sr^{2+} but was available for the sorbed Sr species (Section 4.2 and Figure 14). Figure 56 displays the concentration profiles of the adsorbed species $^{60}Co^{2+}$ and Sr^{2+}. Simulated results show good agreement to the experimental data (i.e. total concentration profiles for HTO, Br^-, I^-, Cl^-, Figure 55; concentration profile for adsorbed species Sr^{2+}, Figure 56), except for the region extending from r = 0.0416 m (borehole wall) to about 0.08 m (Figure 55). Within this region, the experimental results consistently

indicate back diffusion towards the borehole compared to the predicted profiles at 728 days. This process together with the apparent discrepancy of the simulated and experimental results of cobalt will be discussed in Task3.2b.

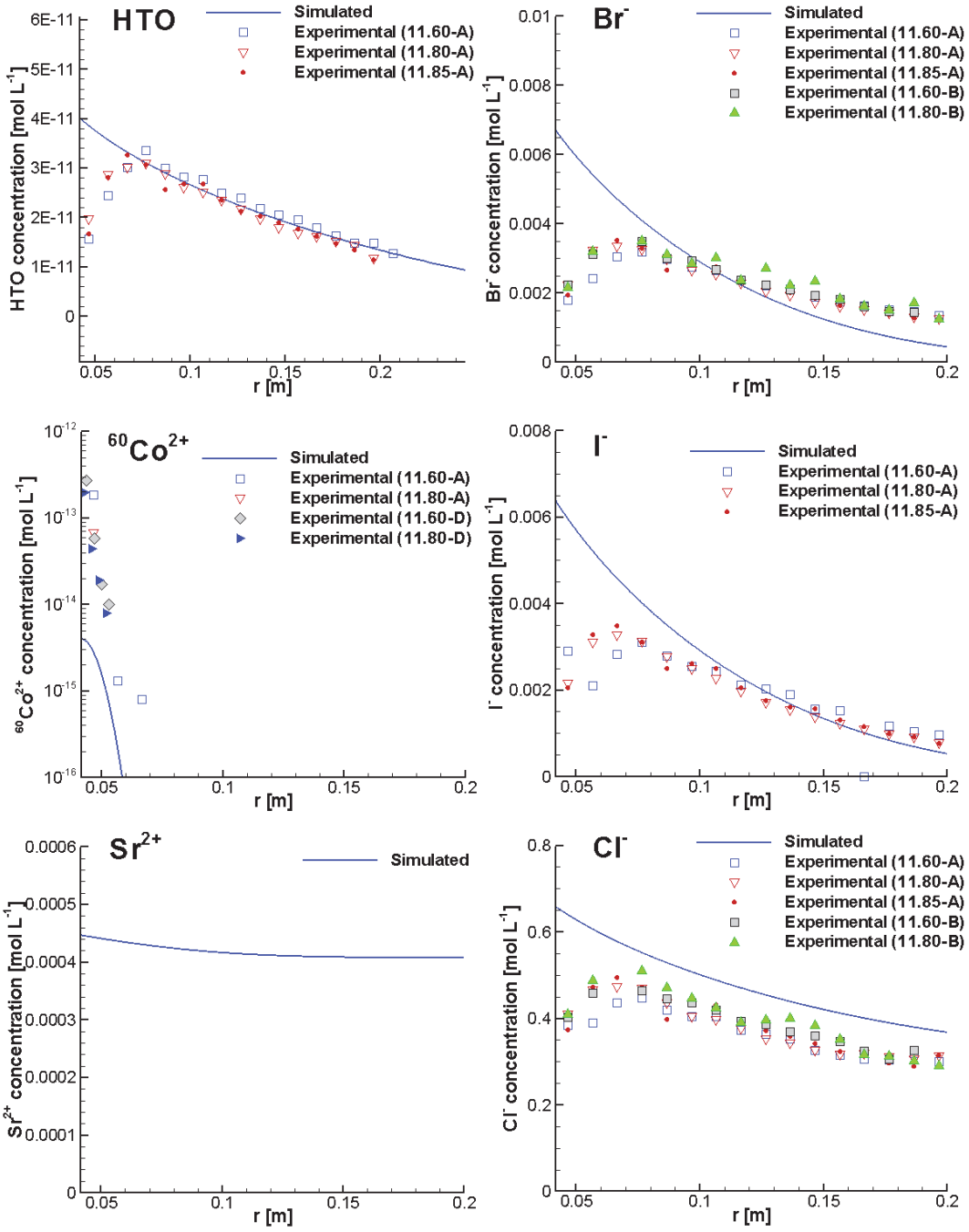

Figure 55: Simulated Total Concentration Profiles for HTO, $^{60}Co^{2+}$, Br^-, Sr^{2+}, and Cl^- in the Opalinus Clay at 728 days and Comparison to the Experimental Total Concentration Profiles in the Porewater of the Overcored Opalinus Clay Samples at 735 Days

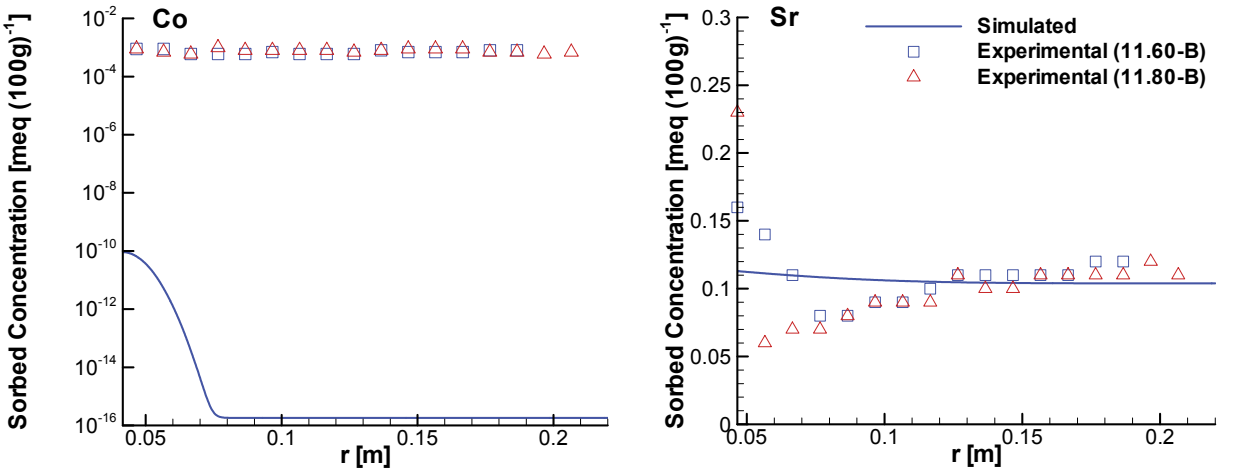

Figure 56: Simulated Concentration Profiles of Adsorbed Species (Co and Sr) at 728 Days and Comparison to the Experimental Data in the Overcored Opalinus Clay Samples at 735 Days

5.4.1.2 Simulations for Cs^+

Simulated aqueous concentration time curves for Cs^+ and the major ions are depicted in Figure 57 and Figure 58, respectively. These results show very good agreement to the experimental data, except for Mg^{2+}, even though the material and diffusion parameters were calibrated based on a more limited set of experimental data (up to 413 days). Due to the solution replacement at the beginning of Phase II, the equilibrium of the major ions in the synthetic porewater with the Opalinus Clay is strongly disturbed. The concentrations of K^+, Cl^- increased substantially, while the concentration of Na^+ doubled. The concentrations of Ca^{2+} and Mg^{2+} decreased slightly. The concentration of SO_4^{2-} decreased two orders of magnitude (compare Table 8 and Table 10). Consequently, the concentrations of K^+, Cl^- decrease in the borehole solution and diffuse into the Opalinus Clay over time. Due to the substantial increase of the concentration and the high selectivity coefficient of K^+, it is strongly adsorbed on the ion exchange sites and replaces Na, Sr, Ca and Mg from the ion exchange sites (Figure 59). The desorption process leads to back diffusion of Na^+, Ca^{2+} and Mg^{2+}, which explains the concentration increase of Ca^{2+} and Mg^{2+} and the slight concentration increase of Na^+ (Figure 58). The concentration of SO_4^{2-} increases as a result of back diffusion from the gap and clay. These effects slow down with time when the concentration gradients decrease.

The simulated concentration profiles of HTO and major ions in the porewater as well as adsorbed species in the Opalinus Clay at 728 days (just before overcoring) are depicted in Figure 60, Figure 61, Figure 62, respectively. The comparison of the simulated and experimental profiles of total concentrations (i.e. including aqueous and adsorbed species) of the major cations is depicted in Figure 63, and shows good agreement for Ca, and follows the observed trends for Na, K and Mg. All profiles show a decrease of concentration from the borehole wall into the clay as expected. Comparing the simulated results at 728 days with the experimental data of the overcored samples (at 735 days) shows a relatively poor fit to the experimental data, indicating that calibrating to aqueous concentration data is insufficient to fully capture system behavior. A consistent back diffusion can clearly be seen by comparing the

simulated and experimental concentration profiles in the area near the borehole wall (Figure 60 and Figure 61, and Figure 62). This will be discussed in Task 3.2b.

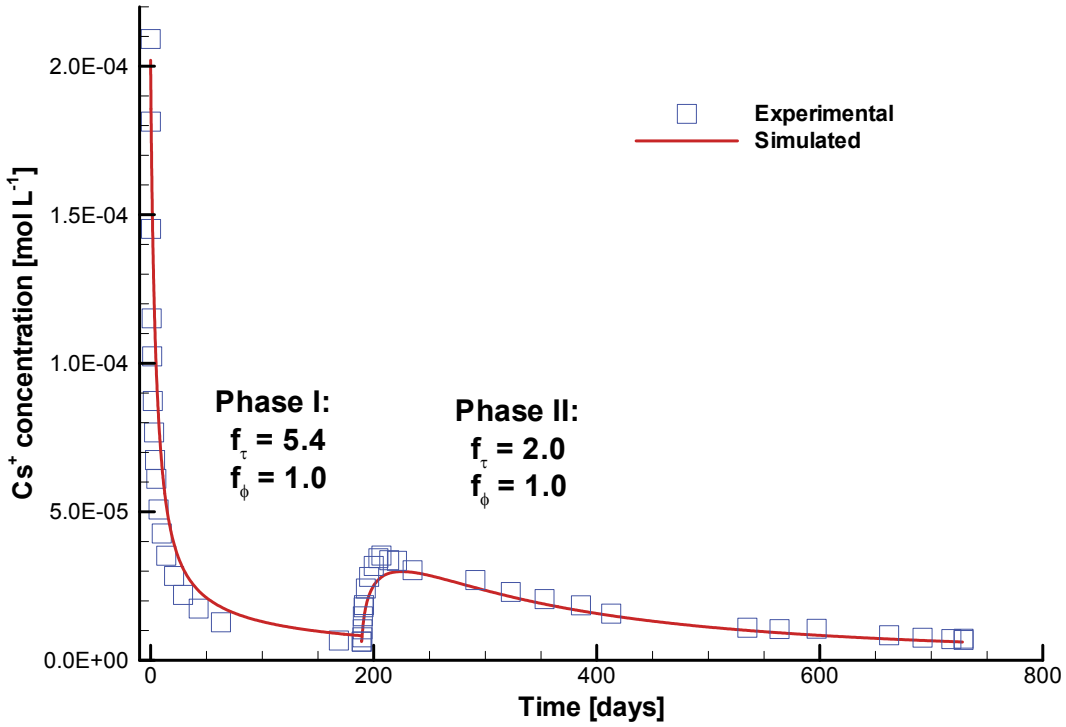

Figure 57: Comparison of Simulated and Experimental Concentration Time Curves for Cs^+ in the Borehole Solution for the DR-A In-situ Diffusion Experiment – from the Start until before Overcoring (728 days) Based on Task 3.1b

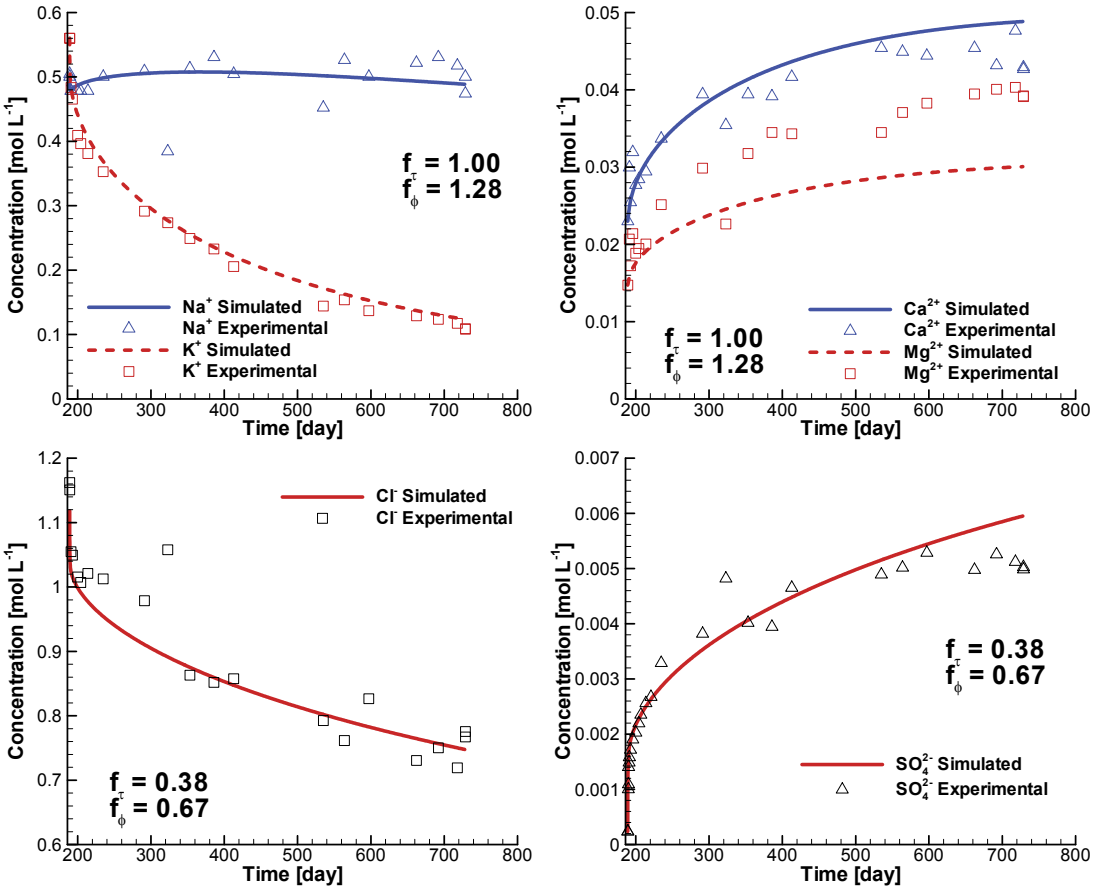

Figure 58: Comparison of Simulated and Experimental Concentration Time Curves for Major Ions in Borehole Solution during the DR-A In-situ Diffusion Experiment - from the Start until right before Overcoring (728 days) Based on Task 3.1b

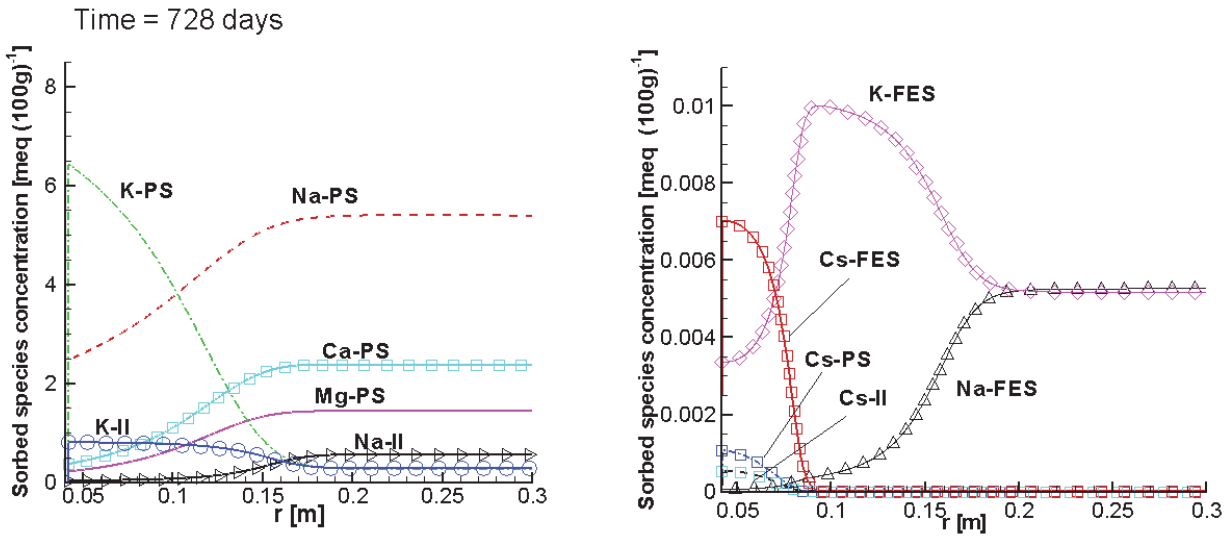

Figure 59: Simulated Concentration Profiles for Adsorbed Species on Three Exchange Sites in the Opalinus Clay at 728 days

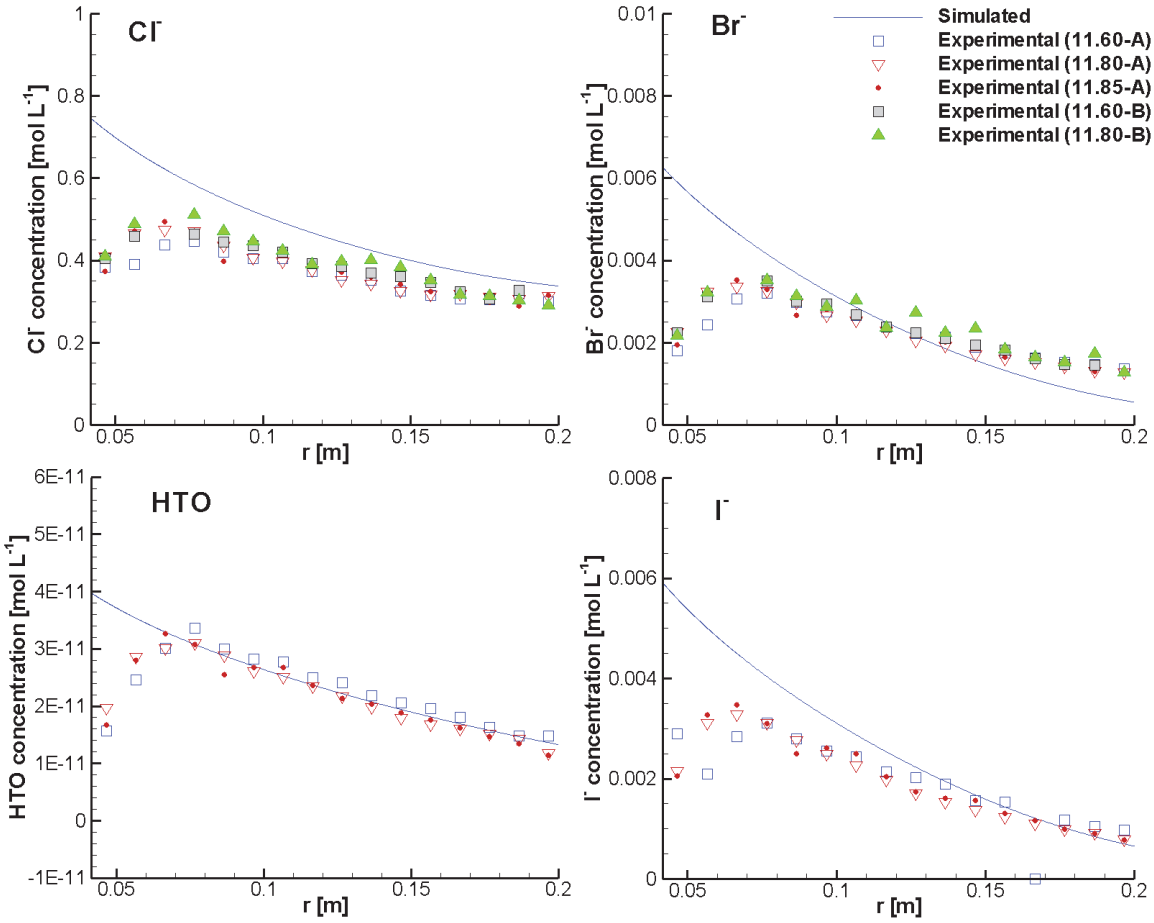

Figure 60: Simulated Total Concentration Profiles for Cl^-, HTO, Br^-, and I^- in the Opalinus Clay at 728 days and Comparison to the Experimental Total Concentration Profiles in the Porewater of the Overcored Opalinus Clay Samples

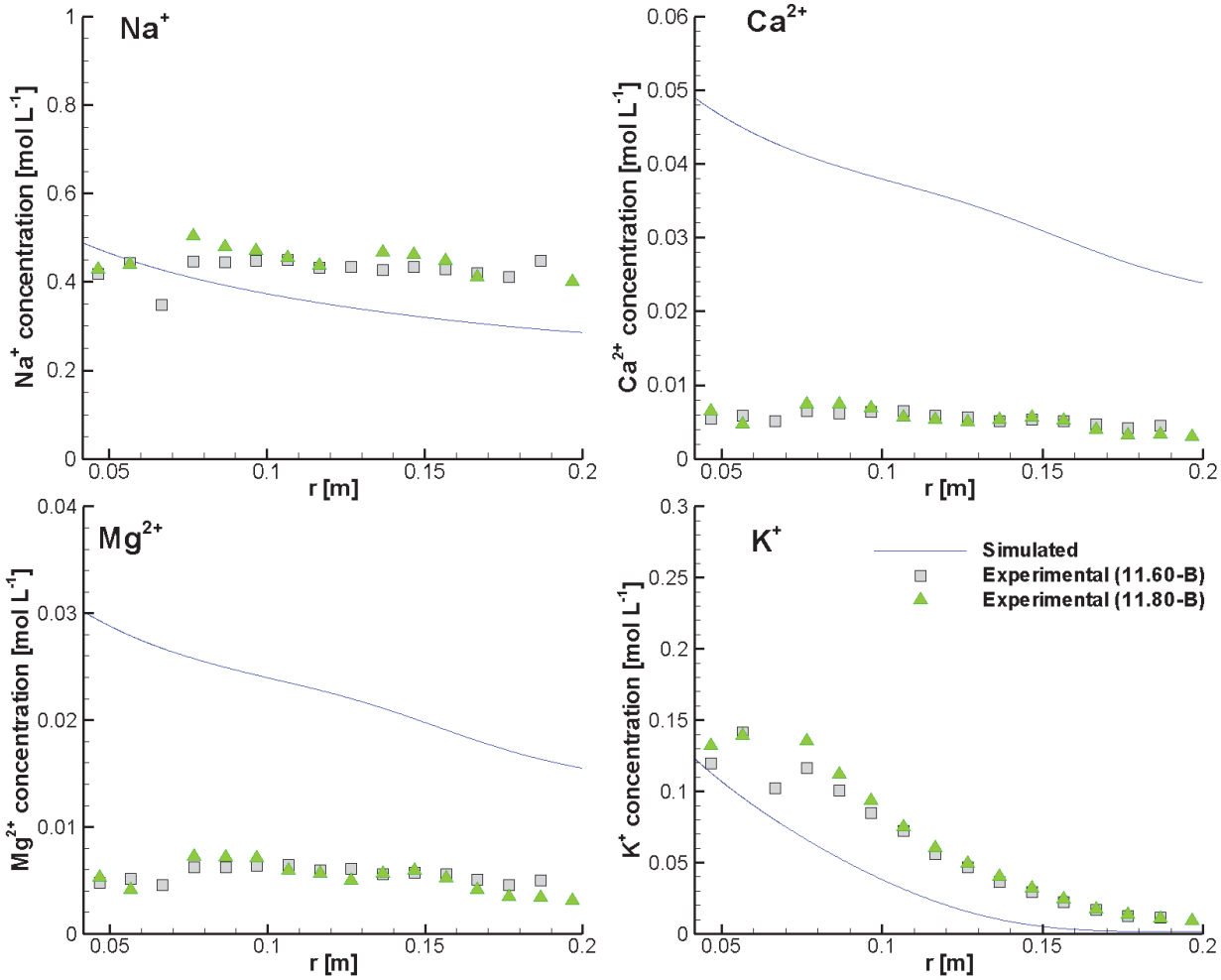

Figure 61: Simulated Concentration Profiles for Aqueous Na^+, Mg^{2+}, Ca^{2+}, and K^+ in the Opalinus Clay at 728 days and Comparison to the Experimental Total Concentration Profiles in the Porewater of the Overcored Opalinus Clay Samples

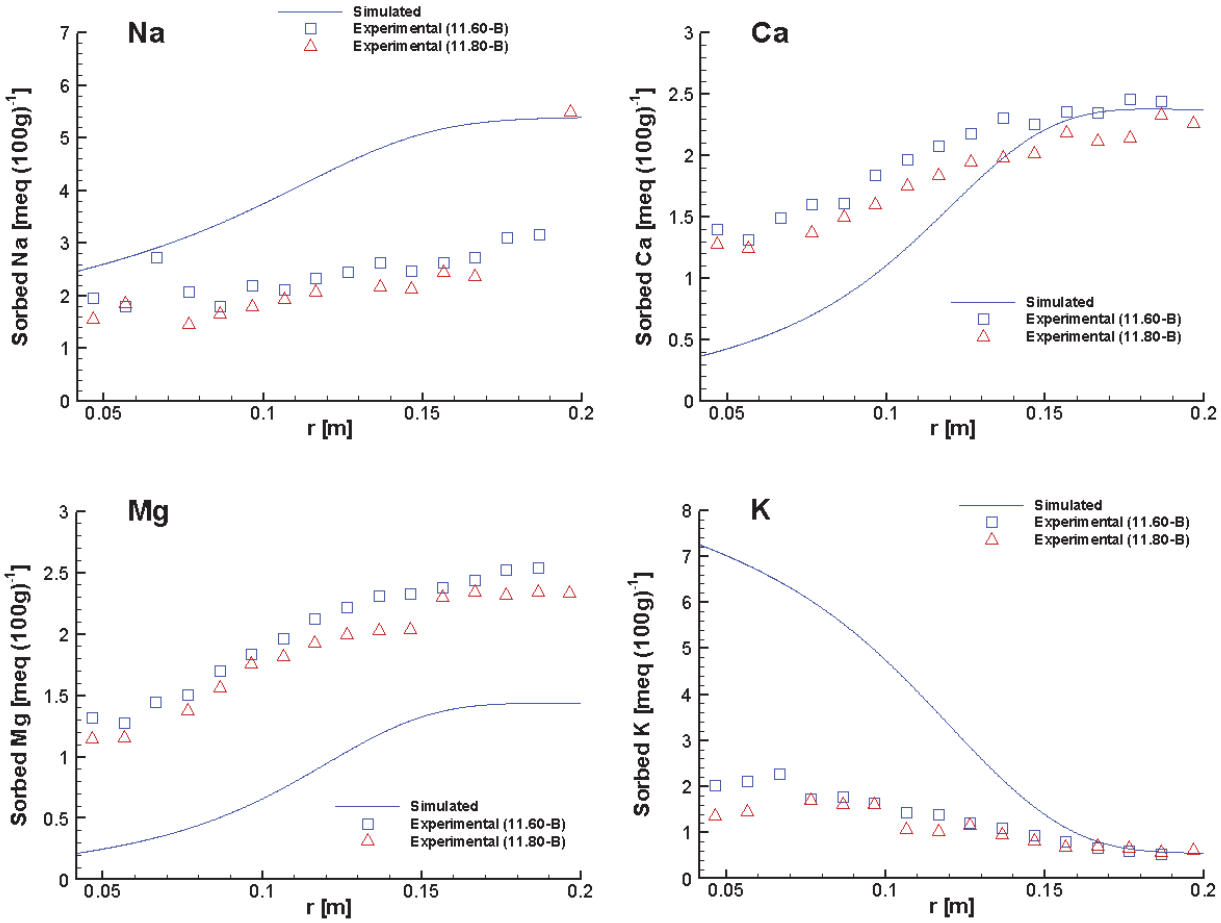

Figure 62: Simulated Concentration Profiles for Adsorbed Species in the Opalinus Clay at 728 days and Comparison to the Experimental Total Concentration Profiles in the Overcored Opalinus Clay Samples

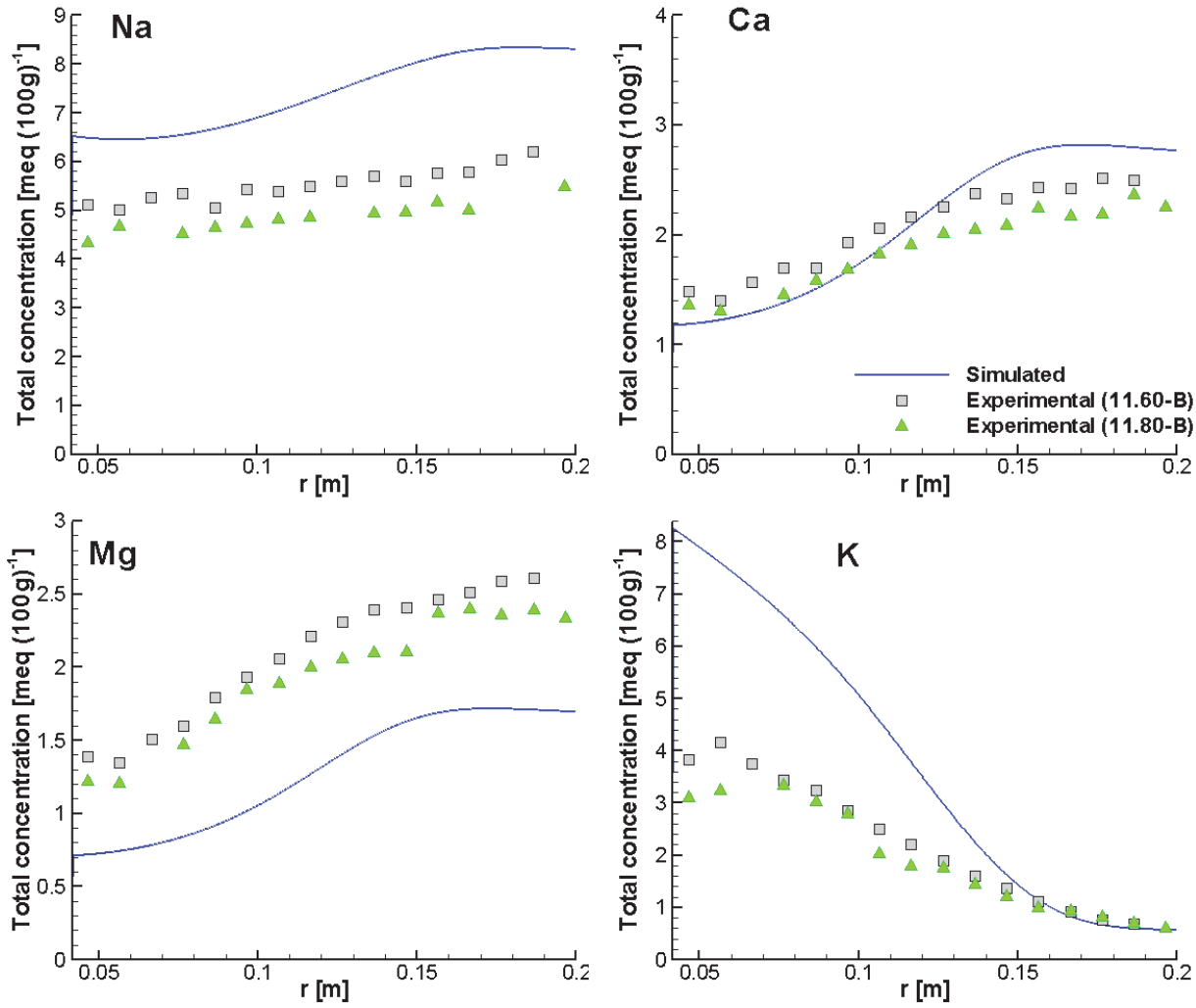

Figure 63: Comparison of Simulated and Experimental Total Concentration (including Aqueous and Sorbed Species) Profiles for Elements Na, Ca, Mg and K of the Overcored Samples at 735 Days (Task 3.2a)

5.4.2 Task 3.2b: Extended Simulations Including the Effect of Overcoring

5.4.2.1 Simulations for $^{60}Co^{2+}$, $^{85}Sr^{2+}$, HTO, Br^- and I^-

The simulated concentration profiles of the components in the porewater of the overcored samples consistently showed back diffusion of HTO, Br^-, I^-, and Cl^- (Figure 64). As a result, the simulations presented in section 5.4.1.1 were revised to bring the core into contact with Opalinus porewater during the overcoring phase (728 days – 735 days). The simulated total concentration profiles for HTO, Br^-, I^-, Cl^-, Co^{2+}, and Sr^{2+} in the Opalinus Clay are depicted in Figure 63.

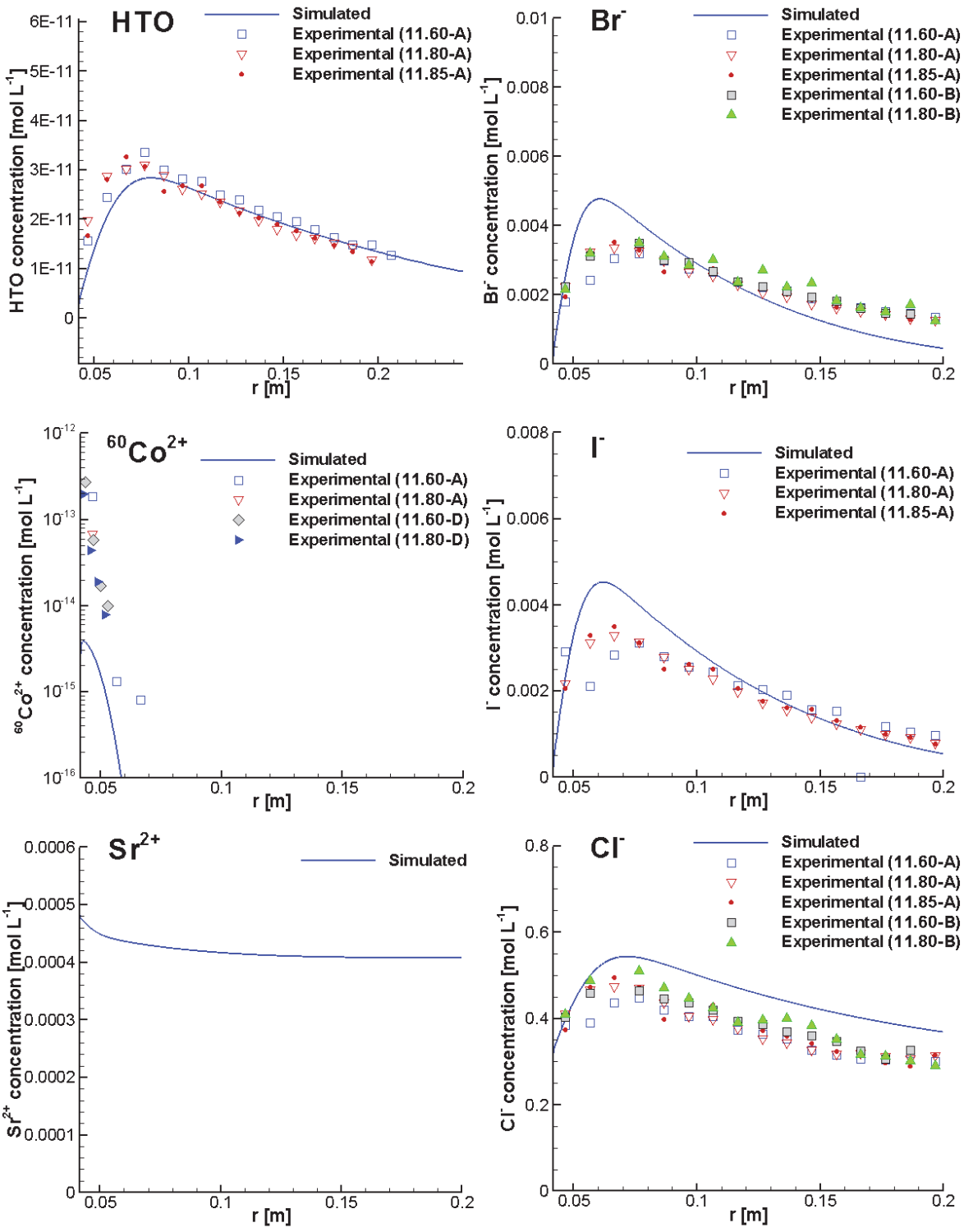

Figure 64: Comparison of Simulated and Experimental Total Concentration Profiles at 735 Days for HTO, $^{60}Co^{2+}$, Br^-, Sr^{2+}, and Cl^- in the Porewater of the Overcored Opalinus Clay Samples

The revised simulation results show good agreement to the experimental data for all dissolved species (note that no experimental data for Sr^{2+} in the porewater were available). The simulated concentrations of dissolved Co^{2+} are slightly lower than observed, which can be considered very good agreement considering analysis uncertainties in the range of 5% to 80% (NAGRA 2014). The simulated profiles of sorbed strontium (including both Sr and $^{85}Sr^{2+}$) showed good agreement to the experimental data (Figure 65). However, simulated concentrations of the adsorbed cobalt are much lower than the experimental data (Figure 65).

Considering the assumption made for the simulations that no Co^{2+} exists in the original formation porewater, the only cobalt source is $^{60}Co^{2+}$ injected in the borehole solution at 2.18×10^{-13} mol L^{-1} (Table 9), which decreases with time. Using the linear adsorption model with constant K_d , the sorbed amount of cobalt can be obtained according to:

$$C_{sorb} = K_d c \qquad \text{Equation 5-1}$$

in which C_{sorb} is the sorbed concentration per weight of solid, c is the concentration in solution per unit volume of solution. The K_d for $^{60}Co^{2+}$ is 90.0 L kg^{-1} (Wersin et al. 2008). The maximum sorbed cobalt concentration should be 3.92×10^{-9} meq $(100g)^{-1}$, which is five orders of magnitude lower than the measured data. Therefore, the measured sorbed cobalt on the Opalinus Clay sample is not caused by the diffusion of the injected $^{60}Co^{2+}$ only (i.e. other sources of background cobalt exist, which are included in the observational data).

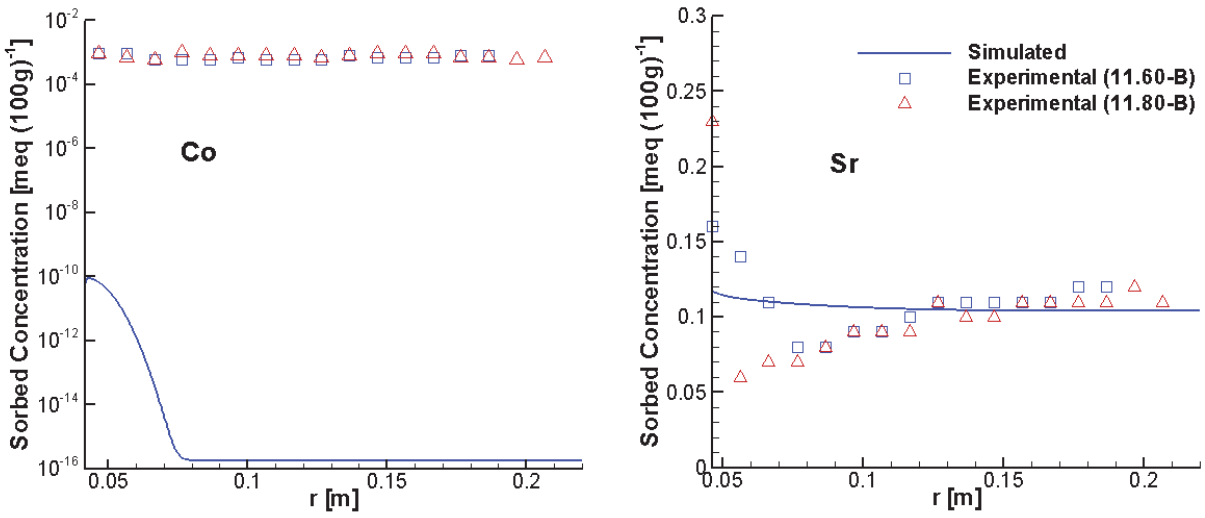

Figure 65: Comparison of Simulated and Experimental Concentration Profiles for Adsorbed Species in the Overcored Opalinus Clay Samples at 735 Days

5.4.2.2 Simulations for Cs^{+}

Building on the simulation described in Section 5.4.1.2, back diffusion due to contact of formation porewater with the borehole wall during the one week overcoring period was simulated. The solution change in the borehole implies a rapid drop of concentrations of HTO

and dissolved ions in the borehole at 728 days (compare the concentrations of major ions in borehole right before overcoring in Figure 58 to the original formation porewater composition in Table 8). Consequently, HTO and ions near the borehole wall diffuse back into the borehole as depicted in Figure 66 and Figure 67. Simulated concentration profiles show very good agreement to the observed data even though the calibrated diffusion parameters were based on Phase II data (until 413 days only) without modification. Because no experiemtal data for Cs (neither in porewater nor as adsorbed species) was obtained from the overcored samples, no comparison of simulated and experimental data for Cs could be undertaken. For the adsorbed species, multisite ion exchange is the main controlling process. Figure 68 depicts the simulated concentration profiles of adsorbed species on different exchange sites (i.e. –PS, -II and –FES, see Table 15) by the end of the overcoring (i.e. 735 days). The adsorbed K-PS concentration near the borehole wall decreases significantly due to the substantial decline of K^+ concentration caused by back diffusion. Consequenly, a large fraction of adsorbed K-PS is released from the echanged sites, and the sites are occupied by other adsorbed apecies such as Na-X, Mg-X_2 and Ca-X_2 etc. (-X represents the sum of three sites) (Figure 68). The simulated Ca-X_2 and Mg-X_2 underetstimate the adsorbed concentrations, while the simulated Na-X and K-X overestimate the adsorbed concentrations (Figure 69). The comparison of the simulated to the experimental profiles of the total concentrations (i.e. including both aqueous and adsorbed species) shows very good agreement for Ca, overestimation for Na and K, underestimation of Mg. Nevertheless, the trend of the concentration distributions at 735 days shows very good agreement for all four elements.

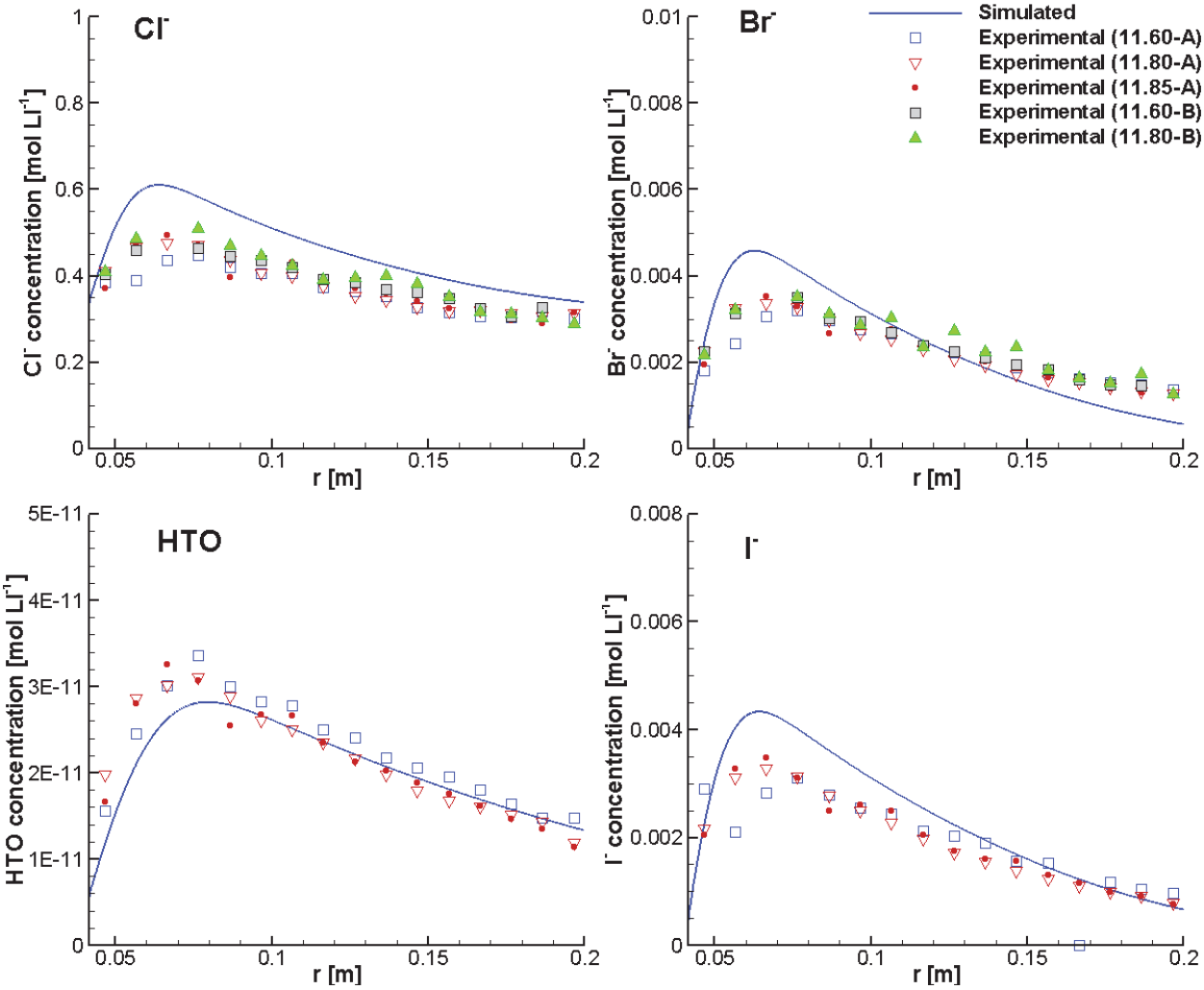

Figure 66: Comparison of Simulated and Experimental Total Concentration Profiles for Cl^-, HTO, Br^- and I^- in the Porewater of the Overcored Opalinus Clay Samples at 735 Days

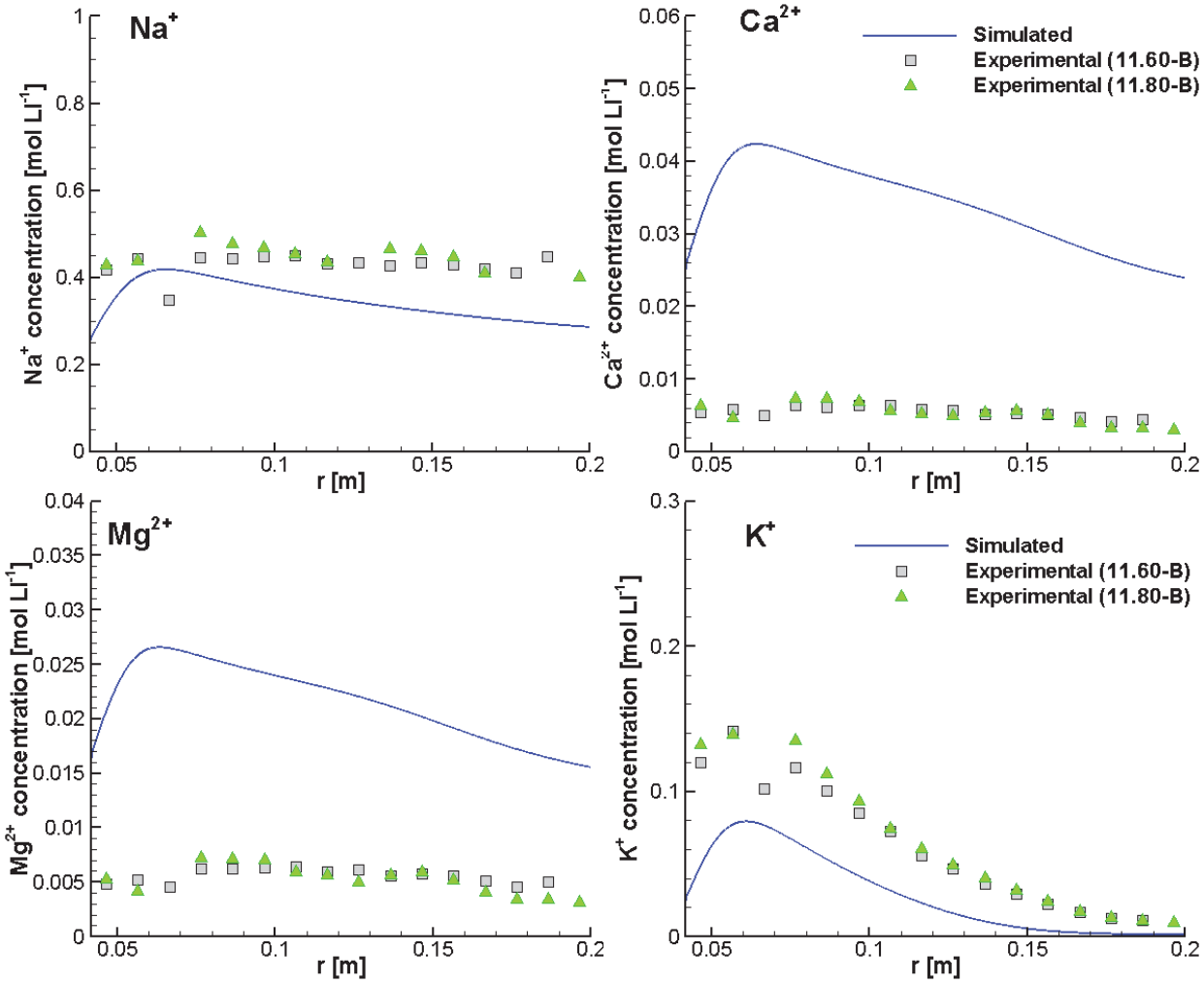

Figure 67: Comparison of Simulated and Experimental Total Concentration Profiles for Na^+, Mg^{2+}, Ca^{2+} and K^+ in the Porewater of the Overcored Opalinus Clay Samples at 735 Days

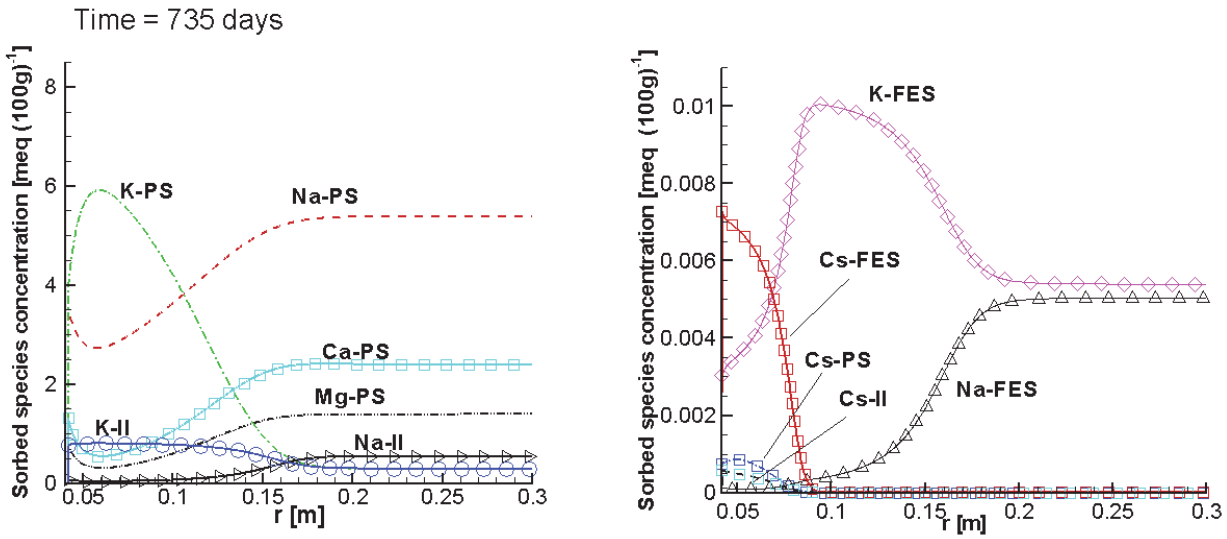

Figure 68: Simulated Concentration Profiles for Adsorbed Species on Three Exchange Sites in the Opalinus Clay after overcoring at 735 days

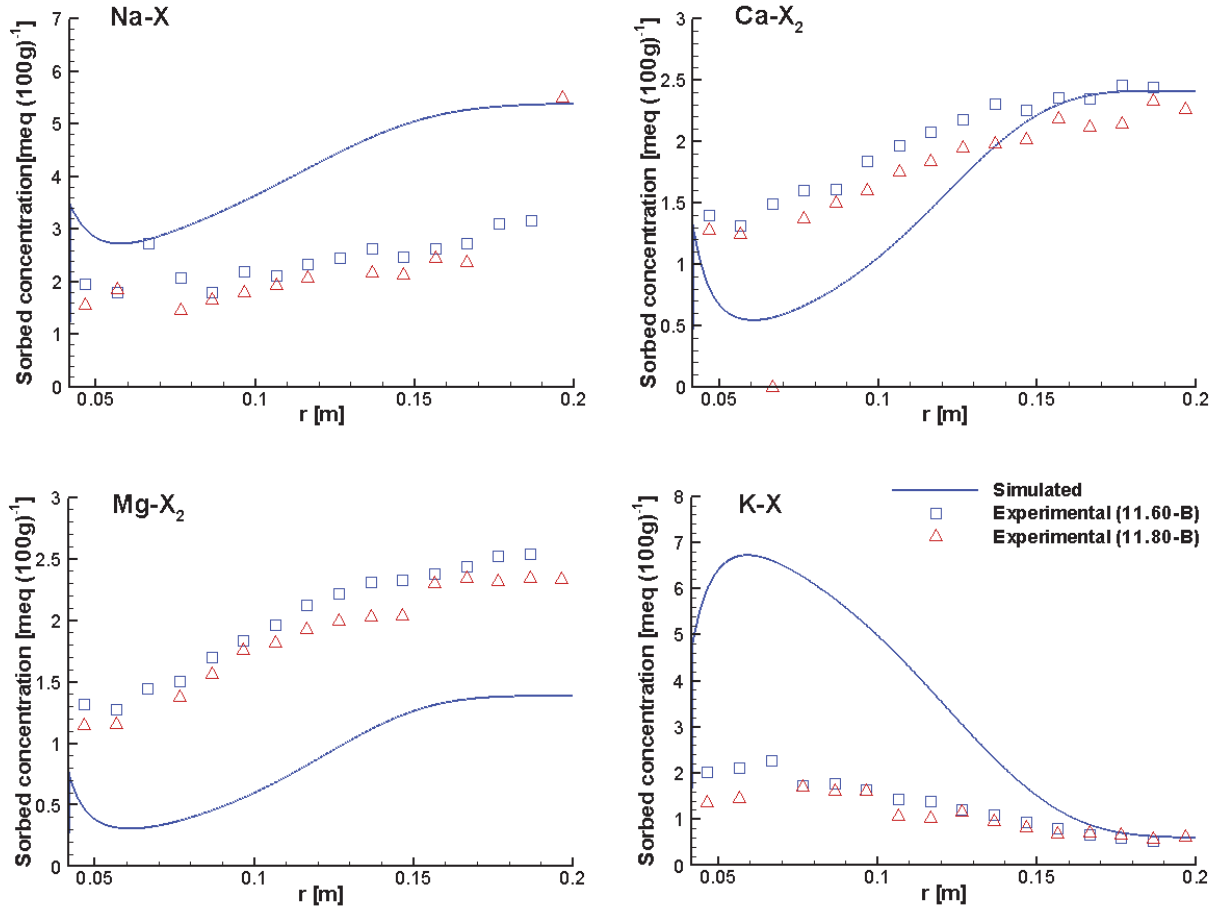

Figure 69: Comparison of Simulated and Experimental Concentration Profiles for Total Adsorbed Species in the Overcored Opalinus Clay Samples at 735 Days

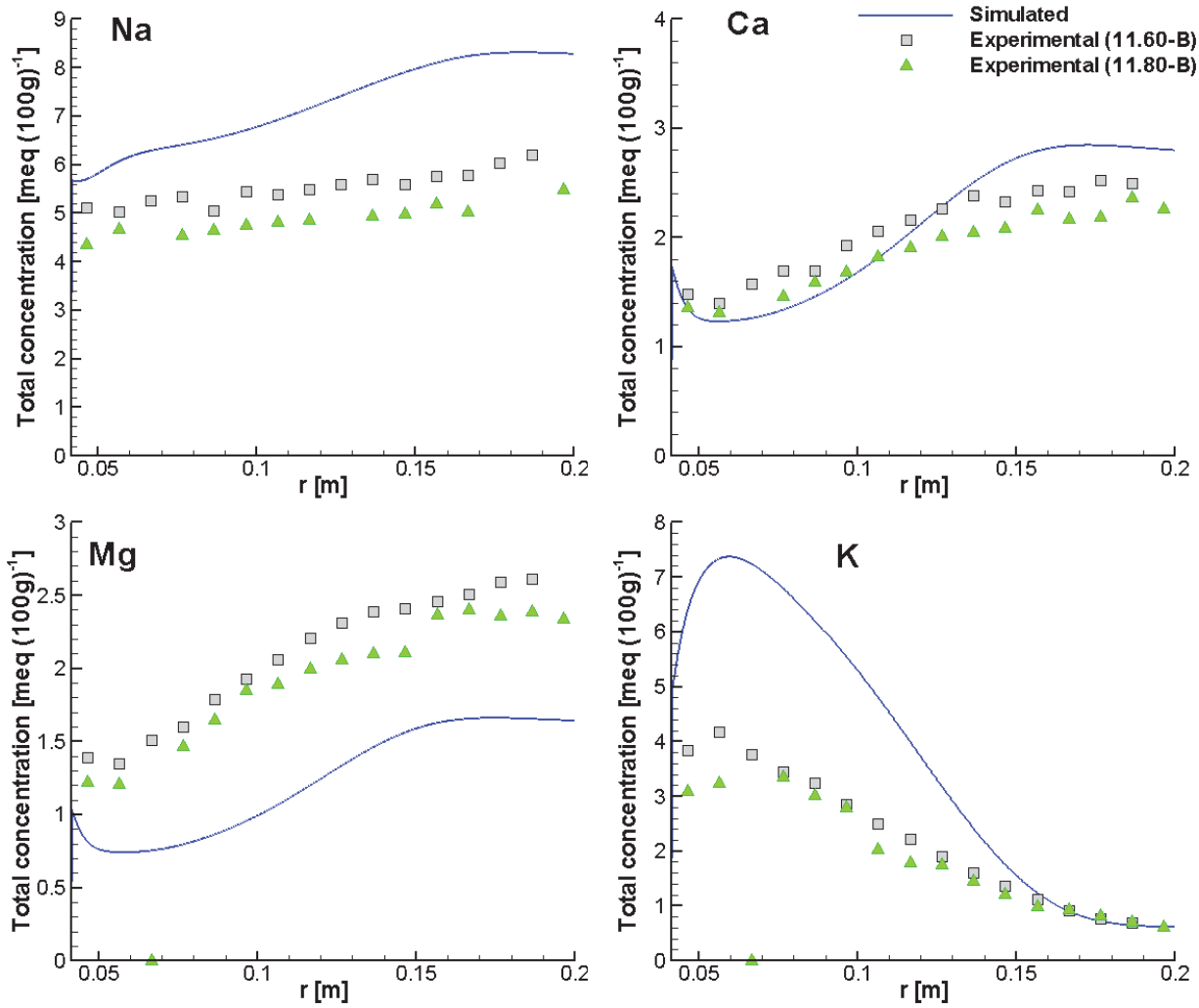

Figure 70: Comparison of Simulated and Experimental Total Concentration (including Aqueous and Sorbed Species) Profiles for Elements Na, Ca, Mg and K of the Overcored Samples at 735 Days (Task 3.2b)

After completion of the contract period for this work, a second DR-A technical meeting was held in December of 2014 in Zürich, Switzerland. In response to discussions at this workshop, several revised simulations of the experiment were undertaken. Considering that these simulations were conducted after conclusion of the contract period, the results are included in Appendix A.

6. CONCLUSIONS AND OUTLOOK

MIN3P-THCm was used to simulate a series of benchmarking tasks and Phase I and II of the DR-A in-situ diffusion experiment that was conducted in shaley facies of the Opalinius Clay. Generally, excellent agreement was achieved with other modelling groups (e.g. results from Flortran, presented by Gimmi (2012), and from CrunchFlow, presented by Soler (2012)) for the

benchmarking tasks (Task 1 and Task 2.1). Comparison of MIN3P-THCm simulation results and observational data for the DR-A in-situ diffusion experiment led to good agreement for HTO and anions, but it was more difficult to obtain a favorable comparison for reactive cations Co^{2+}, Sr^{2+}, Eu^{3+}, and Cs^{+}.

To facilitate these simulations, a new hybrid multicomponent diffusion (HMD) model was developed and implemented in MIN3P-THCm. This model extends, in an empirical manner, the multicomponent diffusion approach by including species-dependent effective porosity and effective tortuosity to account for anion exclusion and cation surface diffusion. This formulation enables simultaneous simulation of diffusion and geochemical interaction among multiple aqueous species and, in waste repository safety assessment, is applicable to study transport in low permeability natural and engineered barriers. The application of this numerical simulation tool to the DR-A in-situ diffusion experiment illustrates that it is a simple, but relatively effective, approach for simulations involving several tracers. The advantage of using the HMD model is that diffusion experiments with multiple tracers can be simulated during a single simulation by using factors that modify effective porosity and/or tortuosity of individual species, to account for processes such as anion exclusion, and interlayer/surface diffusion in clayey materials.

In addition, a multisite ion exchange (MIE) model for Cs^{+} in Opalinus Clay was implemented in MIN3P-THCm. This model was verified against CrunchFlow and applied to the benchmarking cases and the DR-A in-situ diffusion experiment. Very good agreement was achieved with other modelling teams for the benchmarking tasks and for the simulations of the experiment, indicating that the MIE model implementation is consistent with CrunchFlow and Flotran. For the tracers $^{60}Co^{2+}$ and $^{85}Sr^{2+}$, with extremely low concentrations, a linear sorption model was sufficient for the simulation of the DR-A experiment.

The simulations of the DR-A experiment revealed that it is difficult to obtain good simulation results for cations, in particular strongly sorbing cations such as $^{60}Co^{2+}$ and Eu^{3+}. Therefore, a sensitivity analysis and alternative conceptual models were investigated using MIN3P-THCm. The results suggest that the presence of colloidal clay particles in the gap and the filter may provide a possible explanation for the observed rapid decline of tracer concentrations in the borehole at early time. The colliods are interpreted to be an experimental artifact that retain strongly sorbing cations within the borehole test interval. The presence of colloids is restricted to the borehole; colloidal transport does not take place within the clay matrix due to pore size restrictions. For Eu^{3+}, additional adsorption on equipment, such as the Teflon filter, may explain the experimental data.

The simulated results for Phase II of the DR-A experiment show that diffusion parameters calibrated for Phase I have to be modified in order to obtain good agreement with the experimental data. These modifications include an increase of the effective porosity and tortuosity of the Opalinus Clay, as well as, a decrease of the surface diffusion effect for cations. Such modifications are consistent with the hypothesis that the DDL thickness, which is not mechanistically simulated, declines in response to the replacement of the Phase I borehole solution by a solution with higher ionic strength. As a result, the parameter set was recalibrated for Phase II based on observational data up to 413 days. Good agreement could be obtained for the tracers and major ions in the borehole solution, even when extending the simulation to 728 days, corresponding to the termination of the experiment and overcoring. Results for the overcore spatial concentration profiles perpendicular to the borehole also showed overall good agreement for dissolved ion concentrations. However, simulated concentrations did not agree as well for the adsorbed species on the clay surface of the overcored samples.

Nevertheless, the current model is capable of simulating conservative and reactive tracer diffusion into clayey materials such as the Opalinus Clay, with limited uncertainties regarding peneration depths and porewater concentrations.

ACKNOWLEDGEMENTS

This study was funded by the Mont Terri Consortium, Switzerland and NWMO, Canada. Valuable discussions with several colleges – Thomas Gimmi (PSI and University of Bern), Olivier Leupin (NAGRA), Josep Soler (IDAEA-CSIC), especially Tammy Yang (NWMO) and Monique Y. Hobbs (NWMO) – helped to improve this report.

REFERENCES

Appelo, C.A.J. and D. Postma. 2003. Geochemistry, Groundwater and Pollution, A.A. Balkema, Rotterdam, Netherlands.

Appelo, C.A.J. and P. Wersin. 2007. Multicomponent diffusion modeling in clay systems with application to the diffusion of tritium, iodide and sodium in Opalinus Clay. Environmental Science & Technology, 41, 5002-5007.

Appelo, C.A.J., A. Vinsot, S. Mettler and S. Wechner. 2008. Obtaining the porewater composition of a clay rock by modelling the in- and out-diffusion of anions and cations from an in-situ experiment. Journal of Contaminant Hydrology, 101, 67-76.

Appelo, C.A.J., L.R. Van Loon and P. Wersin. 2010. Multicomponent diffusion of a suite of tracers (HTO, Cl, Br, I, Na, Sr, Cs) in a single sample of Opalinus Clay. Geochimica et Cosmochimica Acta, 74, 1201-1219.

Baeyens, B. and M.H. Bradbury. 1994. Physico-Chemical Characterisation and Calculated In-situ Porewater Chemistries for a Low Permeability Palfris Marl Sample from Wellenberg, NAGRA Technical Report NTB 94-22.

Bea Jofre, S.A., K.U. Mayer and K.T.B. MacQuarrie. 2011. Modelling Reactive Transport in Sedimentary Rock Environments - Phase II MIN3P code enhancements and illustrative simulations for a glaciation scenario. Technical report: NWMO TR-2011-13.

Bea Jofre, S.,S. Wilson, K.U. Mayer, G. Dipple, I. Power and P. Gamazo. 2012. Reactive transport modeling of natural carbon sequestration in ultramafic mine tailings Vadose Zone Journal, 11 (2), 1-17

Bear, J. 1972. Dynamics of fluids in porous media, Elsevier Science, New York.

Bossart, P. 2013. Characteristics of the Opalinus Clay at Mont Terri, www.mont-terri.ch.

Bourg, I.C., A.C.M. Bourg and G. Sposito. 2003. Modeling diffusion and adsorption in compacted bentonite: a critical review. Journal of Contaminant Hydrology, 61, 293-302.

Bourke, P.J., N.L. Jefferies, D.A. Lever and T.R. Lineham. 1993. In: Manning, D.A.C., Hall, P.L., Hughes, C.R. (Eds.), Mass Transfer Mechanisms in Compacted Clays. Geochemistry of Clay–Pore Fluid Interactions. Chapman and Hall, London, pp. 331–350.

Bradbury, M. H. and B. Baeyens. 2000. A generalized sorption model for the concentration dependent uptake of caesium by argillaceous rocks, Journal Of Contaminant Hydrology, 42, 141-163.

Bradbury, M. H. and B. Baeyens. 2011. Predictive sorption modelling of Ni(II), Co(II), Eu(III), Th(IV) and U(VI) on MX-80 bentonite and Opalinus Clay: A “bottom-up” approach, Applied Clay Science, 52, 27-33.

Chang, H., W. Um, K. Rod, R.J. Serne, A. Thompson, N. Perdrial and J. Chorover. 2011. Strontium and cesium release mechanisms during unsaturated flow through waste-

weathered Hanford sediments. Environmental Science & Technology, 45, 8313-8320. doi:DOI: 10.1021/es2010368

Diamond, S. 1970. Pore size distributions in clay. Clay and Clay Minerals, 18, 7-23.

Doherty, J. 2010. PEST, Model-independent parameter estimation — User manual (5th ed.): Brisbane, Australia, Watermark Numerical Computing.

Fierz, T. and U. Rösli. 2012. DR-A Experiment: Instrumentation of BDR-A3 and tracer injection, TECHNICAL NOTE 2011-21, Solexperts AG, Switzerland.

Galindez, J.M., C.I. Steefel and U. Maeder. 2011. Continuum model for diffusive transport in the electrical double layer and clay interlamellæ. Proceedings at the Goldschmidt 2011 Conference, Prague, Czech Republic, August 14-19, 2011.

García-Gutiérrez, M., J.L. Cormenzana, T. Missana and M. Mingarro. 2004. Diffusion coefficients and accessible porosity for HTO and 36Cl in compacted FEBEX bentonites. Applied Clay Science, 26 (1-4), 65-73.

Giambalvo, E.R., C.I. Steefel, A.T. Fisher, N.D. Rosenberg and C.G. Wheat. 2002. Effect of fluid-sediment reaction on hydrothermal fluxes of major elements, eastern flank of the Juan de Fuca Ridge. Geochimica et Cosmochimica Acta, 66 (10), 1739–1757.

Gimmi, T., J. Soler and O. Leupin. 2012. Cs sorption parameters for the modeling the DR-A experiment (Task 1.3), (email communication).

Gimmi, T. 2012. DR-A experiment: results of bencmark tasks, Mont Terri Project DR-A Experiment Technical Discussion, Zürich (Üetliberg), 10-11 DEC. 2012 (unpubished, oral presentation).

Gimmi, T. 2013. Summary of initial volumes and concentrations in the DR-A experiment, PSI documentation AN-44-13-03 (unpubished, internal communication).

Gimmi, T., O.X. Leupin, J.M. Soler and L.R. van Loon. 2013. Perturbing a field diffusion experiment: First results of the DR-A test in the Mont Terri Rock Laboratory (Switzerland), Goldschmidt2013, Florence, Italy (abstract).

Glaus, M.A., B. Baeyens, M.H. Bradbury, A. Jakob, L.R. Van Loon and A. Yaroshchuk. 2007. Diffusion of 22Na and 85Sr in montmorillonite: evidence of interlayer diffusion being the dominant pathway at high compaction, Environmental Science & Technology, 41 (2), 478–485.

Henderson, T., K.U. Mayer, B. Parker and T. Al. 2009. Three-dimensional density-dependent flow and multicomponent reactive transport modeling of chlorinated solvent oxidation by potassium permanganate. Journal of Contaminant Hydrology, 106, 195-211.

Lauber, M., B. Baeyens and M.H. Bradbury. 2000. Physicochemical characterisation and sorption measurements of Cs, Sr, Ni, Eu, Th, Sn and Se on Opalinus Clay from Mont Terri. Nagra Technical Report NTB 00-11, Wettingen, Switzerland.

Leupin O. 2012. Task definitions and DR-A field diffusion experimental results at Mont Terri Underground Laboratory (email communications).

Lide, D. R. 1994. CRC Handbook of chemistry and physics: a ready-reference book of chemical and physical data 74th Edition, CRC Press/The chemical Rubber Co., Boca Raton, FL. U.S.A.

Maes, A. and A. Cremers. 1986. High selective ion exchange in clay minerals and zeolites.- In: Davis J.A. and Hayers, K.F. (eds): Geochemical processes at mineral surfaces.- ACS Symposium Series 323, 254-295.

Mayer, K.U. 1999. A numerical model for multicomponent reactive transport in variably-saturated porous media, PH.D. – thesis, Department of Earthe Sciences, University of Waterloo, Waterloo, Ontario, Canada.

Mayer, K.U., E.O. Frind and D.W. Blowes. 2002. Multicomponent reactive transport modeling in variably saturated porous media using a generalized formulation for kinetically controlled reactions. Water Resources Research, 38, 1174. doi:10:1029/2001WR000862

Mayer, K.U. and K. T. B. MacQuarrie. 2010. Solution of the MoMaS reactive transport benchmark with MIN3P - Model formulation and simulation results, Computers and Geosciences, 14,405-419, doi:10.1007/s10596-009-9158-6

Melkior, T., E.C. Gaucher, C. Brouard, S. Yahiaoui, D. Thoby, Ch. Clinard, E. Ferrage, D. Guyonnet, C. Tournassat and D. Coelho. 2009. Na^+ and HTO diffusion in compacted bentonites: effect of surface chemistry and related texture, Journal of Hydrology, 370 (1–4), 9–20.

Molera, M., T. Eriksen and M. Jansson. 2003. Anion diffusion pathways in bentonite clay compacted to different dry densities, Applied Clay Science, 23 (1–4), 69-76.

Muurinen, A., M. Olin and K. Uusheimo. 1990. Diffusion of sodium and copper in compacted sodium bentonite at room temperature. MRS Proceedings 176 (Scientific Basis for Nuclear Waste Management XIII), 641– 647, doi:10.1557/PROC-176-641..

NAGRA. 2012. Mont Terri DR-A field diffusion experiment results (unpublished, internal data exchange).

NAGRA. 2014. Mont Terri DR-A field diffusion experiment results (continued until overcoring) and chemical analysis of the porewater and sorbed species of the overcored samples (unpublished, internal data exchange).

O'Reilly, D.E. and E.M. Peterson. 1971. Self-Diffusion Coefficients and Rotational Correlation Times in Polar Liquids. II, The Journal of Chemical Physcis, 55, 2155-2164.

Palut, J. -M., T. Fierz, J. Eikenberg, F. van Dorp, A. Moeri, P. Bossart, C. Aubry, M. Garcia-Guttierez and Y. Drouiller. 2002. The diffusion in-situ experiment DI: field activity and data report. Mont Terri TECHNICAL REPORT 2000-03.

Palut, J.- M., Ph. Montarnal, A. Gautschi, E. Tevissen and E., Mouche. 2003. Characterisation of HTO Diffusion Properties by an In-situ Tracer Experiment in Opalinus Clay at Mont Terri. Journal of Contaminant Hydrology, 61, 203-218.

Pearson, F.J. 1999. In: Aplin, A.C., Macquaker, J.H.S. (Eds.): What is the porosity of mudrock? Muds and Mudstones: Physical and Fluid Flow Properties. The Geological Society of London, pp. 9-21.

Preočanin, T., A. Selmani, P. Lindqvist-Reis, F. Heberling, N. Kallay and J. Lützenkirchen. 2012. Surface charge at Teflon/aqueous solution of potassium chloride interfaces. Colloids and Surfaces A: Physicochemical and Engineering Aspects, 412, 120-128.

Rasouli, P. 2015. The role of multicomponent diffusion and electrochemical migration for reactive transport in porous media, PhD-thesis, University of British Columbia (in progress).

Samper, J., C. Yang, A. Naves, A. Yllera, A. Hernández, J. Molinero, J.M. Soler, P. Hernán, J.C. Mayor and J. Astudillo. 2006. A fully 3-D anisotropic numerical model of the DI-B in-situ diffusion experiment in the Opalinus Clay formation, Physics and Chemistry of the Earth, Parts A/B/C, 31, (10–14), 531–540.

Shackelford, C.D. and S.M. Moore. 2013. Fickian diffusion of radionuclides for engineered containment barriers: Diffusion coefficients, porosities, and complicating issues, Engineering Geology, 152 (1), 133–147, DOI: 10.1016/j.enggeo.2012.10.014.

Soler J. M. 2010. DR-A Experiment: Reactive Transport Scoping Calculations. Mont Terri Project, Technical Note TN 2010-09, 31pp.

Soler, J.M. 2012. DR-A experiment modeling: Task 1, Mont Terri Project DR-A Experiment Technical Discussion, Zürich (Üetliberg), 10-11 DEC. 2012 (unpubished, oral presentation).

Soler, J.M. 2013. DR-A experiment: Diffusion, retention and perturbation Reactive transport scoping calculation. Change in the salinity of the circulation solution. Mont Terri Project Technical Note 2013-47

Soler, J. M., O.X. Leupin, T. Gimmi and L.R. van Loon. 2014. The DR-A in-situ diffusion experiment at Mont Terri: Effects of changing salinity on diffusion and retention properties. In proceeding of: XXXVII Scientific Basis for Nuclear Waste. DOI: 10.1557/opl.2014.629

Steefel, C.I. 2008. CrunchFlow. Software for Modeling Multicomponent Reactive Flow and Transport. Lawrence Berkeley National Laboratory, Berkeley, CA, USA.

Steefel, C.I., S. Carroll, P. Zhao and S. Roberts. 2003. Cesium migration in Hanford sediment: a multisite cation exchange model based on laboratory transport experiments, Journal of Contaminant Hydrololgy, 67 (1-4), 219-46.

Tournassat, C. and C.A.J. Appelo. 2011. Modelling approaches for anion-exclusion in compacted Na-bentonite. Geochimica et Cosmochimica Acta, 75, 3698-3710.

van Loon, L.R., B. Baeyens and M.H. Bradbury. 2009. The sorption behaviour of caesium on Opalinus Clay: A comparison between intact and crushed material. Applied Geochemistry, 24, 999-1004.

van Loon, L.R., M.A. Glaus and W. Müller. 2007. Anion exclusion effects in compacted bentonites: Towards a better understanding of anion diffusion, Applied Geochemistry, 22, 2536-2552.

van Loon, L.R., J.M. Soler and M.H. Bradbury. 2003. Diffusion of HTO, ^{36}Cl and ^{125}I in Opalinus Clay samples from Mont Terri – effect of confining pressure. Journal of Contaminant Hydrology, 61, 73–83.

Wersin, P. E, E. Curti and C.A.J. Appelo. 2004. Modelling bentonite–water interactions at high solid/liquid ratios: swelling and diffuse double layer effects, Applied Clay Science, 26 (1–4), 249–257.

Wersin, P., J.M. Soler, L.V. Loon, J. Eikenberg, B. Baeyens, D. Grolimund, T. Gimmi and S. Dewonck. 2008. Diffusion of HTO, Br^-, I^-, Cs^+, 85-Sr^{2+} and 60-Co^{2+} in a clay formation: Results and modelling from an in-situ experiment in Opalinus Clay. Applied Geochemistry, 23, 678-691.

Xie, M., S.S. Agus, T. Schanz and O. Kolditz. 2004. An upscaling method and a numerical analysis of swelling/shrinking processes in a compacted bentonite/sand mixture. International Journal for Numerical and Analytical Methods in Geomechanics, 28, 1479–1502. doi: 10.1002/nag.396

Yi, S., J.Samper, A. Naves and J.M. Soler. 2012. Inverse estimation of the effective diffusion of the filter in the In-situ fiffusion and retention (DR) experiment, Transport in Porous Media, 93,415-429, DOI 10.1007/s11242-012-9960-9.

Yllera, A., A. Hernández, M. Mingarro, A. Quejido, L.A. Sedano, J.M. Soler, J. Samper, J. Molinero, J.M. Barcala, P.L. Martín, M. Fernández, P. Wersin, P. Rivas and P. Hernán. 2003. DI-B experiment: planning, design and performance of an in-situ diffusion experiment in the Opalinus Clay formation. Applied Clay Science, 26, 181-196.

Zachara, J. M., S. C. Smith, C. Liu, J. P. McKinley, R. J. Serne and P. L. Gassman. 2002. Sorption of Cs to micaceous subsurface sediments from the Hanford site, USA, Geochimica et Cosmochimica Acta, 66(2), 193–211.

APPENDIX A: REVISED SIMULATION OF THE DR-A IN-SITU DIFFUSION EXPERIMENT PHASE I

CONTENTS

LIST OF FIGURES

Page

A REVISED SIMULATION OF THE DR-A IN-SITU DIFFUSION EXPERIMENT PHASE I

After completion of the contract period for this work, a second Mont Terri DR-A workshop was held in December of 2014 in Zürich, Switzerland. In response to discussions at this workshop, several revised simulations of the experiment were undertaken. Considering that these simulations were conducted after conclusion of the contract period, the results are included in the appendix, and are summarized in the following sections.

A.1. TASK 2.2A: OPEN GAP SCENARIO WITH HIGHER SORPTION DISTRIBUTION COEFFICIENT

During the Mont Terri workshop held in 2014, it was reported that the sorption distribution coefficient (K_d) for $^{60}Co^{2+}$ on Opalinus Clay may be as high as 420 L kg^{-1} (Table 3 in Wersin et al. 2008). It is therefore appropriate to consider a higher K_d value in the simulations, although this value was calibrated to be 90 L kg^{-1} during the DI-A2 in-situ diffusion experiment (Wersin et al. 2008). In addition, it was reemphasized that advective mixing in the borehole may result in faster transport through the filter, which can be mimicked by using a much higher effective diffusion coefficient for the filter. This corresponds to the well-mixed filter approch (Soler 2013). By using a K_d value of around 200 L kg^{-1} for $^{60}Co^{2+}$, in combination with the well-mixed filter approach, good agreement between observed and simulated data was achieved by some modelling groups. Therefore, a recalculation with similar parameters was undertaken using MIN3P-THCm. In the simulations an effective diffusion coefficient of 3.0x10^{-5} m^2 s^{-1} was assumed for the filter. Using an effective filter porosity of 0.45, a D_0 for $^{60}Co^{2+}$ of 0.732x10^{-9} m^2 s^{-1}, and a tortuosity of 9.1x10^4, the desired effective diffusion coefficient was obtained. A K_d of 200 L kg^{-1} for $^{60}Co^{2+}$ was selected.

A.1.1. Task 2.2a_A1: Reference Case (Well-Mixed Filter Approach with K_d of $^{60}Co^{2+}$ Set at 200 L kg^{-1})

For this case, the model set-up was the same as for Task 2.2a described in Section 5.2.2.1 (see Figure 38) except for using a higher K_d value for $^{60}Co^{2+}$ (200 L kg^{-1}) and applying the well-mixed filter approach. Simulated concentration time curves for HTO, Br^-, I^-, $^{60}Co^{2+}$ and $^{85}Sr^{2+}$ are presented in Figure A-1. The concentrations of HTO, Br^- and I^- in the borehole solution are decreasing faster than the observational data at early time, but show good agreement later on, confirming that the influence of the filter is decreasing with time. The mismatch at early time also suggests that advective mixing in the filter may be more restricted than in the simulations. In other words, the simulated enhanced tracer migration through the filter causes an increased mixing between water in the borehole solution and the gap, appearing to overestimate the mobility of the tracers. The simulated concentration time curve for $^{60}Co^{2+}$ shows a poorer agreement with the experimental data; however, the fit is improved compared to the base case similation presented in Figure 38, in which a lower K_d for $^{60}Co^{2+}$ (90 L kg^{-1}) was applied and the well-mixed filter approch was not considered. The simulated concentration of $^{85}Sr^{2+}$ generally exceeds the experimental data. It should be noted that this simulation did not consider enhanced cation diffusion in the DDL, which may contribute to the residual differences.

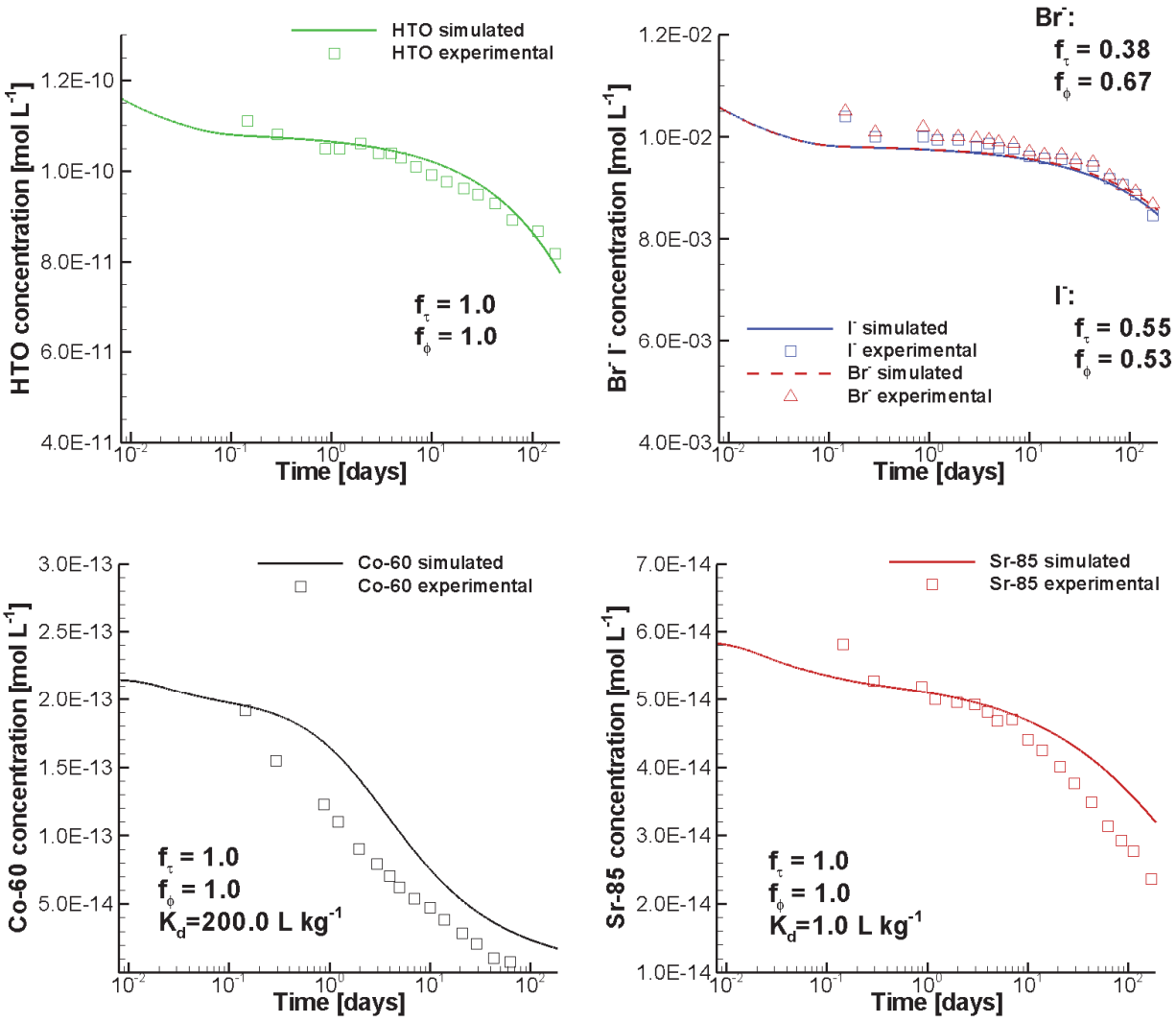

Figure A-1: Comparison of Simulated (Lines) and Experimental (Symbols) Results for HTO, Br^-, I^-, $^{60}Co^{2+}$ and $^{85}Sr^{2+}$ Concentrations for the DR-A In-situ Diffusion Experiment Phase I (Case Task 2.2a_A1)

A.1.2. Task 2.2a_A2: Increased the mobility of $^{60}Co^{2+}$ and $^{85}Sr^{2+}$

Based on the results presented above, it is clear there are still some differences between the simulated and experimental results. Increasing the mobility of $^{60}Co^{2+}$ and $^{85}Sr^{2+}$ to mimic enhanced cation diffusion through the DDL can be achieved by setting the tortuosity correction factors to 10.0 and 3.5. Using this approach, the simulated results show better agreement with the experimental results (Figure A-2), in particular for ^{85}Sr.

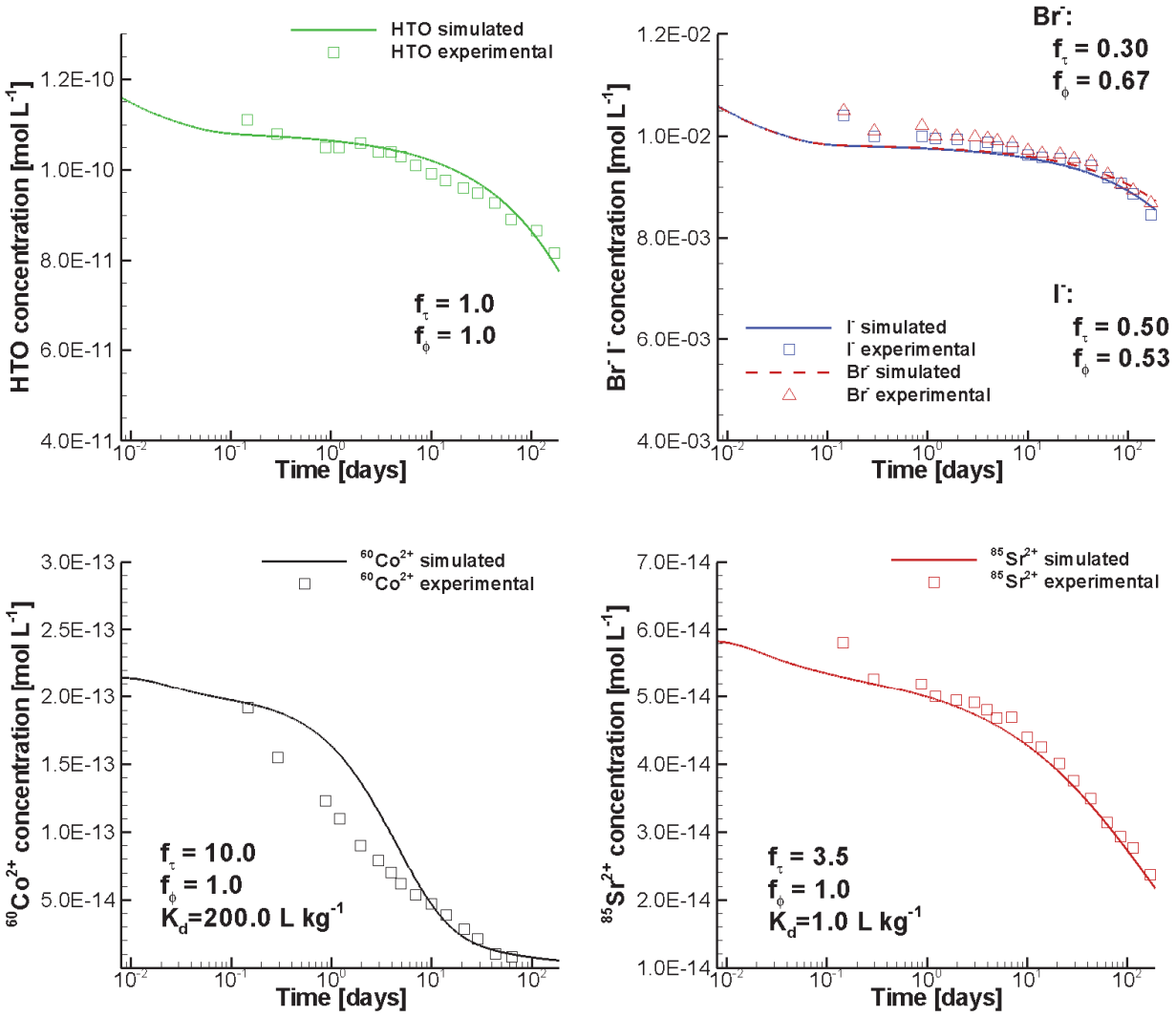

Figure A-2: Comparison of Simulated (Lines) and Experimental (Symbols) Concentration Time Curves for HTO, Br^-, I^-, $^{60}Co^{2+}$ and $^{85}Sr^{2+}$ in the Borehole Solution during the DR-A Field Diffusion Experiment Phase I (Case Task 2.2a_A2)

It is also possible to better match the concentration time curves by increasing both the sorption selectivity coefficient and the tortuosity correction factor (Figure A-2) and/or the mobility of ions in the filter. Therefore, several additional simulations were conducted (not all shown). For example, using the well-mixed filter approach in combination with an increased K_d for $^{60}Co^{2+}$ (i.e. 240 L kg^{-1}), and a tortuosity correction factor of 4.8, the fit to the observational data can be further improved (Figure A-3). Nevertheless, a perfect agreement cannot be reached, even when using extreme values of K_d set as high as 450 L kg^{-1} (results not shown).

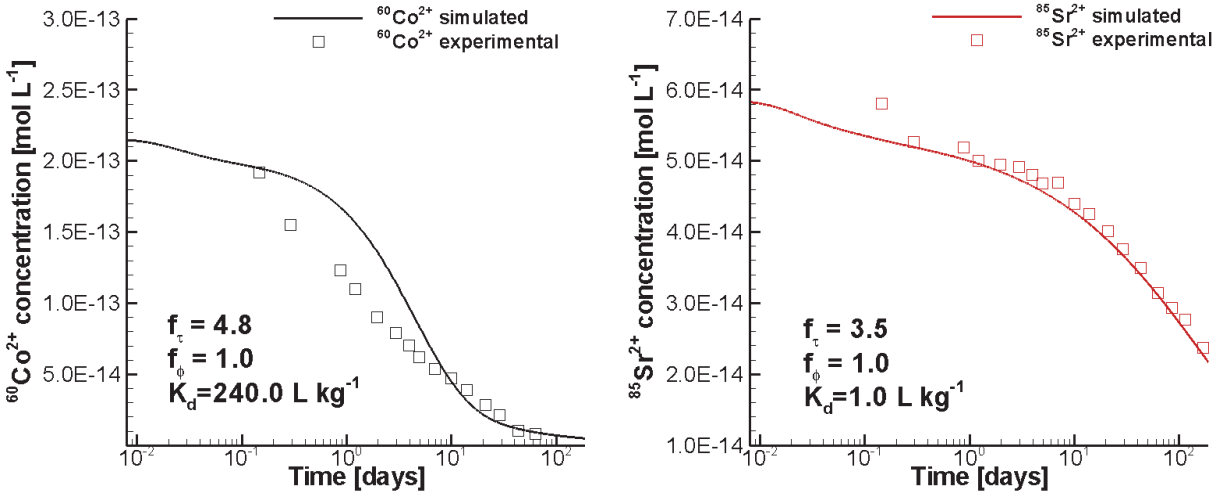

Figure A-3: Comparison of Simulated (Lines) and Experimental (Symbols) Concentrations for HTO, Br^-, I^-, $^{60}Co^{2+}$ and $^{85}Sr^{2+}$ during the DR-A In-situ Diffusion Experiment Phase I (K_d of $^{60}Co^{2+}$ Set to 240.0 L kg^{-1} and Tortuosity Correction Factor for $^{60}Co^{2+}$ Set to 4.8)

A.1.3. Task 2.2d_A3: Cs Diffusion and Retardation Using MIE Model and the Well-mixed Filter Approach

Based on the results presented above, it appears that the well-mixed filter approach may have merit, although the visible discrepancies for HTO and anionic tracers (Br^- and I^-) at early time indicate that this approach may overestimate porewater mixing in the filter. Applying this approach to the simulation of Cs^+ diffusion and adsorption, based on the Task 2.2d Case 4 (see Section 5.2.2.4), leads to the current simulation. According to the well-mixed filter approach, the effective diffusion coefficient for Cs^+ in the filter is set to $D_e = 3.0\times10^{-5}$ m^2 s^{-1} (Soler 2013). For this simulation, the simulated concentation time curve for Cs^+ in the circulation chamber shows good agreement with the experimental data (Figure A-4). In comparison to Task 2.2d Case 4, the simulated concentration time curve is much closer to the experimental data up to 30 days due to enhanced mass transfer across the filter (compare to Figure 42). In this case the correction factor for tortuosity was set to 5.4 (same value as in Task 2.2d Case 4) to mimic enhanced cation diffusion in the DDL.

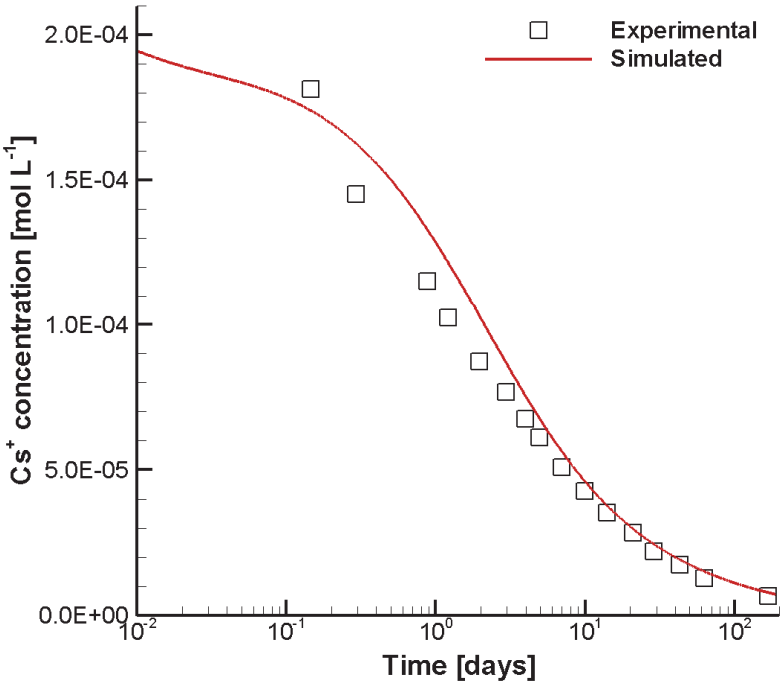

Figure A-4: Comparison of Simulated (Lines) and Experimental (Symbols) Concentrations for Cs^+ for the DR-A In-situ Diffusion Experiment Phase I (Case Task 2.2d_A3)

A.2. REVISED SIMULATION OF THE DR-A IN-SITU DIFFUSION EXPERIMENT PHASE II – LINEAR SORPTION MODEL FOR THE SIMULATION OF $^{60}CO^{2+}$ AND $^{85}SR^{2+}$

The revised simulations of Phase II of the DR-A experiment followed the same approach as for Phase I (i.e. the well-mixed filter approach was used and the linear sorption coefficient K_d for $^{60}Co^{2+}$ was set to 200 L kg^{-1}). Furthermore, the concentration distribution of adsorbed $^{85}Sr^{2+}$ was adjusted to account for decay because the half-life ($T_{1/2}$) of $^{85}Sr^{2+}$ (64.9 days, Sattler 1962) is relatively short in comparison to the experimental time period. By the end of Phase I (189 days), the residual fraction (*f*) of $^{85}Sr^{2+}$ can be estimated as 13.28% according to the equations:

$$f = \frac{N_t}{N_0} = e^{-\lambda t}$$

$$\lambda = \frac{ln2}{T_{1/2}}$$

in which:

λ is the decay constant;
N_0 is the initial quantity of the substance;
N_t is the quantity that remains after a time t.

This residual fraction (13.28 %) was applied to correct the concentration profiles of sorbed $^{85}Sr^{2+}$ at 189 days, which was set as the initial condition for the simulation of Phase II. For aqueous $^{85}Sr^{2+}$, no correction was made. For $^{60}Co^{2+}$, no adjustment was undertaken because its half-life is 5.271 years (Unterweger 2002), much longer than the experimental time period. After 189 days, about 95 % of $^{60}Co^{2+}$ remains and thus the decay of $^{60}Co^{2+}$ can be considered insignificant within Phase I of the experiment.

A.2.1. Task 3.1A_A4: Linear Sorption and Well-mixed Filter Approach – Direct Prediction

The model set-up was the same as for Task 3.1a (section 5.3.1). The simulation is based on Task 2.2a_A2 and directly uses the calibrated diffusion parameters as described above for Phase II of the experiment. Figure A-5 compares the simulated and observed aqueous concentration time curves for the tracers HTO, Br^-, I^-, $^{60}Co^{2+}$ and $^{85}Sr^{2+}$ in the circulation chamber. The discrepancies between the simulated and experimental results for all tracers indicate that the diffusion parameters of the Opalinus Clay likely have changed in response to the replacement of the borehole solution with a solution of elevated ionic strength, as demonstrated in Figure 48. For HTO, Br^- and I^-, the simulation underestimates concentration decreases in the circulation chamber. For $^{85}Sr^{2+}$, the simulation substantially overestimates concentration decreases. In comparison to Task 3.1a (Figure 48), the simulated results of $^{60}Co^{2+}$ improved for Phase I of the experiment, but cannot be evaluated for Phase II because no measured data is available. The simulated results of $^{85}Sr^{2+}$ for Phase II of the experiment generally show more discrepancy to the experimental data for the revised simulations. For HTO, Br^- and I^-, differences of the simulated results are limited between the cases. However, to obtain a similar match, the effective tortuosity factors (f_τ) had to be decreased from 0.38 (Task 3.1a) to 0.30 to compensate for the increase of the tortuosity of the filter.

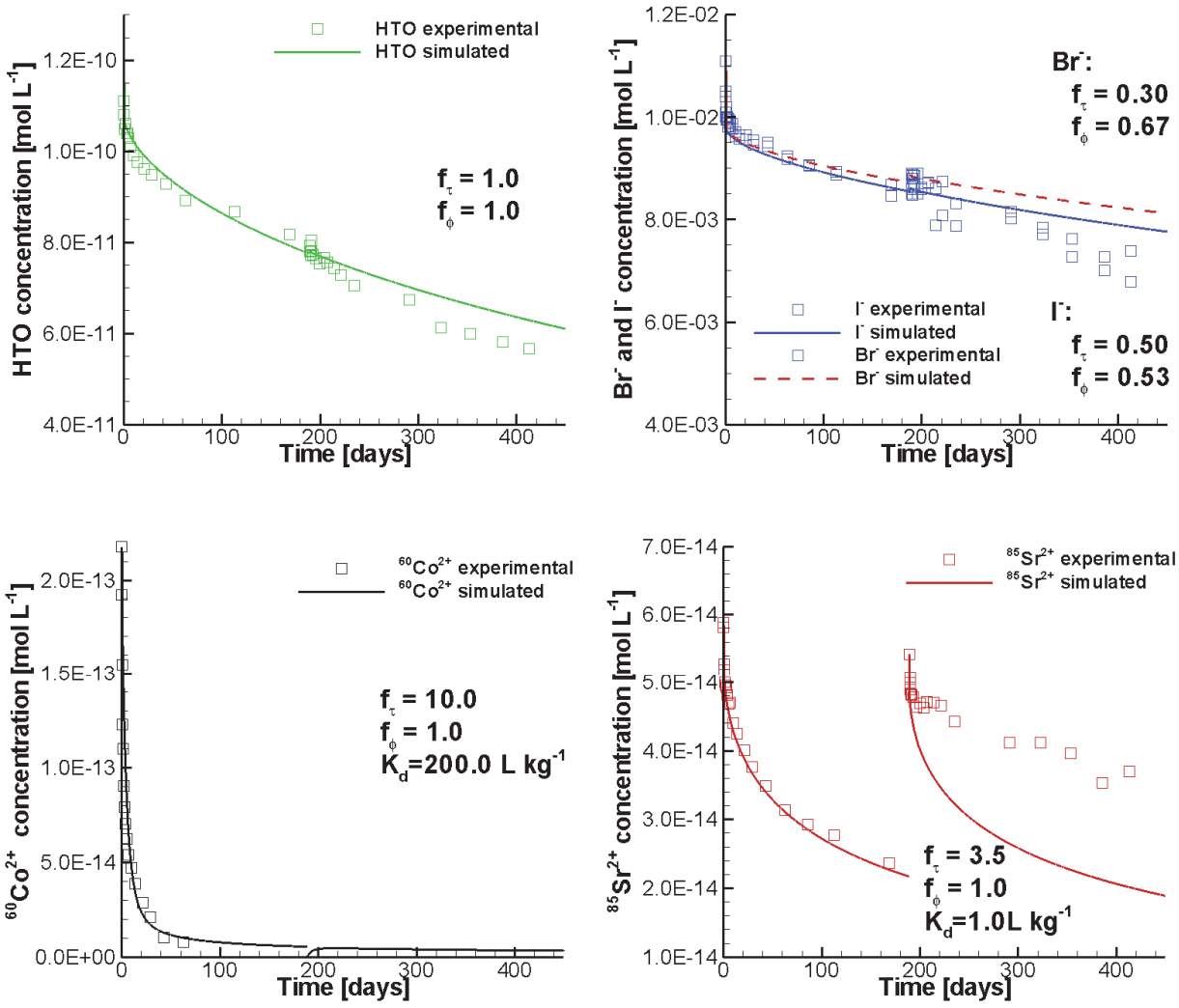

Figure A-5: Comparison of Simulated (Lines) and Experimental (Symbols) Concentration Time Curves for HTO, Br^-, I^-, $^{60}Co^{2+}$ and $^{85}Sr^{2+}$ during Phase I and Phase II

A.2.2. Task 3.1B_A5: Linear Sorption and Well-mixed Filter Approach – Calibration of Diffusion Parameters during Phase II

The model set-up was the same as for Task 3.1B (section 5.3.2). This simulation also builds on Task 2.2a_A2, but to account for the replacement of the borehole solution after Phase I, diffusion parameters for Phase II were recalibrated based on the experimental data up to 413 days. The best fit parameters for matching the measured concentration time curve for HTO were: effective porosity of 0.19, and effective tortuosity of 0.15, which are both higher than those calibrated for Phase I of the DR-A diffusion experiment (same as for Task 3.1b in section 5.3.2). The tortuosity correction factors for individual ionic species were also recalibrated (Figure A-6).

The tortuosity correction factors for I^- and Br^- were increased, while a decrease was required for $^{60}Co^{2+}$ and $^{85}Sr^{2+}$. Figure A-6 shows the comparison of simulated and observed aqueous concentration time curves in the circulation chamber after the diffusion parameter recalibration. Using this approach, the match of the results to the expermental data is comparable to the fit obtained in Task 3.1b (Figure 51) for HTO and $^{85}Sr^{2+}$. However, a slight improvement in agreement can be seen for $^{60}Co^{2+}$ and the anionic tracers (compare Figure 51 and Figure A-6).

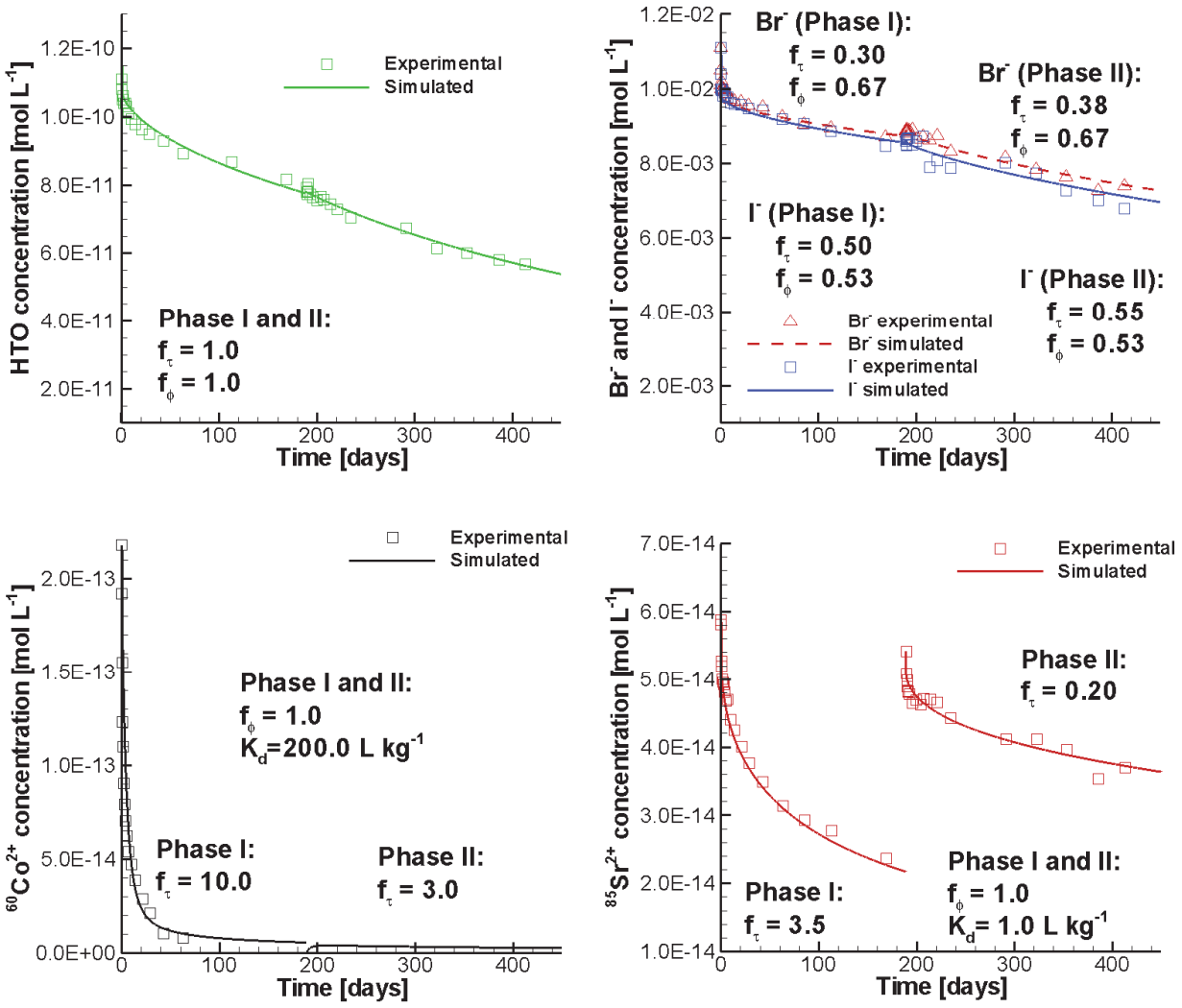

Figure A-6: Comparison of Simulated (Lines) and Experimental (Symbols) Concentration Time Curves for HTO, Br^-, I^-, $^{60}Co^{2+}$ and $^{85}Sr^{2+}$ for Phase I and Phase II (K_d of $^{60}Co^{2+}$ Set to 200.0 L kg^{-1} and Tortuosity Correction Factors Set to ^{60}Co: 3.0, ^{85}Sr: 0.20, I^-: 0.55, Br^-: 0.38)

A.2.3. Task 3.2A_A6: Linear Sorption and Well-mixed Filter Approach – Extended Prediction until 728 Days (Just Before Overcoring)

The model set-up was the same as for Task 3.2a (section 5.4.1). This simulation is based on Task 3.1B_A5 and extends to the time until just prior to overcoring (i.e. 728 days). Figure A-7 depicts the simulated concentration time curves for HTO, Br^-, I^-, $^{60}Co^{2+}$ and $^{85}Sr^{2+}$. The predicted concentrations for HTO, Br^-, I^- and Sr^{2+} in the borehole circulation solution show very good agreement with the experimental observations (Figure A-7). For $^{60}Co^{2+}$, no experimental results were obtained during Phase II.

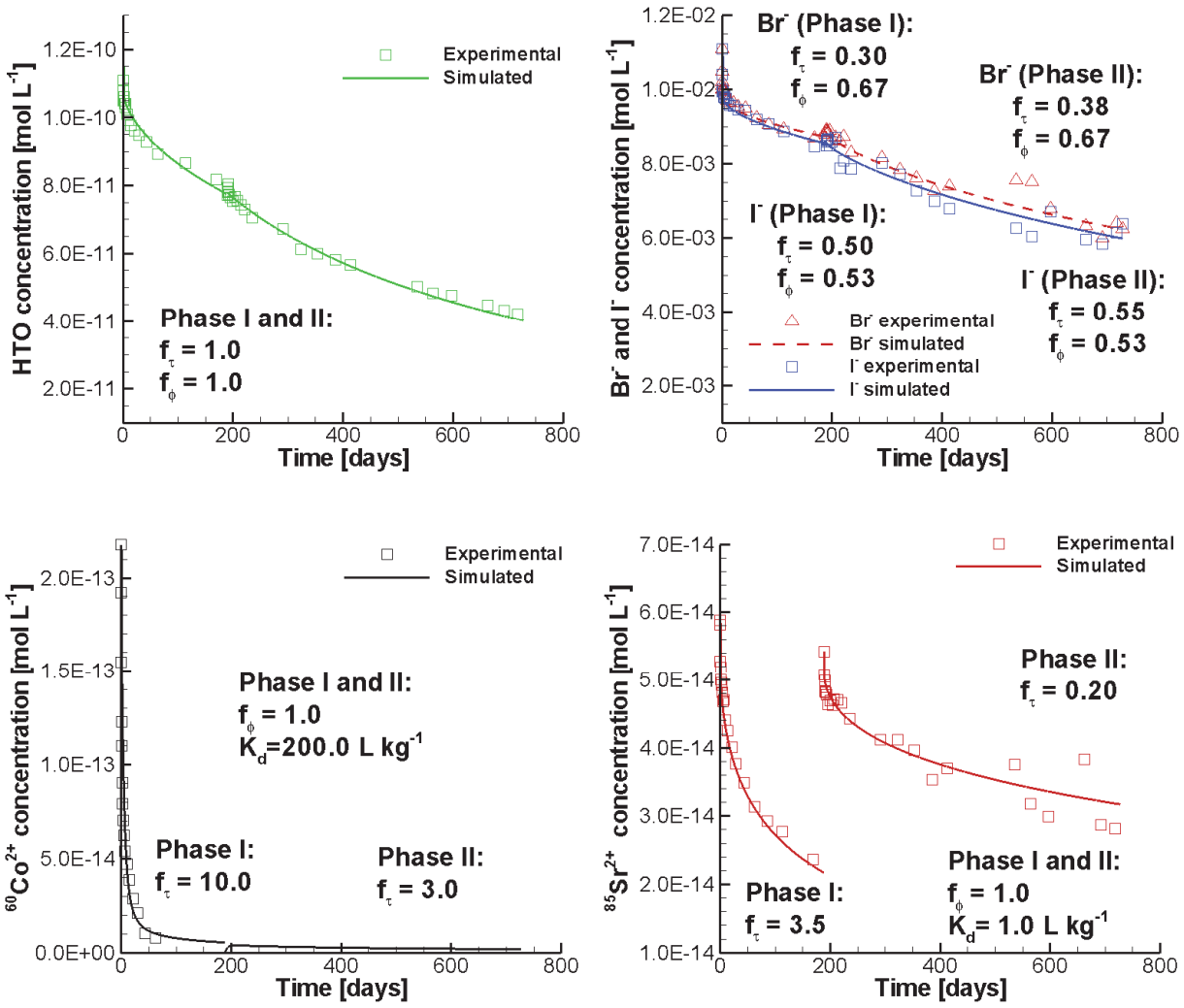

Figure A-7: Comparison of Simulated (Lines) and Experimental (Symbols) Concentration Time Curves for HTO, Br^-, I^-, $^{60}Co^{2+}$ and $^{85}Sr^{2+}$ During Phase I and Phase II (K_d of $^{60}Co^{2+}$ Set to 200.0 L kg^{-1} and Tortuosity Correction Factors Set to $^{60}Co^{2+}$: 3.0, ^{85}Sr: 0.20, I^-: 0.55, Br^-: 0.38)

The simulated concentration profiles for HTO, $^{60}Co^{2+}$, Br^-, and I^- in the Opalinus Clay porewater at 728 days are depicted in Figure A-8 and are compared to the experimental data obtained from porewater extracted from the overcored samples. The simulated concentration profiles for HTO, Br^-, and I^- show very good agreement with the experimental results, except for the region near the borehole wall (i.e. from r=0.0416 m to r≈0.07 m). This region was affected by direct contact with Opalinus Clay formation porewater during the overcoring. However, a larger discrepancy (one to two orders of magnitude) can be seen when comparing the simulated and experimental concentrations of $^{60}Co^{2+}$. The simulated concentrations for $^{60}Co^{2+}$ are less than $2.0x10^{-15}$ mol L^{-1}, similar to concentrations that remain in the borehole solution. It is likely that the measured concentrations include a contribution from the sorbed phase, explaining the observed differences. In comparison to Task 3.2a, very little improvement can be seen (compare results to Figure 55).

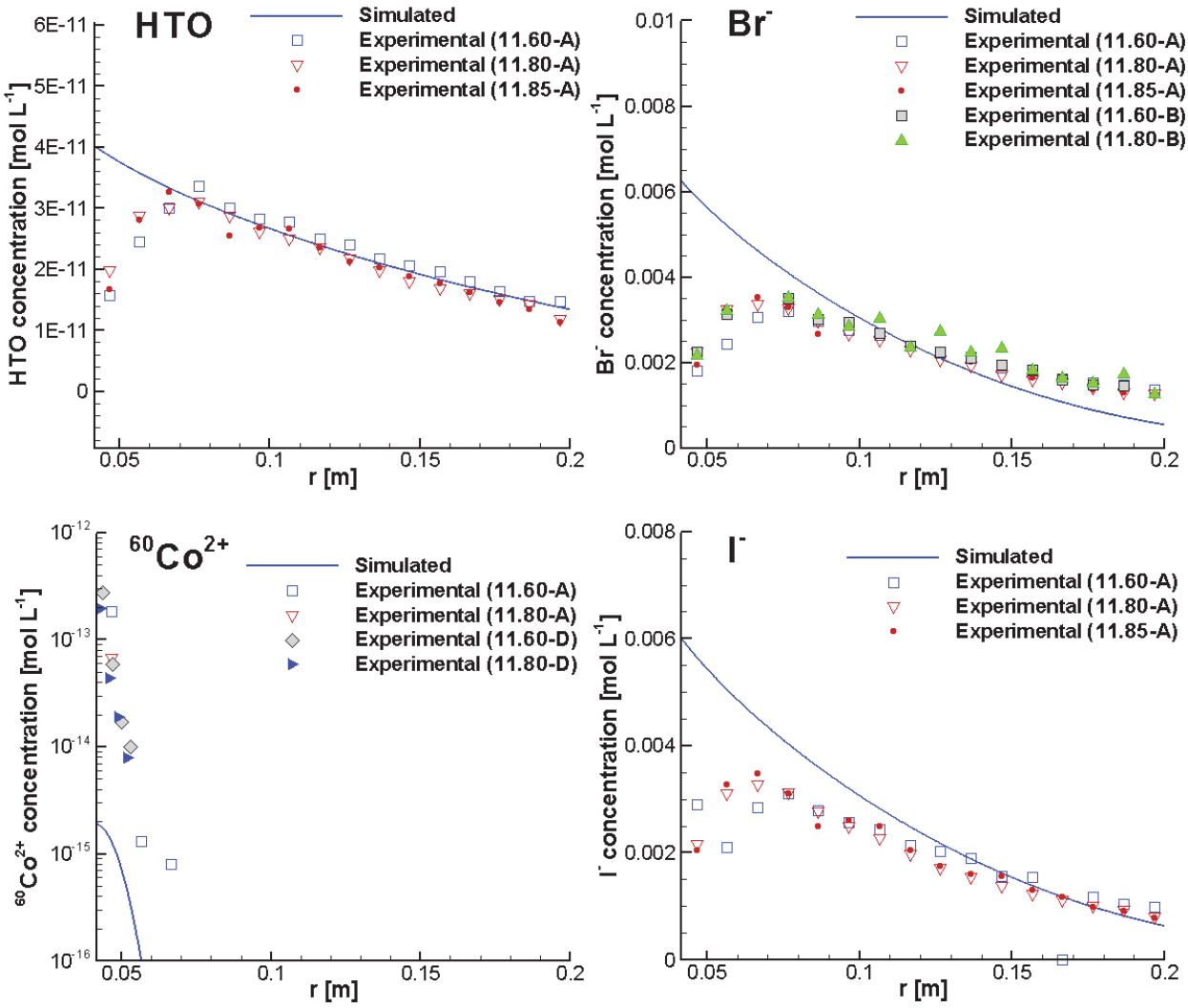

Figure A-8: Simulated Concentration Profiles for HTO, $^{60}Co^{2+}$, Br^- and I^- in the Opalinus Clay at 728 days and Comparison to the Experimental Concentration Profiles from Overcored Samples

A.3. REVISED SIMULATION OF PHASE II OF THE DR-A IN-SITU DIFFUSION EXPERIMENT – MULTISITE ION EXCHANGE (MIE) MODEL FOR THE SIMULATION OF CS^+ DIFFUSION AND RETARDATION

A.3.1. Task 3.1A_A7: MIE Model and Well-mixed Filter Approach – Direct Prediction

This simulation directly applies the diffusion parameters obtained via calibration for Phase I, Task 2.2D_A3 (Appendix A.1.3). Figure A-9 depicts the simulated and experimental concentration time curves for Cs^+ during both Phase I and Phase II. It can be seen that the predicted Cs^+ concentrations during Phase II are higher than the observed data from approximately 190 to 280 days, and lower than the experimental data after 300 days, indicating that diffusion parameters changed in response to the perturbation. Figure A-10 depicts the simulated and observed concentration time curves for the major ions Na^+, K^+, Ca^{2+}, Mg^{2+}, Cl^- and SO_4^{2-}. The simulated results agree well with the trends of the experimental data. In comparison to Task 3.1a (Figure 49), the simulated results of the current case show better agreement to the experimental data for Phase I of the experiment, but slightly worse agreement for Phase II of the experiment starting at 300 days. However, the simulated concentration peak values around 210 days exceed the experimental data for both simulation approaches in a similar manner.

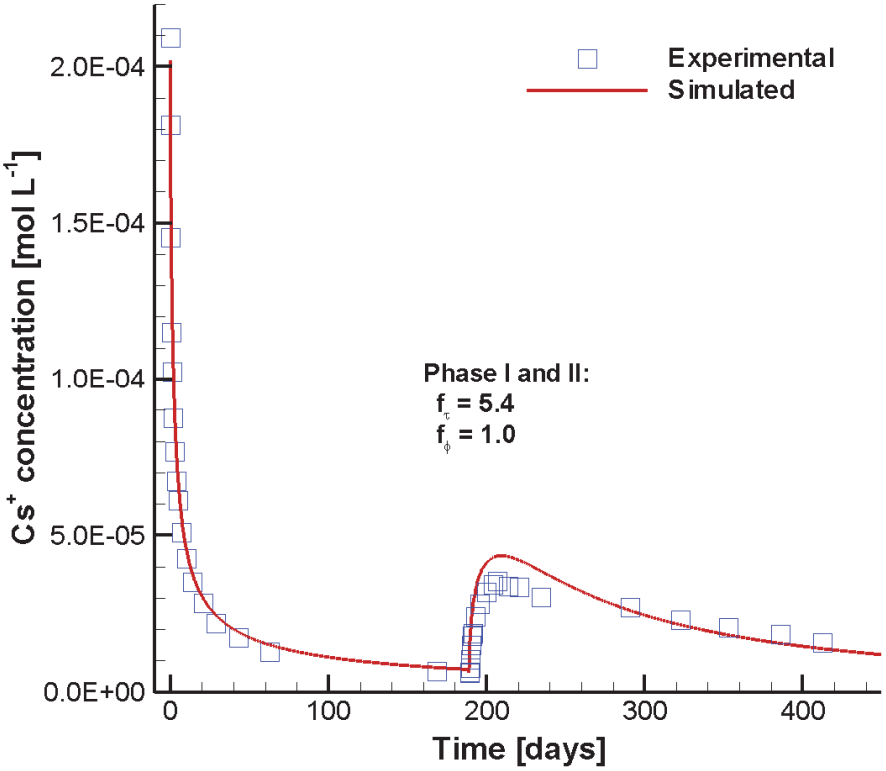

Figure A-9: Comparison of Simulated (Lines) and Experimental (Symbols) Concentration Time Curves for Cs^+ during Phase I and Phase II of the DR-A In-situ Diffusion Experiment (Task 3.1A_A7)

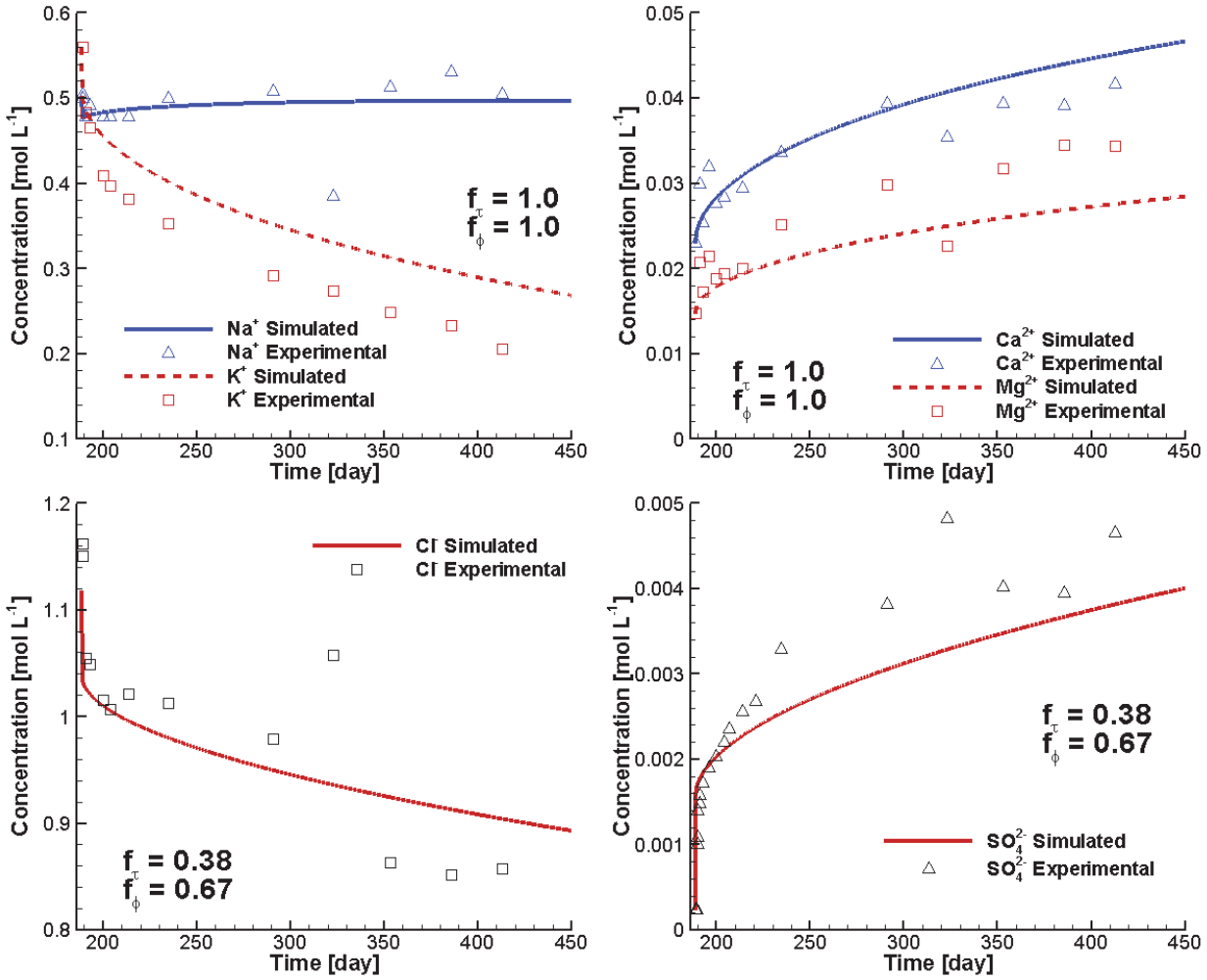

Figure A-10: Comparison of Simulated (Lines) and Experimental (Symbols) Concentration Time Curves for Major Ions during Phase II of the DR-A In-situ Diffusion Experiment (Task 3.1A_A7)

A.3.2. Task 3.1B_A8: MIE Model and Well-mixed Filter Approach – Calibration of Diffusion Parameters

As discussed above, the perturbation after completion of Phase I likely modified the diffusion parameters of the Opalinus Clay. The effective porosity (ϕ_e) and tortuosity (τ_e) of the Opalinus Clay were therefore recalibrated using the concentration time curve of the neutral tracer HTO up to 413 days. The newly calibrated diffusion parameters for Phase II were: ϕ_e for HTO of 0.19 (instead of 0.15 during Phase I), and τ_e of 0.15 (instead of 0.11 during Phase I). Figure A-11 shows very good agreement between the simulated and experimental time curves for Cs^+, using a porosity correction factor of 1.5 and a tortuosity correction factor of 1.0. In comparison to the simulated results of Task 3.1b (Figure 52,), better agreement to the experimental data was achieved for Cs^+. Both simulations capture the concentration increase of Cs^+ in the borehole due to the multisite ion exchange after the replacement of the circulation solution with higher K^+ concentration. However, to achieve this level of agreement, it was necessary to apply different

correction factors during Phase II of the experiment. Nevertheless, the effective diffusion coefficients for Cs^+ (calculated according to $D_e = f_e \phi_e f_\tau \tau_e D_0$) are very close. Figure A-12 shows good agreement between the simulated and observed concentration time curves for the major ions except Ca^{2+} if the tortuosity correction factors for the cations Na^+, K^+, Ca^{2+} and Mg^{2+} are 1.3. For the anions Cl^- and SO_4^{2-}, the calibrated porosity correction factor was 0.67, and the tortuosity correction factor was 0.38. In comparison to the simulated results of Task 3.1b (Figure 53), similar agreement to the experimental data was achieved for the anions, Na^+ and K^+. However, while the agreement with the experimental data for Mg^{2+} increased using the current approach, a less favorable fit with the experimental data was achieved for Ca^{2+} using the current approach in comparison to Task 3.1b.

Figure A-13 depicts the concentrations of sorbed species on the three different ion exchange sites. At 450 days, the most abundant sorbed species of Cs^+ is Cs-FES, because the FES site has the highest selectivity coefficient even though the total fraction of FES sites is only 0.1% of the total ion exchange sites. For all other major cations, the sorbed species on the PS site are dominant (Figure A-13). Nevertheless, only a narrow region near the borehole wall is strongly influenced by multisite ion exchange. At 450 days, the penetration depth of the influenced region is less than 10 cm from the borehole wall.

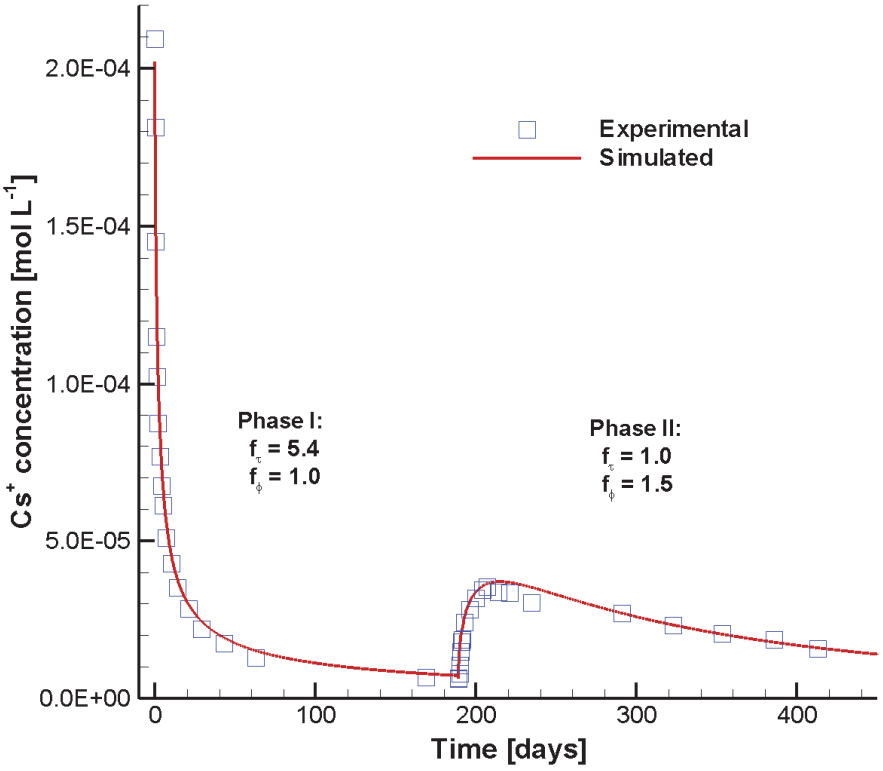

Figure A-11: Comparison of Simulated (Lines) and Experimental (Symbols) Cs^+ Concentration Time Curves for Phase I and Phase II of the DR-A In-situ Diffusion Experiment after Diffusion Parameter Calibration (Task 3.1B_A8)

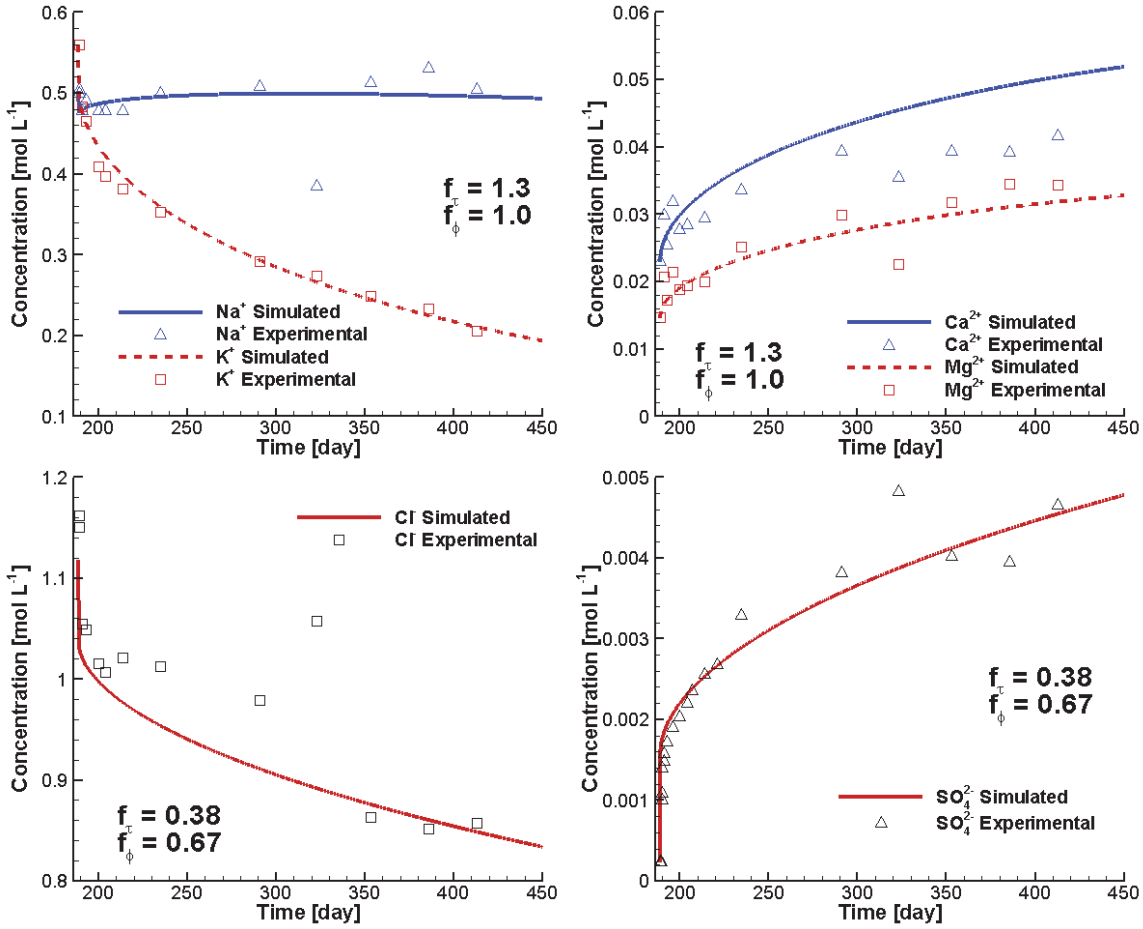

Figure A-12: Comparison of Simulated (Lines) and Experimental (Symbols) Concentration Time Curves of Major Ions during the DR-A In-situ Diffusion Experiment Phase II after Diffusion Parameter Calibration (Task 3.1B_A8)

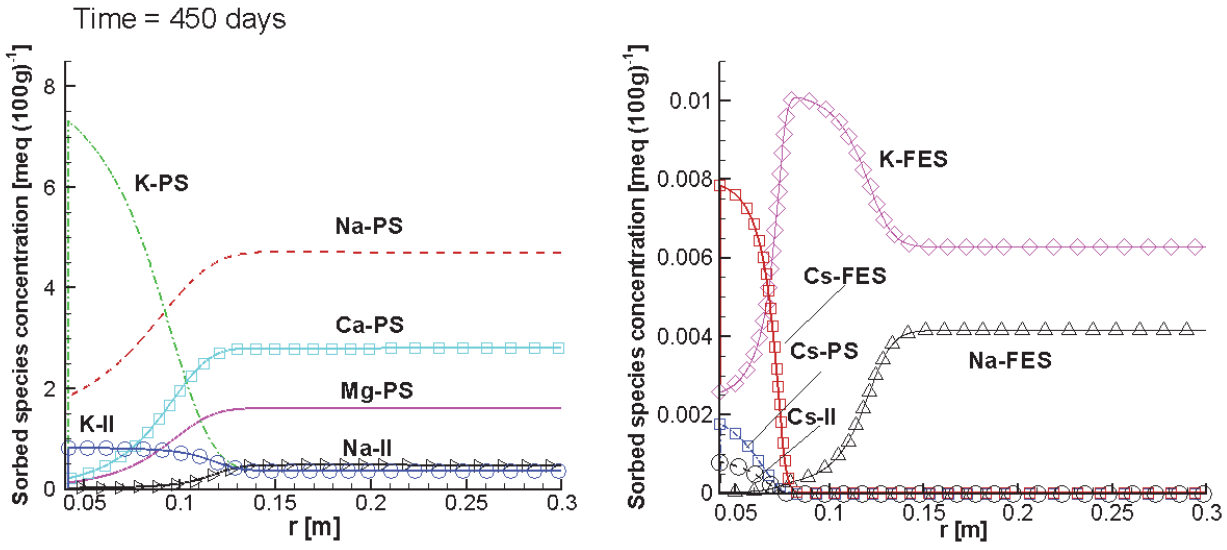

Figure A-13: Simulated Profiles of Sorbed Species on Three Ion Exchange Sites (-PS, -FES and –II) at 450 days

A.3.3. Task 3.2A_A9: MIE Model and Well-mixed Filter Approach – Further Prediction until 728 Days (Just Before Overcoring)

Based on the calibrated diffusion parameters described in the previous section (Section A.3.2), a predictive simulation was conducted until 728 days (just before the overcoring). The predicted Cs^+ time curve shows very good agreement with the experimental observations (Figure A-14). The simulated concentration time curves for the major ions also show good agreement to the experimental data (Figure A-15) with the exception of Ca^{2+}, which is slightly over predicted compared to the experimental observations. The predicted concentration time curves of Cs^+, Na^+, K^+, Cl^- and SO_4^{2-} in the borehole from 420 to 735 days are in very good agreement to the experimental data, similar to the simulated results in Task3.2A depicted in Figure 57 (Cs^+) and in Figure 58 (Na^+, K^+, Cl^- and SO_4^{2-}). However, the predicted concentration time curves of Ca^{2+} in the borehole show better agreement to the experimental data in Task 3.2a than in the current simulation. The opposite behavior can be observed for the predictions of Mg^{2+} (i.e. better fit in current simulation in comparison to Task 3.2A). The predicted profiles for the aqueous species HTO, Br^-, Cl^- and I^- also exhibit good agreement with the experimental data except for the region close to the borehole wall (Figure A-16). The discrepancies near the borehole wall are the result of back diffusion from the clay towards the borehole during overcoring, which is further discussed in Section A.4.2.

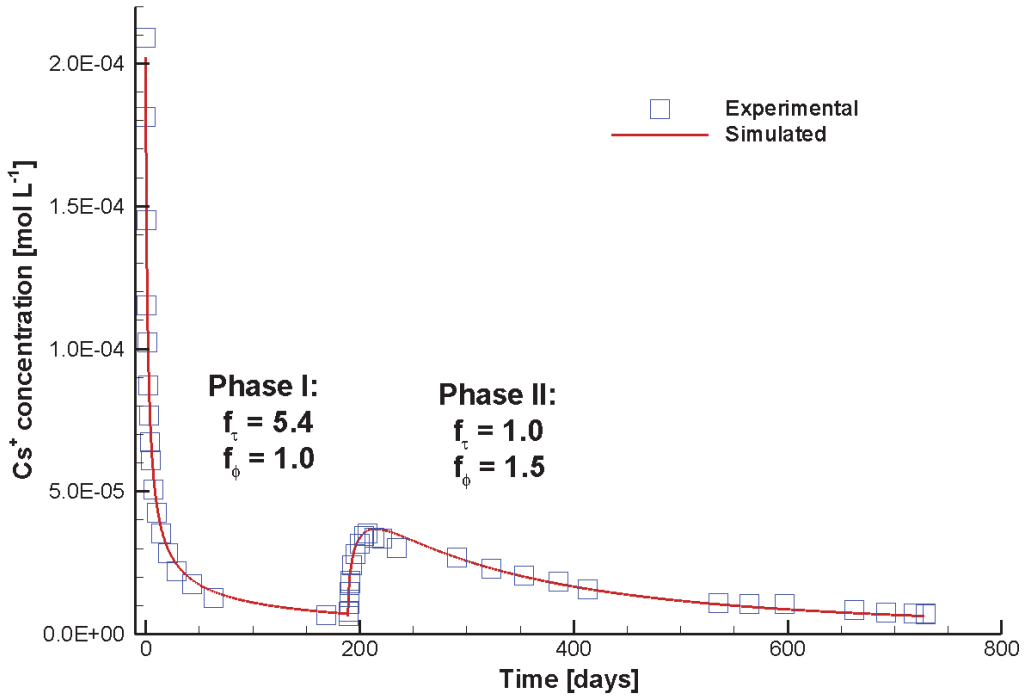

Figure A-14: Comparison of Simulated (Lines) and Experimental (Symbols) Results for Cs^+ Concentrations for Phase I and Phase II of the DR-A In-situ Diffusion Experiment up to 728 Days (Task 3.2A_A9)

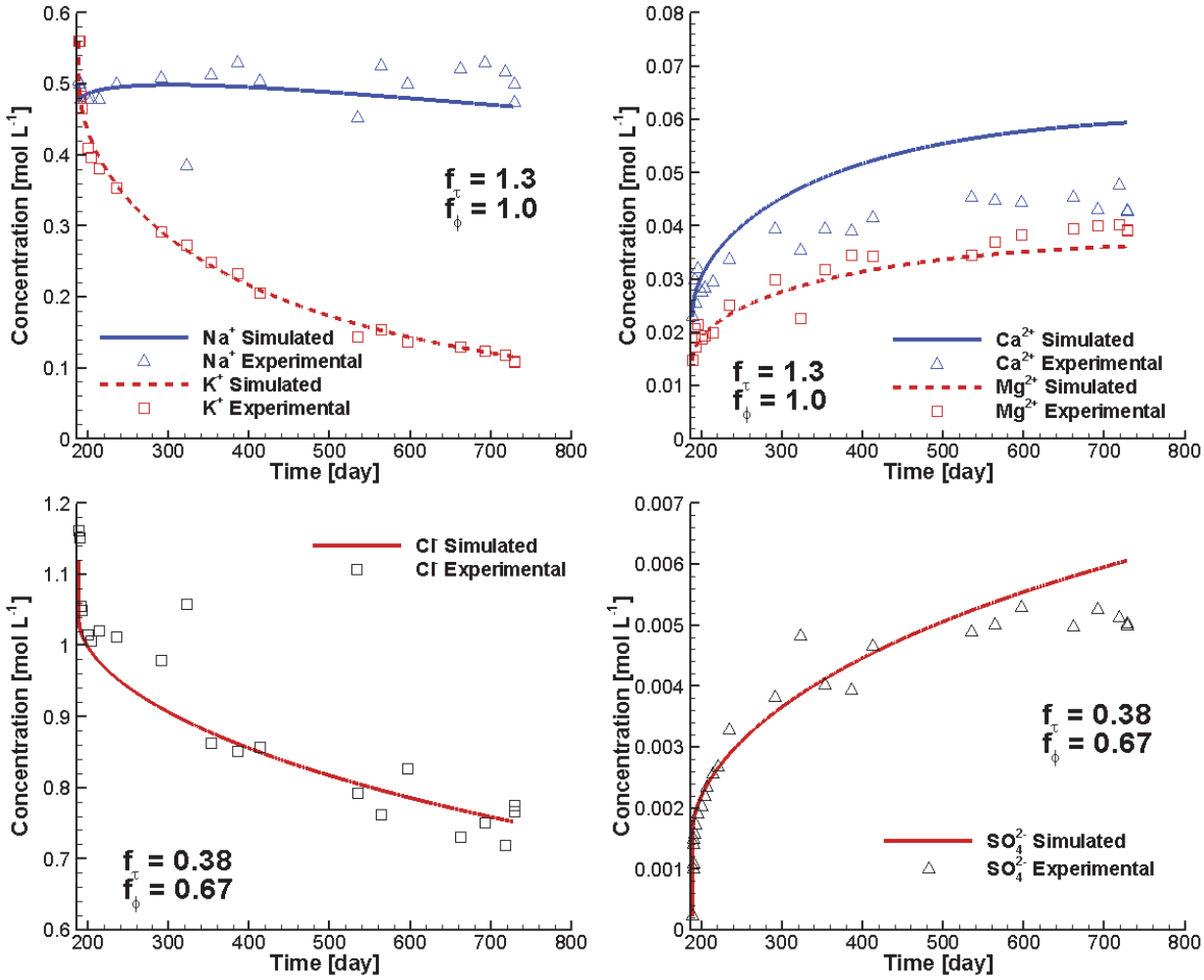

Figure A-15: Comparison of Simulated (Lines) and Experimental (Symbols) Results for Major Ions for Phase II of the DR-A In-situ Diffusion Experiment up to 728 Days (Task 3.2A_A9)

The predicted total concentration profiles (i.e. including both aqueous and sorbed species) of the major elements Na, Ca, Mg and K in the Opalinus Clay agree well with the general trends observed in the experimental data (Figure A-17). The total concentrations of K far from the clay-borehole interface are in very good agreement to the experimental data, but the predicted background total concentrations of Ca are higher than the observed data, and concentrations for Mg are lower than the measured data. This might be occurring because the ion exchange sites for both Ca and Mg are limited to PS sites only (see Table 15). This could lead to underestimation of the total sorbed amount of both species. The profiles of the fractions of sorbed species on the three sorption sites at 728 days are depicted in Figure A-18. In comparison to Figure A-13 (at 450 days), all profiles maintain the same shape, but the penetration depth associated with ion migration from the borehole increases to approximately 12 cm. The predicted concentration profiles for HTO and anions in the overcored sample are very similar to those obtained in Task 3.2A and are in good agreement to the measured data (compare Figure A-16 and Figure 60). However, the current approach provides better

agreement to the experimental data for the adsorbed species, particularly for sorbed Na and Mg (compare Figure A-17 and Figure 63).

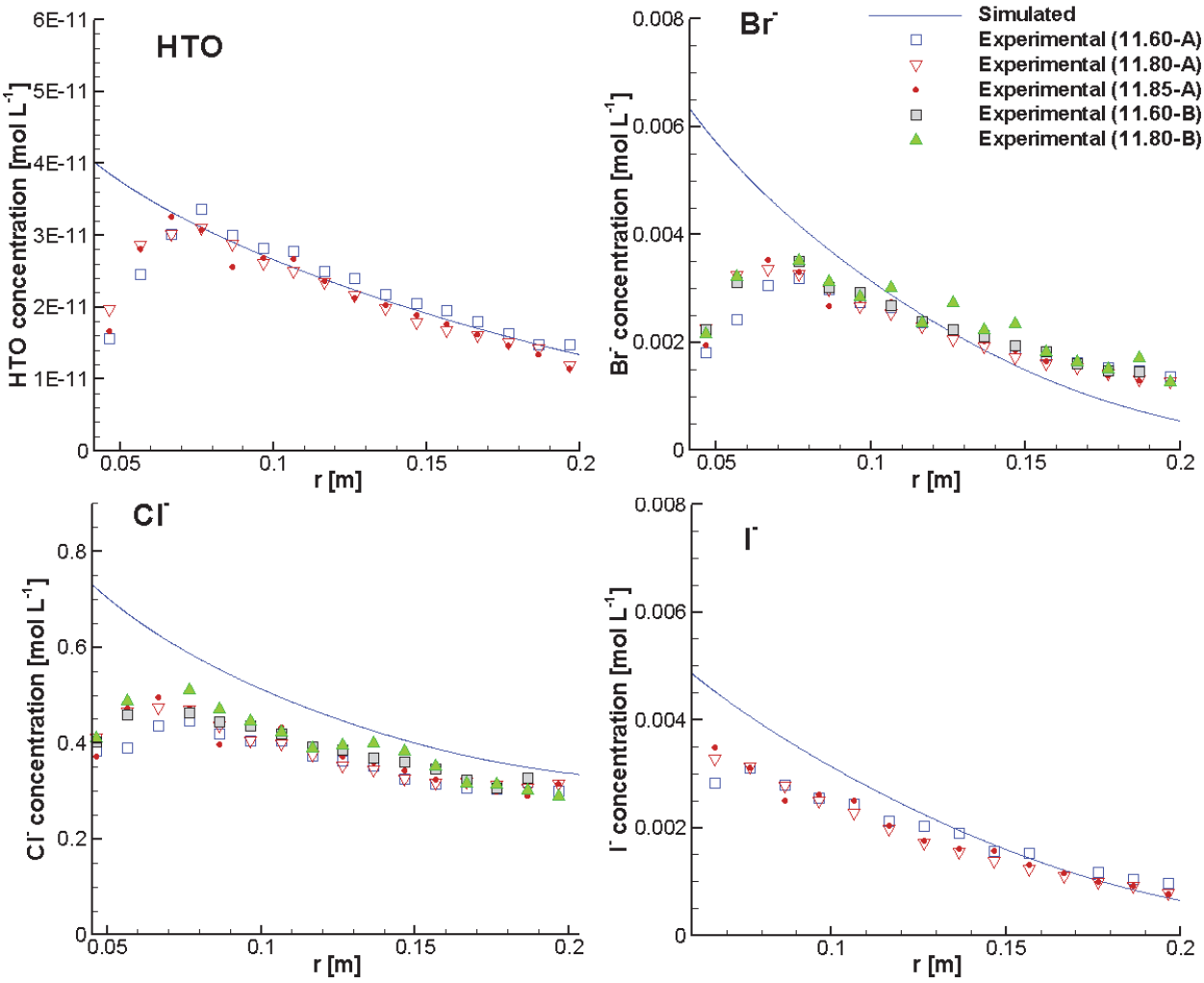

Figure A-16: Simulated Total Concentration Profiles for HTO, Br^-, Cl^- and I^- and Comparison to the Experimental Results in the Porewater of the Overcored Samples at 728 Days (Task 3.2A_A9)

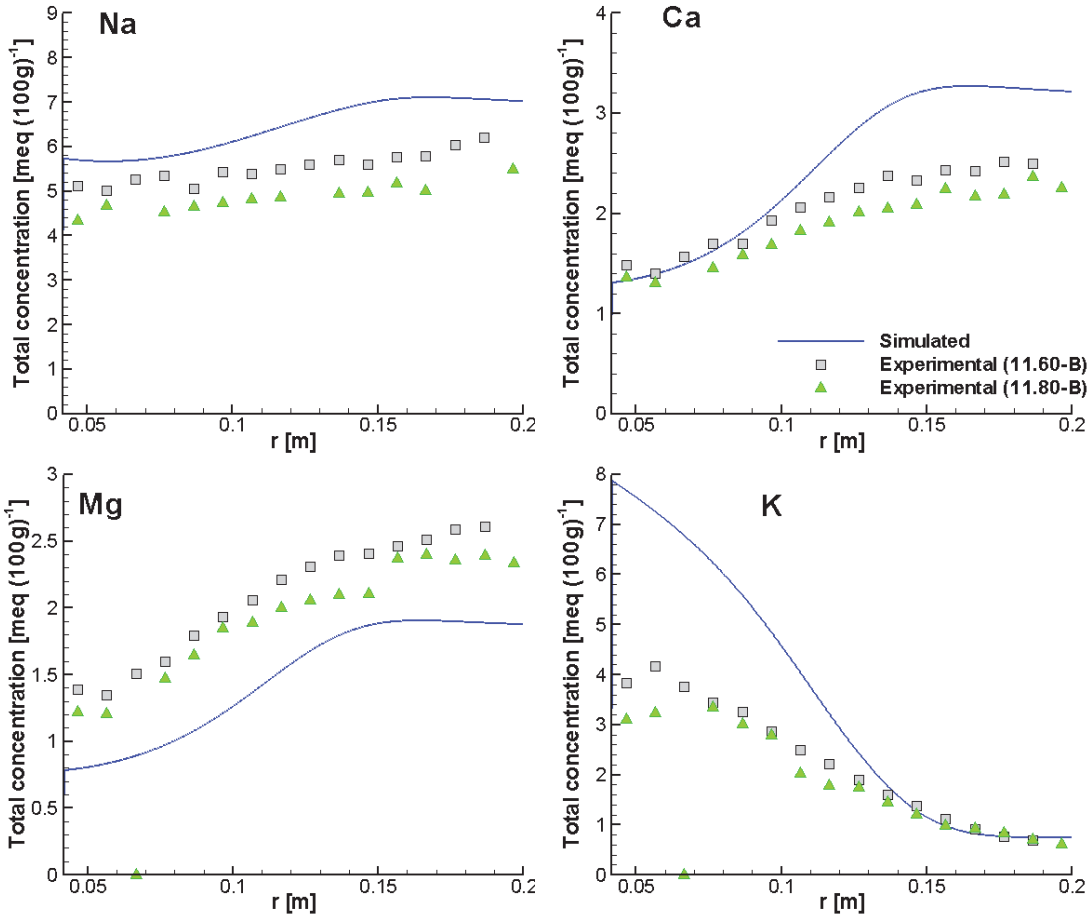

Figure A-17: Simulated Total Concentration Profiles for Na^+, Ca^{2+}, Mg^{2+} and K^+ and Comparison to the Experimental Results in the Porewater of the Overcored Samples at 728 Days (Task 3.2A_A9)

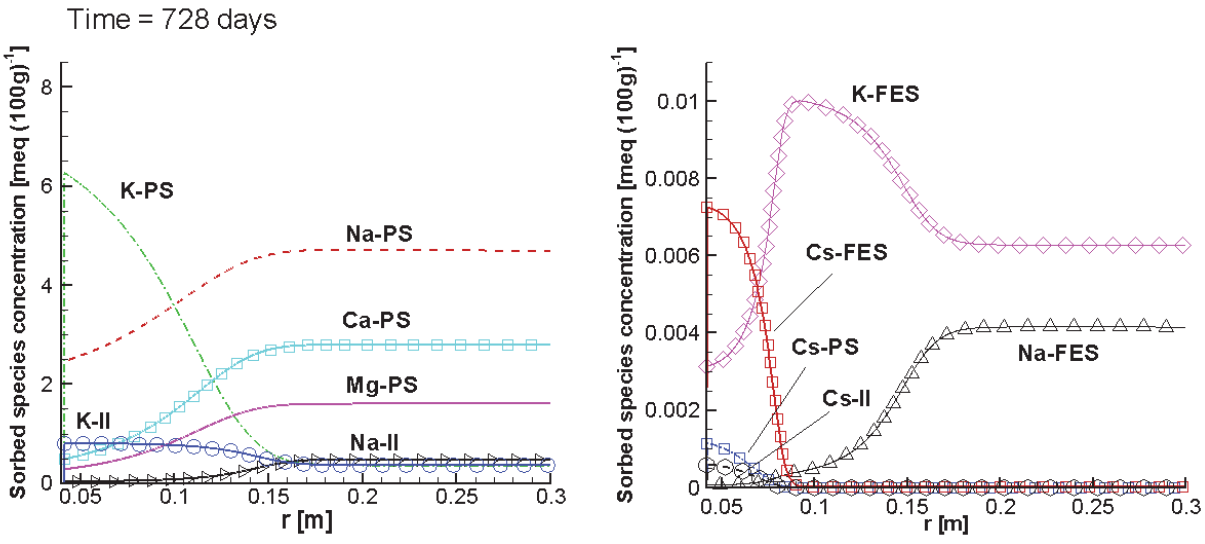

Figure A-18: Simulated Profiles of Sorbed Species on Three Ion Exchange Sites (-PS, -FES and –II) at 728 Days

A.4. REVISED SIMULATION OF THE DR-A IN-SITU DIFFUSION EXPERIMENT - OVERCORING

A.4.1. Task 3.2B_A10: Linear Sorption Approach (Without Filter) – Extended Prediction Including Overcoring Period (from 728 to 735 Days)

This calculation simulates the back diffusion process during overcoring using a linear sorption model for $^{60}Co^{2+}$ and $^{85}Sr^{2+}$ retardation. For this simulation, the circulation chamber and the filter are no longer present. The porewater gathered in the borehole was assumed to be Opalinus Clay formation water with the chemical composition as listed in Table 8, characterized by much lower concentrations for most major ions except SO_4^{2-}, and no tracers (see Figure A-7, Figure A-8; Figure A-15 and Figure A-16). Consequently, back diffusion of tracers and most major ions from the clay towards the borehole center can be expected.

Figure A-19 depicts the simulated and experimental total concentration profiles for HTO, $^{60}Co^{2+}$, Br^- and I^- at 735 days. The simulated concentration profiles for HTO, Br^-, and I^- at 735 days show very good agreement with the experimental results. However, the concentration profile for $^{60}Co^{2+}$ shows more discrepancy to the experimental data (Figure A-19) in comparison to the simulated profiles in Task 3.2b (Figure 64) (see also discussion in Section A.2.3).

Figure A-20 depicts the simulated and experimental profiles for the total concentrations of Co and Sr. Simulated total concentrations of Sr (including Sr and $^{85}Sr^{2+}$ present as aqueous and sorbed species) show relatively good agreement to the experimental data. However, the simulated total concentrations of $^{60}Co^{2+}$ (in the range less than $1.0x10^{-10}$ meq $(100g)^{-1}$) are much lower than the experimental data (in the range of $6.0x10^{-4}$ to $9.0x10^{-4}$ meq $(100g)^{-1}$). This can be explained by the presence of stable Co background concentrations with the isotope $^{60}Co^{2+}$ being only a small fraction of the measured total cobalt concentration as discussed in section 5.4.2.1. Simulated profiles of the total sorbed concentrations of both Co and Sr in the current simulation are slightly higher than those in Task 3.2b (compare Figure A-20 and Figure 65).

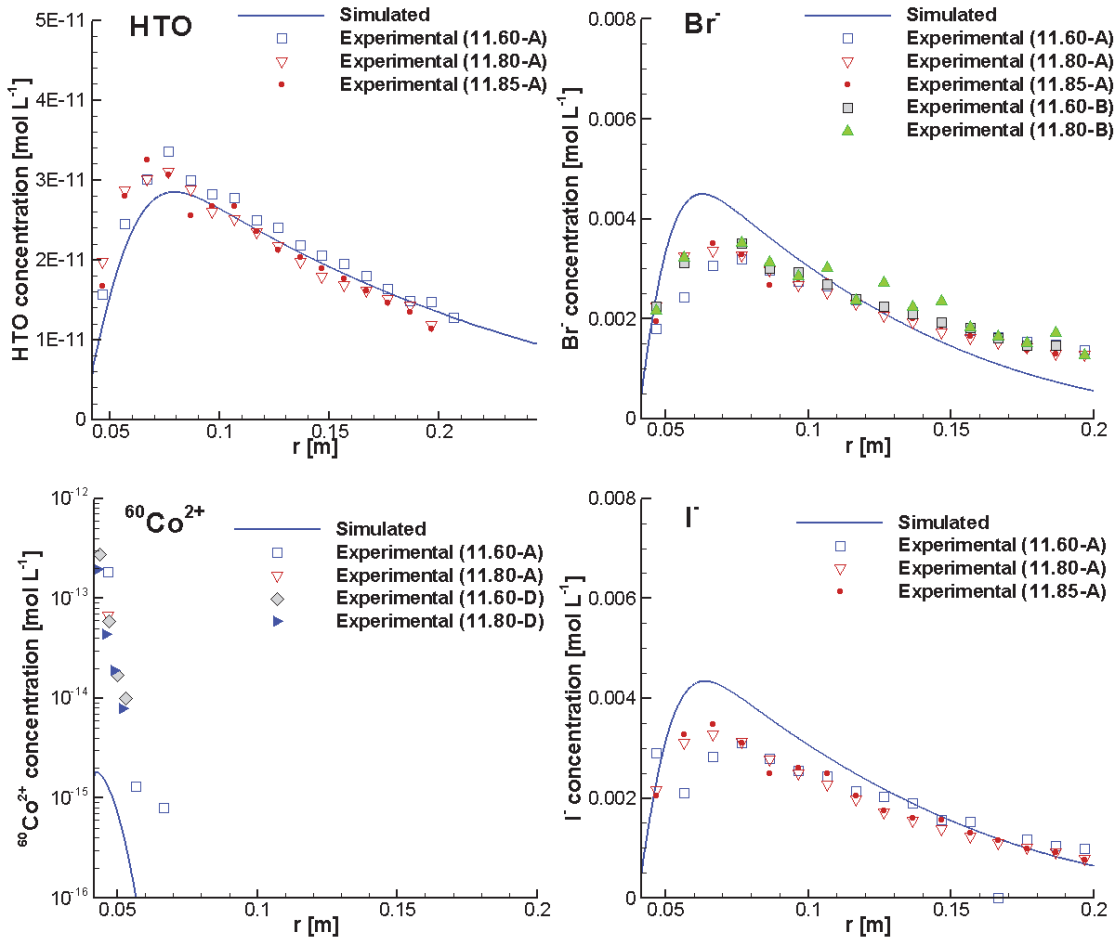

Figure A-19: Comparison of the Simulated Total Concentration Profiles for HTO, $^{60}Co^{2+}$, Br^- and I^- in the Opalinus Clay at 735 days and in the Porewater of the Overcored Opalinus Clay Samples (Task3.2B_A10)

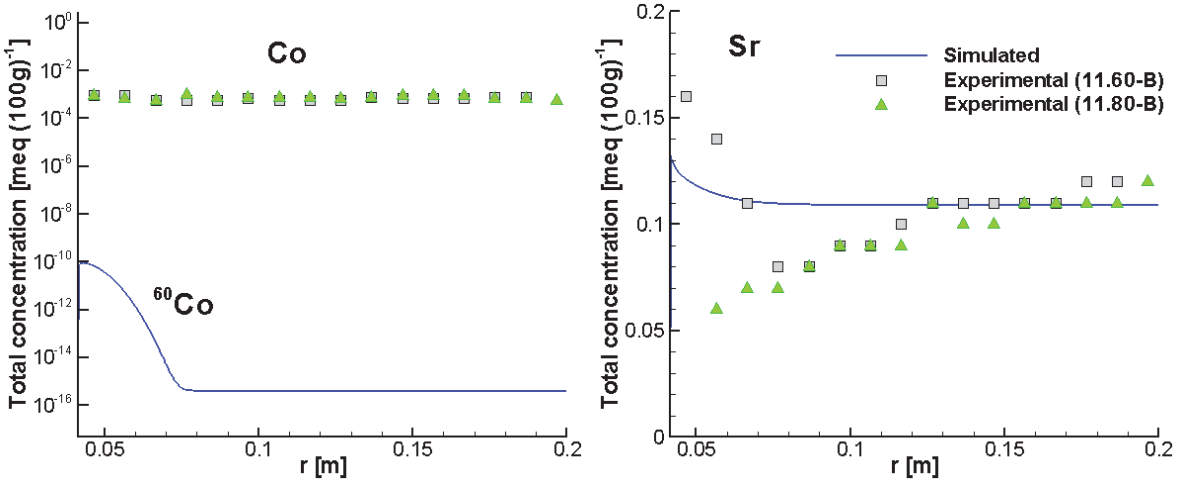

Figure A-20: Comparison of Simulated and Experimental Profiles of Sorbed Concentration of Co (left) and Sr (right) in the Overcored Opalinus Clay Samples at 735 Days (Task3.2B_A10)

A.4.2. Task 3.2B_A11: Multisite Ion Exchange Model (Without Filter)– Extended Prediction of the Overcoring (from 728 to 735 Days)

This case simulates the overcoring process by applying the multisite ion exchange model to simulate Cs^+ retardation during the one week period of overcoring. The back diffusion of HTO, Br^-, I^- and Cl^- from the Opalinus Clay towards the borehole is well simulated (Figure A-21). Experimental data for the Cs^+ concentration profile is not available; therefore no comparison can be made for Cs. The simulated concentration profiles for the cations Na^+, Ca^{2+}, Mg^{2+} and K^+ follow the trends of the experimental data observed in the overcored samples (Figure A-23). However, the background concentration of Ca is higher, and that of Mg is lower than the experimental results. The background total concentration of K agrees well with the experimental data, but shows higher concentration in the range near the borehole. The simulated profiles of the total concentrations (i.e. including aqueous and sorbed species) of Na, Ca, Mg and K follow the trends of the experimental data (Figure A-23).

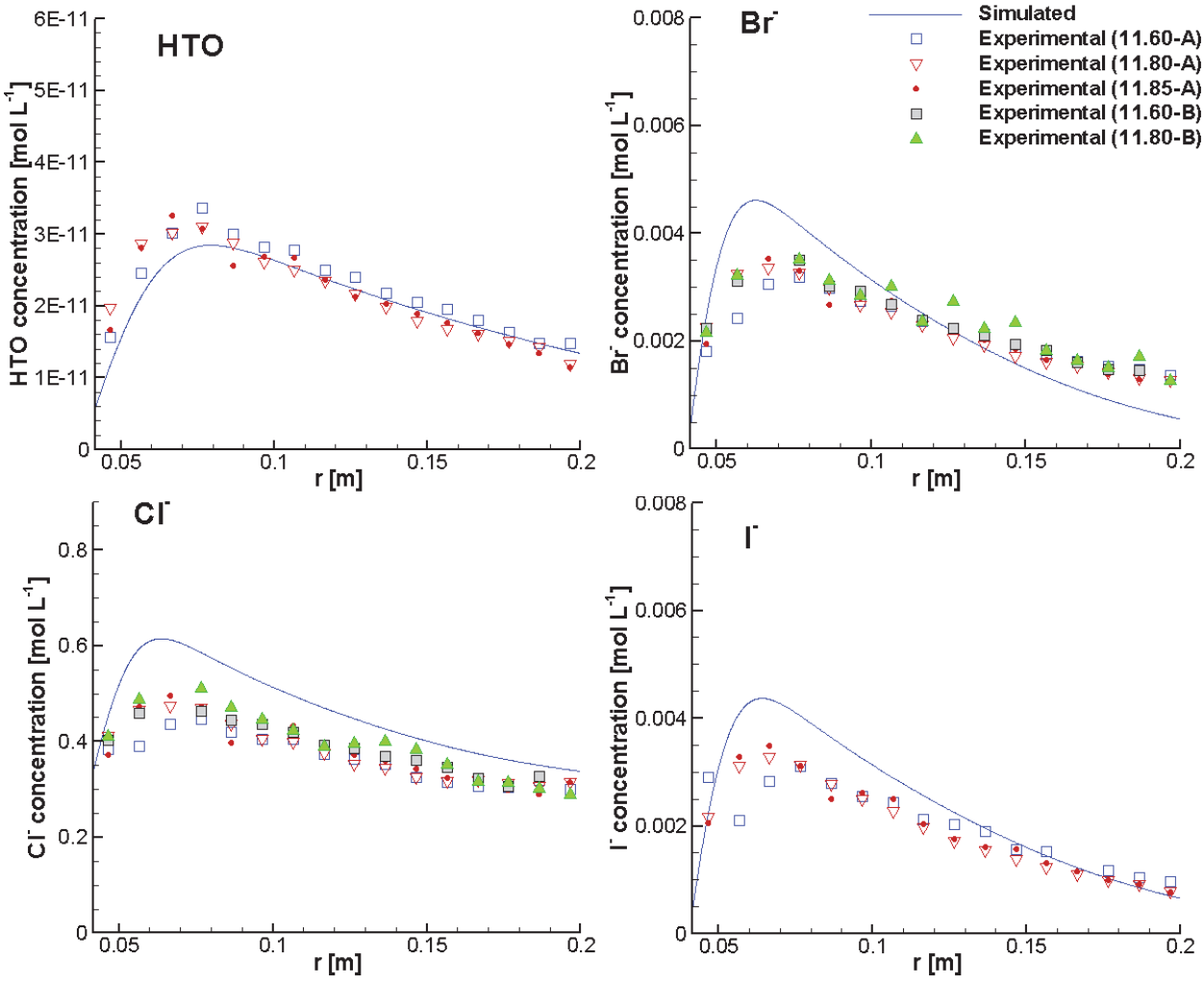

Figure A-21: Comparison of Simulated and Experimental Concentration Profiles for HTO, Br^-, Cl^- and I^- in the Porewater of the Overcored Samples at 735 Days (Task 3.2B_A11)

In comparison to the simulated results in Task 3.2B (Figure 66 to Figure 70), the predicted profiles of HTO and anions in the current simulation are almost identical and in good agreement to the experimental data (compare Figure A-21 to Figure 66). Concentrations of adsorbed species and total concentrations (adsorbed and aqueous) show improved agreement to the experimental data in comparison to Task 3.2B, especially for Na and Mg (compare Figure 69, Figure A-23 to Figure 70).

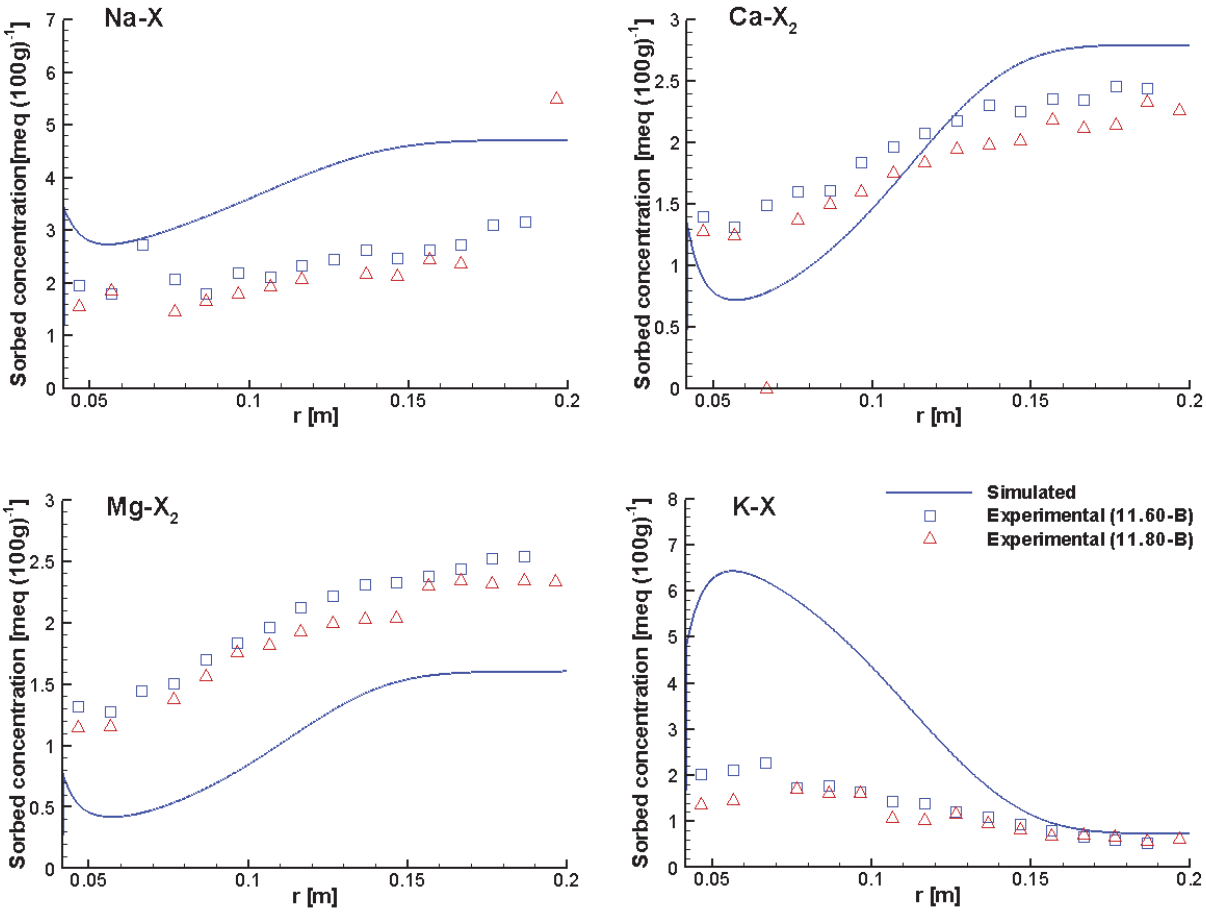

Figure A-22: Comparison of Simulated and Experimental Total Concentration Profiles of sorbed species of the Overcored Samples at 735 Days (Task 3.2B_A11)

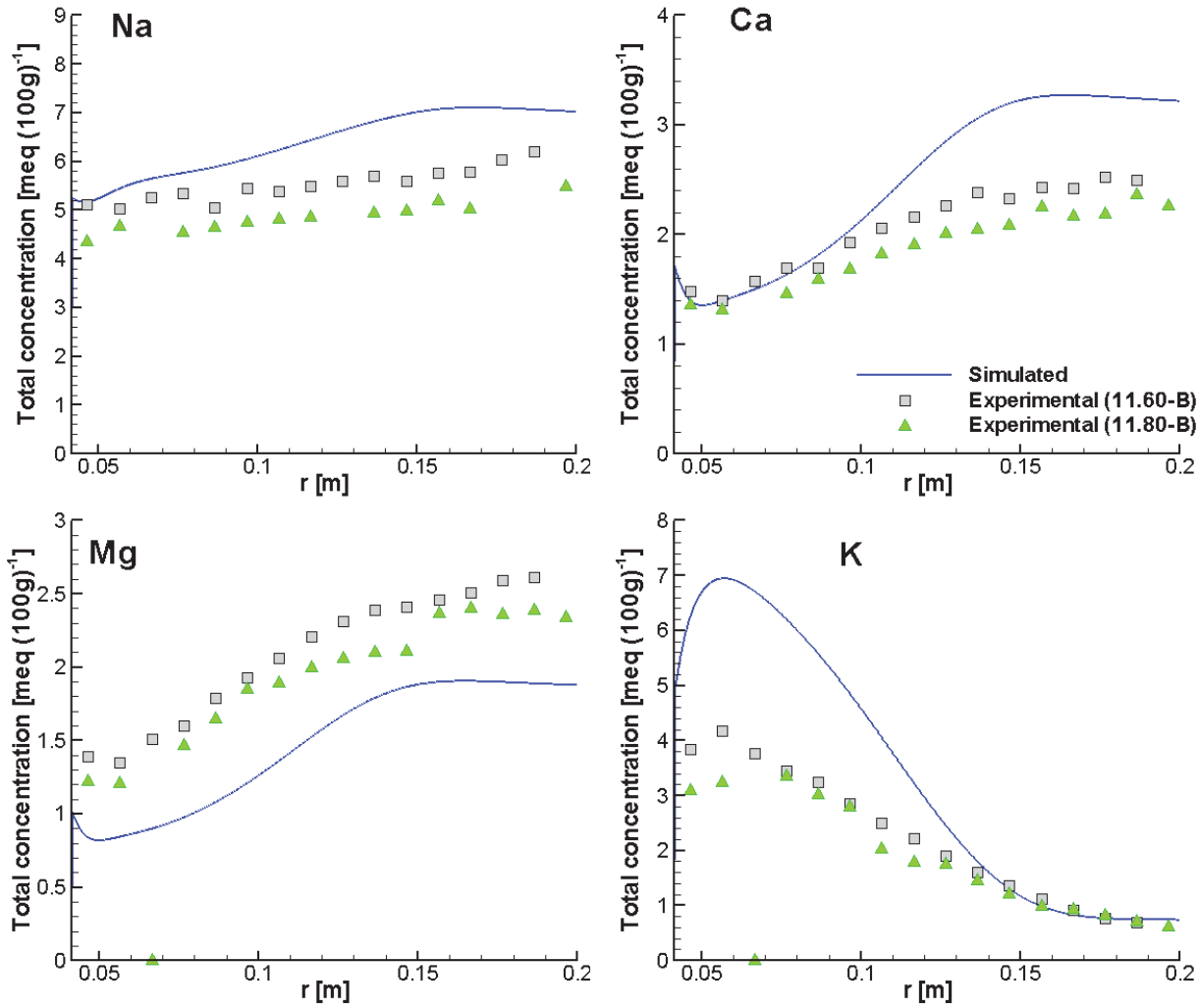

Figure A-23: Comparison of Simulated and Experimental Total Concentration (including Aqueous and Sorbed Species) Profiles for Elements Na, Ca, Mg and K of the Overcored Samples at 735 Days (Task 3.2B_A11)

A.5. SUMMARY

Several alternative simulations were conducted to evaluate the impact of different modelling approaches on the simulation results and the ability to match experimental data. It could be shown that slightly better agreement to the experimental data can be obtained for the strongly sorbing tracers by using higher sorption coefficients (for Co) and a larger tortuosity for the filter to mimic advective mixing in the filter, following the approach proposed by other modelling teams. Including advective mixing in the filter led to larger discrepancies between the experimental and simulated data for HTO and anions at earlier stages of the experiment, but showed limited influence shortly after experiment initiation (0.5 days). The predicted spatial concentration profiles for HTO and anions showed good agreement to the experimental data of the overcored samples, very similar to previous simulations reported in the main body of the report. For the major cations, slightly better agreement was achieved for the ion exchanged species Na-X and Mg-X_2. However, the alternative simulations continued to show some discrepancies between the simulated and experimental results, specifically for Ca, suggesting

the need for a more mechanistic model that accounts for ion migration in the diffuse double layer model. Overall, the differences between the alternative simulations presented in this appendix and the simulations presented in the main body of the report are relatively small. All simulations closely follow the trends observed in the experimental data, and the choice of simulation approach does not affect interpretation of the results in terms of ion migration into the Opalinus clay.

REFERENCES

Sattler, A. R. 1962. Decayy of Sr^{85}, Physical Review, 127, 854–859.

Soler, J.M. 2013. DR-A experiment: Diffusion, retention and perturbation Reactive transport scoping calculation. Change in the salinity of the circulation solution. Mont Terri Project Technical Note 2013-47

Unterweger, M.P. 2002. Half-life measurements results at the National Institute of Standards and Technology, Proceedings of the Conference on Radionuclide Metrology and its Applications, ICRM'01, Applied Radiation and Isotopes, 56, 125-130.

Wersin, P., J.M. Soler, L.V. Loon, J. Eikenberg, B. Baeyens, D. Grolimund, T. Gimmi and S. Dewonck. 2008. Diffusion of HTO, Br^-, I^-, Cs^+, 85-Sr^{2+} and 60-Co^{2+} in a clay formation: Results and modelling from an in-situ experiment in Opalinus Clay. Applied Geochemistry, 23, 678-691.